Title

Dissolved CO2 and Oxygen Dynamics on Coral Reefs: from Natural Variability and Impacts on Calcification to Projections under Warming

Author

Pezner, Ariel Katharine

Publication Date

2022

Peer reviewed|Thesis/dissertation

UNIVERSITY OF CALIFORNIA SAN DIEGO

Dissolved CO_2 and Oxygen Dynamics on Coral Reefs: from Natural Variability and Impacts on Calcification to Projections under Warming

A Dissertation submitted in partial satisfaction of the requirements
for the degree Doctor of Philosophy

in

Oceanography

by

Ariel Katharine Pezner

Committee in charge:

Professor Andreas Andersson, Chair
Professor Richard Norris
Professor Jonathan Shurin
Professor Jennifer Smith
Professor Jennifer Taylor

2022

The Dissertation of Ariel Katharine Pezner is approved, and it is acceptable in quality and form for publication on microfilm and electronically.

University of California San Diego

2022

DEDICATION

This thesis is dedicated to my parents, Sandra and Richard. Thank you, for everything.

TABLE OF CONTENTS

LIST OF FIGURES

CHAPTER 1

CHAPTER 2

CHAPTER 3

CHAPTER 4

LIST OF TABLES

CHAPTER 3

CHAPTER 4

ACKNOWLEDGEMENTS

There are many people who have supported me, trained me, and mentored me throughout my scientific journey who I would like to acknowledge here.

First, I would like to thank my thesis advisor, Dr. Andreas Andersson. Thank you, Andreas, for providing me with the opportunity to complete my Ph.D. and the intellectual freedom to pick projects I am passionate about. You have supported me in exploring so many different avenues with my research as well as my endeavors and passions outside of the lab. I have learned so much from my time at Scripps and I am a better scientist having been your student. Thank you for creating a lab environment that is collaborative and supportive and for encouraging us to maintain a balance of work and life. I am really honored to have been a part of the SCOOBY Lab.

I would also like to thank my committee members, Richard Norris, Jonathan Shurin, Jennifer Smith, and Jennifer Taylor for helping me expand upon my scientific questions and for dedicating their time to provide feedback on my work.

Much of the work presented in this dissertation would not have been possible without the help, time, and encouragement of the SCOOBY Lab members over the years. Thank you to Heather Page, Tyler Cyronak, Alyssa Griffin, Travis Courtney, Samuel Kekuewa, Max Rintoul, and Rhys Tallentire for your help in the lab, in the field, and over Zoom. Thank you, Travis, for being the best officemate and mentor – sharing an office with you during many of the low and high points of this Ph.D. was invaluable. And to Travis, Sam, and Max -- our time in the field in Dongsha, Taiping, and Okinawa were some of the highlights of my Ph.D. experience. Thank you for being the best SCUBA buddies and field partners and for all the shared laughs, memories, and meals.

In addition to the SCOOBY Lab, there are many other people and institutions I must thank for their contributions to this work. For our work in Taiwan, thank you so much to Dr. Keryea Soong and your team at National Sun Yat-sen University for the opportunities to visit both Dongsha Atoll and Taiping Island and all of the coordination involved with those trips. Thank you to Yi Wei, Yi-Bei Liang, Hai-Jin Zhang, and Joy Ru-Yu Cheng for your assistance, translation, and friendship during our visits to Taiwan and even in Japan. And thank you to the Dongsha Atoll National Marine Park employees and the Coast Guard Administration of Taiwan for your hospitality and support of our work. For our work in Japan, thank you to Dr. Satoshi Mitarai and your team at the Okinawa Institute of Science and Technology for the opportunity to work in Onna and for your hospitality and assistance in Okinawa. I also thank all of the many co-authors from the following chapters for their contributions to this work. Thank you also to Dr. Sarah Davies, Dr. Colleen Bove, and the rest of the Davies Lab at Boston University for their mentorship, support, and friendship during my last year. Even though our work is not part of this dissertation, having a small place in your lab has meant so much to me.

I also would like to thank some of my earlier mentors for stimulating my love of science and passion for research. I would not be at this point in my career today without the inspiration, support, and encouragement from Dr. Mark Ewoldsen, Dr. Ulli Seibt, and Dr. Daniel Blumstein. Dr. E, thank you for inspiring my love of environmental science and encouraging me to pursue it. Ulli, thank you for trusting me with my first independent research project and for mentoring me during my time at UCLA. Dan, thank you for the opportunity to have my first marine field experience in Mo'orea. You challenged me every day of our field course and I am a better scientific writer and scientist because of you.

At Scripps, there are so many people to thank for making the last five years so incredible. Thank you to the members of the 2017 cohort for your friendship and support over these years. Thank you to the administration staff including Gilbert Bretado and Shelley Weisel and others for always knowing the answers to my questions and for keeping so much of Scripps running. And thank you to the GRD Office for all of your help processing purchases and all of our travel. To Alaina Smith, Olivia Pereira, Kayla Wilson, Kelli Mullane, and Stephanie Matthews, thank you for the laughs, the experiences, and the friendship we have all shared. Most of my best memories from this time involve you.

Thank you to the UCLA Mixed Student Union and the SIO Women and Minorities in Science groups and all of their members and board members over the years. Both MSU and WMIS were important communities for me throughout my education, and I am so proud of the work we have accomplished. My identity as a multiracial woman is an integral part of my role as a scientist and I look forward to continuing to serve and uplift the underrepresented in science throughout my career.

Thank you to all of my friends outside of Scripps for your love and support over the years, especially Sahar Moheize, Janna Johnson, and Tammy Hsu. Thank you to Brett Sonnichsen for your endless support in the last few years. And most of all, thank you to my parents, Sandra and Richard, for being truly the best parents, cheerleaders, role models, and best friends I could have ever asked for. You gave me the world and encouraged me to be whoever I wanted to be and I am so proud to be your daughter, I love you.

This work would not have been possible without the funding from a variety of different sources. This work was funded by my National Science Foundation Graduate Research Fellowship (NSF GRFP) DGE-2038238, as well as the following grants awarded to

Dr. Andreas J Andersson: NSF OCE 18-29778, NSF OCE 14-16518, NSF OCE 12-55042, and UC San Diego Academic Senate Marine Sciences Research Grant #A105437.

Chapter 2, in full, is a reprint of the material as it appears in Lateral, vertical, and temporal variability of seawater carbonate chemistry at Hog Reef, Bermuda. Pezner, Ariel K.; Courtney, Travis A.; Page, Heather N.; Beatty, Cory M.; DeGrandpre, Michael D.; Andersson, Andreas J., Frontiers in Marine Science, 2021. The dissertation author was the primary investigator and author of this paper.

Chapter 3, in full, is currently in review at Nature Climate Change as Global coral reefs will experience moderate to severe hypoxia before the end of the century. Pezner, Ariel K.; Courtney, Travis A.; Barkley, Hannah C.; Chou, Wen-Chen; Chu, Hui-Chuan; Clements, Samantha M.; Cyronak, Tyler; DeGrandpre, Michael D.; Kekuewa, Samuel A. H.; Kline, David I.; Liang, Yi-Bei; Martz, Todd R.; Mitarai, Satoshi; Page, Heather N.; Rintoul, Max S.; Smith, Jennifer E.; Soong, Keryea; Takeshita, Yui; Tresguerres, Martin; Wei, Yi; Yates, Kimberly K.; Andersson, Andreas J. The dissertation author was the primary investigator and author of this paper.

Chapter 4, in full, is currently being prepared for submission for publication of the material. Pezner, Ariel K.; Charles, Christopher D.; Chou, Wen-Chen; Chu, Hui-Chuan; Courtney, Travis A.; Frable, Bejamin W.; Kekuewa, Samuel A. H.; Soong, Keryea; Wei, Yi; Andersson, Andreas J. The dissertation author was the primary investigator and author of this material.

VITA

2017 Bachelor of Science in Environmental Science (Minors: Conservation Biology and Atmospheric & Oceanic Sciences), University of California Los Angeles

2020 Master of Science in Oceanography, University of California San Diego

2022 Doctor of Philosophy in Oceanography, University of California San Diego

PUBLICATIONS

Pezner, Ariel K., Courtney, Travis A., Page, Heather N., Beatty, Cory M., DeGrandpre, Michael D., Andersson, Andreas J. Lateral, vertical, and temporal variability of seawater carbonate chemistry at Hog Reef, Bermuda. Frontiers in Marine Science, 2021. https://doi.org/10.3389/fmars.2021.562267

Pezner, Ariel K., Pivovaroff, Alexandria L., Sun, Wu, Sharifi, M. Rasoul, Rundel, Philip W., Seibt, Ulli. Plant functional traits predict the drought response of native California plant species. International Journal of Plant Sciences, 2019, 181:256-265. https://doi.org/10.1086/706451

Johnson, Gina C.*, **Pezner, Ariel K.*,** Sura, Shayna M., Fong, Peggy. Nutrients and herbivory, but not sediments, have opposite and independent effects on the tropical macroalga *Padina Boryana*. Journal of Experimental Marine Biology and Ecology, 2018, 507: 17-22. https://doi.org/10.1016/j.jembe.2018.07.004 *Authors contributed equally to this manuscript

Pezner, Ariel K., Lim, Anthony R., Kang, Jane J., Armenta, Tiffany C., Blumstein, Daniel T. Hiding behavior in Christmas tree worms on different time scales. Behavioral Ecology, 2017, 28:154-163. https://doi.org/10.1093/beheco/arw140

ABSTRACT OF THE DISSERTATION

Dissolved CO_2 and Oxygen Dynamics on Coral Reefs: from Natural Variability and Impacts on Calcification to Projections under Warming

by

Ariel Katharine Pezner

Doctor of Philosophy in Oceanography

University of California San Diego, 2022

Professor Andreas Andersson, Chair

Coral reefs globally are facing impacts from ocean warming, acidification, and oxygen loss as a result of anthropogenic climate change. Understanding the spatiotemporal patterns of reef carbonate chemistry and oxygen variability, as well as how low pH or oxygen conditions might affect coral physiology, is key to predicting how global reefs will be impacted in the future. In this dissertation, I leveraged dissolved oxygen data from autonomous sensors deployed at 32 sites around the world to explore present-day oxygen variability and project

changes in hypoxia exposure under modeled ocean warming. I show that hypoxia is pervasive on global coral reefs, with 84 % of the reef habitats surveyed experiencing weak to moderate hypoxia and 13 % experiencing severe hypoxia under present-day conditions. Calculations of reef oxygen loss under 5 warming scenarios reveal that warming will increase the duration, intensity, and severity of hypoxic events on reefs, leading to severely hypoxic conditions on more than a third of these reef habitats by 2100. In case studies of reefs in Bermuda and Taiwan, I examined multidimensional variability in carbonate chemistry and oxygen across a reef and assessed the potential for seagrass beds to serve as refugia for corals from ocean acidification and deoxygenation. In Bermuda, data from spatial seawater surveys and a suite of autonomous sensors at the surface and benthos revealed strong signals of both benthic and water column productivity that interacted with local geomorphology and hydrodynamics to create the observed patterns in carbonate chemistry and oxygen across the reef. In Taiwan, strong gradients in temperature, pH, and oxygen across the seagrass bed were associated with significant differences in coral skeletal extension rate, density, and $\partial^{13}C$ isotopic composition measured from coral cores. However, there was no evidence that the presence of seagrass significantly impacted coral calcification rates along this gradient. Altogether, this dissertation provides projections of coral reef oxygen loss under rapid climate change and highlights the contributions of local conditions to observed variability in seawater chemistry with complex impacts on coral growth.

CHAPTER 1: Introduction

Despite covering just 0.1-0.5% of the ocean floor (Smith, 1978; Copper, 1994; Spalding and Grenfell, 1997), coral reefs are some of the most ecologically and economically valuable ecosystems on the planet. As the foundation species for coral reef ecosystems, corals provide three-dimensional structural complexity and habitat used by countless other reef species, supporting the immense biodiversity observed on coral reefs (Fisher et al., 2015). It is estimated that coral reefs provide more than $375 billion in ecosystem services every year (Costanza and Folke, 1997), including fisheries that feed more than 500 million people (Wilkinson, 2004), coastline protection from storms and erosion, pharmacological products, and tourism (Moberg and Folke, 1999). However, coral reefs globally are facing impacts from a combination of stressors such as overfishing, pollution, ocean acidification, warming, and deoxygenation that are threatening their health and survival (Pandolfi et al., 2005; Hoegh-Guldberg et al., 2007; Altieri et al., 2017). Significant declines in coral cover have been recorded across the globe, from the Caribbean (Gardener et al., 2003) to the Great Barrier Reef (De'ath et al., 2012), and these trends are predicted to continue in the future (Hoegh-Guldberg et al., 2007).

Corals create the complex structures observed on coral reefs through the production of their calcium carbonate skeleton via calcification. The ability of corals to calcify relies strongly on the carbonate chemistry of the surrounding seawater (Andersson and Gledhill, 2013), which may be impacted by anthropogenic ocean acidification (OA) (Kleypas and Yates, 2009). Known as the "other CO_2 problem" (Doney et al., 2009), OA is the result of oceanic uptake of excess atmospheric carbon dioxide. The dissolution of atmospheric CO_2 into seawater causes a series of chemical reactions that shift carbonate chemistry equilibrium in seawater, resulting in a decrease

in seawater pH (increase in H^+ ion concentration) and decrease in carbonate ion concentration (CO_3^{2-}) (Zeebe and Wolf-Gladrow, 2001):

$$CO_2 + H_2O \leftrightarrow HCO_3^- + H^+ \leftrightarrow CO_3^{2-} + 2H^+ \quad \text{(Equation 1)}$$

These changes in the carbonate chemistry balance make calcification less energetically favorable, and thus may pose challenges to organismal calcification under OA. Long-term declines in pH have already been observed in oceans around the world (e.g., Midorikawa et al., 2012; Bates et al., 2017), with a mean change in global surface pH of 0.1 units since the Industrial Revolution (Garcia-Soto et al., 2021). Under the most extreme projections of continued anthropogenic CO_2 emissions, mean surface ocean pH is expected to decrease by a total of 0.44 units by the end of the century (Kwiatkowski et al., 2020).

Observing the trends and effects of ocean acidification on coral reefs, however, tends to be more complicated than in the open ocean. As shallow, coastal environments with a high biomass to water volume ratio, carbonate chemistry on coral reefs, both over time and across space, is influenced by a combination of biological processes and physical characteristics of the reef, such as geomorphology and hydrodynamics (Anthony et al., 2011; Zhang et al., 2012; Falter et al., 2013; Lowe and Falter, 2015). Biologically driven changes in carbonate chemistry are a result of the net photosynthesis, respiration, calcification, and dissolution processes occurring on or within the reef benthos (Anthony et al., 2011; Kleypas et al., 2011) and in the water column (Long et al., 2019). Changes in the relative dominance of the organic carbon cycle (photosynthesis and respiration) and the inorganic carbon cycle ($CaCO_3$ precipitation and dissolution) can be observed by measuring or calculating dissolved inorganic carbon (DIC), which represents the total concentration of inorganic carbon species in seawater, and total

alkalinity (TA), the buffering capacity of seawater or charge balance (Zeebe and Wolf-Gladrow, 2001), where:

$$DIC = [CO_2] + [HCO_3^-] + [CO_3^{2-}] \quad \text{(Equation 2)}$$

and

$$TA = [HCO_3^-] + 2[CO_3^{2-}] + [B(OH)_4^-] + [OH^-] - [H^+] \quad \text{(Equation 3)}$$

$$\pm \text{ other minor constituents}$$

Net photosynthesis removes DIC from seawater and increases pH, whereas net respiration adds DIC to seawater and reduces pH. Calcification removes TA and DIC from seawater in a 2:1 ratio, slightly increasing pH, whereas dissolution adds TA and DIC in the same ratio and slightly increases pH (Figure 1.1). When plotted together, we would expect a slope of ~ 1 in a system where the organic and inorganic carbon cycles are closely balanced. If the slope is closer to 0, then the system is dominated by organic carbon cycling (photosynthesis and respiration), whereas a slope closer to 2 would suggest a dominance of the inorganic carbon cycle ($CaCO_3$ precipitation and dissolution, assuming no other processes are significantly influencing TA) (e.g., Cyronak et al., 2018; Figure 1.1).

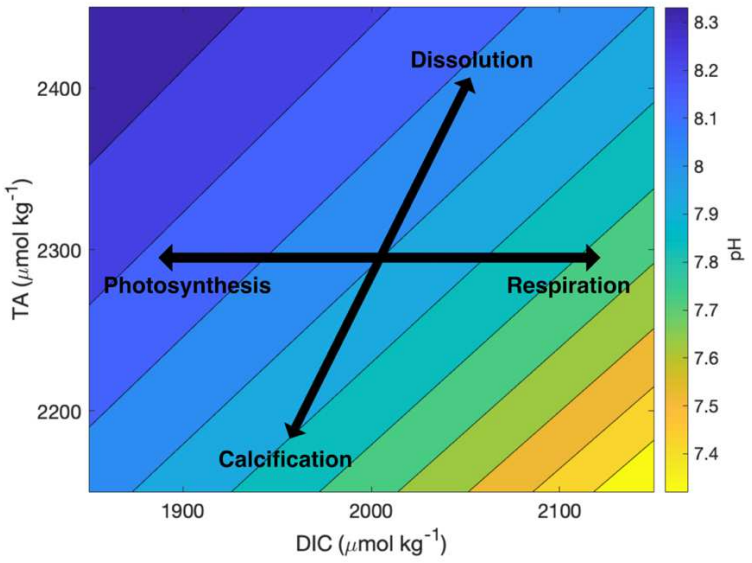

Figure 1.1: Effects of the organic and inorganic carbon cycle processes on TA, DIC, and pH (color bar) (assuming a constant salinity of 35 PSU and temperature of 25 ºC).

Physical characteristics of reefs, such as water residence times and current dynamics can also significantly contribute to observed gradients and variability in seawater carbonate chemistry (Falter et al., 2013; Lowe and Falter, 2015). Reefs with longer residence times and slower flow rates allow the benthos to modify the overlying seawater to a greater extent compared to reefs with short residence times and fast flow rates (Falter et al., 2013). Similarly, the depth of a reef can be a strong predictor of reef temperature and pH variability (Cyronak et al., 2020). Considering how all of these biological and physical factors contribute to observed gradients and variability on reefs is necessary for establishing baseline conditions and improving our ability to predict how observed variability will change when one or more of these factors changes. Combined with biological and physiological experiments, this greater understanding of controls on the seawater carbonate chemistry system on a reef will help us project how corals will be impacted by ocean acidification and other environmental stressors in the future.

In addition to OA, coral reefs are also facing the potential consequences of low oxygen conditions resulting from ocean deoxygenation and hypoxic events. As a result of climate change and coastal nutrient input, hypoxic events are predicted to become more common across the globe (Stramma et al. 2010; Altieri and Gedan 2015; Breitburg et al., 2018). Despite a substantial literature on hypoxic events in temperate zones (Diaz and Rosenberg 2008; Howarth et al. 2011), only recently has the occurrence of hypoxia on coral reefs become a more active area of research (Altieri et al. 2017; Nelson and Altieri 2019; Johnson et al., 2021). Coral reefs have traditionally been assumed to be well-oxygenated systems, however, few studies or even monitoring programs include dissolved oxygen (DO) data in their measurements or analyses and hypoxia research has historically been biased toward temperate areas (Altieri et al., 2017). Thus, it is likely that hypoxic events on coral reefs have actually been historically under-reported, (Altieri

et al., 2017). Recent observations have demonstrated that tropical coral reefs can experience severe hypoxic events and these can lead to mass mortality of reef organisms and bleaching and mortality of the corals (Altieri et al., 2017; Johnson et al., 2018, 2021; Kealoha et al., 2019).

In order to understand the potential implications of ocean deoxygenation and increasing frequency of hypoxic events for coral reefs, it is important to characterize the baseline dissolved oxygen conditions that reefs experience. Much like the carbonate chemistry, oxygen fluxes on coral reefs are driven by a combination of biological metabolic processes, environmental conditions, and physical characteristics of the reef (for a review, see Nelson and Altieri, 2019). Photosynthesis by algae, coral symbionts, and water column primary producers during the day significantly elevate DO on a reef, however, respiration by these organisms as well as the other reef inhabitants at night can significantly reduce DO concentrations (Niggl et al., 2010; Wild et al., 2010). In addition, environmental changes such as nutrient loading, warming, and seasonal stratification can cause increases in biological oxygen demand and thus decreases in DO concentration (Nelson and Altieri, 2019). Similarly, physical characteristics of the reef such as shallow reef depth, long water residence times, and slow currents can prevent re-oxygenation of the seawater from the atmosphere or open ocean and enhance the effects of local biological processes on the overlying water (Nelson and Altieri, 2019).

Notably, the likelihood that corals will experience both acidic and hypoxic conditions may be particularly heightened in areas with high primary producer biomass, such as seagrass beds, mangroves, or near seaweed farms (e.g., Challener et al., 2016; Camp et al., 2017, 2019). While photosynthesis by primary producers during the day can significantly elevate pH and DO concentrations, respiration by primary producers and other organisms at night can lead to extremely low pH and DO levels (to or past the point of hypoxia) (e.g., Challener et al., 2016;

Camp et al., 2017, 2019). The extent to which the benefits of high pH and DO during the day outweigh the costs of low pH and DO at night for corals growing in these conditions is not known. Thus, identifying and studying corals naturally occurring in such systems can be useful for in situ experiments of the effects of both low oxygen and pH on coral growth.

The broad goal of this dissertation research was to characterize the variability of carbonate chemistry and DO on coral reefs. In addition, I also quantify the impacts of this variability on coral growth and calcification in a naturally variable environment. The following chapters employ a variety of field and laboratory techniques including autonomous sensor deployments, spatial water surveys, and coral skeletal growth and isotope analyses to address specific questions within these general objectives.

In **Chapter 2**, I characterize the multidimensional variability in carbonate chemistry and DO across Hog Reef, Bermuda: laterally across the surface, vertically with depth, and over time, using a combination of discrete seawater sampling and autonomous instrumentation. Using these tools, I assess the drivers of the observed variability and test the assumption of well-mixed conditions on the reef.

In **Chapter 3**, I leverage autonomous sensor data from 32 deployments on reef sites at 12 locations around the globe to establish baseline DO conditions on each reef and quantify the current hypoxia exposure under present-day conditions. Using location-specific model predictions of sea surface temperature rise by 2100, I calculate the projected effect of 5 warming scenarios, including an acute heatwave scenario, on the oxygen solubility and the biological oxygen demand for each site to understand how hypoxic event intensity, duration, and severity will change under warming.

In **Chapter 4**, I characterize the variability of water chemistry and DO across a seagrass bed over both time and space. Using massive *Porites* coral cores, I compare the calcification rates, density, growth rates, and skeletal stable isotopic compositions of corals residing along a natural gradient of seawater chemistry and DO across the seagrass bed to determine if differences in exposure to naturally variable pH and DO affect coral growth.

Chapter 5 is the conclusion to the dissertation, where key findings from the previous chapters are discussed.

REFERENCES

Altieri, A. H., and Gedan, K. B. (2015). Climate change and dead zones. *Global Change Biology* 21, 1395–1406. doi: 10.1111/gcb.12754.

Altieri, A. H., Harrison, S. B., Seemann, J., Collin, R., Diaz, R. J., and Knowlton, N. (2017). Tropical dead zones and mass mortalities on coral reefs. *Proceedings of the National Academy of Sciences* 114, 3660–3665. doi: 10.1073/pnas.1621517114.

Andersson, A., and Gledhill, D. (2012). Ocean acidification and coral reefs: Effects on breakdown, dissolution, and net ecosystem calcification. *Annual Review of Marine Science* 5. doi: 10.1146/annurev-marine-121211-172241.

Anthony, K. R. N., A. Kleypas, J., and Gattuso, J.-P. (2011). Coral reefs modify their seawater carbon chemistry - implications for impacts of ocean acidification. *Global Change Biology* 17, 3655–3666. doi: 10.1111/j.1365-2486.2011.02510.x.

Bates, N. R. (2017). Twenty years of marine carbon cycle observations at Devils Hole Bermuda provide insights into seasonal hypoxia, coral reef calcification, and ocean acidification. *Frontiers in Marine Science* 4. doi: 10.3389/fmars.2017.00036.

Breitburg, D., Levin, L. A., Oschlies, A., Grégoire, M., Chavez, F. P., Conley, D. J., Garçon, V., Gilbert, D., Gutiérrez, D., Isensee, K., Jacinto, G. S., Limburg, K. E., Montes, I., Naqvi, S. W. A., Pitcher, G., Rabalais, N. N., Roman, M. E., Rose, K. A., Seibel, B. A., Telszewski, M., Yasuhara, M., and Zhang, J. (2018). Declining oxygen in the global ocean and coastal waters. *Science* 359, eaam7240. doi: 10.1126/science.aam7240.

Camp, E. F., Edmondson, J., Doheny, A., Rumney, J., Grima, A. J., Huete, A., and Suggett, D. J. (2019). Mangrove lagoons of the Great Barrier Reef support coral populations persisting under extreme environmental conditions. *Marine Ecological Progress Series.* 625, 1–14. doi: 10.3354/meps13073.

Camp, E. F., Nitschke, M. R., Rodolfo-Metalpa, R., Houlbreque, F., Gardner, S. G., Smith, D. J., Zampighi, M., Suggett, D. J. (2017). Reef-building corals thrive within hot-acidified and deoxygenated waters. *Scientific Reports* 7, 2434. doi: 10.1038/s41598-017-02383-y.

Challener, R. C., Robbins, L. L., and McClintock, J. B. (2016). Variability of the carbonate chemistry in a shallow, seagrass-dominated ecosystem: implications for ocean acidification experiments. *Marine Freshwater Research* 67, 163. doi: 10.1071/MF14219.

Copper, P. (1994). Ancient reef ecosystem expansion and collapse. *Coral Reefs* 13, 3–11.

Costanza, R., and Folke, C. (1997). "Valuing ecosystem services with efficiency, fairness and sustainability as goals," in *Nature's Services: Societal Dependence on Natural Ecosystems*, ed. G. C. Daily (Washington, D.C.: Island Press), 49–70.

Cyronak, T., Andersson, A. J., Langdon, C., Albright, R., Bates, N. R., Caldeira, K., Carlton, R., Corredor, J. E., Dunbar, R. B., Enochs, I., Erez, J., Eyre, B. D., Gattuso, J.-P., Gledhill, D.,

Kayanne, H., Kline, D. I., Koweek, D. A., Lantz, C., Lazar, B., Manzello, D., McMahon, A., Meléndez, M., Page, H. N., Santos, I. R., Schulz, K. G., Shaw, E., Silverman, J., Suzuki, A., Teneva, L., Watanabe, A., and Yamamoto, S. (2018). Taking the metabolic pulse of the world's coral reefs. *PLoS ONE* 13, e0190872. doi: 10.1371/journal.pone.0190872.

Cyronak, T., Takeshita, Y., Courtney, T. A., DeCarlo, E. H., Eyre, B. D., Kline, D. I., Martz, T., Page, H., Price, N. N., Smith, J., Stoltenberg, L., Tresguerres, M., and Andersson, A. J. (2020). Diel temperature and pH variability scale with depth across diverse coral reef habitats. *Limnology and Oceanography Letters* 5, 193–203. doi: 10.1002/lol2.10129.

De'ath, G., Fabricius, K. E., Sweatman, H., and Puotinen, M. (2012). The 27-year decline of coral cover on the Great Barrier Reef and its causes. *Proceedings of the National Academy of Sciences* 109, 17995–17999. doi: 10.1073/pnas.1208909109.

Diaz, R. J., and Rosenberg, R. (2008). Spreading dead zones and consequences for marine ecosystems. *Science* 321, 926–929. doi: 10.1126/science.1156401.

Doney, S. C., Fabry, V. J., Feely, R. A., and Kleypas, J. A. (2009). Ocean acidification: The other CO_2 problem. *Annual Review of Marine Science* 1, 169–192. doi: 10.1146/annurev.marine.010908.163834.

Falter, J. L., Lowe, R. J., Zhang, Z., and McCulloch, M. (2013). Physical and biological controls on the carbonate chemistry of coral reef waters: Effects of metabolism, wave forcing, sea level, and geomorphology. *PLoS ONE* 8, e53303. doi: 10.1371/journal.pone.0053303.

Fisher, R., O'Leary, R., Low-Choy, S., Mengersen, K., Knowlton, N., Brainard, R., and Caley, M. J. (2015). Species richness on coral reefs and the pursuit of convergent global estimates. *Current Biology* 25, 500–505.

Garcia-Soto, C., Cheng, L., Caesar, L., Schmidtko, S., Jewett, E. B., Cheripka, A., Rigor, I., Caballero, A., Chiba, S., Báez, J. C., Zielinski, T., and Abraham, J. P. (2021). An overview of ocean climate change indicators: Sea surface temperature, ocean heat content, ocean ph, dissolved oxygen concentration, Arctic sea ice extent, thickness and volume, sea level and strength of the AMOC (Atlantic Meridional Overturning Circulation). *Frontiers in Marine Science*. doi: 10.3389/fmars.2021.642372.

Gardner, T. A., Côté, I. M., Gill, J. A., Grant, A., and Watkinson, A. R. (2003). Long-term region-wide declines in Caribbean Corals. *Science* 301, 958–960. doi: 10.1126/science.1086050.

Hoegh-Guldberg, O., Mumby, P. J., Hooten, A. J., Steneck, R. S., Greenfield, P., Gomez, E., Harvell, C. D., Sale, P. F., Edwards, A. J., Caldeira, K., Knowlton, N., Eakin, C. M., Iglesias-Prieto, R., Muthiga, N., Bradbury, R. H., Dubi, A., and Hatziolos, M. E. (2007). Coral reefs under rapid climate change and ocean acidification. *Science* 318, 1737–1742. doi: 10.1126/science.1152509.

Howarth, R., Chan, F., Conley, D. J., Garnier, J., Doney, S. C., Marino, R., and Billen, G. (2011). Coupled biogeochemical cycles: eutrophication and hypoxia in temperate estuaries and coastal marine ecosystems. *Frontiers in Ecology and the Environment* 9, 18–26. doi: 10.1890/100008.

Johnson, M. D., Rodriguez, L. M., and Altieri, A. H. (2018). Shallow-water hypoxia and mass mortality on a Caribbean coral reef. *Bulletin of Marine Science* 94, 143–144. doi: 10.5343/bms.2017.1163.

Johnson, M. D., Swaminathan, S. D., Nixon, E. N., Paul, V. J., and Altieri, A. H. (2021). Differential susceptibility of reef-building corals to deoxygenation reveals remarkable hypoxia tolerance. *Scientific Reports* 11, 23168. doi: 10.1038/s41598-021-01078-9.

Kealoha, A. K., Doyle, S. M., Shamberger, K. E. F., Sylvan, J. B., Hetland, R. D., and DiMarco, S. F. (2020). Localized hypoxia may have caused coral reef mortality at the Flower Garden Banks. *Coral Reefs* 39, 119–132. doi: 10.1007/s00338-019-01883-9.

Kleypas, J. A., Anthony, K. R. N., and Gattuso, J.-P. (2011). Coral reefs modify their seawater carbon chemistry – case study from a barrier reef (Moorea, French Polynesia). *Global Change Biology* 17, 3667–3678. doi: 10.1111/j.1365-2486.2011.02530.x.

Kleypas, J. A., and Yates, K. K. (2009). Coral reefs and ocean acidification. *Oceanography* 22, 108–117.

Kwiatkowski, L., Torres, O., Bopp, L., Aumont, O., Chamberlain, M., Christian, J. R., Dunne, J. P., Gehlen, M., Ilyina, T., John, J. G., Lenton, A., Li, H., Lovenduski, N. S., Orr, J. C., Palmieri, J., Santana-Falcón, Y., Schwinger, J., Séférian, R., Stock, C. A., Tagliabue, A., Takano, Y., Tjiputra, J., Toyama, K., Tsujino, H., Watanabe, M., Yamamoto, A., Yool, A., and Ziehn, T.(2020). Twenty-first century ocean warming, acidification, deoxygenation, and upper-ocean nutrient and primary production decline from CMIP6 model projections. *Biogeosciences* 17, 3439–3470. doi: 10.5194/bg-17-3439-2020.

Long, M. H., Rheuban, J. E., McCorkle, D. C., Burdige, D. J., and Zimmerman, R. C. (2019). Closing the oxygen mass balance in shallow coastal ecosystems. *Limnology and Oceanography* 64, 2694–2708. doi: 10.1002/lno.11248.

Lowe, R. J., and Falter, J. L. (2015). Oceanic forcing of coral reefs. *Annual Review of Marine Science* 7, 43–66. doi: 10.1146/annurev-marine-010814-015834.

Midorikawa, T., Inoue, H. Y., Ishii, M., Sasano, D., Kosugi, N., Hashida, G., Nakaoka, S.-I., and Suzuki, T. (2012). Decreasing pH trend estimated from 35-year time series of carbonate parameters in the Pacific sector of the Southern Ocean in summer. *Deep Sea Research Part I: Oceanographic Research Papers* 61, 131–139. doi: 10.1016/j.dsr.2011.12.003.

Moberg, F., and Folke, C. (1999). Ecological goods and services of coral reef ecosystems. *Ecological Economics* 29, 215–233.

Nelson, H. R., and Altieri, A. H. (2019). Oxygen: The universal currency on coral reefs. *Coral Reefs* 38, 177–198. doi: 10.1007/s00338-019-01765-0.

Niggl, W., Haas, A. F., and Wild, C. (2010). Benthic community composition affects O_2 availability and variability in a Northern Red Sea fringing reef. *Hydrobiologia* 644, 401–405. doi: 10.1007/s10750-010-0200-4.

Pandolfi, J. M., Jackson, J. B. C., Baron, N., Bradbury, R. H., Guzman, H. M., Hughes, T. P., Kappel, C. V., Micheli, F., Ogden, J. C., Possingham, H. P., and Sala, E. (2005). Are U.S. coral reefs on the slippery slope to slime? *Science* 307, 1725–1726. doi: 10.1126/science.1104258.

Smith, S. (1978). Coral-reef area and the contributions of reefs to processes and resources of the world's oceans. *Nature* 273, 225–226.

Spalding, M., and Grenfell, A. (1997). New estimates of global and regional coral reef areas. *Coral Reefs* 16, 225–230.

Stramma, L., Schmidtko, S., Levin, L. A., and Johnson, G. C. (2010). Ocean oxygen minima expansions and their biological impacts. *Deep Sea Research Part I: Oceanographic Research Papers* 57, 587–595. doi: 10.1016/j.dsr.2010.01.005.

Wild, C., Niggl, W., Naumann, M. S., and Haas, A. F. (2010). Organic matter release by Red Sea coral reef organisms—Potential effects on microbial activity and in situ O_2 availability. *Marine Ecology Progress Series* 411, 61–71. doi: 10.3354/meps08653.

Wilkinson, C. ed. (2004). *Status of Coral Reefs of The World: 2004*. Townsville, Queensland, Australia: Australian Institute of Marine Science.

Zeebe, R. E., and Wolf-Gladrow, D. (2001). *CO_2 in seawater: Equilibrium, kinetics, isotopes*. Gulf Professional Publishing.

Zhang, Z., Falter, J., Lowe, R., and Ivey, G. (2012). The combined influence of hydrodynamic forcing and calcification on the spatial distribution of alkalinity in a coral reef system. *Journal of Geophysical Research* 117. doi: 10.1029/2011JC007603.

CHAPTER 2: Lateral, Vertical, and Temporal Variability of Seawater Carbonate Chemistry at Hog Reef, Bermuda

Ariel K. Pezner, Travis A. Courtney, Heather N. Page, Sarah N. Giddings, Cory M. Beatty, Michael D. DeGrandpre, and Andreas J. Andersson

frontiers in Marine Science

ORIGINAL RESEARCH
published: 11 February 2021
doi: 10.3389/fmars.2021.562267

Lateral, Vertical, and Temporal Variability of Seawater Carbonate Chemistry at Hog Reef, Bermuda

Ariel K. Pezner[1], Travis A. Courtney[1], Heather N. Page[1,2], Sarah N. Giddings[1], Cory M. Beatty[3], Michael D. DeGrandpre[3] and Andreas J. Andersson[1]*

[1] Scripps Institution of Oceanography, University of California, San Diego, La Jolla, CA, United States, [2] Sea Education Association, Woods Hole, MA, United States, [3] Department of Chemistry and Biochemistry, University of Montana, Missoula, MT, United States

Spatial and temporal carbonate chemistry variability on coral reefs is influenced by a combination of seawater hydrodynamics, geomorphology, and biogeochemical processes, though their relative influence varies by site. It is often assumed that the water column above most reefs is well-mixed with small to no gradients outside of the benthic boundary layer. However, few studies to date have explored the processes and properties controlling these multi-dimensional gradients. Here, we investigated the lateral, vertical, and temporal variability of seawater carbonate chemistry on a Bermudan rim reef using a combination of spatial seawater chemistry surveys and autonomous *in situ* sensors. Instruments were deployed at Hog Reef measuring current flow, seawater temperature, salinity, pH_T, pCO_2, dissolved oxygen (DO), and total alkalinity (TA) on the benthos, and temperature, salinity, DO, and pCO_2 at the surface. Water samples from spatial surveys were collected from surface and bottom depths at 13 stations covering ~3 km^2 across 4 days. High frequency temporal variability in carbonate chemistry was driven by a combination of diel light and mixed semi-diurnal tidal cycles on the reef. Daytime gradients in DO between the surface and the benthos suggested significant water column production contributing to distinct diel trends in pH_T, pCO_2, and DO, but not TA. We hypothesize these differences reflect the differential effect of biogeochemical processes important in both the water column and benthos (organic carbon production/respiration) vs. processes mainly occurring on the benthos (calcium carbonate production/dissolution). Locally at Hog Reef, the relative magnitude of the diel variability of organic carbon production/respiration was 1.4–4.6 times larger than that of calcium carbonate production/dissolution, though estimates of net organic carbon production and calcification based on inshore-offshore chemical gradients revealed net heterotrophy (−118 ± 51 mmol m^{-2} day^{-1}) and net calcification (150 ± 37 mmol $CaCO_3$ m^{-2} day^{-1}). These results reflect the important roles of time and space in assessing reef biogeochemical processes. The spatial variability in carbonate chemistry parameters was larger laterally than vertically and was generally observed in conjunction with depth gradients, but varied between sampling events, depending on time of day and modifications due to current flow.

Keywords: carbonate chemistry, ocean acidification, calcification, coral reef, Hog Reef, Bermuda, reef metabolism

OPEN ACCESS

Edited by:
Hajime Kayanne, The University of Tokyo, Japan

Reviewed by:
Daniel Aagren Nielsen, University of Technology Sydney, Australia
Atsushi Watanabe, Ocean Policy Research Institute, Japan

****Correspondence:***
Ariel K. Pezner
apezner@ucsd.edu

Specialty section:
This article was submitted to Coral Reef Research, a section of the journal Frontiers in Marine Science

Received: *14 May 2020*
Accepted: *11 January 2021*
Published: *11 February 2021*

Citation:
Pezner AK, Courtney TA, Page HN, Giddings SN, Beatty CM, DeGrandpre MD and Andersson AJ (2021) Lateral, Vertical, and Temporal Variability of Seawater Carbonate Chemistry at Hog Reef, Bermuda. Front. Mar. Sci. 8:562267. doi: 10.3389/fmars.2021.562267

INTRODUCTION

Coral reefs are some of the most ecologically diverse and economically valuable ecosystems in the world, providing ecosystem services such as coastline protection, fisheries provisioning, tourism revenue, nutrient cycling, and habitat creation that amount to billions of dollars annually (e.g., Spurgeon, 1992; Moberg and Folke, 1999; Brander et al., 2007; Costanza et al., 2014). However, anthropogenic stressors on local and global scales, including temperature rise (e.g., Hughes et al., 2003), overfishing (e.g., Jackson et al., 2001), hypoxia (Nelson and Altieri, 2019), and ocean acidification (e.g., Hoegh-Guldberg et al., 2007) are threatening reef function around the world. Coral reefs may be particularly susceptible to the effects of ocean acidification due to the large presence of marine calcifiers whose calcium carbonate ($CaCO_3$) structures serve as the reef foundation (Kleypas et al., 1999; Hoegh-Guldberg et al., 2007; Kleypas and Yates, 2009). Increasingly acidified conditions resulting from changes in seawater carbonate chemistry are predicted to drive declines in calcification by organisms such as corals (e.g., Langdon et al., 2000; for a metanalysis see Chan and Connolly, 2013) and increases in bioerosion and $CaCO_3$ dissolution rates (e.g., Andersson and Gledhill, 2013; Schönberg et al., 2017) which could result in many reefs potentially shifting to net dissolving instead of net calcifying by the end of the century (Hoegh-Guldberg et al., 2007; Silverman et al., 2009; Eyre et al., 2018).

An individual reef's response to acidified conditions, however, may be strongly dependent on the biogeochemistry of the particular system (Andersson et al., 2014). Locally, carbonate chemistry is in part controlled by the metabolic processes occurring on the benthos such as calcification, $CaCO_3$ dissolution, primary production, and respiration (Anthony et al., 2011; Kleypas et al., 2011). The net sum of total calcification and $CaCO_3$ dissolution is referred to as Net Community Calcification (NCC); whereas, the net sum of primary production and total respiration is referred to as Net Community Production (NCP). Changes in NCC affect the balance of both total alkalinity (TA) and dissolved inorganic carbon (DIC) in a ratio of 2:1, whereas changes in NCP in reef environments mainly affect DIC (Zeebe and Wolf-Gladrow, 2001; Andersson and Gledhill, 2013). Consequently, positive NCC results in a decrease in seawater pH while positive NCP results in an increase in pH, and vice versa for negative NCC and NCP, respectively (Zeebe and Wolf-Gladrow, 2001). Concurrent with these metabolic processes, physical factors such as the reef geomorphology, hydrodynamics, and residence time also influence local variability in carbonate chemistry, as these physical properties control the flow trajectory and contact time between seawater and the benthos (Anthony et al., 2011; Zhang et al., 2012; Falter et al., 2013; Lowe and Falter, 2015; Page et al., 2018). It has been hypothesized that these metabolic and physical processes together may modulate local seawater chemistry to the extent they can either alleviate or exacerbate acidification over reefs compared to the open ocean (Bates et al., 2010; Anthony et al., 2011, 2013; Andersson et al., 2014; Cyronak et al., 2014). However, how these biological and physical drivers interact and contribute to local seawater carbonate chemistry variability in different coral reef habitats and across vertical, lateral, and temporal scales has not been fully characterized (Page et al., 2018; Takeshita et al., 2018).

Many previous studies have demonstrated carbonate chemistry variability as a function of time at the surface or at the bottom in numerous coral reef locations (e.g., Gray et al., 2012; Sutton et al., 2014; DeCarlo et al., 2017) with fewer studies characterizing the spatial and lateral variability across different habitats (Suzuki and Kawahata, 2003; Watanabe et al., 2006; Andersson et al., 2014). In terms of vertical variability, most studies assume that the water column above a shallow reef is well-mixed with small to no gradients above the benthic boundary layer (e.g., Falter et al., 2013; Page et al., 2018). However, given that flow regime, residence time, and benthic productivity have the potential to form strong gradients in water chemistry from upstream to downstream (Anthony et al., 2011; Takeshita et al., 2018), there may also be gradients between surface and bottom that are not often quantified (Watanabe et al., 2006; Andersson et al., 2007). Spatial gradients in any direction also change through time, on hourly to seasonal (e.g., Gagliano et al., 2010; Gray et al., 2012; Guadayol et al., 2014) and annual to decadal time scales (e.g., Pelejero et al., 2005; Wei et al., 2015). This variability has been characterized in Bermuda over shorter timescales (days) (e.g., Takeshita et al., 2018) and longer timescales (seasons to years) (e.g., Bates et al., 2010; Andersson et al., 2014; Yeakel et al., 2015; Bates, 2017). However, there is a scarcity of studies examining vertical, lateral, and temporal variations in reef carbonate chemistry simultaneously.

Compared to low latitude, tropical coral reefs, the high latitude reefs in Bermuda experience significant seasonal and inter-annual variations in seawater chemistry as a result of variations in seawater temperature and local reef metabolism (Andersson et al., 2014; Courtney et al., 2017), as well as larger scale ocean processes linked to the North Atlantic Oscillation (NAO) (Yeakel et al., 2015). In addition, this ocean region has been identified as an area with one of the fastest changing chemical environments under ocean acidification (Andersson et al., 2019). Furthermore, it has been suggested that the coral community structure of Bermuda, which is made up of coral taxa with relatively stress-tolerant life histories, may represent one potential stable state of coral reefs in a future high CO_2 world (Courtney et al., 2017), making it an important area to study. Here, the main objective was to compare the spatial variability of seawater chemistry laterally across a reef, at surface and at depth, and through time, in order to capture variability in four dimensions. We also estimated the relative contributions of biogeochemical processes to variability in DIC and TA locally and relative to the open ocean end-member during the study period. Understanding the variability of local seawater chemistry, both spatially and temporally, as well as the drivers of this variability, will be important for predicting the scope and magnitude of ocean acidification impacts on coral reefs.

MATERIALS AND METHODS

Study Site

The study was conducted at Hog Reef (32.457°N, 64.835°W), a rim-reef on the northern edge of the Bermuda carbonate platform (**Figure 1**). Depth varies across Hog Reef, ranging from ∼4 to 25 m with a mean (± 1 SD) of 10.3 ± 3.3 m, generally increasing offshore but with high structural complexity and variability (Courtney et al., 2016; Takeshita et al., 2018; **Figures 1**, **2**). Mean (± 1 SD) benthic cover at Hog Reef has been previously described as 35 ± 3% macroalgae, 27 ± 5% hard coral, 20 ± 4% turf algae, 16 ± 2% soft coral, and < 5% sand, rock, rubble, and coralline algae (Marine Environmental Program, 2007; Courtney et al., 2016). Residence time of the water on this rim reef has been estimated to be about 1–4 days using various tracer methods (Morris et al., 1977; Venti et al., 2012). Tides in this area can be characterized as mixed semi-diurnal, with a mean tidal range of 0.90 ± 0.11 m. Tide information (mean sea level, MSL; m) data were accessed from the NOAA Tides and Currents Database for the nearest tide station (St. Georges Island, Bermuda Station[1]). Bathymetry data was accessed from Sutherland et al. (2014) and the satellite image of Hog Reef is courtesy of the Digital Globe Foundation.

Autonomous Sensors

In order to capture high frequency variability and diel cycles on the reef, a suite of autonomous sensors was deployed at Hog Reef (**Figure 1d** and **Table 1**). To characterize water flow, an Aquadopp acoustic doppler current profiler (ADCP, 1 MHz; Nortek) was deployed at the bottom (∼7 m water depth) from September 1–7, 2017. The Aquadopp measured current speeds and directions in 0.5 m depth bins from 0.4 m above the profiler to 5.4 m above the profiler. However, due to interference in the first two cells by nearby biota and reef structures, only cells from 1.4 to 5.4 m above the profiler were analyzed. Averages of 1 Hz data over 1 min were stored at 10 min intervals.

Seawater pH_T (defined on the total H^+ scale), pCO_2, and TA were measured with a suite of instruments from Sunburst Sensors between September 1–22, 2017, including a Submersible Autonomous Moored Instrument for pH (SAMI-pH), two SAMI-CO_2 that also recorded temperature and dissolved O_2 with Aanderaa 4531 Oxygen Optodes, a CTD (Microcat, Sea-Bird Scientific), and the recently developed SAMI for Alkalinity (SAMI-alk), which is one of the first *in situ* instruments for autonomous measurements of total alkalinity (Spaulding et al., 2014). SAMI-pH accuracy and precision are ± 0.005 and ± 0.001, respectively, based on repeat analyses of tris buffer. SAMI-CO_2 accuracy and precision are ± 5 and ± 1 μatm, respectively, based on comparisons with an infrared CO_2 analyzer. The Aanderaa Oxygen Optode accuracy is reported as < 1 μM. Accuracy for the CTD temperature and conductivity is ± 0.002°C and ± 0.0003 S m^{-1}, respectively. Spaulding et al. (2014) found an accuracy and precision for SAMI-alk of −2 ± 13 μmol kg^{-1} based on comparison with discrete samples collected during a deployment. All instruments collected measurements every 15 minutes, except the SAMI-alk which collected measurements every 2 h (with one measurement omitted per day due to *in situ* calibrations at varying times, i.e., 11 measurements per day). Initial offsets of sensor data were corrected based on water samples collected at the time of deployment and no other offsets were applied. Initial SAMI-CO_2 calibrations are referenced to an infrared method calibrated with NOAA certified gases. See **Table 1** for a summary of the deployment specifics.

In addition to the Sunburst Sensors instruments, time series data for air and seawater pCO_2 were obtained from a NOAA PMEL MAPCO2 buoy moored on Hog Reef (32.457°N, 64.835°W). The MAPCO2 buoy measures the mole fraction of CO_2 (xCO_2) in seawater and air equilibrated with seawater every 3 h using a LI-COR LI-820 CO_2 infrared gas analyzer calibrated with a reference gas that meets World Meteorological Organization standards (Sutton et al., 2014, 2019). Accuracy and precision of these xCO_2 measurements are estimated to be < ± 2 and < ± 0.7 μmol mol^{-1}, respectively (Sutton et al., 2014). The buoy is also equipped with a Sensirion SHT71 sensor to measure relative humidity and temperature (Sutton et al., 2014). Sea surface temperature and salinity were also continuously recorded by a Sea-Bird Electronics 16 plus V2, with accuracies of ± 0.005°C and ± 0.0005 S/m for temperature and conductivity, respectively. Air and seawater pCO_2 were calculated from these parameters using equations from Zeebe and Wolf-Gladrow (2001), with uncertainty estimated to be < 2.0 μatm (Sutton et al., 2014).

Spatial Surveys of Carbonate Chemistry

Autonomous moored sensor measurements were coupled with discrete water samples collected at 13 stations covering an area of ∼3 km^2 on Hog Reef (**Figure 1**). A total of 4 spatial surveys were completed via boat, each over a span of ∼2 h, with afternoon surveys (∼13:00–15:00) on September 1 and September 4 and morning surveys (∼10:00–12:00) on September 4 and September 7. Spatial surveys consisted of three overlapping transects, with the PMEL MAPCO2 buoy as a common center point, and spanned the width of the rim reef (**Figures 1b,c**). Using a 5 liter Niskin bottle, water samples were collected at the surface (0.5–1.0 m) and bottom (4–20 m depending on the station's local water depth) at all stations, with one intermediate sample collected at the deepest stations (**Figure 1d**). *In situ* temperature and salinity were measured with a YSI 556 Handheld Multiparameter Instrument (accuracy: temperature ± 0.15°C, salinity ± 1%). Water samples for DIC and TA (N = 114) were collected according to best practices in 250 ml Pyrex glass sample bottles and immediately fixed with 100 μl of a saturated $HgCl_2$ solution (Dickson et al., 2007).

DIC was analyzed using an Automated Infra-Red Inorganic Carbon Analyzer (AIRICA, Marianda) with a Li-COR 7000 as detector. TA was analyzed via open-cell potentiometric acid titration system developed by the Dickson Lab at Scripps Institution of Oceanography (Dickson et al., 2007). Some samples (n = 29) were reanalyzed using a small volume, open-cell Metrohm Titrando automatic titrator system to validate results due to occasional occurrences of non-ideal titration curves. Accuracy (± precision) of TA and DIC measurements

[1]https://tidesandcurrents.noaa.gov/stationhome.html?id=2695540#info

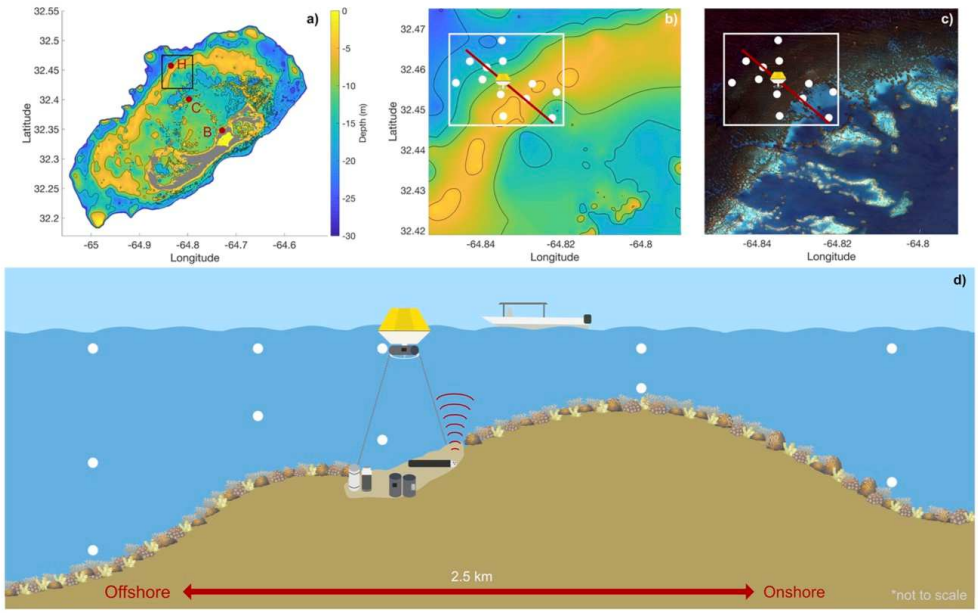

FIGURE 1 | Details of study site: **(a)** Depth contour map of the Bermuda platform, indicating Hog Reef (H), Crescent Reef (C), and Bailey's Bay (B) (letters and red circles) with a section of the rim reef including Hog Reef boxed in black **(b,c)**; **(b)** Depth contour map of Hog Reef from black box in **(a)** with spatial survey locations (white circles), buoy location, onshore-offshore reef transect (red line), and spatial survey area in white (see **Figures 5–7**); **(c)** High-resolution satellite image of Hog Reef, Bermuda processed by Dr. Tyler Cyronak under an imagery grant from the DigitalGlobe Foundation from black box in **(a)** with spatial survey locations (white circles), buoy location, onshore-offshore reef transect (red line), and spatial survey area in white (see **Figures 5–7**); **(d)** Conceptual diagram of the onshore-offshore transect and sampling scheme with the Hog Reef buoy, 6 autonomous sensors, and boat spatial survey water sampling locations (white circles) on exaggerated reef contour (not to scale). Coral icon images attributed to Tracey Saxby and Diana Kleine, Integration and Application Network, University of Maryland Center for Environmental Science (ian.umces.edu/imagelibrary/).

were calculated as the mean offsets (± SD) from Certified Reference Materials (CRM) provided by the Dickson Lab and were 1.3 ± 3.5 μmol kg^{-1} (n = 57) for DIC, −0.46 ± 1.5 μmol kg^{-1} (n = 24) for the Dickson TA system, and 1.76 ± 3.0 μmol kg^{-1} (n = 21) for the Metrohm TA system. CO2SYS for Excel (Lewis and Wallace, 1998) and MATLAB (van Heuven et al., 2011), were used to calculate additional carbonate chemistry parameters using the first and second dissociation constants of carbonic acid (K_1 and K_2) from Mehrbach et al. (1973) refit by Dickson and Millero (1987), the dissociation constants of bisulfate (K_{HSO4}) from Dickson (1990) and total boron by Uppström (1974), and total scale pH (pH_T).

Data Analysis and Calculations

Current Data

Current profiler data was collected in earth coordinates and corrected for the magnetic declination of the earth at the deployment site to account for differences between magnetic and true north. The magnetic declination at Hog Reef (32.457°N 64.835°W) on 1 September 2017 was 14.74°W ± 0.33° of true north[2]. All data are reported in compass coordinates where 0° is north and 90° is east. A principal component analysis was then performed on the corrected, depth-averaged u (east) and v (north) current velocities for both the entire duration of the deployment, as well as for individual days using the *princax* function in MATLAB (developed by Rich Signell, United States Geological Survey). The angle of maximum variance (θ) and the major and minor axes of a principal ellipse were computed to identify the angle containing the most variance. Mean depth-averaged flow velocity was also calculated and denoted on plots with a quiver arrow emanating from the instrument deployment location, with angle and length denoting current direction and speed, respectively.

Variability and Frequency Analyses

Variability for each parameter recorded by the autonomous sensors was calculated as the mean daily range (maximum—minimum) (from 00:00 h to 23:45 h, or as close to these times as sampling frequency would allow) ± one standard deviation. Variability in measured parameters from the spatial

[2]https://www.ngdc.noaa.gov/geomag/calculators/magcalc.shtml#declination

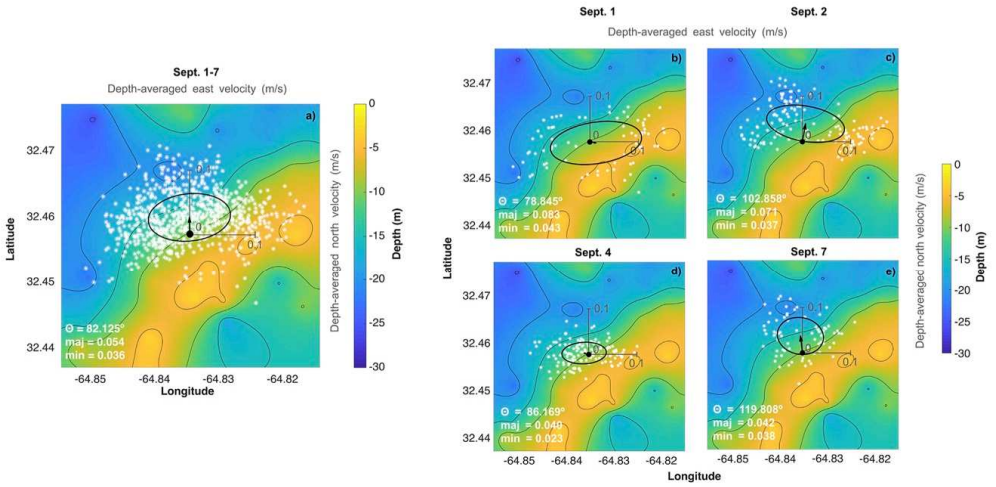

FIGURE 2 | Depth-averaged current velocity **(a)** over the entire deployment (September 1–7) and for individual days corresponding to dates of the water chemistry spatial surveys **(b)** September 1, **(c)** September 2, **(d)** September 4, and **(e)** September 7 overlaid on the bathymetry of the deployment site. White stars correspond to individual velocity measurements over that time period and the arrow beginning at the black dot corresponds to the mean velocity vector. The ellipse represents the variability (1 SD) of the velocity on that day (i.e., the velocity variability (1 SD) traces out an ellipse starting at the black dot pointing toward the ellipse—for example, over the full deployment period, the mean flow is approximately off-reef to the north but varies strongly in the east/west direction, with minimal variability southwards). The origin for the velocity plots (individual measurements, ellipse, and mean velocity vector) is at the mooring represented by the black circle on each plot and *x* and *y*-axis scales of 0.1 m/s are included in light gray.

TABLE 1 | Summary of instrument deployment configuration at Hog Reef.

Instrument	Deployment depth	Parameters measured	Sampling frequency	Deployment dates
MAPCO2 Buoy	surface	xCO_2 (air, seawater)	3 h	2010–2019
SAMI-CO_2, Aanderaa Optode	surface	pCO_2, T, DO	15 min	1–22 September
CTD	7 m	T, S	15 min	1–22 September
SAMI-pH	7 m	pH_T, T	15 min	1–22 September
SAMI-alk	7 m	TA, T	2 h	1–22 September
SAMI-CO_2	7 m	pCO_2, T, DO	15 min	1–22 September
ADCP	7 m	current speed, direction, T, P	10 min	1–7 September

Variables measured are: xCO_2, mole fraction of carbon dioxide; pCO_2, partial pressure of carbon dioxide; T, temperature; DO, dissolved oxygen; S, salinity; pH_T, total scale pH; TA, total alkalinity; current speed; current direction; and P, pressure.

surveys was calculated as the mean range of a parameter ± 1 standard deviation on one sampling date over the surface or bottom (for lateral variability) across all sampling dates. Vertical variability was calculated as the mean of the absolute differences in a parameter between surface and bottom across the survey area for one sampling date ± 1 standard deviation, across all sampling dates.

Frequency analyses were performed on all parameters measured by the autonomous sensors in order to determine the dominant frequencies of variability using the *plomb* function in MATLAB to create Lomb-Scargle periodograms (**Figure 3**; raw data are shown in **Supplementary Figure 1**). A high-pass filter (*highpass*; pass band frequency of 1 day^{-1}) was used to remove additional low frequency signals and distill the diel frequency signal in temperature at surface and bottom. A Savitzky-Golay filter (*sgolayfilt*; order 3 and frame length 7) and then a high-pass filter (*highpass*; pass band frequency of 1 day^{-1}) was used to distill the frequency signals in total alkalinity at 7 m as well as calculated relative NCC ($r_{NCC\ TA}$). These filtered total alkalinity, $r_{NCC\ TA}$, and temperature data were only used to create the Lomb-Scargle periodograms (**Figure 3**, right column) which are plotted next to the raw, unfiltered time series data (**Figure 3**, main column; for a comparison, see **Supplementary Figures 4–6**).

Biogeochemical Drivers of Variability

Instrument time series data were used to approximate the relative contribution from biogeochemical processes to the observed variability in DIC and TA at Hog Reef. A time series of DIC at 7 m was calculated from the time series of TA (from the SAMI-alk at 7 m) and pCO_2 (from the SAMI-CO_2 at 7 m)

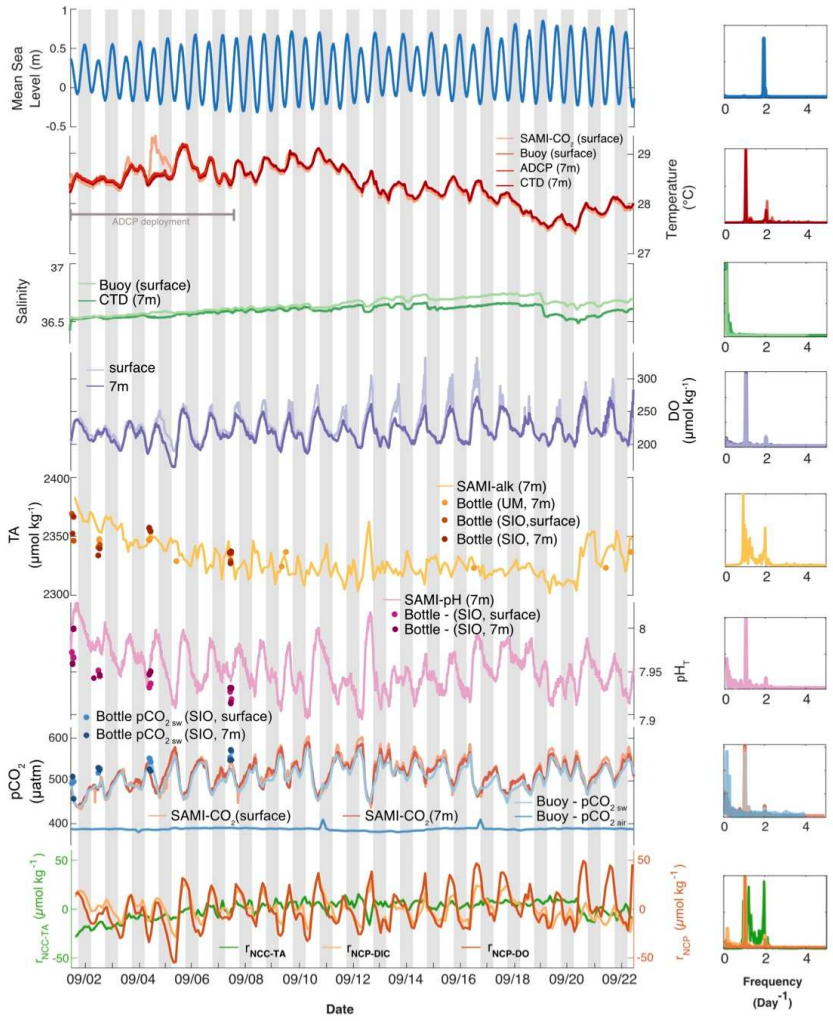

FIGURE 3 | (Left) Temporal variability in environmental conditions and seawater chemistry on Hog Reef for September 2017 at surface (lighter colors) and bottom (darker colors). Temperature, salinity, dissolved oxygen, TA, pH_T, and pCO_2 were measured with autonomous moored sensors. Measurements of bottom temperature (at 7 m depth) from multiple sensors were essentially indistinguishable, thus only one was plotted. Measured TA and calculated pH_T and pCO_2 from discrete TA and DIC seawater samples were plotted as circles ("SIO" samples were analyzed in the Andersson Lab at Scripps Institution of Oceanography and "UM" samples were analyzed in the DeGrandpre Lab at the University of Montana Missoula). Mean sea level data were accessed from the NOAA Tides and Currents Database (St. George's Island). Relative NCC and NCP (r_{NCC-TA}, r_{NCP-DO}, and $r_{NCP-DIC}$) were estimated from sensor-derived water chemistry data using a mean anomaly (as described in the text). Gray bars indicate nighttime hours. (**Right**) Lomb-Scargle periodograms of autonomous moored sensor parameters as well as calculated r_{NCC-TA}, r_{NCP-DO}, and $r_{NCP-DIC}$.

(**Supplementary Figure 3**), interpolated to a frequency of every 2 h from 1 September 2017 at 15:00 to 22 September 2017 at 11:00 in order to match the lower sampling frequency of the SAMI-alk. Note that DIC calculated from pH_T and TA also gave similar DIC values. TA, DIC, and DO were normalized (nTA, nDIC, nDO) to mean salinity from the interpolated time series (36.59 PSU).

For a well-mixed reef habitat, NCC is routinely calculated based on Eulerian measurements of TA according

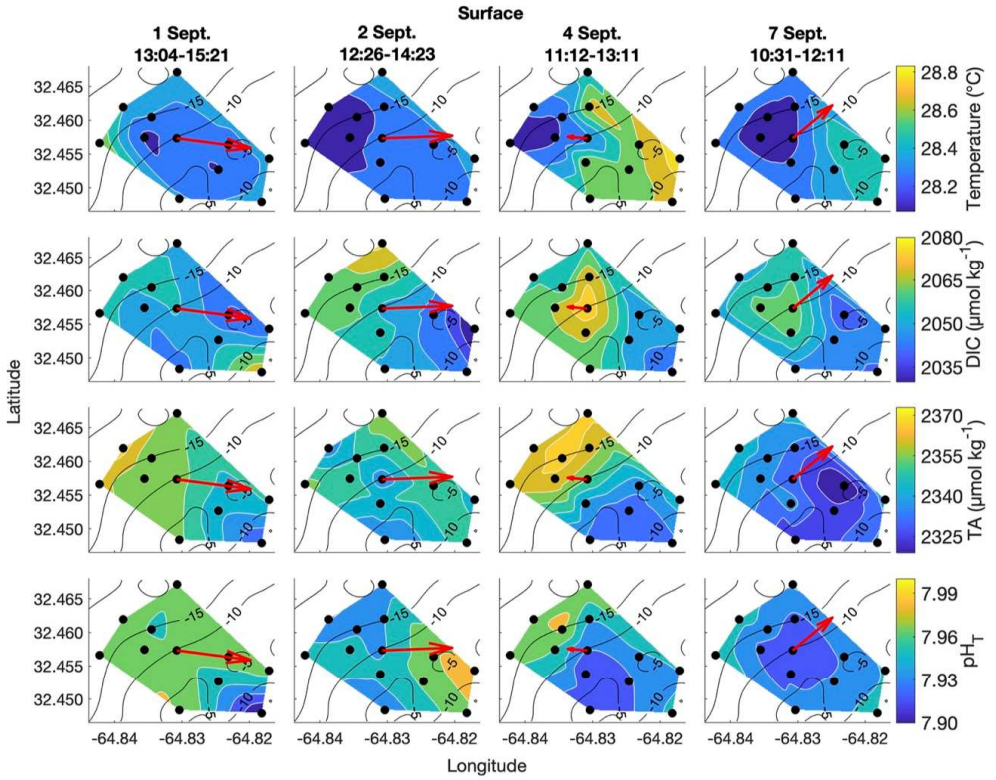

FIGURE 4 | Lateral spatiotemporal variability at the surface in temperature, DIC, TA, and pH_T (calculated from measured DIC and TA) on September 1, 2, 4, and 7. Plots also contain bathymetry contours (black) and the mean depth-averaged velocity vector averaged over the sampling period (red).

to (e.g., Silverman et al., 2007; Langdon et al., 2010; Koweek et al., 2015a):

$$NCC_{\mathrm{TA}} = -\frac{1}{2}\Delta nTA\frac{\rho h}{\tau} = -\frac{1}{2}(nTA_{reef} - nTA_{offshore})\frac{\rho h}{\tau} \quad (1)$$

where ΔnTA refers to the difference between nTA on the reef and offshore, τ is the mean residence time, ρ is the seawater density, and h is the mean height of the water column. Furthermore, NCP can be calculated based on measurements of DIC and TA or DO with corrections for gas exchange:

$$\begin{aligned} NCP_{\mathrm{DIC}} &= -\left(\Delta nDIC - \frac{1}{2}\Delta nTA\right)\frac{\rho h}{\tau} + F_{CO_2,gas} \\ &= \left[-\left(nDIC_{reef} - nDIC_{offshore}\right)\right. \\ &\quad \left.-\left(-\frac{1}{2}\left(nTA_{reef} - nTA_{offshore}\right)\right)\right]\frac{\rho h}{\tau} + F_{CO_2,gas} \quad (2) \end{aligned}$$

$$\begin{aligned} NCP_{\mathrm{DO}} &= \Delta nDO\frac{\rho h}{\tau} + F_{O_2,gas} \\ &= \left(nDO_{reef} - nDO_{offshore}\right) + F_{O_2,gas} \quad (3) \end{aligned}$$

where ΔnDIC and ΔnDO refer to the differences between the reef and offshore, and $F_{CO2,gas}$ and $F_{O2,gas}$ represent sea-air CO_2 and O_2 gas exchange, respectively. Relative to biogeochemical processes on coral reefs with relatively short residence times (hours to days), sea-air CO_2 gas exchange is often small and therefore assumed to be negligible while O_2 flux is more strongly affected (e.g., Yeakel et al., 2015).

Here, we used two different approaches to assess the biogeochemical processes underlying the observed chemical condition and variability at Hog Reef. In one approach, NCC and NCP were calculated according to Eqs 1 and 2 relative to the offshore values of TA and DIC measured at the Bermuda Atlantic Time-series Station (BATS), adopting the best estimates of the mean depth (10.3 ± 3.3 m) and residence time at Hog Reef (2.5 ± 0.4 days; Venti et al., 2012). However, because

neither τ nor h were directly measured in this study and even small errors in these parameters can generate large errors in NCC and NCP (Courtney and Andersson, 2019), these calculations are admittedly uncertain. A Monte Carlo analysis was used to propagate the potential errors of τ and h through iterative calculations of NCC and NCP using randomly generated numbers (n = 10,000) within the range of uncertainties for each parameter. The resulting mean and range were used as approximations of the mean ± uncertainty in NCC and NCP. Furthermore, it is important to recognize that these estimates of NCC and NCP based on inshore-offshore chemical gradients represent integrated metabolic signals over multiple tidal cycles and habitats beyond the Hog Reef study site because currents here are not unidirectional and seawater is moving back and forth across this site multiple times before escaping (Venti et al., 2012; Takeshita et al., 2018).

In a second approach, the local biogeochemical variability was assessed based on relative changes in NCC and NCP, rather than actual rates. In the absence of detailed τ or h measurements, the relative contributions of NCC and NCP can be assessed by their ratio, termed R_{OI} by Suzuki (1998), which represents the ratio of organic to inorganic carbon production (Suzuki, 1998; Suzuki and Kawahata, 2003):

$$\frac{NCP_{\mathrm{DIC}}}{NCC_{\mathrm{TA}}} = \left[-(\Delta nDIC - \frac{1}{2}\Delta nTA)\right] / \left[-\frac{1}{2}\Delta nTA\right] \quad (4)$$

or

$$\frac{NCP_{\mathrm{DO}}}{NCC_{\mathrm{TA}}} = [-\Delta nDO] / \left[-\frac{1}{2}\Delta nTA\right] \quad (5)$$

However, in the present case, to highlight the diel variability and the relative magnitude of the numerator and denominator of Eqs 4 and 5 at Hog Reef, the temporal variabilities of these terms were assessed independently relative to the local mean over the sampling period rather than the offshore conditions. We refer to these terms as $r_{\mathrm{NCC\text{-}TA}}$, $r_{\mathrm{NCP\text{-}DIC}}$, and $r_{\mathrm{NCP\text{-}DO}}$:

$$r_{\mathrm{NCC-TA}} = -\frac{1}{2}\Delta nTA = -\frac{1}{2}\left(nTA_{reef} - nTA_{reef\_mean}\right) \quad (6)$$

$$\begin{aligned} r_{\mathrm{NCP-DIC}} &= -\left(\Delta nDIC - \frac{1}{2}\Delta nTA\right) = \\ &= -\left(nDIC_{reef} - nDIC_{reef\_mean}\right) \\ &\quad -\left(-\frac{1}{2}(nTA_{reef} - nTA_{reef\_mean})\right) \end{aligned} \quad (7)$$

$$r_{\mathrm{NCP-DO}} = \Delta nDO = nDO_{reef} - nDO_{reef\_mean} \quad (8)$$

It is important to note that $r_{\mathrm{NCC\text{-}TA}}$, $r_{\mathrm{NCP\text{-}DIC}}$, and $r_{\mathrm{NCP\text{-}DO}}$ are not metabolic rates, nor do they reflect the net trophic or calcification status of the water at Hog Reef. Instead these terms simply highlight the approximate relative magnitude of variability in TA and DIC attributed to NCC and NCP at Hog Reef and its surrounding habitats on diel timescales. The spatial representation of these terms roughly corresponds to the hypothetical reef area covered by a parcel of seawater over one tidal cycle. This has previously been referred to as the "effective reef footprint" which translates to the spatial and temporal extent of the benthic communities' influence on the overlying seawater chemistry (Courtney et al., 2016). The temporal variability in $r_{\mathrm{NCC\text{-}TA}}$, $r_{\mathrm{NCP\text{-}DIC}}$, and $r_{\mathrm{NCP\text{-}DO}}$ was calculated as the mean daily range (from 00:00 h to 00:00 h, or as close to these times as sampling frequency would allow) ± 1 standard deviation.

RESULTS

Fine Scale Temporal and Vertical Variability

Vertical profiles of current speeds and directions as well as pressure recorded at Hog Reef clearly showed the mixed semidiurnal tidal cycle, with a mean current speed of 0.08 ± 0.04 m s^{-1} (**Supplementary Figure 2**). Tide station data revealed a mean tidal range of 0.90 ± 0.11 m during the deployment (**Figure 3**, also measured by the ADCP, **Supplementary Figure 2**). From the principal component analysis of the depth-averaged velocities for the full deployment period (1–7 September), the angle of maximum variance (θ) was 82° with a flow speed of 0.054 m s^{-1} compared to 0.036 m s^{-1} for the orthogonal (352°) component. The direction of the mean quiver pointed approximately north at 0.025 m s^{-1}. Consequently, water flowed predominantly offshore at Hog Reef (**Figure 2a**), with significant variance in the east/west (approximately along-reef) direction resulting in an elliptical benthic footprint with a semi-major axis of 1.2 km and semi-minor axis of 0.8 km based on the hypothetical distance traveled by a parcel of water over 6 hours. Additional principal component analyses of the depth-averaged velocities for individual days corresponding to our spatial survey sampling dates revealed that θ varied between these days, changing from 79° on September 1 (**Figure 2b**), 103° on September 2 (**Figure 2c**), 86° on September 4 (**Figure 2d**), and 120° on September 7 (**Figure 2e**). The direction of the mean quiver for each day revealed that mean flow varied from along-reef and slightly inshore on September 1 (**Figure 2b**), to off-reef to the northeast on September 2 (**Figure 2c**), to slightly off-reef to the northwest on September 4 (**Figure 2d**), and off-reef approximately north on September 7 (**Figure 2e**) with differing degrees of variance.

High frequency measurements by autonomous sensors at Hog Reef showed distinct diel variability in temperature, DO, pH_T, and pCO_2, but less so with respect to TA, which was confirmed by a frequency analysis of all data (**Figure 3**, right column). A secondary local maximum and minimum of some of these parameters were also apparent on most days (**Figure 3**), with secondary peaks in the power spectra at ∼2 day^{-1}, reflecting the influence from the mixed semi-diurnal tide (**Figure 3**). This was particularly prominent for the TA data. Surface and bottom (7 m) temperatures generally agreed, with the exception of September 3–4 with a maximum vertical difference of 0.84°C (**Figure 3**). Mean temperature (± 1 SD) during the deployment was 28.38 ± 0.40°C at

the surface and 28.36 ± 0.38°C at the bottom. The mean diel temperature range (± 1 SD) in surface and bottom waters over the month-long deployment was 0.38 ± 0.15 and 0.40 ± 0.11°C, respectively (**Figure 3**). Salinity remained relatively constant throughout the deployment with a mean (± 1 SD) of 36.64 ± 0.06 PSU at the surface and 36.59 ± 0.04 PSU at the bottom. We note that there was drift between the salinity measurements at the surface and 7 m beginning midway through the deployment resulting in higher mean salinity at the surface compared to the bottom. Calculations of density at the surface and bottom produced an unstable water column during the latter half of the deployment, with a mean density (± 1 SD) over the deployment of 1023.6 ± 0.2 kg m^{-3} at the surface and 1023.5 ± 0.1 kg m^{-3} at the bottom, suggesting that the drift was a sensor error and not a real signal. Given a lack of post-deployment cross-calibration between instruments, we cannot confirm which sensor experienced the drift, though the drift may be an artifact of potential biofouling due to the absence of a pump for the CTD deployed at the bottom.

DO concentrations at the surface during peak production hours were higher than at the bottom, though the mean (± 1 SD) concentrations at surface and bottom over the deployment were similar (226 ± 22 and 220 ± 18 μmol kg^{-1}, respectively). The mean diel range (± 1 SD) in DO, however, appeared qualitatively different at the surface (78 ± 29 μmol kg^{-1}) and bottom (54 ± 16 μmol kg^{-1}) (**Figure 3**). Furthermore, mean TA and pH_T (± 1 SD) at the bottom were 2331 ± 16 μmol kg^{-1} and 7.953 ± 0.025, with mean diel ranges (± 1 SD) of 26 ± 13 μmol kg^{-1} and 0.07 ± 0.02, respectively (**Figure 3**; no autonomous measurements were made at the surface of these parameters, **Table 1**). Changes in pH_T positively tracked changes in DO (Spearman's rank correlation coefficient, $\rho = 0.61$, $p < 0.001$) which also mirrored changes in pCO_2 over the deployment (pH_T and pCO_2: $\rho = -0.99$, $p < 0.001$; pCO_2, and DO: $\rho = -0.66$, $p < 0.001$). Mean seawater pCO_2 (± 1 SD) measured by the SAMI-CO_2 instruments was 518 ± 35 μatm at the surface and 516 ± 30 μatm at the bottom, with mean diel ranges (± 1 SD) of 70 ± 25 and 76 ± 28 μatm, respectively (**Figure 3**), the differences of which are within the instruments' accuracy. Mean buoy seawater pCO_2 measured at the surface, however, was slightly lower (508 ± 30 μatm; mean ± 1 SD) than that measured by the SAMI-CO_2 at the surface, with the difference between these values outside of the buoy instrument's accuracy. However, buoy pCO_2 had a similar mean diel range (± 1 SD) of 70 ± 25 μatm compared to the SAMI-CO_2 instruments. Buoy pCO_2 measured in air was relatively constant (387 ± 3 μatm; mean ± 1 SD) with a small diel signal (5 ± 6 μatm; mean range ± 1 SD), which however, was disproportionally influenced by two anomalous measurements on September 11 and 16th which were outside the range of expected accuracy and precision.

Overall, parameters that were measured (TA) or calculated (pH_T and pCO_2) from discrete bottle samples collected at the instrument site during spatial surveys showed good agreement with instrument data for the majority of samples, though there were disagreements on a few occasions (**Figure 3**). The degraded precision compared to the fundamental replicate reproducibility is likely due to spatial and temporal mismatches between the sensors and discrete sampling. Bottle samples were collected as close to the sensors as physically possible from a boat, but small differences in sampling depth as well as water movement and/or potential boundary layers around the instruments may have led to these observed disagreements. In addition, there is also some error introduced to measurements of pCO_2 and pH_T calculated from DIC and TA that may contribute in part to these differences (Millero, 2007).

Lateral Spatiotemporal Variability

Spatial surveys over Hog Reef revealed noticeable variability in most parameters across the 3 km^2 survey area. Some lateral gradients appeared to follow inshore to offshore depth gradients, but the structure of these gradients varied between sampling dates and with changes in the direction of bulk water flow as measured by the current meter (**Figures 4**, **5**). Mean surface temperature (± 1 SD) across the four surveys was 28.38 ± 0.15°C at the surface and 28.28 ± 0.14°C at the bottom whereas mean salinity (± 1 SD) was the same at both surface and bottom (36.6 ± 0.0 PSU) at the precision of the YSI. The mean ranges (± 1 SD) of these parameters were 0.41 ± 0.14°C and 0.1 ± 0.0 PSU across the surface, and 0.38 ± 0.12°C and 0.1 ± 0.0 PSU across the bottom across the four surveys, respectively (**Figures 4**, **5**). Temperature was lower on the northwestern side of the survey area over the deeper reef drop off, and higher in the southeast above the shallow reef lagoon area (**Figures 4**, **5**) as would be expected due to depth-dependent heating.

DIC and TA were lower over the shallower, inshore areas of the reef, and higher over the deeper drop off (**Figures 4**, **5**). Mean DIC (± 1 SD) at the surface and bottom was 2058 ± 9 and 2056 ± 8 μmol kg^{-1} with a lateral mean range (± 1 SD) of 32 ± 7 and 27 ± 1 μmol kg^{-1}, respectively. Mean surface TA (± 1 SD) was 2347 ± 12 μmol kg^{-1} whereas mean bottom TA was 2349 ± 13 μmol kg^{-1} with a mean lateral range (± 1 SD) of 31 ± 7 and 27 ± 7 μmol kg^{-1}, respectively (**Figure 3**). Seawater pH_T calculated from measurements of DIC and TA was similar across the four surveys, with a mean surface value (± 1 SD) of 7.95 ± 0.02 and mean bottom value of 7.96 ± 0.02, but tended to be lower above the shallower reef areas (**Figures 4**, **5**) compared to deeper areas. The lateral mean ranges (± 1 SD) in pH_T were similar for surface (0.06 ± 0.01 pH_T units) and bottom (0.06 ± 0.00 pH_T units).

Vertical Spatiotemporal Variability

Vertical variability was small for all parameters of the spatial survey area and with no clear spatial trend (**Figure 6**). The mean temperature and salinity differences (± 1 SD) between surface and bottom were 0.11 ± 0.07°C and 0.0 ± 0.0 PSU, respectively, across the four surveys, which are less than the precision of the YSI 556 Handheld Multiparameter Instrument measurements themselves (**Figure 6**). Mean absolute differences (± 1 SD) in carbonate chemistry parameters between surface and bottom were 5 ± 2 μmol kg^{-1} for DIC, 6 ± 3 μmol

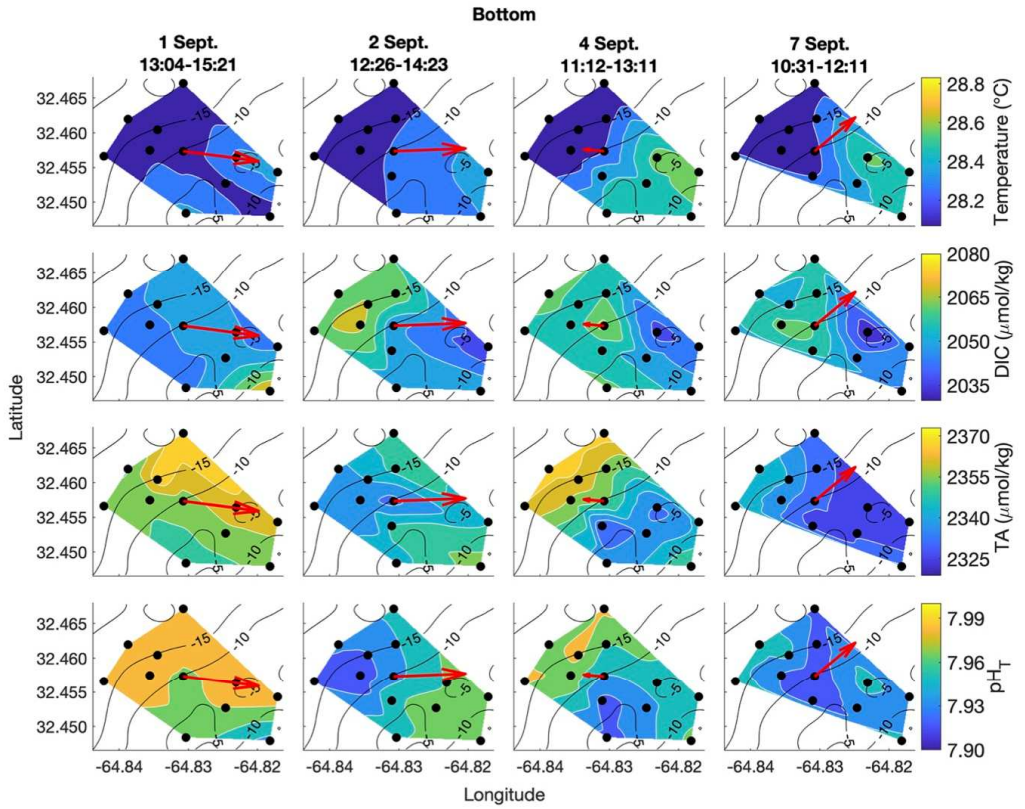

FIGURE 5 | Lateral spatiotemporal variability at the bottom in temperature, DIC, TA, and pH_T (calculated from measured DIC and TA) on September 1, 2, 4, and 7. Plots also contain bathymetry contours (black) and the mean depth-averaged velocity vector averaged over the sampling period (red).

kg^{-1} for TA, and 0.01 ± 0.01 for pH_T across the four surveys (**Figure 6**) and were close to the precision of the respective measurements.

Biogeochemical Drivers of Carbonate Chemistry Variability

On the local scale, $r_{NCP\ DIC}$, $r_{NCP\ DO}$, and $r_{NCC\ TA}$ were calculated relative to a $nDIC_{mean}$ of 2043 μmol kg^{-1}, nDO_{mean} of 220 μmol kg^{-1}, and nTA_{mean} of 2331 μmol kg^{-1}. The variability of $r_{NCP\text{-}DO}$ and $r_{NCP\text{-}DIC}$ followed a diel cycle, with maximum values in the late afternoon and minimum values in the early morning (as confirmed by the frequency analysis; **Figure 3**). However, the mean diel range (± 1 SD) in $r_{NCP\text{-}DO}$ (51 ± 15 μmol kg^{-1}) was larger than the mean diel range for $r_{NCP\text{-}DIC}$ (32 ± 11 μmol kg^{-1}) (**Figure 3**). The diel variability in $r_{NCP\text{-}DO}$ and $r_{NCP\text{-}DIC}$ also corresponded to the diel cycle of pH_T measured independently at Hog Reef, i.e., peaks in $r_{NCP\text{-}DIC}$ and $r_{NCP\text{-}DO}$ corresponded to peaks in pH_T (**Figure 3**). Diel variability in $r_{NCC\text{-}TA}$ was smaller than both $r_{NCP\text{-}DO}$ and $r_{NCP\text{-}DIC}$ (13 ± 6 μmol kg^{-1}; mean range ± 1 SD) and $r_{NCC\text{-}TA}$ did not show any strong correlation to either $r_{NCP\text{-}DO}$ or $r_{NCP\text{-}DIC}$ with a correlation coefficient (r) < 0.1 in both cases. The local diel variabilities in $r_{NCP\text{-}DIC}$ and $r_{NCC\text{-}TA}$ were also clearly evident in biogeochemical assessments based on inshore-offshore chemical gradients (**Figures 7B,C**). Offshore TA and DIC at the surface at BATS[3] in September 2017 was 2396 and 2046 μmol kg^{-1}, respectively, which combined with the mean depth and residence time of the Hog Reef area, revealed NCP of −118 ± 51 mmol m^{-2} day^{-1} (mean ± 1 SD) and NCC of 150 ± 37 mmol $CaCO_3$ m^{-2} day^{-1}. Consequently, these calculations indicate that the integrated metabolic signals encompassing multiple tidal cycles and potentially multiple habitats were net heterotrophic and net calcifying, with the diel variabilities characterized on

[3]http://bats.bios.edu/bats-data/

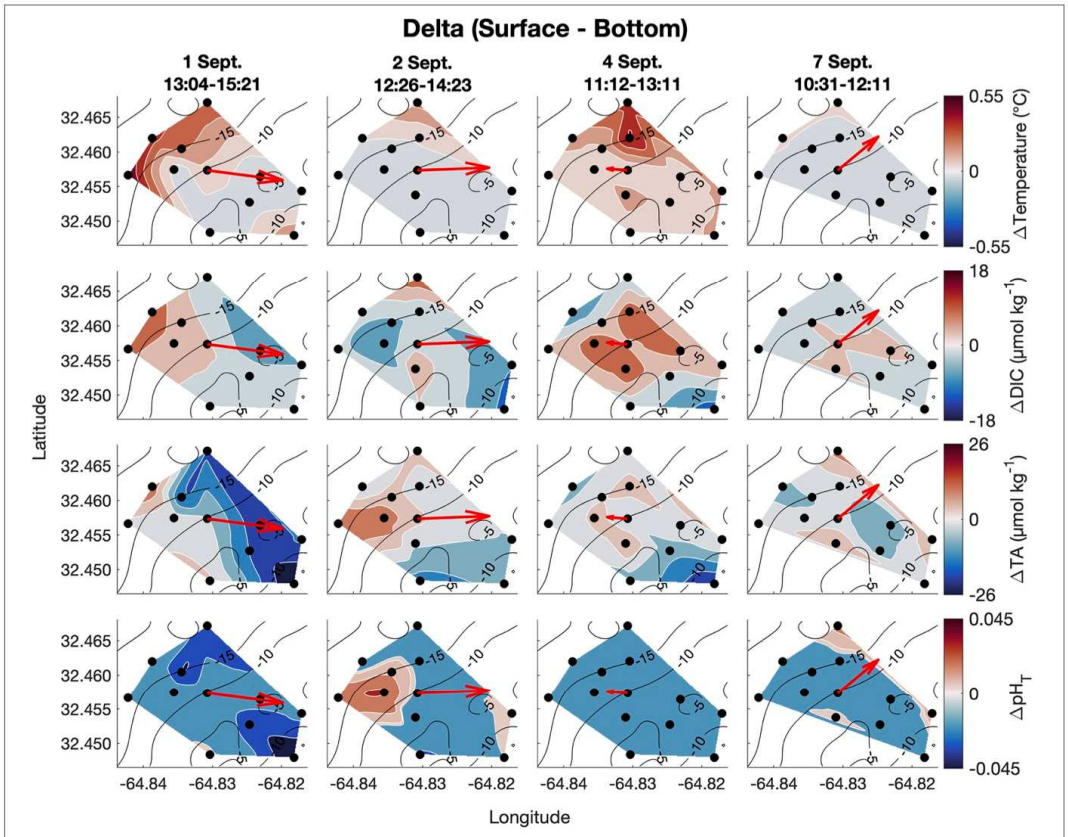

FIGURE 6 | Vertical spatiotemporal variability of the difference between surface and bottom temperature, DIC, TA, and pH_T (calculated from measured DIC and TA; bottom values subtracted from surface values) on September 1, 2, 4, and 7. Plots also contain bathymetry contours (black) and the mean depth-averaged velocity vector averaged over the sampling period.

Hog Reef superimposed on these larger scale net metabolic signals (**Figure 7**).

DISCUSSION

Fine Scale Temporal and Vertical Variability

The results of this study suggest that variability in the parameters measured at Hog Reef was mainly diel, and was likely influenced by a combination of light, benthic and water column production, calcification and dissolution, and local tidal flow. In particular, temperature, DO, pH_T, and pCO_2 exhibited distinct local extremes in the afternoon and after midnight each day. This dominant frequency of variability of ~ 1 day^{-1} was linked to the daily light cycle and its effects on seawater temperature and primary production (**Figure 3**). Seawater pCO_2 variability was inverse to that of DO and pH_T, reflecting CO_2 uptake by primary production during the day and release via respiration at night. These diel patterns are ubiquitous for shallow marine systems and have been documented for many reef systems in Bermuda (Bates et al., 2001, 2010; Sutton et al., 2014; Page et al., 2017; Takeshita et al., 2018) and around the globe (e.g., Hofmann et al., 2011; Gray et al., 2012; Guadayol et al., 2014; Koweek et al., 2015a,b; DeCarlo et al., 2017; Page et al., 2018; Cyronak et al., 2020).

In contrast to the autonomous measurements of temperature, DO, pH_T, and pCO_2, which revealed distinct diel trends, autonomous measurements of TA revealed higher frequency temporal variability and a less distinct diel trend (**Figure 3**). This may be related to the fact that the relative magnitude of the diel variability in calcification and $CaCO_3$ dissolution (r_{NCC}) was small compared to that of photosynthesis and respiration ($r_{NCP\text{-}DO}$ and $r_{NCP\text{-}DIC}$) at Hog Reef, making changes in seawater TA less pronounced compared to changes in DIC, DO, pH_T, and

pCO_2 (**Figure 3** and **Supplementary Figure 3**; Takeshita et al., 2018). Furthermore, frequency analyses revealed that TA varied strongly at frequencies of both 1 day^{-1} (diel light cycle) as well as 2 day^{-1} (relating to the tidal cycle) (**Figure 3**, right). This suggests that flow dynamics had a strong influence on the temporal variability in TA, which depending on the flow trajectory and history, would reveal a chemical signature that did not necessarily track the diel light cycle, and led to the prominence of variability at a higher frequency (**Figure 3**). We hypothesize that the reason other parameters (i.e., DO, pH_T, and seawater pCO_2) revealed a strong diel trend that was not muddled by the tidal cycle is because photosynthesis and respiration were also quantitatively important in the water column, as opposed to just the benthos, whereas calcification and $CaCO_3$ dissolution mainly occurred on the benthos. Consequently, changes in the seawater TA appeared to mainly reflect biogeochemical processes that predominantly occurred in the benthos (calcification and dissolution) with the chemical signal modified by hydrodynamics, while changes in DIC, DO, pH_T, and pCO_2 were also strongly influenced by water column photosynthesis and respiration. This hypothesis is supported by the fact that there were notable differences in the magnitude of DO variability at the surface and the bottom throughout the deployment period. While DO minima at night were similar for surface and bottom, daytime maxima were much higher in the surface, suggesting that there was higher total net primary productivity measured at the surface compared to the benthos during the day. Furthermore, the largest differences between surface and bottom DO occurred during neap tides, potentially indicating amplified gradients during times of reduced water flow and mixing (e.g., Falter et al., 2013; Lowe and Falter, 2015). Long et al. (2019) reported that water column production at Hog Reef accounted for more than half (58%) of the total oxygen flux, compared to just 39% from the benthos, during an overlapping study interval with our observations (Long et al., 2019), lending further support to the hypothesized contribution from water column productivity compared to the benthos.

The observed gradient in DO between surface and bottom was at times partly corroborated by independent pCO_2 measurements by the SAMI-CO_2 at the bottom and the MAPCO2 buoy at the surface. Surface pCO_2 measured by the buoy was consistently lower than pCO_2 measured at 7 m by the SAMI-CO_2, as would be expected given the DO gradient between surface and 7 m. However, because of inconsistencies between measurements of pCO_2 by the MAPCO2 and SAMI-CO_2 at the surface, it is difficult to make any strong conclusions based on these observations. It should also be noted that variations in seawater temperature and NCC between day (net calcification) and night (decreased calcification and increased $CaCO_3$ dissolution) influence seawater pCO_2 opposite to changes resulting from the day-night cycle in NCP (Cyronak et al., 2020), resulting in a dampened pCO_2 diel amplitude. Consequently, pCO_2 measurements are less sensitive relative to the DO measurements as a measure of net productivity differences between the surface and bottom. On coral reefs in general, the benthos is assumed to be the main contributor to coral reef organic carbon production with only minor influence from the water column. Few studies have actually quantified the relative contributions of each (e.g., Long et al., 2019), but based on the present observations and the Long et al. (2019) study, it is clear that this needs to be assessed in more detail in future studies. The relative contributions from the water column and benthos to NCP are likely to change as a function of depth so that the contribution from the benthos becomes increasingly important as the depth decreases. This may in fact explain the observations from Cyronak et al. (2020) that coral reef pH_T variability can be largely predicted based on depth and mean pH_T conditions.

Compared to our observations at Hog Reef, other studies that have characterized TA autonomously on coral reef environments in Kāne'ohe Bay, Hawai'i (Spaulding et al., 2014, same sensor as this study; Briggs et al., 2020, solid-state sensor) and Heron Island, Australia (McMahon et al., 2018, VINDTA 3c) observed more distinct diel variability and a greater daily amplitude in TA that closely tracked the diel variability in other carbonate chemistry parameters (i.e., pH_T and pCO_2). These study locations were characterized by much shallower depths than Hog Reef, and thus, higher benthic biomass to water volume ratio, resulting in greater influence by benthic processes on water chemistry and consequently larger changes in seawater TA. The higher biomass to water volume ratio was also evident from greater daily changes in seawater pH_T and pCO_2 at these locations (Drupp et al., 2013; McMahon et al., 2018; Page et al., 2018). It should be noted that making high quality autonomous measurements of TA on coral reefs is an important and active area of research since it provides an additional master variable to constrain the carbonic acid system. Furthermore, because calcification and $CaCO_3$ dissolution are central processes on coral reefs, and strongly influenced by global environmental change (Hoegh-Guldberg et al., 2007; Hughes et al., 2018), these processes are critical to monitor. Direct measurements of TA (as opposed to calculated TA) offer the most accurate and precise approach to estimate NCC. Thus, high frequency measurements of TA are important for understanding the drivers and dynamics of calcification and dissolution processes on coral reefs and could reveal temporal trends, relationships, and the effects of episodic events (e.g., storms) otherwise not detected from low frequency measurements (Spaulding et al., 2014; McMahon et al., 2018; Briggs et al., 2020).

Lateral and Vertical Spatiotemporal Variability

Lateral spatial gradients in carbonate chemistry across Hog Reef appeared to be influenced by the bathymetry and the general direction of water flow across or along the reef (**Figures 5**, **6**). The observed gradients in DIC, TA, and pH_T generally decreased from offshore to inshore as a result of the uptake of TA and DIC via calcification and primary production, with an exacerbated signal in shallower areas where smaller volumes of water were being modified by the reef community (such as in Falter et al., 2013; Takeshita et al., 2018). The current data and spatial survey data together highlight the influence of hydrodynamics on the structure of the observed gradients (**Figures 5**, **6**). On most days, the mean direction of depth-averaged flow was oriented in line

with the irregularities in the structure of the inshore-offshore gradients observed (e.g., September 2, 4, 7 in **Figures 5**, **6**). It should also be noted that September 4 was an extremely calm and sunny day, and thus, favorable for generating strong chemical gradients. While current speed and direction do not fully account for the gradients observed, the present results highlight the need to combine spatial water chemistry surveys with complementary hydrodynamic data, in order to better interpret observed chemical gradients. Furthermore, given the much larger gradients observed laterally compared to vertically, we find that the general assumption of a well-mixed water column over coral reefs is mostly a reasonable assumption at the spatial scale and depth of the current study, but the presence of stratification and/or disparate contributions from the benthos and water column biogeochemical processes, may invalidate this assumption. Furthermore, this assumption varies from place to place and needs to be given site-specific considerations.

Lateral spatial gradients in seawater carbonate chemistry have previously been characterized in Bermuda (e.g., Andersson et al., 2014; Venti et al., 2014; Takeshita et al., 2018) and in many other reef systems (e.g., Watanabe et al., 2006; Shamberger et al., 2011; Albright et al., 2015; Courtney et al., 2018; Page et al., 2018). Combined with mean residence time and depth, these gradients provide the information required to calculate rates of NCC and NCP, but accurately characterizing residence time is a non-trivial task associated with large uncertainties (Lowe et al., 2009; Venti et al., 2012; Teneva et al., 2013; Courtney and Andersson, 2019). The present data highlight the potential challenges in quantifying local rates of NCC and NCP based on spatial chemical gradients, as the water on the reef flows in different directions depending on the time of day and depth. In addition, the history of any given water parcel flowing over different habitats depends on the tide, current speeds and directions, and benthic composition. Compared to Hog Reef, there are clearly other locations that are more suitable for this task where even-depth and quasi-unidirectional flow or no flow (e.g., slack tide) may assist in quantifying rates of NCC and NCP. Other approaches based on gradients in the benthic boundary layer (e.g., benthic gradient flux or eddy covariance: Long et al., 2013; Takeshita et al., 2016, 2018) may also provide a way to accurately characterize rates at locations such as Hog Reef but are limited to a small benthic footprint ($\sim$100 m^2). Although the objective of this study was not to quantify metabolic rates, the different approaches explored here to assess biogeochemical drivers (local temporal variability, inshore-offshore gradients, and TA-DIC relationships) revealed the importance of the temporal and spatial scales considered, and how they might be related (**Figures 7**, **8**).

Biogeochemical Drivers of Carbonate Chemistry Variability

Calculations of $r_{\text{NCP-DIC}}$, $r_{\text{NCP-DO}}$, and $r_{\text{NCC-TA}}$ using a mean anomaly highlighted the variability of localized processes occurring on Hog Reef and adjacent habitats (i.e., habitat-specific biogeochemical processes and the respective mixing between offshore, rim reef, and lagoon seawater). On average, these terms roughly represented a benthic reef area on the order of 3 km^2, but there were times when the footprint may have been larger (**Figure 2**). The magnitude of the local, short-term variability in organic carbon processes ($r_{\text{NCP-DIC}}$ and $r_{\text{NCP-DO}}$) was greater than that of inorganic carbon processes ($r_{\text{NCC-TA}}$) occurring at Hog Reef during the study period with the diel range of both $r_{\text{NCP-DO}}$ and $r_{\text{NCP-DIC}}$ exceeding that of $r_{\text{NCC-TA}}$ (4.6 $\pm$ 2.4 μmol kg^{-1} for $r_{\text{NCP-DO}}$: $r_{\text{NCC-TA}}$ and 2.8 $\pm$ 1.4 μmol kg^{-1} for $r_{\text{NCP-DIC}}$: $r_{\text{NCC-TA}}$; mean ratio $\pm$ SD) (**Figure 3**). This was in agreement with a previous study at the same site that measured benthic NCC and NCP based on chemical gradients in the benthic boundary layer (Takeshita et al., 2018). Furthermore, the temporal variability in $r_{\text{NCP-DIC}}$ agreed well with $r_{\text{NCP-DO}}$ calculated from changes in DO, though the amplitude of the diel variability in $r_{\text{NCP-DO}}$ was larger than that of $r_{\text{NCP-DIC}}$. This disagreement may be in part due to deviation from the assumed photosynthetic quotient of 1 (Smith and Marsh, 1973; Takeshita et al., 2018; Bolden et al., 2019) with a Type II linear regression between $r_{\text{NCP-DO}}$ and $r_{\text{NCP-DIC}}$ yielding a slope of 1.8 ($p < 0.001$), but could also arise from other factors (e.g., sea-air gas exchange was not accounted for and DIC was not measured directly but calculated from pCO_2 and TA; **Supplementary Figure 3**).

Direct estimates of NCP and NCC based on the chemical gradients between Hog Reef and offshore (BATS), showed substantial net heterotrophy and net calcification (**Figure 7C**). These estimates reveal the cumulative influence on seawater chemistry from a reef area potentially larger than Hog Reef and for seawater residence time extending multiple tidal cycles, with the influence from the local daily metabolism superimposed on this larger scale reef metabolic signal. The generality of these results (i.e., heterotrophy and calcification) is probably robust, but the absolute values need to be viewed with caution since the flow trajectory, mean depth, and residence time are associated with substantial uncertainty (Courtney and Andersson, 2019). Nonetheless, the estimated mean rates of NCC and NCP are comparable to previous estimates from Bermuda in September (NCC: $\sim$50–200 mmol m^{-2} day^{-1}, NCP: $\sim$ 0–−250 mmol m^{-2} day^{-1}; (Bates et al., 2010; Yeakel et al., 2015; Courtney et al., 2016, 2017; Takeshita et al., 2018), although several of these estimates used similar methodology and are thus not quite independent comparisons (Yeakel et al., 2015; Courtney et al., 2016, 2017), and Takeshita et al. (2018) only measured NCP and NCC over 3 days.

The importance of scale, illuminated by the different approaches used to assess the importance of biogeochemical processes on Hog Reef, was also evident from graphical assessment and correlation analysis of TA-DIC data. In contrast to many other studies that have characterized TA and DIC on coral reefs over temporal or spatial scales (e.g., Cyronak et al., 2018 and references therein), the current study did not observe a strong correlation between TA and DIC across space (**Figure 8**), which was also the case in Takeshita et al. (2018). The lack of a clear TA-DIC relationship could be explained by both the local dominance of r_{NCP} over r_{NCC} as well as the differences between surface and benthic production (see previous discussion). However, when placed in context with TA and DIC data collected at other reef sites in Bermuda, covering inshore waters from Bailey's Bay to the rim reef at Hog Reef, the data from this study fit well along a linear relationship of nTA and nDIC (normalized to a salinity of 36.7, the mean salinity across

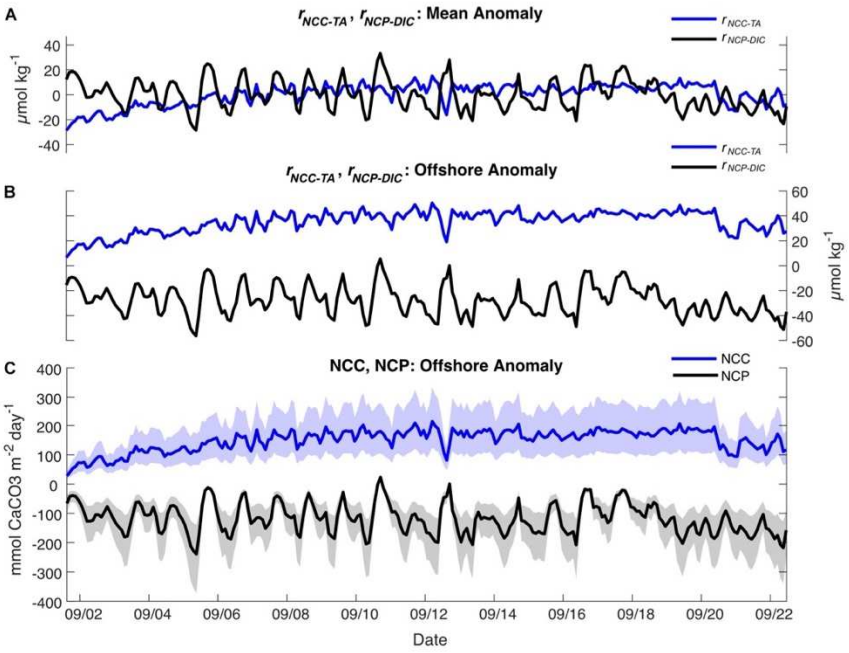

FIGURE 7 | (A) r_{NCC-TA} (blue) and $r_{NCP-DIC}$ (black) calculated relative to the local means; **(B)** r_{NCC-TA} (blue) and $r_{NCP-DIC}$ (black) calculated relative to the offshore value at the BATS Station; **(C)** Rates of NCC (blue) and NCP (black) (mean ± shaded uncertainty) calculated relative to the offshore value at the BATS Station.

data from all studies) with a slope close to 1 (slope = 0.97, R^2 = 0.86; **Figure 8**). This implies that NCC and NCP are closely balanced at this larger spatial and temporal scale, and that relatively small changes in mean pH_T occur as a function of time and space (Suzuki and Kawahata, 2003; Andersson and Gledhill, 2013; Andersson et al., 2014; Cyronak et al., 2018). However, this does not mean that pH_T is invariable; for a given habitat, seawater pH_T may vary largely on diel timescales depending on the relative importance of the organic to inorganic carbon cycle (Cyronak et al., 2018; Takeshita et al., 2018). These observations are directly related to the functional scale (biological, temporal, and spatial) of the study and has been discussed extensively in Cyronak et al. (2018) and Takeshita et al. (2018).

CONCLUDING REMARKS

The results of this study highlight that seawater carbonate chemistry on coral reefs varies considerably over time and space, with variability linked to diel cycles and local hydrodynamics. By measuring variability in carbonate chemistry and other parameters simultaneously over time and at multiple spatial scales, we showed that physical and biological processes interact on a reef on different scales to result in the net variability in carbonate chemistry and environmental parameters. The general assumption of a well-mixed water column with small vertical chemical gradients (compared to lateral or temporal gradients) over shallow coral reefs may be a reasonable assumption for many reefs, but is site dependent and needs to be assessed on a case-by-case basis. Notably, the present study showed a decoupling between the variability of TA and other carbonate chemistry parameters, which could be attributed to different contributions from benthic and water column biogeochemical processes as well as hydrodynamics. This observation deserves additional attention in other reef locations characterized by different depth, flow, and community compositions. In general, because of their relatively high latitude (32°N), Bermudan reefs experience higher seasonal variability in many properties compared to more tropical reefs. It has been predicted that future changes in ocean pH may increase the variability, and thus the range, of extreme pCO_2 values that reefs are exposed to due to reduced seawater buffering capacity (Jury et al., 2013; Shaw et al., 2013). However, whether naturally more variable reef environments extend protections to corals and reef organisms under a regime of changing ocean pH is unclear (Dufault et al., 2012; Comeau et al., 2014; Camp et al., 2016; Rivest et al., 2017; Kapsenberg and Cyronak, 2019). Characterizing the present-day variability of carbonate chemistry at multiple scales, as well as the interactions between hydrodynamics, geomorphology, and biogeochemistry, on reefs such as those in Bermuda will

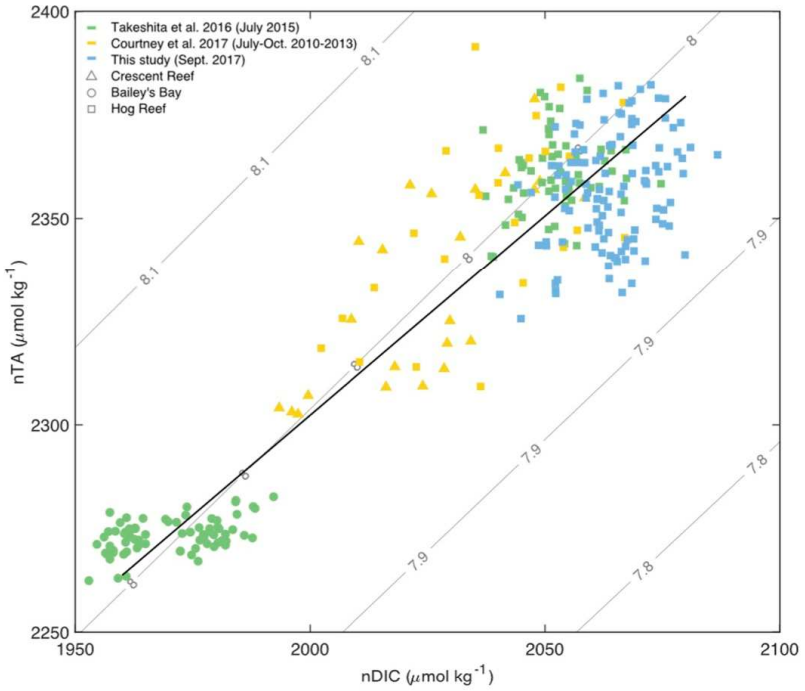

FIGURE 8 | Salinity normalized (36.7 PSU) TA and DIC for water sample data from sites across the Bermuda carbonate platform: Crescent Reef (triangles), Bailey's Bay (circles), and various expeditions to Hog Reef (squares) ranging from 2010 to 2017 with a Type II linear regression for all data (black) and pH contours. Only data from July to October of each year were used from Courtney et al. (2017; yellow). All data from Takeshita et al. (2016; green) were collected in July 2015. All bottle sample data from the present study were collected in September 2017 (blue).

help us better predict how reefs will change as a result of future acidification.

DATA AVAILABILITY STATEMENT

The datasets presented in this study can be found in online repositories. The names of the repository/repositories and accession number(s) can be found below: BCO-DMO Dataset #783568 https://www.bco-dmo.org/dataset/783568 and BCO-DMO Project #73787 https://www.bco-dmo.org/project/737878.

AUTHOR CONTRIBUTIONS

AA, TC, HP, and MD designed the study. TC, HP, AA, and CB deployed the instruments and collected the data. AP performed the laboratory work and analyzed the data with inputs from AA, TC, and SG. AP wrote the first draft of the manuscript with input from AA. All authors contributed to subsequent drafts of the manuscript.

FUNDING

This study was supported by funding from the NSF GRFP (AP, TC, and HP), NSF OCE 18-29778 (AP), NSF OCE 14-16518 and 12-55042 (AA), and NSF OCE 14-59255 (MD).

ACKNOWLEDGMENTS

We thank Dr. Matthew Long and Jennie Rheuban (Woods Hole Oceanographic Institution) for assistance during sensor deployment and recovery and Dr. Tyler Cyronak for processing and providing imagery of Hog Reef.

SUPPLEMENTARY MATERIAL

The Supplementary Material for this article can be found online at: https://www.frontiersin.org/articles/10.3389/fmars.2021.562267/full#supplementary-material

REFERENCES

Albright, R., Benthuysen, J., Cantin, N., Caldeira, K., and Anthony, K. (2015). Coral reef metabolism and carbon chemistry dynamics of a coral reef flat. *Geophys. Res. Lett.* 42, 3980–3988. doi: 10.1002/2015GL063488

Andersson, A. J., Bates, N. R., and Mackenzie, F. T. (2007). Dissolution of carbonate sediments under rising pCO2 and ocean acidification: observations from Devil's Hole, Bermuda. *Aquat. Geochem.* 13, 237–264. doi: 10.1007/s10498-007-9018-8

Andersson, A. J., and Gledhill, D. (2013). Ocean acidification and coral reefs: effects on breakdown, dissolution, and net ecosystem calcification. *Annu. Rev. Mar. Sci.* 5, 321–348. doi: 10.1146/annurev-marine-121211-172241

Andersson, A. J., Venn, A. A., Pendleton, L., Brathwaite, A., Camp, E. F., Cooley, S., et al. (2019). Ecological and socioeconomic strategies to sustain Caribbean coral reefs in a high-CO_2 world. *Reg. Stud. Mar. Sci.* 29:100677. doi: 10.1016/j.rsma.2019.100677

Andersson, A. J., Yeakel, K. L., Bates, N. R., and de Putron, S. J. (2014). Partial offsets in ocean acidification from changing coral reef biogeochemistry. *Nat. Clim. Chang.* 4, 56–61. doi: 10.1038/nclimate2050

Anthony, K. R. N., Diaz-Pulido, G., Verlinden, N., Tilbrook, B., and Andersson, A. J. (2013). Benthic buffers and boosters of ocean acidification on coral reefs. *Biogeosci. Discuss.* 10, 1831–1865.

Anthony, K. R. N., Kleypas, A. J., and Gattuso, J.-P. (2011). Coral reefs modify their seawater carbon chemistry - implications for impacts of ocean acidification. *Glob. Change Biol.* 17, 3655–3666. doi: 10.1111/j.1365-2486.2011.02510.x

Bates, N. R. (2017). Twenty years of marine carbon cycle observations at Devil's Hole, Bermuda provide insights into seasonal hypoxia, coral reef calcification, and ocean acidification. *Front. Mar. Sci.* 4:36. doi: 10.3389/fmars.2017.00036

Bates, N. R., Amat, A., and Andersson, A. J. (2010). Feedbacks and responses of coral calcification on the Bermuda reef system to seasonal changes in biological processes and ocean acidification. *Biogeosciences* 7, 2509–2530. doi: 10.5194/bg-7-2509-2010

Bates, N. R., Samuels, L., and Merlivat, L. (2001). Biogeochemical and physical factors influencing seawater fCO2 and air sea CO_2 exchange on the Bermuda coral reef. *Limnol. Oceanogr.* 46, 833–846. doi: 10.4319/lo.2001.46.4.0833

Bolden, I. W., Sachs, J. P., and Gagnon, A. C. (2019). Temporally-variable productivity quotients on a coral atoll: implications for estimates of reef metabolism. *Mar. Chem.* 217:103707. doi: 10.1016/j.marchem.2019.103707

Brander, L. M., Van Beukering, P., and Cesar, H. S. J. (2007). The recreational value of coral reefs: a meta-analysis. *Ecol. Econ.* 63, 209–218. doi: 10.1016/j.ecolecon.2006.11.002

Briggs, E. M., De Carlo, E. H., Sabine, C. L., Howins, N. M., and Martz, T. R. (2020). Autonomous ion-sensitive field effect transistor-based total alkalinity and pH measurements on a barrier reef of Kāne'ohe Bay. *ACS Earth Space Chem.* 4, 355–362. doi: 10.1021/acsearthspacechem.9b00274

Camp, E. F., Smith, D. J., Evenhuis, C., Enochs, I., Manzello, D., Woodcock, S., et al. (2016). Acclimatization to high-variance habitats does not enhance physiological tolerance of two key Caribbean corals to future temperature and pH. *Proc. R Soc. B Biol. Sci.* 283:20160442. doi: 10.1098/rspb.2016.0442

Chan, N. C. S., and Connolly, S. R. (2013). Sensitivity of coral calcification to ocean acidification: a meta-analysis. *Glob. Change Biol.* 19, 282–290. doi: 10.1111/gcb.12011

Comeau, S., Edmunds, P. J., Spindel, N. B., and Carpenter, R. C. (2014). Diel pCO2 oscillations modulate the response of the coral *Acropora hyacinthus* to ocean acidification. *Mar. Ecol. Prog. Ser.* 501, 99–111. doi: 10.3354/meps10690

Costanza, R., de Groot, R., Sutton, P., van der Ploeg, S., Anderson, S. J., Kubiszewski, I., et al. (2014). Changes in the global value of ecosystem services. *Glob. Environ. Change* 26, 152–158. doi: 10.1016/j.gloenvcha.2014.04.002

Courtney, T. A., and Andersson, A. J. (2019). Evaluating measurements of coral reef net ecosystem calcification rates. *Coral Reefs* 38, 997–1006. doi: 10.1007/s00338-019-01828-2

Courtney, T. A., Andersson, A. J., Bates, N. R., Collins, A., Cyronak, T., de Putron, S. J., et al. (2016). Comparing chemistry and census-based estimates of net ecosystem calcification on a rim reef in Bermuda. *Front. Mar. Sci.* 3:181. doi: 10.3389/fmars.2016.00181

Courtney, T. A., De Carlo, E. H., Page, H. N., Bahr, K. D., Barro, A., Howins, N., et al. (2018). Recovery of reef-scale calcification following a bleaching event in Kāne'ohe Bay, Hawai'i: post-bleaching recovery of reef-scale calcification. *Limnol. Oceanogr. Lett.* 3, 1–9. doi: 10.1002/lol2.10056

Courtney, T. A., Lebrato, M., Bates, N. R., Collins, A., de Putron, S. J., Garley, R., et al. (2017). Environmental controls on modern scleractinian coral and reef-scale calcification. *Sci. Adv.* 3:e1701356. doi: 10.1126/sciadv.1701356

Cyronak, T., Andersson, A. J., Langdon, C., Albright, R., Bates, N. R., Caldeira, K., et al. (2018). Taking the metabolic pulse of the world's coral reefs. *PLoS One* 13:e0190872. doi: 10.1371/journal.pone.0190872

Cyronak, T., Schulz, K. G., Santos, I. R., and Eyre, B. D. (2014). Enhanced acidification of global coral reefs driven by regional biogeochemical feedbacks. *Geophys. Res. Lett.* 41, 5538–5546. doi: 10.1002/2014GL060849

Cyronak, T., Takeshita, Y., Courtney, T. A., DeCarlo, E. H., Eyre, B. D., Kline, D. I., et al. (2020). Diel temperature and pH variability scale with depth across diverse coral reef habitats. *Limnol. Oceanogr. Lett.* 5, 193–203. doi: 10.1002/lol2.10129

DeCarlo, T. M., Cohen, A. L., Wong, G. T. F., Shiah, F.-K., Lentz, S. J., Davis, K. A., et al. (2017). Community production modulates coral reef pH and the sensitivity of ecosystem calcification to ocean acidification. *J. Geophys. Res. Oceans* 122, 745–761. doi: 10.1002/2016JC012326

Dickson, A. G. (1990). Thermodynamics of the dissociation of boric acid in synthetic seawater from 273.15 to 318.15 K. *Deep Sea Res. Part Oceanogr. Res. Pap.* 37, 755–766. doi: 10.1016/0198-0149(90)90004-F

Dickson, A. G., and Millero, F. J. (1987). A comparison of the equilibrium constants for the dissociation of carbonic acid in seawater media. *Deep Sea Res. Part Oceanogr. Res. Pap.* 34, 1733–1743. doi: 10.1016/0198-0149(87)90021-5

Dickson, A. G., Sabine, C. L., Christian, J. R., Bargeron, C. P., North Pacific Marine Science, and Organization (eds) (2007). *Guide to Best Practices for Ocean CO_2 Measurements*. Sidney, BC: North Pacific Marine Science Organization.

Drupp, P. S., De Carlo, E. H., Mackenzie, F. T., Sabine, C. L., Feely, R. A., and Shamberger, K. E. (2013). Comparison of CO_2 dynamics and air-sea gas exchange in differing tropical reef environments. *Aquat. Geochem.* 19, 371–397. doi: 10.1007/s10498-013-9214-7

Dufault, A. M., Cumbo, V. R., Fan, T.-Y., and Edmunds, P. J. (2012). Effects of diurnally oscillating pCO2 on the calcification and survival of coral recruits. *Proc. R. Soc. B Biol. Sci.* 279, 2951–2958. doi: 10.1098/rspb.2011.2545

Eyre, B. D., Cyronak, T., Drupp, P., De Carlo, E. H., Sachs, J. P., and Andersson, A. J. (2018). Coral reefs will transition to net dissolving before end of century. *Science* 359, 908–911. doi: 10.1126/science.aao1118

Falter, J. L., Lowe, R. J., Zhang, Z., and McCulloch, M. (2013). Physical and biological controls on the carbonate chemistry of coral reef waters: effects of metabolism, wave forcing, sea level, and geomorphology. *PLoS One* 8:e53303. doi: 10.1371/journal.pone.0053303

Gagliano, M., McCormick, M. I., Moore, J. A., and Depczynski, M. (2010). The basics of acidification: Baseline variability of pH on Australian coral reefs. *Mar. Biol.* 157, 1849–1856. doi: 10.1007/s00227-010-1456-y

Gray, S. E. C., DeGrandpre, M. D., Langdon, C., and Corredor, J. E. (2012). Short-term and seasonal pH, pCO2 and saturation state variability in a coral-reef ecosystem. *Glob. Biogeochem. Cycles* 26:2011GB004114. doi: 10.1029/2011GB004114

Guadayol, Ò, Silbiger, N. J., Donahue, M. J., and Thomas, F. I. M. (2014). Patterns in temporal variability of temperature, oxygen and pH along an environmental gradient in a coral reef. *PLoS One* 9:e85213. doi: 10.1371/journal.pone.0085213

Hoegh-Guldberg, O., Mumby, P. J., Hooten, A. J., Steneck, R. S., Greenfield, P., Gomez, E., et al. (2007). Coral reefs under rapid climate change and ocean acidification. *Science* 318, 1737–1742. doi: 10.1126/science.1152509

Hofmann, G. E., Smith, J. E., Johnson, K. S., Send, U., Levin, L. A., Micheli, F., et al. (2011). High-frequency dynamics of ocean pH: a multi-ecosystem comparison. *PLoS One* 6:e28983. doi: 10.1371/journal.pone.0028983

Hughes, T. P., Baird, A. H., Bellwood, D. R., Card, M., Connolly, S. R., Folke, C., et al. (2003). Climate change, human impacts, and the resilience of coral reefs. *Science* 301, 929–933. doi: 10.1126/science.1085046

Hughes, T. P., Kerry, J. T., Baird, A. H., Connolly, S. R., Dietzel, A., Eakin, C. M., et al. (2018). Global warming transforms coral reef assemblages. *Nature* 556, 492–496. doi: 10.1038/s41586-018-0041-2

Jackson, J. B. C., Kirby, M. X., Berger, W. H., Bjorndal, K. A., Botsford, L. W., Bourque, B. J., et al. (2001). Historical overfishing and the recent collapse of coastal ecosystems. *Science* 293, 629–637. doi: 10.1126/science.1059199

Jury, C. P., Thomas, F. I. M., Atkinson, M. J., and Toonen, R. J. (2013). Buffer capacity, ecosystem feedbacks, and seawater chemistry under global change. *Water* 5, 1303–1325. doi: 10.3390/w5031303

Kapsenberg, L., and Cyronak, T. (2019). Ocean acidification refugia in variable environments. *Glob. Change Biol.* 25, 3201–3214. doi: 10.1111/gcb.14730

Kleypas, J. A., Anthony, K. R. N., and Gattuso, J.-P. (2011). Coral reefs modify their seawater carbon chemistry - case study from a barrier reef (Moorea, French Polynesia). *Glob. Change Biol.* 17, 3667–3678. doi: 10.1111/j.1365-2486.2011.02530.x

Kleypas, J. A., Buddemeier, R. W., Archer, D., Gattuso, J.-P., Langdon, C., and Opdyke, B. N. (1999). Geochemical consequences of increased atmospheric carbon dioxide on coral reefs. *Science* 284, 118–120. doi: 10.1126/science.284.5411.118

Kleypas, J. A., and Yates, K. K. (2009). Coral reefs and ocean acidification. *Oceanography* 22, 108–117.

Koweek, D. A., Dunbar, R. B., Monismith, S. G., Mucciarone, D. A., Woodson, C. B., and Samuel, L. (2015a). High-resolution physical and biogeochemical variability from a shallow back reef on Ofu, American Samoa: an end-member perspective. *Coral Reefs* 34, 979–991. doi: 10.1007/s00338-015-1308-9

Koweek, D. A., Dunbar, R. B., Rogers, J. S., Williams, G. J., Price, N., Mucciarone, D., et al. (2015b). Environmental and ecological controls of coral community metabolism on Palmyra Atoll. *Coral Reefs* 34, 339–351. doi: 10.1007/s00338-014-1217-3

Langdon, C., Gattuso, J.-P., and Andersson, A. (2010). "Measurements of calcification and dissolution of benthic organisms and communities," in *Guide to Best Practices for Ocean Acidification Research and Data Reporting*, eds U. Riebesell, V. J. Fabry, L. Hansson, and J.-P. Gattuso (Luxembourg: Office for Official Publications of the European Communities), 213–232.

Langdon, C., Takahashi, T., Sweeney, C., Chipman, D., Goddard, J., Marubini, F., et al. (2000). Effect of calcium carbonate saturation state on the calcification rate of an experimental coral reef. *Glob. Biogeochem. Cycles* 14, 639–654. doi: 10.1029/1999GB001195

Lewis, E., and Wallace, D. (1998). *CO2SYS - Program Developed for the CO_2 System Calculations*. Oak Ridge, TE: Oak Ridge National Laboratory, US Department of Energy: Carbon Dioxide Information Analysis Center.

Long, M. H., Berg, P., de Beer, D., and Zieman, J. C. (2013). In situ coral reef oxygen metabolism: an eddy correlation study. *PLoS One* 8:e058581. doi: 10.1371/journal.pone.0058581

Long, M. H., Rheuban, J. E., McCorkle, D. C., Burdige, D. J., and Zimmerman, R. C. (2019). Closing the oxygen mass balance in shallow coastal ecosystems. *Limnol. Oceanogr.* 64, 2694–2708. doi: 10.1002/lno.11248

Lowe, R. J., and Falter, J. L. (2015). Oceanic forcing of coral reefs. *Annu. Rev. Mar. Sci.* 7, 43–66. doi: 10.1146/annurev-marine-010814-015834

Lowe, R. J., Falter, J. L., Monismith, S. G., and Atkinson, M. J. (2009). A numerical study of circulation in a coastal reef-lagoon system. *J. Geophys. Res. Oceans* 114:C005081. doi: 10.1029/2008JC005081

Marine Environmental Program (2007). *Marine Environmental Program Annual Report, 2006-2007*. St.George's: Bermuda Insitute of Ocean Sciences.

McMahon, A., Santos, I. R., Schulz, K. G., Cyronak, T., and Maher, D. T. (2018). Determining coral reef calcification and primary production using automated alkalinity, pH and pCO2 measurements at high temporal resolution. *Estuar. Coast. Shelf Sci.* 209, 80–88. doi: 10.1016/j.ecss.2018.04.041

Mehrbach, C., Culberson, C. H., Hawley, J. E., and Pytkowicx, R. M. (1973). Measurement of the apparent dissociation constants of carbonic acid in seawater at atmospheric pressure. *Limnol. Oceanogr.* 18, 897–907. doi: 10.4319/lo.1973.18.6.0897

Millero, F. J. (2007). The marine inorganic carbon cycle. *Chem. Rev.* 107, 308–341.

Moberg, F., and Folke, C. (1999). Ecological Goods and Services of Coral Reef Ecosystems. *Ecol. Econ.* 29, 215–233.

Morris, B., Barnes, J., Brown, F., and Markham, J. (1977). *The Bermuda Marine Environment: A Report of the Bermuda Inshore Waters Investigations, 1976-1977*. St.George's: Bermuda Biological Station.

Nelson, H. R., and Altieri, A. H. (2019). Oxygen: the universal currency on coral reefs. *Coral Reefs* 38, 177–198. doi: 10.1007/s00338-019-01765-0

Page, H. N., Courtney, T. A., Collins, A., De Carlo, E. H., and Andersson, A. J. (2017). Net community metabolism and seawater carbonate chemistry scale non-intuitively with coral cover. *Front. Mar. Sci.* 4:161. doi: 10.3389/fmars.2017.00161

Page, H. N., Courtney, T. A., De Carlo, E. H., Howins, N. M., Koester, I., and Andersson, A. J. (2018). Spatiotemporal variability in seawater carbon chemistry for a coral reef flat in Kāne'ohe Bay, Hawai'i. *Limnol. Oceanogr.* 64, 913–934. doi: 10.1002/lno.11084

Pelejero, C., Calvo, E., McCulloch, M., Marshall, J. F., Gagan, M. K., Lough, J. M., et al. (2005). Preindustrial to modern interdecadal variability in coral reef pH. *Science* 309, 2204–2207. doi: 10.1126/science.1113692

Rivest, E. B., Comeau, S., and Cornwall, C. E. (2017). The role of natural variability in shaping the response of coral reef organisms to climate change. *Curr. Clim. Change Rep.* 3, 271–281. doi: 10.1007/s40641-017-0082-x

Schönberg, C. H. L., Fang, J. K. H., Carreiro-Silva, M., Tribollet, A., and Wisshak, M. (2017). Bioerosion: the other ocean acidification problem. *ICES J. Mar. Sci.* 74, 895–925. doi: 10.1093/icesjms/fsw254

Shamberger, K. E. F., Feely, R. A., Sabine, C. L., Atkinson, M. J., DeCarlo, E. H., Mackenzie, F. T., et al. (2011). Calcification and organic production on a Hawaiian coral reef. *Mar. Chem.* 127, 64–75. doi: 10.1016/j.marchem.2011.08.003

Shaw, E. C., McNeil, B. I., Tilbrook, B., Matear, R., and Bates, M. L. (2013). Anthropogenic changes to seawater buffer capacity combined with natural reef metabolism induce extreme future coral reef CO_2 conditions. *Glob. Change Biol.* 19, 1632–1641. doi: 10.1111/gcb.12154

Silverman, J., Lazar, B., Cao, L., Caldeira, K., and Erez, J. (2009). Coral reefs may start dissolving when atmospheric CO_2 doubles. *Geophys. Res. Lett.* 36:L036282.

Silverman, J., Lazar, B., and Erez, J. (2007). Effect of aragonite saturation, temperature, and nutrients on the community calcification rate of a coral reef. *J. Geophys. Res. Oceans* 112:C003770. doi: 10.1029/2006JC003770

Smith, S. V., and Marsh, J. A. Jr. (1973). Organic carbon production on the windward reef flat of Eniwetok Atoll. *Limnol. Oceanogr.* 18, 953–961. doi: 10.4319/lo.1973.18.6.0953

Spaulding, R. S., DeGrandpre, M. D., Beck, J. C., Hart, R. D., Peterson, B., De Carlo, E. H., et al. (2014). Autonomous in situ measurements of seawater alkalinity. *Environ. Sci. Technol.* 48, 9573–9581. doi: 10.1021/es501615x

Spurgeon, J. P. G. (1992). The economic valuation of coral reefs. *Mar. Pollut. Bull.* 24, 529–536. doi: 10.1016/0025-326X(92)90704-A

Sutherland, M. G., McLean, S. H., Love, M. R., Carignan, K. S., and Eakins, B. W. (2014). *Digital Elevation Models of Bermuda: Data Sources, Processing and Analysis*. Washington, DC: NOAA.

Sutton, A. J., Feely, R. A., Maenner-Jones, S., Musielwicz, S., Osborne, J., Dietrich, C., et al. (2019). Autonomous seawater pCO2 and pH time series from 40 surface buoys and the emergence of anthropogenic trends. *Earth Syst. Sci. Data* 11, 421–439. doi: 10.5194/essd-2018-114

Sutton, A. J., Sabine, C. L., Maenner-Jones, S., Lawrence-Slavas, N., Meinig, C., Feely, R. A., et al. (2014). A high-frequency atmospheric and seawater pCO2 data set from 14 open-ocean sites using a moored autonomous system. *Earth Syst. Sci. Data* 6, 353–366.

Suzuki, A. (1998). Combined effects of photosynthesis and calcification on the partial pressure of carbon dioxide in seawater. *J. Oceanogr.* 54, 1–7. doi: 10.1007/BF02744376

Suzuki, A., and Kawahata, H. (2003). Carbon budget of coral reef systems: an overview of observations in fringing reefs, barrier reefs and atolls in the Indo-Pacific regions. *Tellus B Chem. Phys. Meteorol.* 55, 428–444. doi: 10.3402/tellusb.v55i2.16761

Takeshita, Y., Cyronak, T., Martz, T. R., Kindeberg, T., and Andersson, A. J. (2018). Coral reef carbonate chemistry variability at different functional scales. *Front. Mar. Sci.* 5:175. doi: 10.3389/fmars.2018.00175

Takeshita, Y., McGillis, W., Briggs, E. M., Carter, A. L., Donham, E. M., Martz, T. R., et al. (2016). Assessment of net community production and calcification of a coral reef using a boundary layer approach. *J. Geophys. Res. Oceans* 121, 5655–5671. doi: 10.1002/2016JC011886

Teneva, L., Dunbar, R. B., Mucciarone, D. A., Dunckley, J. F., and Koseff, J. R. (2013). High-resolution carbon budgets on a Palau back-reef modulated by interactions between hydrodynamics and reef metabolism. *Limnol. Oceanogr.* 58, 1851–1870. doi: 10.4319/lo.2013.58.5.1851

Uppström, L. R. (1974). The boron/chlorinity ratio of deep-sea water from the Pacific Ocean. *Deep Sea Res. Oceanogr. Abstr.* 21, 161–162. doi: 10.1016/0011-7471(74)90074-6

van Heuven, S., Pierrot, D., Rae, J. W. B., Lewis, E., and Wallace, D. (2011). *MATLAB Program Developed for CO_2 System Calculations*. Oak Ridge, TN: Carbon Dioxide Information Analysis Center, Oak Ridge National Laboratory, US Department of Energy.

Venti, A., Andersson, A., and Langdon, C. (2014). Multiple driving factors explain spatial and temporal variability in coral calcification rates on the Bermuda platform. *Coral Reefs* 33, 979–997. doi: 10.1007/s00338-014-1191-9

Venti, A., Kadko, D., Andersson, A. J., Langdon, C., and Bates, N. R. (2012). A multi-tracer model approach to estimate reef water residence times: a multi-tracer residence time model. *Limnol. Oceanogr. Methods* 10, 1078–1095. doi: 10.4319/lom.2012.10.1078

Watanabe, A., Kayanne, H., Hata, H., Kudo, S., Nozaki, K., Kato, K., et al. (2006). Analysis of the seawater CO_2 system in the barrier reef-lagoon system of Palau using total alkalinity-dissolved inorganic carbon diagrams. *Limnol. Oceanogr.* 51, 1614–1628. doi: 10.4319/lo.2006.51.4.1614

Wei, G., Wang, Z., Ke, T., Liu, Y., Deng, W., Chen, X., et al. (2015). Decadal variability in seawater pH in the West Pacific: Evidence from coral d11B records. *J. Geophys. Res. Oceans* 120, 7166–7181. doi: 10.1002/2015JC011066

Yeakel, K. L., Andersson, A. J., Bates, N. R., Noyes, T. J., Collins, A., and Garley, R. (2015). Shifts in coral reef biogeochemistry and resulting acidification linked to offshore productivity. *Proc. Natl. Acad. Sci. U.S.A.* 112, 14512–14517. doi: 10.1073/pnas.1507021112

Zeebe, R. E., and Wolf-Gladrow, D. (2001). *CO_2 in Seawater: Equilibrium, Kinetics, Isotopes*. Houston, TX: Gulf Professional Publishing.

Zhang, Z., Falter, J., Lowe, R., and Ivey, G. (2012). The combined influence of hydrodynamic forcing and calcification on the spatial distribution of alkalinity in a coral reef system. *J. Geophys. Res. Oceans* 117:C007603. doi: 10.1029/2011JC007603

Conflict of Interest: The authors declare that the research was conducted in the absence of any commercial or financial relationships that could be construed as a potential conflict of interest.

frontiers

Supplementary Material

1 Supplementary Figures

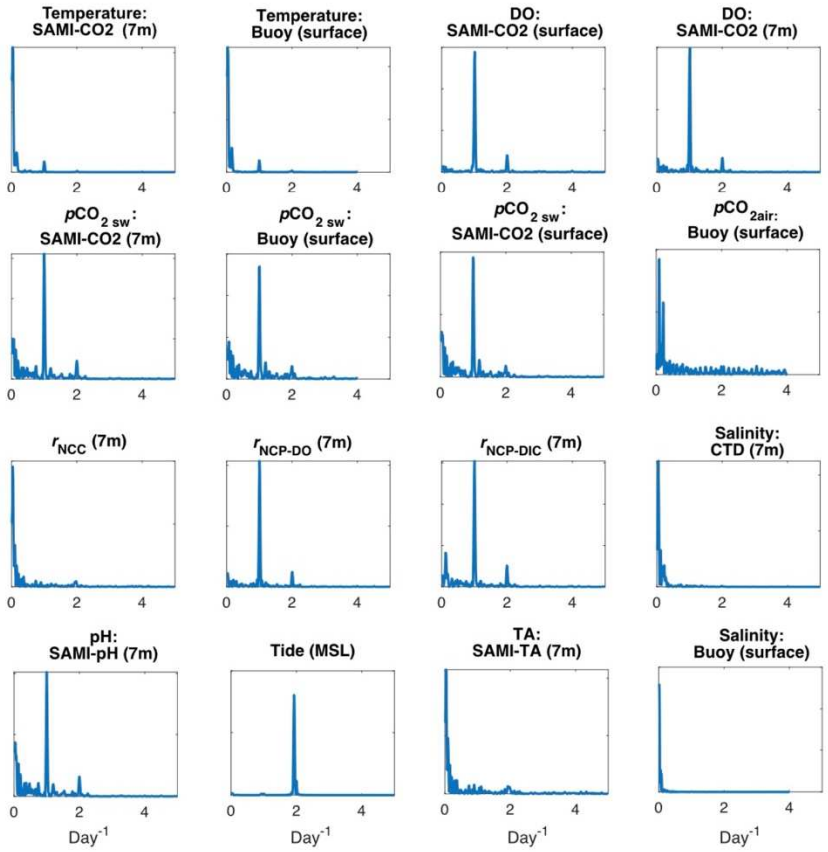

Supplementary Figure 1. Lomb-Scargle periodograms of raw (non-filtered) autonomous moored sensor parameters as well as calculated $r_{NCC\text{-}TA}$, $r_{NCP\text{-}DO}$, and $r_{NCP\text{-}DIC}$ (mean anomaly).

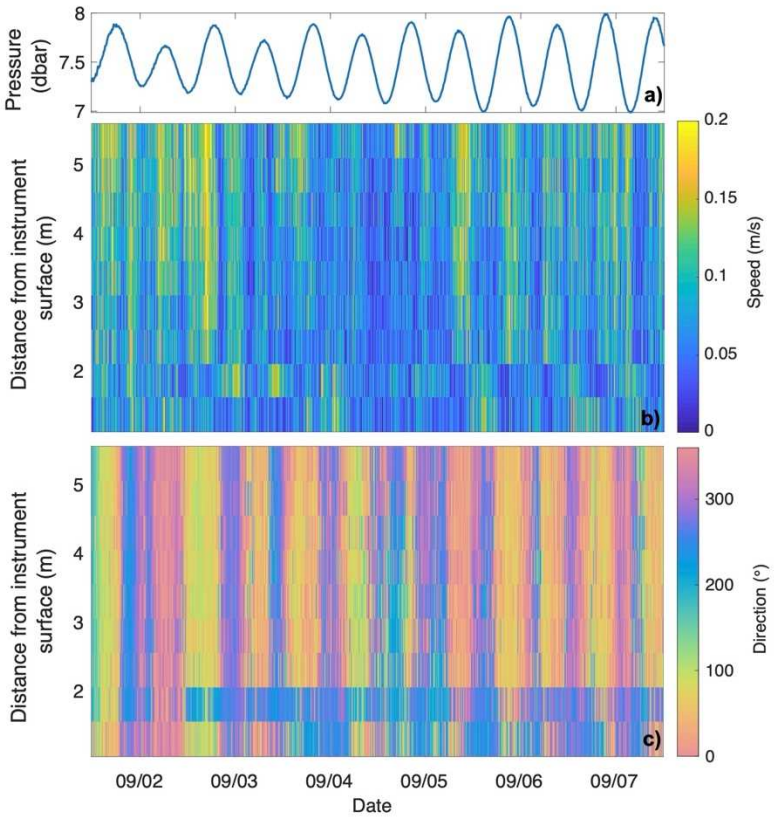

Supplementary Figure 2. Temporal variability of **(A)** pressure at the instrument face, **(B)** current speed, and **(C)** current direction over the deployment period throughout depth from the ADCP.

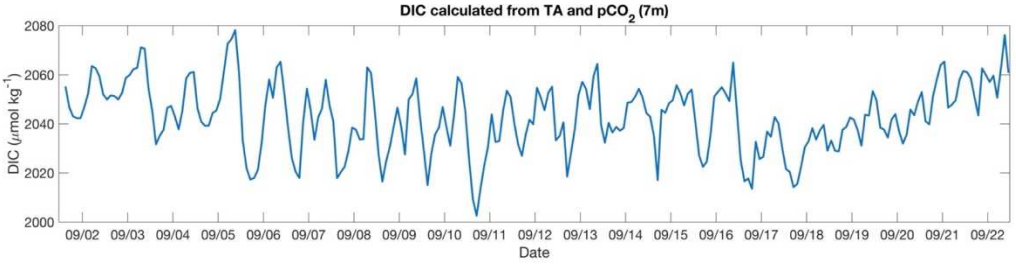

Supplementary Figure 3. Dissolved inorganic carbon (DIC) calculated from total alkalinity (TA) from the SAMI-TA and pCO_2 from the SAMI-CO2 measured at 7m.

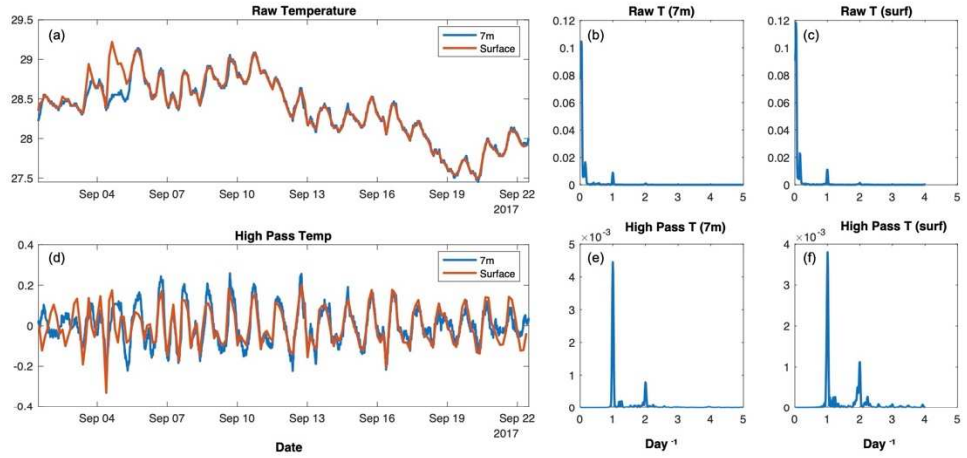

Supplementary Figure 4. (a) Time series of raw temperature data at 7m (blue) and surface (orange); (b,c) Lomb-Scargle periodograms of raw (non-filtered) temperature at 7m and surface; (d) time series of temperature data with a highpass filter at 7m and surface; and (e,f) Lomb-Scargle periodograms of filtered temperature at 7m and surface.

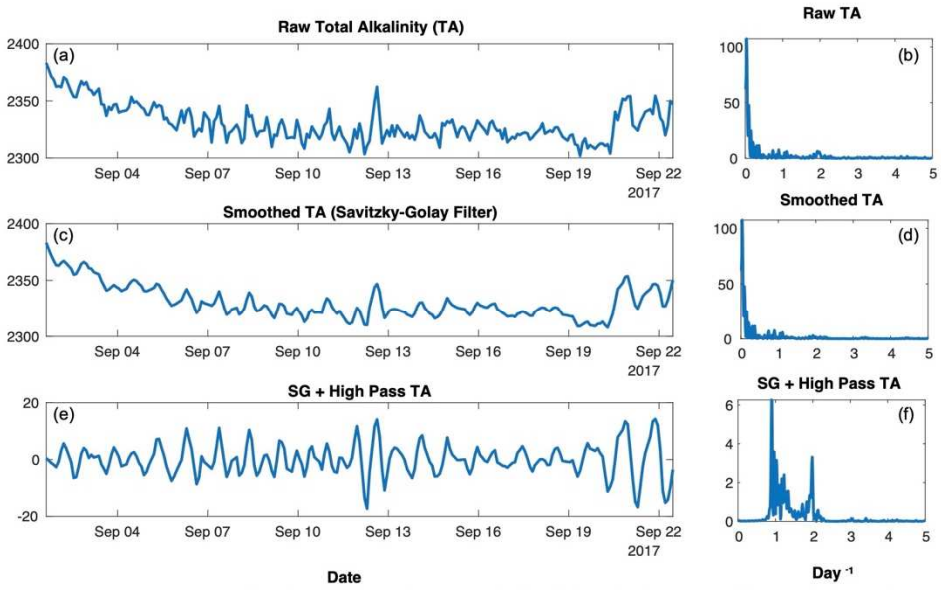

Supplementary Figure 5. (a) Time series of raw total alkalinity (TA) at 7m; (b) Lomb-Scargle periodogram of raw (non-filtered) TA; (c) time series of TA smoothed with a Savitzky-Golay filter; (d) Lomb-Scargle periodogram of smoothed TA; (e) time series of smoothed TA with a high pass filter; and (f) Lomb-Scargle periodogram of smoothed and filtered TA.

3

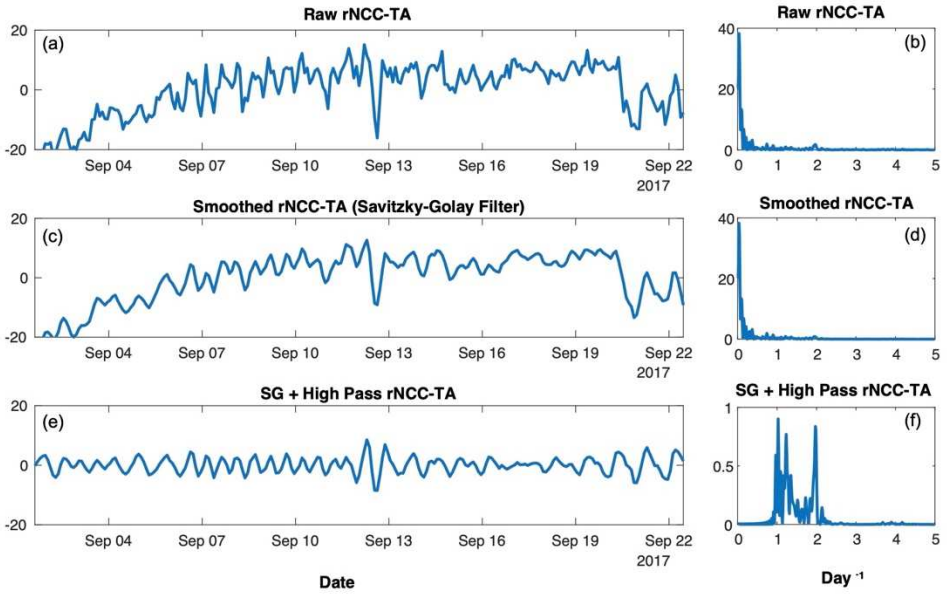

Supplementary Figure 6. (a) Time series of raw $r_{NCC\text{-}TA}$ (mean anomaly); (b) Lomb-Scargle periodogram of raw (non-filtered) $r_{NCC\text{-}TA}$; (c) time series of $r_{NCC\text{-}TA}$ smoothed with a Savitzky-Golay filter; (d) Lomb-Scargle periodogram of smoothed $r_{NCC\text{-}TA}$; (e) time series of smoothed $r_{NCC\text{-}TA}$ with a high pass filter; and (f) Lomb-Scargle periodogram of smoothed and filtered $r_{NCC\text{-}TA}$.

ACKNOWLEDGEMENTS

Chapter 2, in full, is a reprint of the material as it appears in Lateral, vertical, and temporal variability of seawater carbonate chemistry at Hog Reef, Bermuda. Pezner, Ariel K.; Courtney, Travis A.; Page, Heather N.; Beatty, Cory M.; DeGrandpre, Michael D.; Andersson, Andreas J., Frontiers in Marine Science, 2021. The dissertation author was the primary investigator and author of this paper.

CHAPTER 3: Global coral reefs will experience moderate to severe hypoxia before the end of the century

Ariel K. Pezner, Travis A. Courtney, Hannah C. Barkley, Wen-Chen Chou, Hui-Chuan Chu, Samantha M. Clements, Tyler Cyronak, Michael D. DeGrandpre, Samuel A. H. Kekuewa, David I. Kline, Yi-Bei Liang, Todd R. Martz, Satoshi Mitarai, Heather N. Page, Max S. Rintoul, Jennifer E. Smith, Keryea Soong, Yui Takeshita, Martin Tresguerres, Yi Wei, Kimberly K. Yates, Andreas J. Andersson

Abstract: Declining dissolved oxygen concentrations in coastal waters are predicted to threaten marine ecosystems globally. However, current and future oxygen concentrations and the occurrence of hypoxic events on coral reefs remain underexplored. Here, we report present-day hypoxia exposure and modeled changes in hypoxic event duration, frequency, intensity, and severity under future warming at 32 representative reef sites. 84% of these reefs experienced weak to moderate ($\leq$153 μmol kg^{-1}) hypoxia and 13% experienced severe ($\leq$61 μmol kg^{-1}) hypoxia during our observations, demonstrating that hypoxia is already pervasive on some reefs at present-day. Projected ocean warming will increase the total duration, intensity, and severity of hypoxia on coral reefs, with more than 94% and 31% of these reefs experiencing weak to moderate and severe hypoxia, respectively, by 2100 under a high-end warming scenario. These projected increases in hypoxia duration, intensity, and severity could have serious consequences for many coral reef taxa worldwide.

Earth's global ocean has been steadily losing oxygen due to warming-induced decreases in oxygen solubility, accelerated respiration, increases in water column stratification, and coastal eutrophication (*1-3*). Since the 1950s, the open ocean has lost more than 2% of its dissolved oxygen, oxygen minimum zones have expanded and shoaled, and hundreds of coastal sites have reported severe hypoxic conditions (*1, 3-5*). These trends will continue in the future, as ocean surface oxygen concentrations are projected to decrease by an additional 3.2 to 3.7% by 2100, with these changes expected to emerge across 59 to 80% of the ocean by 2050 (*4*). While trends of deoxygenation in the open ocean and the occurrence of temperate hypoxic and anoxic zones are relatively well-documented (*1-3*), there has been less focus on tropical coastal ecosystems such as coral reefs (*6-8*) despite mounting evidence that modern hypoxic events can lead to mass mortality of coral reef taxa (e.g., *6-9*).

Traditionally, coral reefs have been assumed to be well-oxygenated systems and historically, autonomous, high-frequency dissolved oxygen measurements have not been included in reef monitoring efforts (*6-8*). As a result, there is a paucity of high-quality dissolved oxygen measurements from tropical coral reefs and a high likelihood that the occurrence of hypoxia on tropical coral reefs across the globe has been severely underreported (*6*). Acute, severe hypoxic events can be induced on tropical coral reefs through a variety of physical and biological mechanisms such as warming, restricted water flow, increased biological oxygen demand, nutrient and organic matter loading, and/or an influx of oxygen deficient water (*6-9*). As global temperatures continue to rise and marine heatwaves become more frequent and severe (*10*), hypoxic events on coral reefs are likely to become more common as a result of changes in oxygen solubility and biological oxygen demand (*11*). Given the essential role of oxygen in driving aerobic metabolism, hypoxia poses a severe threat to coral reef ecosystems and the

humans that depend on them (*3 ,4, 7, 12*). Thus, characterizing present-day oxygen concentrations and hypoxia exposure on a variety of reefs across different spatiotemporal scales is imperative for defining "normoxia" on tropical coral reefs, understanding current levels of exposure to hypoxic conditions, and for projecting future coral reef oxygen conditions under ocean warming (*7-8, 12*). To date, a number of studies have expressed grave concerns about the potential consequences of declining oxygen on coral reefs (*6-9, 12*). However, there are currently no encompassing synthesis studies characterizing the range of oxygen conditions experienced on different reefs today or how these conditions will change under future warming.

In the present study, we leveraged autonomous sensor data from 32 representative reef site deployments at 12 locations around the globe (Fig. 3.1A, 3.S1, Table 3.S1) to quantify present-day oxygen conditions and hypoxia exposure at a diverse subset of reefs. We also modeled the effect of future warming scenarios on the oxygen solubility and the biological oxygen demand for each site and location to calculate changes in oxygen availability and hypoxic event frequency, duration, intensity, and severity by the year 2100 (See Online Methods). The observational data presented here include reef sites between 23 ºS and 32 ºN in the East and South China Sea; North Atlantic; West, Central, and South Pacific; and Caribbean (Fig. 3.1A). Deployment lengths ranged from 3 to 309 days and occurred between 2015 and 2019 across seasons (Table 3.S1; see Supplementary Materials for detailed site characterization and deployment information.). Oxygen data were recorded at sites ranging from 0.5 to 17 m in depth from a variety of coral reef habitat types (e.g., seagrass-dominated, reef flat, lagoon, patch reef, forereef, and reef crest; Table 3.S1).

Results

Global variability in baseline dissolved oxygen concentration

We observed a large range of oxygen conditions among the different reef habitats, with diel oxygen variability, means, and extremes differing between reef habitats at the same location, as well as between study locations in different regions (Fig. 3.1B-C, 3.S1, Table 3.S3). The mean daily dissolved oxygen concentration across all sites were 173 ± 28 μmol kg^{-1} (mean ± 1 SD) or 88 ± 13 expressed as percent saturation. The mean daily range was 81 ± 52 μmol kg^{-1} (42 ± 28 % saturation) whereas the mean daily minimum oxygen concentration was 136 ± 40 μmol kg^{-1} (69 ± 20 % saturation) and the mean daily maximum was 217 ± 39 μmol kg^{-1} (111 ± 20 % saturation), with large variations between reef locations (Fig. 3.1, 3.2A, Table 3.S3). The smallest mean daily range in oxygen concentration and percent saturation (23 ± 4 μmol kg^{-1} and 12 ± 2 %, respectively) was observed at the forereef in Tutuila, which was one of the deeper sites (15.2 m depth) and directly connected with the surrounding open ocean. In contrast, the largest mean daily range (258 ± 11 μmol kg^{-1} and 139 ± 5 %, respectively) was observed at Taiping 1, which was a shallow (0.5 m) nearshore reef area dominated by seagrass and scattered coral colonies. Oxygen was typically lowest in the early morning at all locations, and highest in the mid-afternoon as a result of nighttime respiration and daytime photosynthesis, respectively (Fig. 3.1B).

Pervasive hypoxia under present-day conditions

While many studies use a threshold of ≤ 2 mg L^{-1} (~61 μmol kg^{-1} depending on seawater density) to define hypoxic conditions, dissolved oxygen thresholds vary as a function of taxa, exposure time, life stage, temperature, and other factors (*8, 13-18)*. Evidence from the few experiments conducted on tropical reef taxa suggests lethal thresholds in reef taxa can be as high

as 4 mg L^{-1} (*16*) and sublethal hypoxia thresholds can be even higher for some species, especially under warming (*15, 18-19*). Thus, a threshold of 2 mg L^{-1} (61 μmol kg^{-1}) may not accurately capture the range of all the potential sublethal and lethal impacts of hypoxia for all reef species. In our analyses, we employed four hypoxia thresholds: "weak hypoxia" of ≤ 5 mg L^{-1} (153 μmol kg^{-1}), a conservative threshold that captures 90% of observed sublethal impacts in temperate benthic marine organisms (*14*), "mild hypoxia" of ≤ 4 mg L^{-1} (122 μmol kg^{-1}), "moderate hypoxia" of ≤ 3 mg L^{-1} (92 μmol kg^{-1}), and "severe hypoxia" as the conventional ≤ 2 mg L^{-1} (61 μmol kg^{-1}) threshold (see Online Methods).

Based on these thresholds, we found that many reef sites already experience oxygen stress. Nearly all reefs in our study (84 %) experienced weak hypoxia, 50 % experienced mild hypoxia, 34 % experienced moderate hypoxia, and 13 % experienced severe hypoxia at some point during the data collection period (Fig. 3.1B-C, 3.2A-E). Across all sites, we identified 1,198 weak hypoxic events lasting 0.5 to 64 hours across all sites and 229 mild to moderate events lasting up to 18 hours (Fig. 3.2B-E). Weak to moderate hypoxic events lasting less than 12 hours were most common, whereas those lasting 12 to 24 hours or more than 24 hours were comparatively rarer (Fig. 3.2B-E). Severe hypoxic events were less common (19 events), observed at only 4 sites, with the longest event being 7.5 hours in duration (Fig. 3.2B-E). The majority of hypoxic observations, regardless of threshold, occurred in the early morning between 2:00 and 7:00 h due to net nighttime respiration (Fig. 3.3).

Hypoxia projections under warming by 2100

To project future changes in oxygen concentrations and resultant hypoxia exposure at each reef site, we employed location-specific projections of ocean warming by the year 2100 to

calculate the cumulative effects of warming on oxygen solubility and biological oxygen demand. Warming projections were adopted from the Coupled Model Intercomparison Project 6 Shared Socio-economic Pathways (Fig. 3.S2, Table 3.S4) – SSP1-2.6 (+0.3 ºC to +1.1 ºC), SSP2-4.5 (+1.1 ºC to +3.4 ºC), SSP3-7.0 (+1.8 ºC to +3.3 ºC), and SSP5-8.5 (+2.8 ºC to +4.1 ºC) from the Community Earth System Model Whole Atmosphere Community Climate Model (See Online Methods) – and a severe, acute heatwave scenario of +6 ºC (*20*). The effect on oxygen solubility was calculated based on thermodynamic principles while the effect on biological oxygen demand was approximated from nighttime respiration signals and a temperature coefficient (Q_{10}) (See Online Methods, Fig. 3.S3, 3.S4).

Our calculations reveal that under the SSP1-2.6 scenario, the number of reef sites assessed in this study experiencing weak hypoxia by the year 2100 would be similar to present-day observations (84%), increasing to 94 % under SSP5-8.5 and 97 % during a 6 ºC heatwave event (Fig. 3.2A, Table 3.S5). Mild and moderate hypoxia would increase from 59 % and 34% of sites, respectively, under SSP1-2.6, to 72 % and 44 % of sites under the SSP5-8.5 scenario (Fig. 3.2A, Table 3.S5) and 75 % and 53 % during a 6 ºC heatwave. Further, under the SSP1-2.6 scenario, 19 % of sites would experience severe hypoxia by the year 2100, increasing to 31 % under the SSP5-8.5 scenario and 34 % during a 6 ºC heatwave event (Fig. 3.2A, Table 3.S5).

Overall, the total number of hypoxic observations will increase for all warming scenarios ranging from an increase of 13 % to 42 % under SSP1-2.6 and 97 % to 287 % under SSP-8.5 (Fig. 3.2F, 3.S5). As a result, the frequency, duration, intensity (i.e., the difference between a threshold and an observation concentration; *21*), and severity (average intensity multiplied by duration; *21*) of hypoxic events crossing each threshold will also increase (See Online Methods, Fig. 3.2, 3.S5-7, Table 3.S5). These projections suggest a shift from more acute to more chronic

hypoxia exposure under increasing warming, the magnitude of which will depend on future atmospheric CO_2 concentrations and the relevant thresholds of hypoxia tolerance for reef taxa (Fig. 3.2, 3.S5-7, Table 3.S5).

Discussion

Understanding what changing oxygen dynamics on coral reefs means for corals and reef ecosystems requires urgent attention from the research community. Field data from previous severe hypoxic events on coral reefs report extremely variable responses of different coral genera (*7*), revealing both sensitive (e.g., *Acropora* and *Pocillopora spp.*) and tolerant (e.g., *Porites spp.*) groups (*6, 22-24*). Similarly, data from the relatively few laboratory hypoxia experiments reveal a wide range of species-specific tolerances to hypoxia intensity and duration, with mortality occurring in fewer than 3 days at oxygen concentrations as high as 4 mg L^{-1} (~122 μmol kg^{-1}) for *Acropora yongeii* (*16*) and after 7 days at as low as 0.5 mg L^{-1} (~15 μmol kg^{-1}) for *Stephanocoenia intersepta* (*6*). In contrast, *Orbicella faveolata* survived more than 11 days at 1 mg L^{-1} (~31 μmol kg^{-1}) with no signs of stress *(17*), suggesting some species or populations may be particularly resilient to oxygen stress. Physiologically, some coral species may be able to cope with varying degrees of hypoxia by increasing anaerobic respiration (*25*) and engaging transcriptional hypoxia-response systems (*26*). However, these strategies may not be equally effective for all corals or sustainable under repeated stress or longer hypoxic events. Studies of coral larvae and recruits demonstrate that hypoxic conditions can impair coral settlement (*27*) and survivorship of coral recruits (*28*), further limiting ecosystem recovery under repeated or long-term hypoxic conditions.

Hypoxia tolerance also varies between reef-associated organisms by orders of magnitude, with some thresholds well above the standard 2 mg L^{-1}. A 2008 meta-analysis of temperate species found molluscs and anemones were the most tolerant to hypoxia whereas crustaceans and fish were the most sensitive (*14*). Aside from direct mortality, hypoxic conditions can lead to changes in behavior, feeding, respiration, reproduction, and/or general performance, which can scale up to impair ecosystem function through loss or migration of key species (*7, 29*). It is also important to understand the tolerance of photosynthetic organisms to hypoxia, as a reduction in photosynthetic activity during the day will have implications for the mean and extreme oxygen conditions on the reef (*7*).

Notably, oxygen loss and hypoxic events are not occurring in isolation from other stressors. Oxygen and temperature are tightly linked in terms of organism metabolism and together may severely limit species performance and restrict habitats that are metabolically viable (*15, 30-32*). For tropical corals, there is evidence that hypoxia exposure and tolerance are related to bleaching susceptibility (*26*). In addition, hypoxic conditions typically co-occur with acidification, as increased respiration decreases both pH and dissolved oxygen concentrations (*32*). The combination of low oxygen and acidification stress has been shown to be mainly additive, with negative impacts across a wide range of taxa (*33*). Coastal eutrophication therefore has the capacity to intensify local hypoxia and acidification, suggesting a reduction of nutrient inputs may improve projected conditions at local scales under ongoing global change (*34*).

Here, we provide the first comprehensive synthesis of oxygen concentrations and variability as well as hypoxia frequency, intensity, severity, and duration on tropical coral reefs. Our findings suggest hypoxia is already pervasive in coral reef habitats around the world and will become more common and severe as ocean temperature increases. While these projections

are specific to the reefs and locations included in this study, the observations here provide broad representation of the different reef systems and environments found around the world. Continued and additional high frequency oxygen data measurements on coral reefs will be imperative for establishing current conditions, tracking potential hypoxic events, expanding the applicability of these predictions, and characterizing impacts on reef communities in the future. At the same time, field and laboratory experiments must aim to further refine accurate and realistic thresholds of oxygen for different coral reef organisms to better predict future impacts on reef ecology and functioning.

Online Methods

Sensor and Deployment Information

The majority of dissolved oxygen data presented in the current study (25 of 32 sites) were recorded by SeapHOx or Sea-Bird Scientific CTD sensor packages with Aanderaa oxygen optodes (Table 3.S1). The remaining oxygen datasets were recorded by Idronaut CTD and oxygen sensor packages (Dongsha 1 and Dongsha 2), Sea-Bird SBE19 Plus CTD and SBE 43 oxygen sensor packages (Baker, Jarvis, Palmyra 3, and Tutuila), or Sea-Bird Scientific CTD and PME miniDOT sensor packages (Taiping 1). Detailed site and deployment information can be found in the Supplementary Materials.

Calibrations and Conversions of Datasets

All sensors were calibrated by the manufacturer or according to manufacturer's instructions by the user as noted in previous publications *(40, 41, 43, 48, 58, 62, 64)*. If applicable, salinity

corrections were implemented according to manufacturer's specifications and analog measurements were converted from voltages to concentrations. Data were assessed for quality and erroneous data points (defined as missing values or values that exceeded the measurement range of the instrument), which were flagged and excluded from any subsequent analyses. Deployment data were restricted to measurements in seawater based on salinity values to exclude extraneous data points collected during instrument transport, initial deployment, or recovery (exposure to air). Density calculations using the Gibbs Seawater Toolbox functions *(70)* in RStudio *(71)* were used to convert all oxygen units to μmol kg^{-1}. See Supplementary Materials for an assessment and discussion on the potential errors and uncertainty of the oxygen measurements.

Calculations

Calculations of Daily Statistics

The mean (Table 3.S3) and absolute daily minimum and maximum (Fig. 3.2A, Table 3.S3) as well as the mean daily range (Table 3.S3) were calculated for each site. These calculations excluded partial days of data (i.e., the first and last days of the deployment were excluded to avoid bias) to ensure means and extremes were calculated over full 24-hour cycles. See code file "PeznerMS.R" [GitHub link to be inserted prior to publication].

Calculations of Intensity, Duration, and Severity

The intensity (*I*), duration (*D*), and severity (*S*) of hypoxic observations and events were calculated by modifying a methodology applied to seawater aragonite saturation states by Hauri et al. (*21*) according to Equations (1-3). Prior to calculations, datasets that were not at a 30-

minute sampling frequency were either subsampled (Dongsha 1, Dongsha 2, Hog 1a, Hog 1b, Dongsha 3, Okinawa 2, Okinawa 3, Taiping 1, Taiping 2, Tutuila, Baker, Jarvis, Palmyra 3) or interpolated (Crocker 1a, 1b, 1c; Palmyra 1b) to a 30-minute sampling frequency to standardize comparisons across datasets. Linear interpolations were performed using the approx() function in RStudio (*71*).

For individual hypoxic observations, the intensity (I_{obs}; µmol kg^{-1}) was calculated as the difference between the observed oxygen concentration (DO_{obs}; µmol kg^{-1}) and a determined threshold of hypoxia (T; µmol kg^{-1}):

$$I_{obs} = T - DO_{obs} \quad \text{(Equation 1)}$$

For hypoxic events, consecutive observations below a given oxygen threshold were identified using the rleid() function of the data.table package (*77*) in RStudio (*71*; see "PeznerMS.R" code file). Intensity of the event (I_{event}; µmol kg^{-1}) was calculated as the difference between the mean oxygen concentration during the event (DO_{event}) and the threshold (T):

$$I_{event} = T - \overline{DO_{event}} \quad \text{(Equation 2)}$$

Severity of the event (S; µmol kg^{-1} hr) was calculated as the product of the event intensity (I_{event}) and duration (D; hours) (*21*):

$$S = D * I_{event} \quad \text{(Equation 3)}$$

For these calculations, we used four hypoxia thresholds: 153 μmol kg^{-1} (~ 5 mg L^{-1}), 122 μmol kg^{-1} (~ 4 mg L^{-1}), 92 μmol kg^{-1} (~ 3 mg L^{-1}), and 61 μmol kg^{-1} (~ 2 mg L^{-1}). While many studies use the threshold of ≤ 2 mg L^{-1} (~61 μmol kg^{-1}) to define severe hypoxic conditions, it has been shown that this threshold, originally identified as the level at which great reductions in benthic macrofauna would be observed in Northern European fjords (7*8*), is inadequate as a threshold for other marine species (*13-14, 79*). We provide the three additional thresholds to better capture a range of organism sensitivities to both lethal and sublethal impacts. Based on Vaquer-Sunyer and Duarte (*14*), we chose a "weak" hypoxia threshold of 153 μmol kg^{-1} (~ 5 mg L^{-1}) as the upper bound of our thresholds, as it is the oxygen concentration that captured 90% of sublethal impacts in temperate benthic marine organisms. We also added thresholds at regular intervals, with a "mild" hypoxia threshold of 122 μmol kg^{-1} (~ 4 mg L^{-1}; an upper bound of lethal oxygen levels determined for the tropical coral *Acropora yongeii*; *16*) and a "moderate" hypoxia threshold of 92 μmol kg^{-1} (~ 3 mg L^{-1}). Calculations of intensity (for events and observations), duration of events, and severity of events were performed for each threshold (Fig. 3.2B-F, 3.S5-7).

CMIP6 Temperature Projection Data

We extracted predicted sea surface temperature (SST) rise values for each location (Fig. 3.S2) from the Coupled Model Intercomparison Project 6 (CMIP6) ensemble member Community Earth System Model Whole Atmosphere Community Climate Model (CESM2-WACCM) (*5, 80-81*). The model was run by the National Center for Atmospheric Research (NCAR) in 2018, with a 0.9º × 1.25º finite volume grid atmosphere with 70 levels coupled with 320 × 384

longitude/latitude ocean with 60 levels (*80-81*). The model used the Historical, SSP1-2.6, SSP2-4.5, SSP3-7.0, and SSP5-8.5 simulations (*5, 80-81*). Monthly SST data from the closest grid cell to each location's latitude and longitude were averaged and compared between present day (mean of the 2015–2020 annual SST) and end of century (mean of 2090–2100 annual SST) to calculate anticipated increase in temperature by 2100 (Table 3.S4). This methodology was used so that the warming estimates would be less dependent on year-to-year climate variability events. See code file "CMIP6_SST_DO_sites.R" for full code used to extract and process these data.

Predicting Changes in Dissolved Oxygen as a Result of Temperature Rise

We calculated changes in DO concentrations as a result of the physical and biological impacts of temperature rise on DO solubility and biological oxygen demand (i.e., total respiration rates), respectively, based on measured DO at each reef site and the projected CMIP6 temperature rise for each location. A simple box model was also used to validate the methodology and calculations used to approximate changes in DO solubility and biological oxygen demand (See Supplementary Material).

Calculating the Impact of Warming on Solubility

Changes in DO solubility were calculated for each site under each climate projection (DO_{sol_SSP126}, DO_{sol_SSP245}, DO_{sol_SSP370}, DO_{sol_SSP585}) and a 6 ºC heatwave scenario ($DO_{sol\_heatwave}$) using Equations 4–5 (*82*) assuming only changes in temperature:

$$T_s = \log\left(\frac{(298.15 - t)}{(273.15 + t)}\right) \qquad \text{(Equation 4)}$$

$$\ln(DO_{sol}) = A_0 + A_1 T_s + A_2 T_s^2 + A_3 T_s^3 + A_4 T_s^4 + A_5 T_s^5 + S(B_0 + B_1 T_s + B_2 T_s^2 + B_3 T_s^3) + C_0 S^2 \quad \text{(Equation 5)}$$

where t is temperature (ºC), T_s is the scaled temperature, DO_{sol} is the solubility (µmol kg^{-1}), A_0 is 5.80818, A_1 is 3.20684, A_2 is 4.11890, A_3 is 4.93845, A_4 is 1.01567, A_5 is 1.41575, B_0 is -7.01211e-03, B_1 is -7.25958e-03, B_2 is -7.93334e-03, B_3 is -5.54491e-03, C_0 is -1.32412e-07, and S is salinity (PSU).

Changes in DO concentration as a result of changes in solubility (ΔDO_{sol}) due to warming from present day were then calculated for each site and projection:

$$\Delta DO_{sol} = DO_{sol\,present} - DO_{sol\,proj} \quad \text{(Equation 6)}$$

where $DO_{sol\_present}$ is the solubility of DO under present-day measured temperature and salinity conditions (µmol kg^{-1}) and DO_{sol_proj} is the solubility of DO for a given temperature rise projection or scenario, calculated from Eqn. 4–5 (µmol kg^{-1}).

Calculating the Impact of Warming on Respiration

The respiration signal of each reef at present day was approximated from the difference between the mean dissolved oxygen ($\overline{DO}$; µmol kg^{-1}) across the entire deployment and the mean daily minimum dissolved oxygen concentration ($\overline{DO_{min}}$; µmol kg^{-1}), according to Equation 7:

$$DO_{offset} = \overline{DO} - \overline{DO_{min}} \quad \text{(Equation 7)}$$

Thus, DO_{offset} (μmol kg^{-1}) reflects the observed changes in DO owing to the net effect of nighttime respiration, air-sea gas exchange, and physical transport processes assuming that on average, the daily mean DO at each location is close to 100% saturation. However, since air-sea gas exchange is quantitatively small relative to respiration rates on coral reefs and the flow is from air to sea at night, gas exchange was assumed to be negligible although it leads to a slight underestimation of the respiration signal. Similarly, day-to-day changes in water transport, current speed, trajectory, and residence time could also influence the observed DO loss, but on average each site is characterized by a set of baseline conditions constrained by the tidal cycle, depth, geomorphology, wind and swell conditions, which favors the application of DO_{offset} as an approximation of the respiration signal at each location. The daily statistics of DO_{offset} were calculated excluding the first and last days of the deployment in order to exclude partial days (less than full 24-hour periods) from the mean.

To assess the biological impacts of each temperature rise scenario on biological oxygen demand, the change in respiration rate was calculated using a Q_{10} relationship according to Equations 8–9 for each site and temperature scenario:

$$T_{rise} = T_2 - T_1 \quad \text{(Equation 8)}$$

$$R_2 = R_1 * Q_{10}^{\left(\frac{T_{rise}}{10}\right)} \quad \text{(Equation 9)}$$

where T_{rise} is the difference between baseline T_1 and T_2, R_2 is the respiration rate under increased temperature T_2, R_1 is the respiration rate at present temperature (T_1), and Q_{10} is the unitless metabolic quotient (*83-84*). In the present study, we assumed a Q_{10} of 2 (i.e., metabolic rate, in this case respiration, doubles for every temperature increase of 10 ºC), based on the literature for coral metabolism (*85-89*). However, because absolute respiration rates were unknown (i.e., R_1), the reduction in DO concentrations due to increased respiration under different warming scenarios was calculated based on the ratio of R_2,and R_1 and the estimated respiration signal DO_{offset} according to Equations 10–11 (Fig. 3.S3):

$$DO_{offset_{Q10}} = DO_{offset} * \left(\frac{R_2}{R_1}\right) \quad \text{(Equation 10)}$$

$$\Delta \mathrm{DO}_{Q10} = DO_{offset_{Q10}} - DO_{offset} \quad \text{(Equation 11)}$$

where DO_{offset_Q10} (µmol kg^{-1}) is the expected change in DO_{offset} (change in DO due to respiration at present) as a result of increased respiration and ΔDO_{Q10} is the decrease in DO concentration, accounting for present-day respiration rates.

Combining the Impacts of Warming on Solubility and Respiration

Combining the physical (changes in solubility) and biological (changes in respiration rate) impacts of temperature rise, expected net reduction in DO concentration for each reef site and under each scenario was calculated using Equations 12-13 (Fig. 3.S3):

$$\Delta DO = \Delta DO_{Q10} + \Delta DO_{sol} \quad \text{(Equation 12)}$$

$$DO_{proj} = DO - \Delta DO \quad \text{(Equation 13)}$$

where ΔDO (μmol kg^{-1}) is the total combined decrease in DO concentration, DO_{proj} is the projected DO concentration (μmol kg^{-1}) for each site and under each warming scenario, and DO is the present-day measured DO concentration at each site (μmol kg^{-1}).

Acknowledgments: We thank Kazumi Inoha, Rong-Wei Syu, and all field station administrators and field assistants who were essential in collecting these datasets.

Funding:

National Science Foundation OCE-1255042 (AJA)

National Science Foundation OCE-1829778 (AJA)

UCSD Marine Sciences Grant #A105437 (AJA)

National Science Foundation Graduate Research Fellowship DGE-2038238 (AKP)

Philanthropic Educational Organization (P.E.O.) International Scholar Award (AKP)

NOAA Coral Reef Conservation Program and NOAA Ocean Acidification Program, through the NOAA National Coral Reef Monitoring Program. (HCB)

U.S. Geological Survey, Coastal and Marine Hazards and Resources Program funded data collection at Crocker Reef, Florida, USA. (KKY)

Internal funding from the Okinawa Institute of Science and Technology (SM)

National Science Foundation OCE-1538495 (DIK and MT)

National Science Foundation OCE-1459255, OPP-1723308 (MDD)

Ministry of Science and Technology of Taiwan #107-2611-M-019-001-MY3 (WCC)

Author contributions:

Conceptualization: AKP, TAC, AJA

Methodology: AKP, TAC, MSR, AJA

Investigation: AKP, TAC, HCB, WCC, HCC, SMC, TC, MDD, SAHK, DIK, YBL, TRM, SM, HNP, MSR, JES, KS, YT, MT, YW, KKY, AJA

Formal Analysis: AKP

Visualization: AKP

Writing – original draft: AKP, AJA

Writing – review & editing: AKP, TAC, HCB, WCC, HCC, SMC, TC, MDD, SAHK, DIK, YBL, TRM, SM, HNP, MSR, JES, KS, YT, MT, YW, KKY, AJA

Supervision – AJA, TAC

Competing interests: Authors declare that they have no competing interests.

Data Availability Statement:

All data included in this study (for all figures and statistics) are freely available at [Dryad link to be inserted prior to publication]. Data may be used if cited appropriately.

Code Availability Statement:

All code files written and used for analyses in this study are freely available on GitHub [GitHub link to be inserted prior to publication]. Code may be used if cited appropriately.

FIGURES

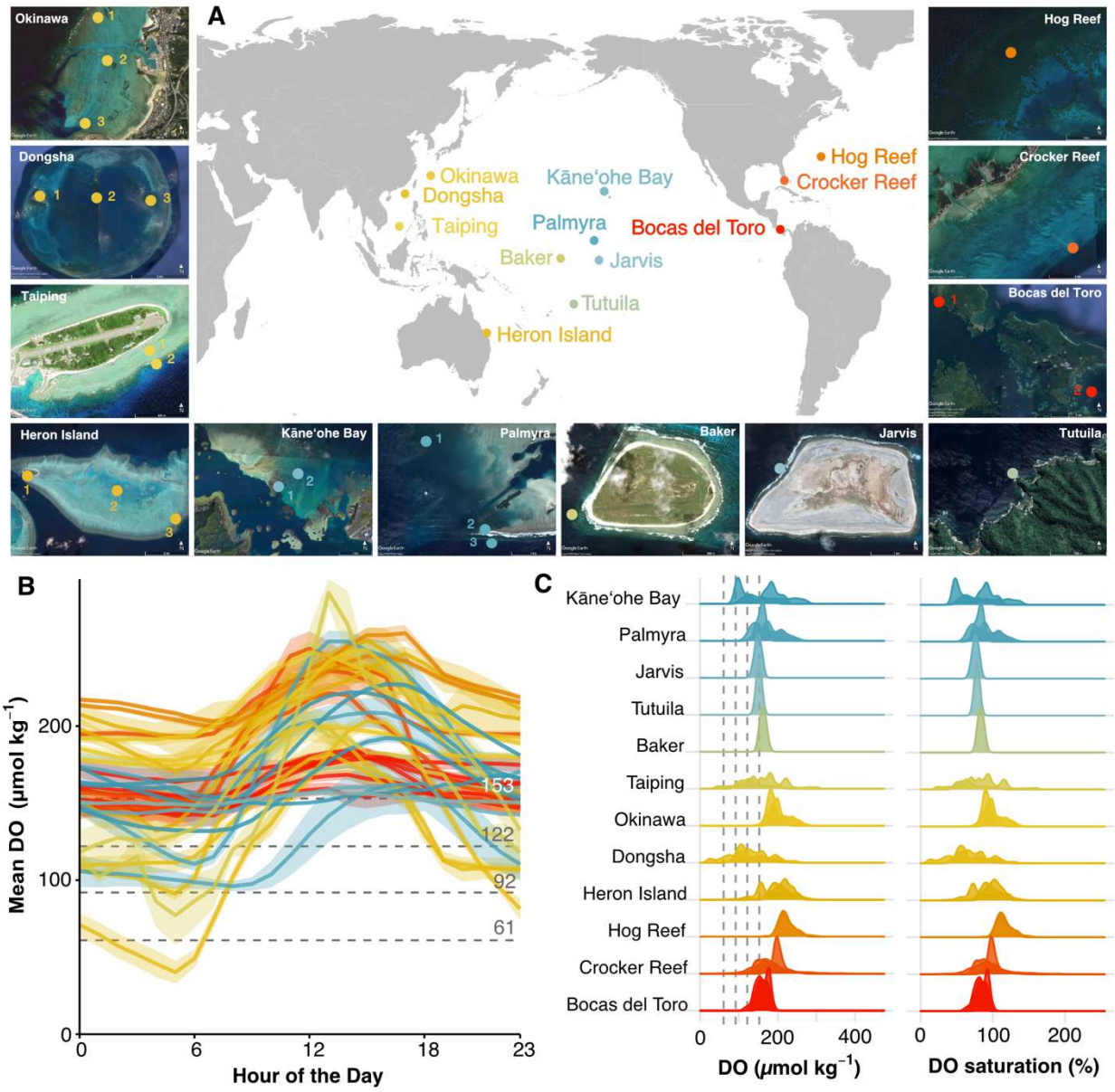

Figure 3.1: Map of deployment sites and locations, hourly oxygen climatologies, and oxygen distributions. (A) Map and satellite images (Google Earth) of each reef location including specific instrument deployment sites (circles) at each location. Some sites had instruments deployed at multiple depths (Table 3.S1). **(B)** Mean ± shaded lower and upper 95 % confidence interval of the hourly climatology of dissolved oxygen (DO) concentrations for all sites. The grey dashed lines indicate the four hypoxia thresholds: 153, 122, 92, and 61 µmol kg^{-1}. **(C)** Ridgeline distributions of dissolved oxygen concentration and percent saturation grouped by location. Vertical grey dashed lines indicate four hypoxia concentration thresholds as in **B**. In all panels the color scheme follows the location colors used in **A**.

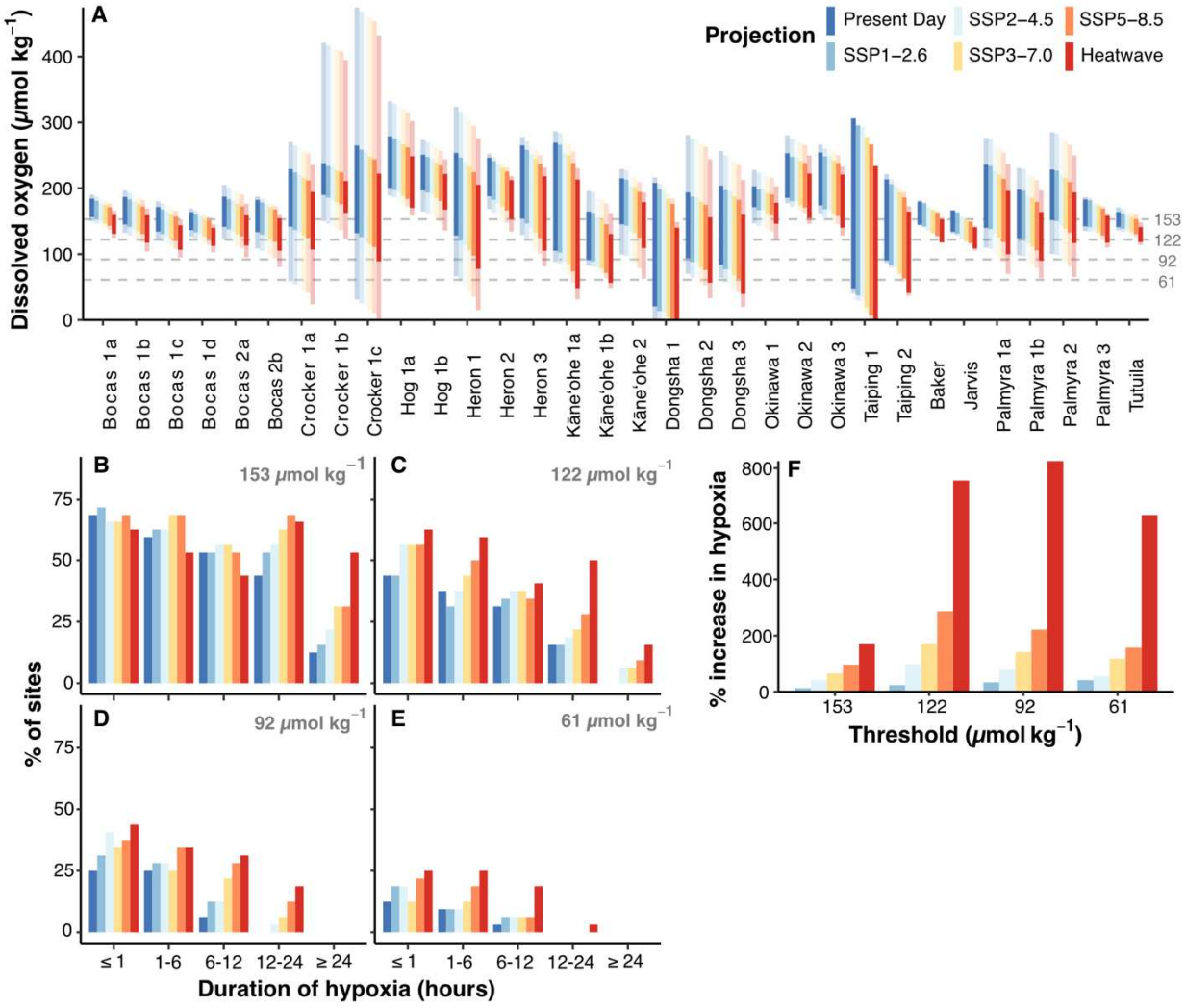

Figure 3.2: Shifts in dissolved oxygen concentration, hypoxic event duration, and occurrence of hypoxia exposure under warming. (A) Vertical dark shaded bars represent the mean daily range of dissolved oxygen for each site at present (Table 3.S3) and future temperature projections for the year 2100 (Table 3.S4). The lower and upper bounds of the vertical light shaded bars represent the lowest daily minimum oxygen and highest daily maximum oxygen concentration, respectively (Table 3.S3). The grey dashed lines indicate four hypoxia thresholds: 153 µmol kg^{-1} (weak), 122 µmol kg^{-1} (mild), 92 µmol kg^{-1} (moderate), and 61 µmol kg^{-1} (severe). **(B-E)** Percent of sites (n = 32) that experience hypoxic events of each listed duration for each warming scenario and hypoxia threshold (153, 122, 92, or 61 µmol kg^{-1}; B-E, respectively). **(F)** Percent increase in the total number of observations below each hypoxia threshold across all sites for each temperature projection relative to present day.

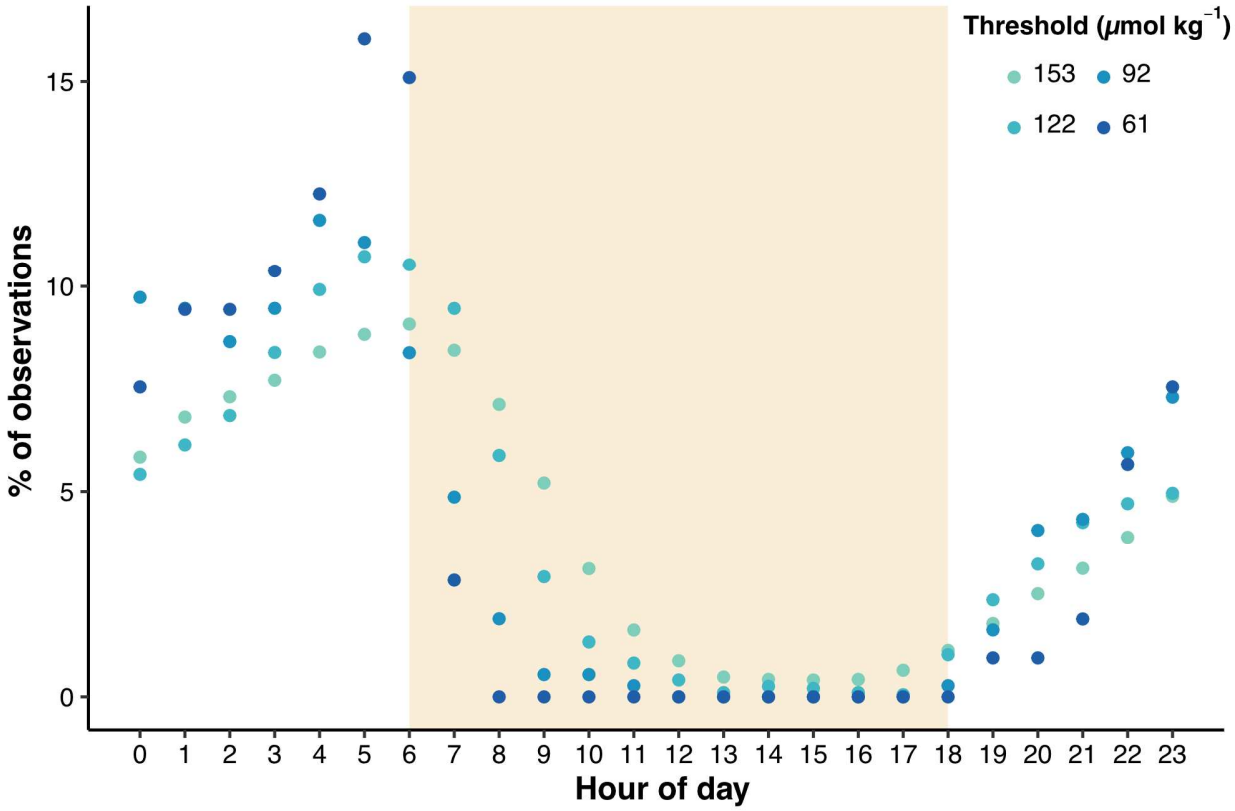

Figure 3.3: Timing of present-day hypoxic observations across all sites. Percent of recorded oxygen observations below each of the four thresholds (153, 122, 92, and 61 μmol kg^{-1}; light to dark blue) occurring at each hour of the day for all sites and deployments. Daylight hours denoted by orange shaded box (local time).

SUPPLEMENTAL FIGURES

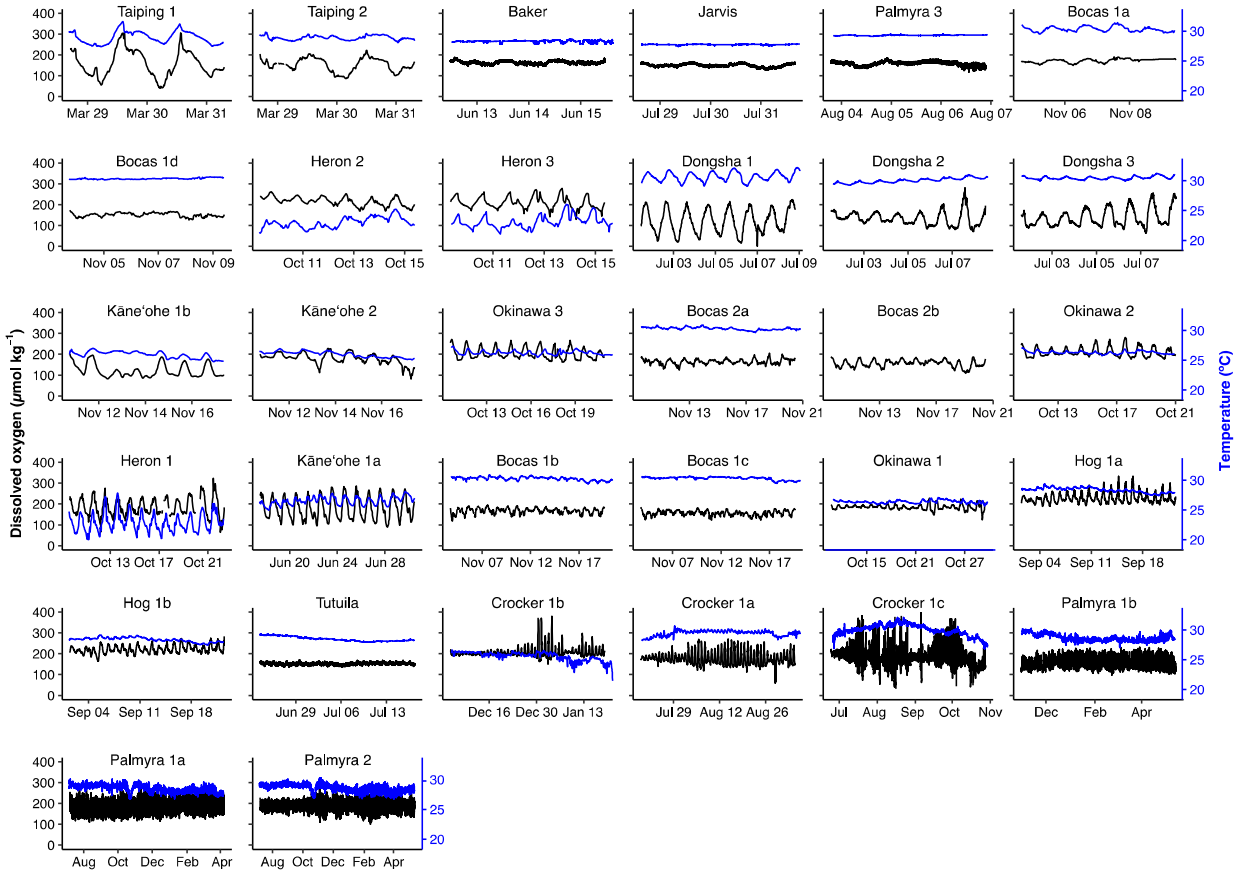

Figure 3.S1: Dissolved oxygen and temperature time series for all sites. Dissolved oxygen (µmol kg^{-1}; black, left y-axis) and temperature (ºC; blue, right y-axis) in order of sites with increasing deployment length (Table 3.S1).

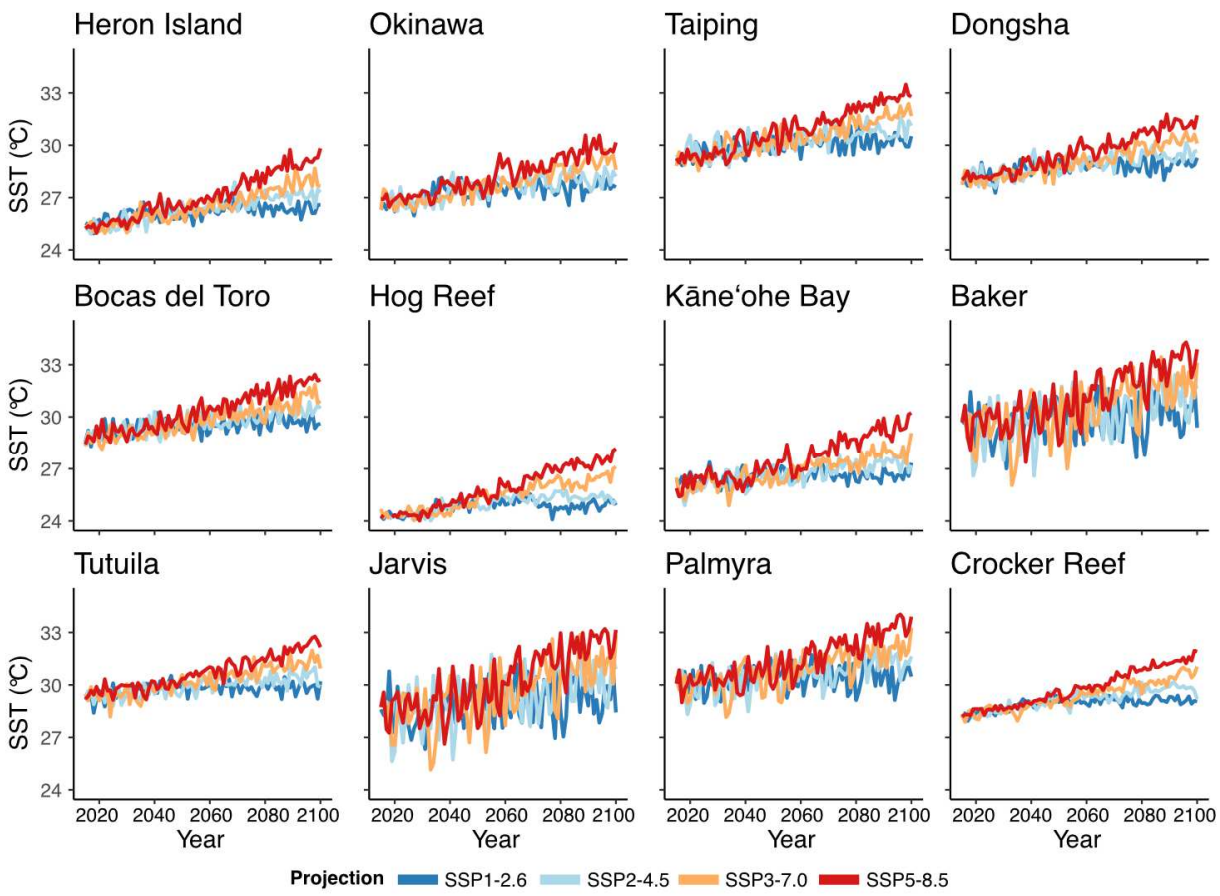

Figure 3.S2: Sea surface temperature predictions for each location. Mean monthly CMIP6 CESM2-WACCM (*80-81*) sea surface temperature (SST) projections at each study location for the SSP1-2.6, SSP2-4.5, SSP3-7.0, and SSP5-8.5 scenarios (blue to red).

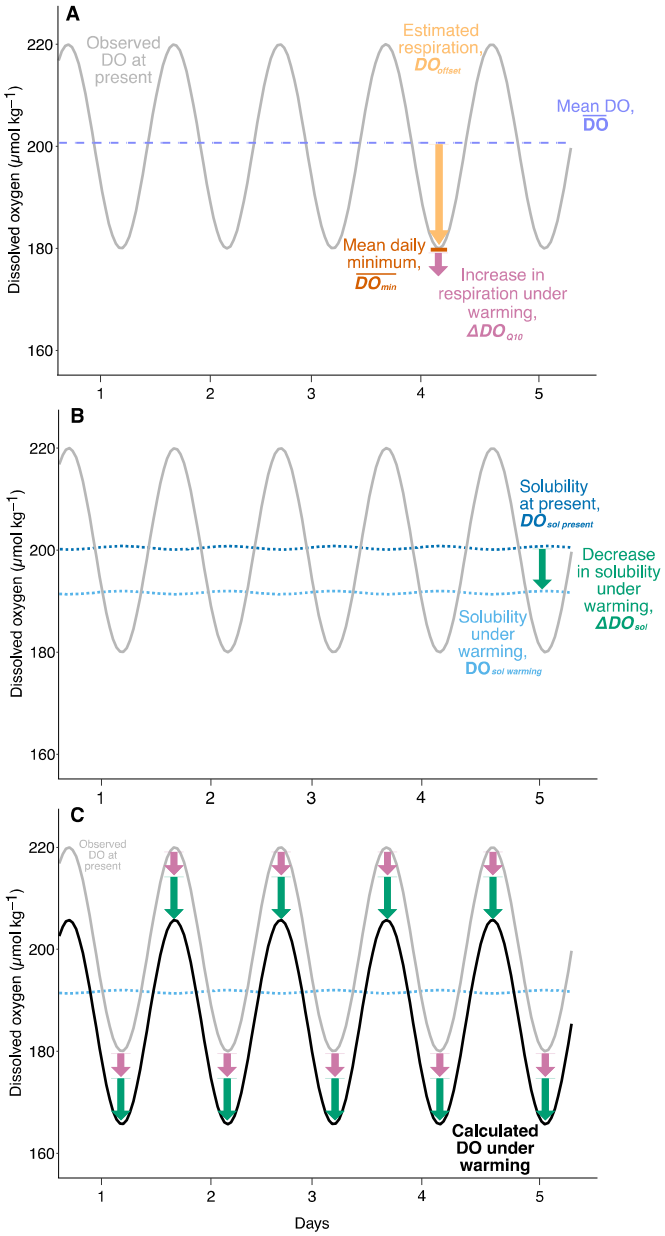

Figure 3.S3: Conceptual diagram of calculation approach used to estimate changes in coral reef dissolved oxygen under warming (Equations 6-13). (A) Present-day dissolved oxygen (DO; µmol kg^{-1}; solid grey line), mean DO value across time series (purple dashed line), estimation of drawdown of DO by respiration (DO_{offset}; yellow arrow) as the difference between mean DO and mean daily minimum (DO_{min}; orange); and increase in respiration under 3 ºC warming (ΔDO_{Q10}; pink arrow). **(B)** Present-day DO (solid grey line), present-day solubility (dashed dark blue line; $DO_{sol\ present}$), solubility of DO under 3 ºC warming (dashed light blue line), and the decrease in solubility under warming (ΔDO_{sol}; green arrow). **(C)** Present-day DO and new calculated DO under warming (black solid line) due to changes in respiration and solubility (green and pink arrows, respectively).

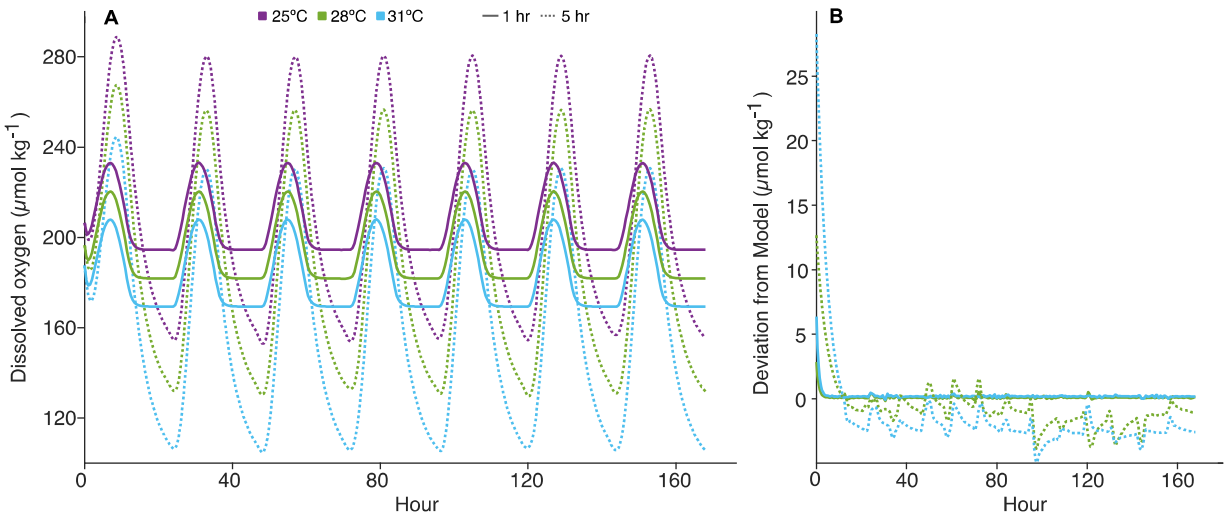

Figure 3.S4: Box model results and comparison of results to calculations. (A) Modeled decreases in dissolved oxygen concentration (µmol kg^{-1}) over 7 days under three temperature scenarios (25 ºC, 28 ºC, 31 ºC; purple, green, blue, respectively) and two residence times (1 hour and 5 hours; solid and dotted lines, respectively). **(B)** Deviation of calculations used in the present study to model decreases in oxygen as a result of warming from box model output using data in A under two warming scenarios (+3 ºC and +6 ºC; blue and green, respectively) and two residence times (1 hour and 5 hours; solid and dotted, respectively).

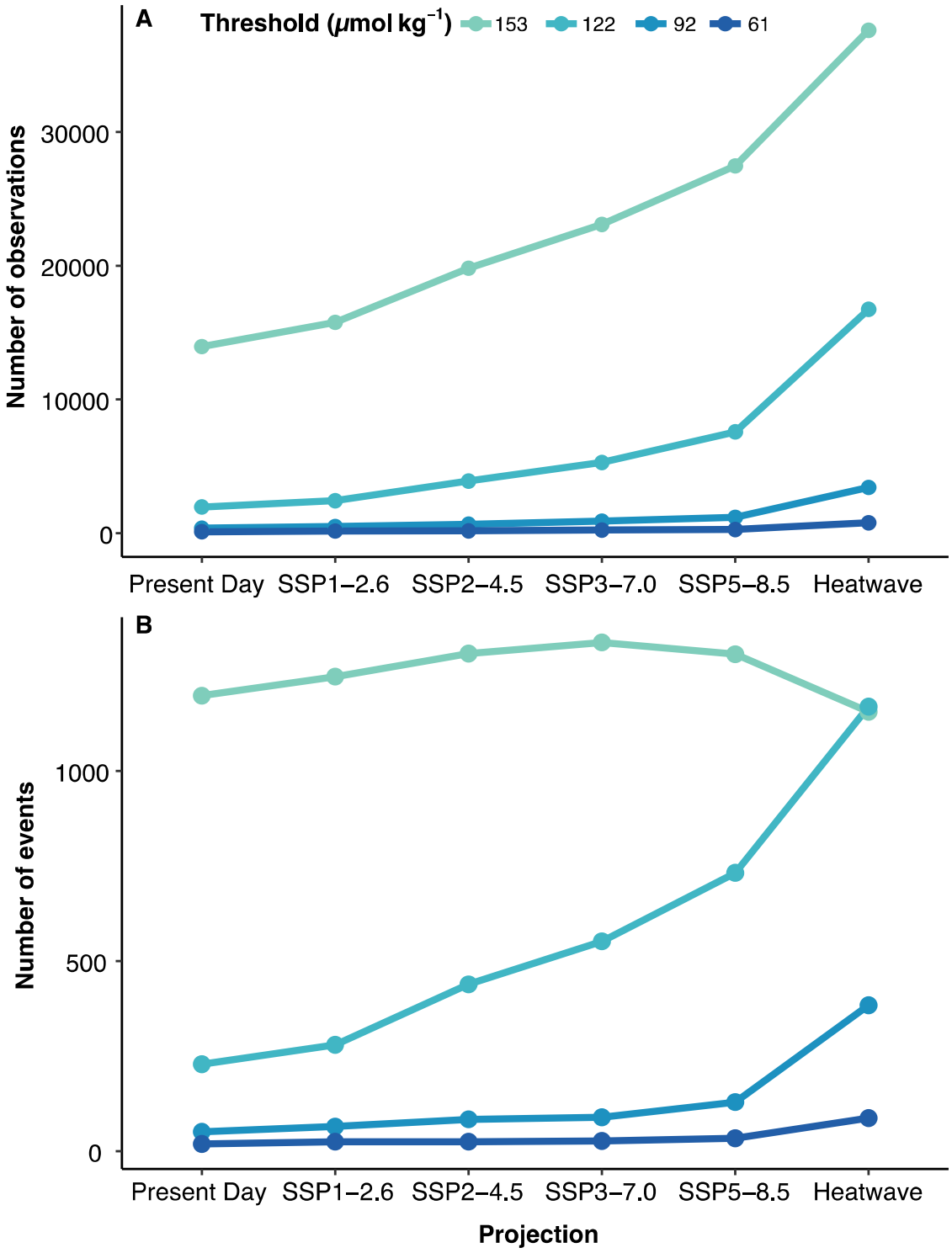

Figure 3.S5: Change in number of hypoxic observations and events under warming. (A) Change in number of observations below each oxygen threshold: 153 µmol kg^{-1}, 122 µmol kg^{-1}, 92 µmol kg^{-1}, and 61 µmol kg^{-1} (weak, mild, moderate, and severe; shades of blue) and **(B)** Change in number of hypoxic events for each warming projection and threshold across all sites.

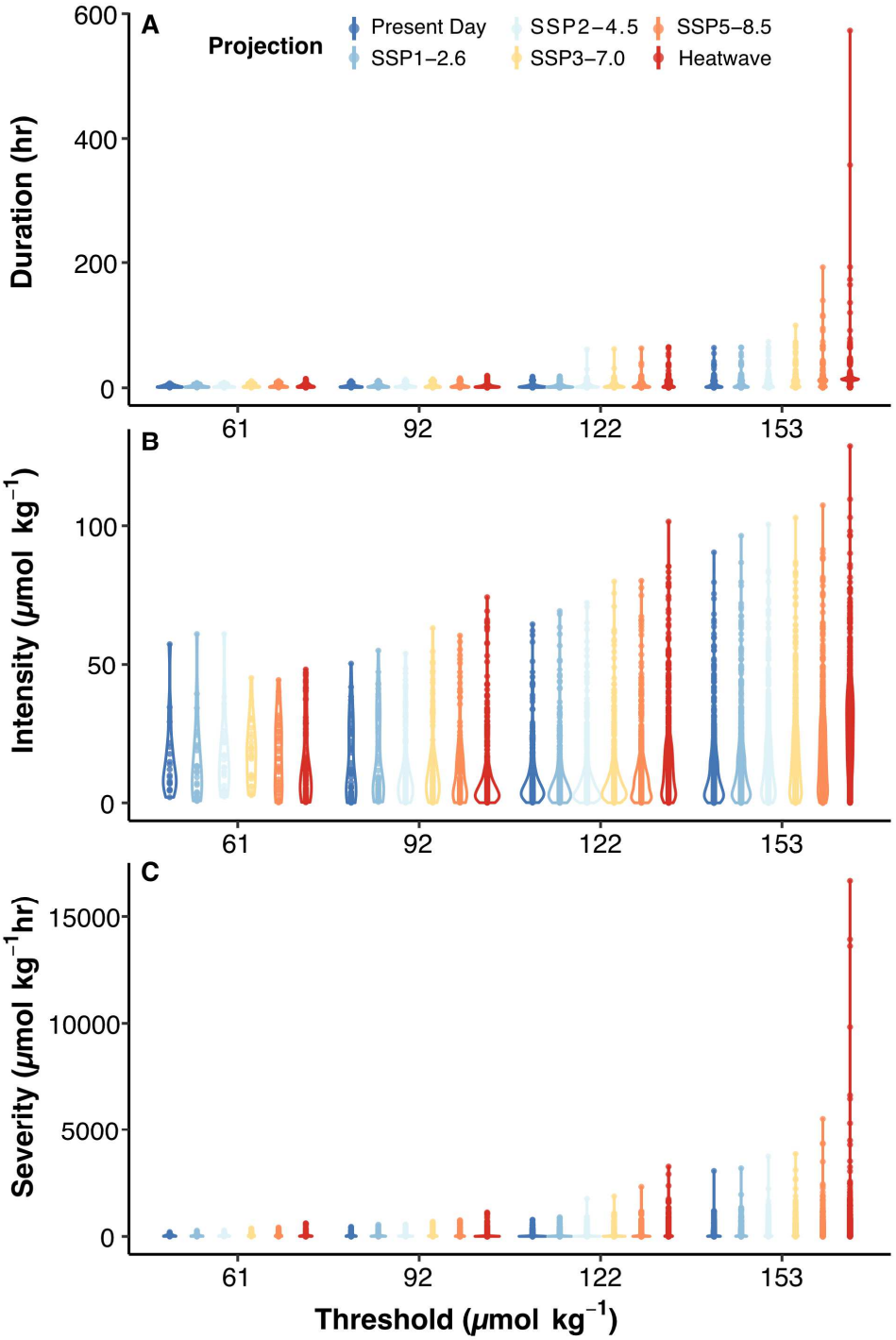

Figure 3.S6 Changes in duration, intensity, and severity of hypoxic events under warming. Distributions of the duration **(A)**, intensity **(B)** and severity **(C)** of all hypoxic events below each threshold (≤153 µmol kg^{-1}, ≤122 µmol kg^{-1}, ≤92 µmol kg^{-1}, or ≤61 µmol kg^{-1}) for each warming projection (blue to red) across all sites.

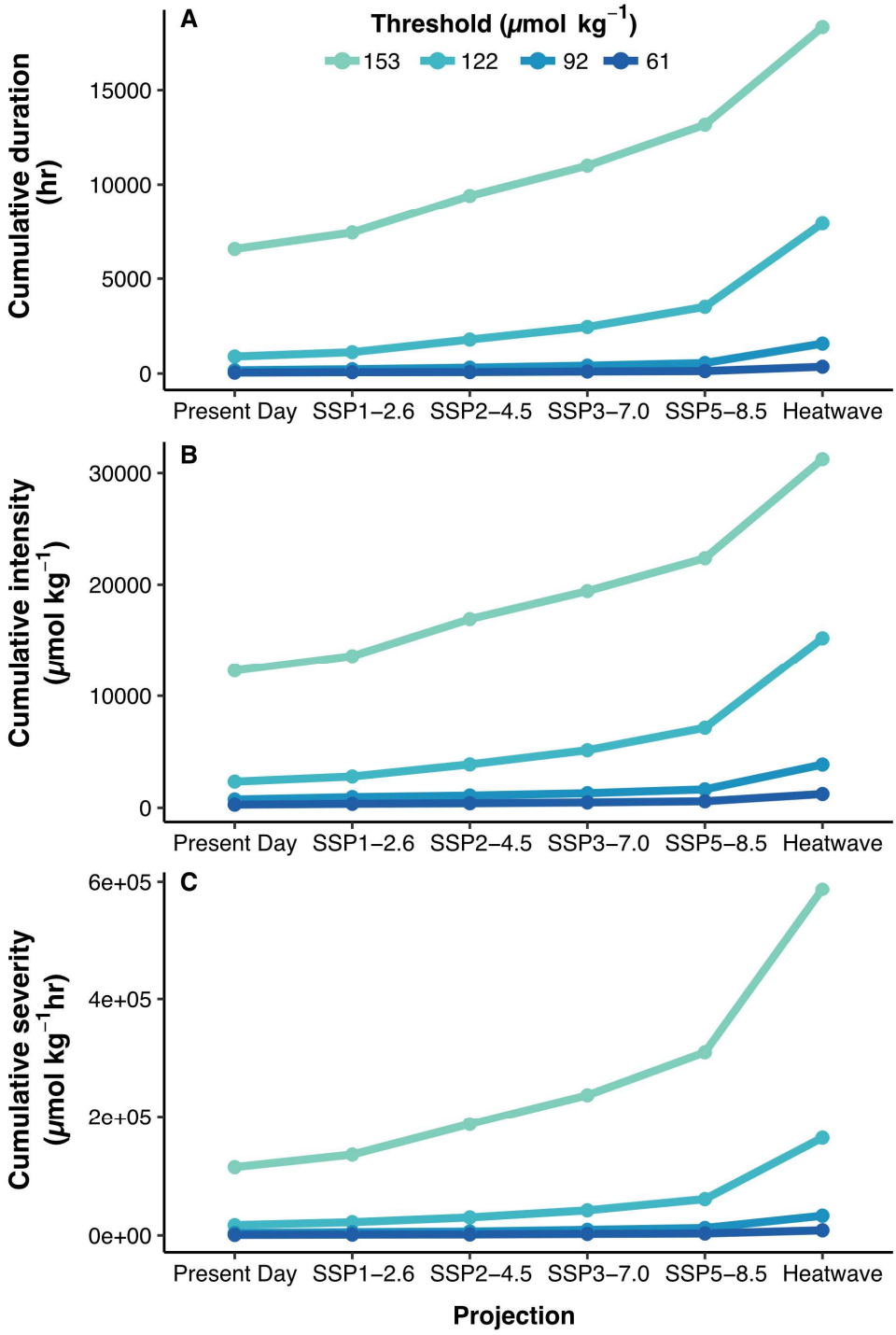

Figure 3.S7: Changes in cumulative duration, intensity, and severity under warming. Cumulative duration **(A)**, cumulative intensity **(B)**, and cumulative severity **(C)** of the hypoxic events below each threshold (≤153 µmol kg^{-1}, ≤122 µmol kg^{-1}, ≤92 µmol kg^{-1}, or ≤61 µmol kg^{-1}; shades of blue) for each warming scenario across all sites.

Table 3.S1: Instrument deployment information for all sites. Instrument column lists instrument package followed by specific oxygen optode model in parentheses if relevant.

Location	Site	Instrument	Deployment Dates	Duration (days)	Depth (m)	Latitude	Longitude	Reef Type	Ref
Bocas del Toro	Bocas 1a	SeapHOx (Aanderaa)	Nov. 4, 2015 – Nov. 9, 2015	5	1	9.377	-82.300	Bay	*41*
Bocas del Toro	Bocas 1b	SeapHOx (Aanderaa)	Nov. 3, 2015 – Nov. 19, 2015	16	3	9.377	-82.300	Bay	*41*
Bocas del Toro	Bocas 1c	SeapHOx (Aanderaa)	Nov. 3, 2015 – Nov. 19, 2015	16	8	9.377	-82.300	Bay	*41*
Bocas del Toro	Bocas 1d	SeapHOx (Aanderaa)	Nov. 3, 2015 – Nov. 9, 2015	6	12	9.377	-82.300	Bay	*41*
Bocas del Toro	Bocas 2a	SeapHOx (Aanderaa)	Nov. 9, 2015 – Nov. 20, 2015	11	3	9.259	-82.108	Nearshore	*41*
Bocas del Toro	Bocas 2b	SeapHOx (Aanderaa)	Nov. 9, 2015 – Nov. 20, 2015	11	8	9.259	-82.108	Nearshore	*41*
Crocker Reef	Crocker 1a	SeapHOx (Aanderaa)	July 19, 2013 – Sept. 3, 2013	47	3.7	24.909	-80.526	Rubble	*58*
Crocker Reef	Crocker 1b	SeapHOx (Aanderaa)	Dec. 4, 2013 – Jan. 19, 2014	46	3.7	24.909	-80.526	Rubble	*58*
Crocker Reef	Crocker 1c	SeapHOx (Aanderaa)	June 24, 2014 – Oct. 27, 2014	126	3.7	24.909	-80.526	Rubble	*58*
Hog Reef	Hog 1a	Sea-Bird (Aanderaa)	Sept. 1, 2017 – Sept. 22, 2017	21	1	32.457	-64.834	Rim Reef	*48*
Hog Reef	Hog 1b	Sea-Bird (Aanderaa)	Sept. 1, 2017 – Sept. 22, 2017	21	7	32.457	-64.834	Rim Reef	*48*
Heron Island	Heron 1	SeapHOx (Aanderaa)	Oct. 9, 2015 – Oct. 22, 2015	13	0.7	-23.444	151.913	Reef Crest	*40*
Heron Island	Heron 2	SeapHOx (Aanderaa)	Oct. 9, 2015 – Oct. 15, 2015	6	2.1	-23.451	151.958	Lagoon	*40*
Heron Island	Heron 3	SeapHOx (Aanderaa)	Oct. 9, 2015 – Oct. 15, 2015	6	1.2	-23.464	151.985	Nearshore	*40*
Kāneʻohe Bay	Kāneʻohe 1a	SeapHOx (Aanderaa)	June 17, 2016 – June 30, 2016	13	1.8	21.458	-157.798	Reef Flat	*43*
Kāneʻohe Bay	Kāneʻohe 1b	SeapHOx (Aanderaa)	Nov. 10, 2016 – Nov. 17, 2016	7	1.8	21.458	-157.798	Reef Flat	*43*
Kāneʻohe Bay	Kāneʻohe 2	SeapHOx (Aanderaa)	Nov. 10, 2016 – Nov. 17, 2016	7	2.5	21.462	-157.792	Rubble	*43*
Dongsha	Dongsha 1	Idronaut CTD	July 1, 2018 – July 8, 2018	7	0.5	20.707	116.721	Nearshore, seagrass	This Study

Table 3.S1: Instrument deployment information for all sites. Instrument column lists instrument package followed by specific oxygen optode model in parentheses if relevant (continued).

Location	Site	Instrument	Deployment Dates	Duration (days)	Depth (m)	Latitude	Longitude	Reef Type	Ref
Dongsha	Dongsha 2	Idronaut CTD	July 1, 2018 – July 8, 2018	7	4	20.705	116.808	Patch Reef	This Study
Dongsha	Dongsha 3	Sea-Bird (Aanderaa)	July 1, 2018 – July 8, 2018	7	4	20.702	116.890	Patch Reef	This Study
Okinawa	Okinawa 1	SeapHOx (Aanderaa)	Oct. 10, 2019 – Oct. 29, 2019	19	0.5	26.452	127.795	Reef Crest	This Study
Okinawa	Okinawa 2	Sea-Bird (Aanderaa)	Oct. 10, 2019 – Oct. 21, 2019	11	2	26.447	127.796	Lagoon	This Study
Okinawa	Okinawa 3	Sea-Bird (Aanderaa)	Oct. 10, 2019 – Oct. 21, 2019	10	10	26.439	127.792	Channel	This Study
Taiping	Taiping 1	Sea-Bird (MiniDOT)	Mar. 28, 2019 – Mar. 31, 2019	3	0.5	10.377	114.370	Nearshore, seagrass	This Study
Taiping	Taiping 2	SeapHOx (Aanderaa)	Mar. 28, 2019 – Mar. 31, 2019	3	1	10.376	114.370	Reef Flat	This Study
Baker	Baker	Sea-Bird (SBE43)	June 12, 2018 – June 15, 2018	3	14.3	0.192	-176.489	Forereef	*62*
Jarvis	Jarvis	Sea-Bird (SBE43)	July 28, 2018 – July 31, 2018	3	17.1	-0.369	-16082	Forereef	*62*
Palmyra	Palmyra 1a	SeapHOx (Aanderaa)	July 7, 2016 – April 8, 2017	275	5	5.889	-162.124	Reef Terrace	This Study
Palmyra	Palmyra 1b	SeapHOx (Aanderaa)	Oct. 30, 2018 – May 14, 2019	196	5	5.889	-162.124	Reef Terrace	This Study
Palmyra	Palmyra 2	SeapHOx (Aanderaa)	July 7, 2016 – May 12, 2017	309	4	5.869	-162.111	Back Reef	This Study
Palmyra	Palmyra 3	Sea-Bird (SBE43)	Aug. 3, 2018 – Aug. 6, 2018	3	12.8	5.866	-162.110	Forereef	*62*
Tutuila	Tutuila	Sea-Bird (SBE43)	June 23, 2018 – July 17, 2018	24	15.2	-14.295	-170.812	Forereef	*64*

Table 3.S2: Assessment of dissolved oxygen measurement bias. Percent (%) of observations below each threshold (153 µmol kg^{-1}, 122 µmol kg^{-1}, 92 µmol kg^{-1}, 61 µmol kg^{-1}) for observed oxygen data (Obs.; left) and oxygen data corrected for a -5% bias (Bias; right) for each projection (Present, SSP1-2.6, SSP2-4.5, SSP3-7.0, SSP5-8.5, and a 6 ºC Heatwave).

	153 µmol kg^{-1}		**122 µmol kg^{-1}**		**92 µmol kg^{-1}**		**61 µmol kg^{-1}**	
Projection	**Obs.**	**Bias**	**Obs.**	**Bias**	**Obs.**	**Bias**	**Obs.**	**Bias**
Present	3.91	2.67	0.547	0.380	0.104	0.0817	0.0297	0.0280
SSP1-2.6	4.41	3.07	0.678	0.467	0.138	0.108	0.0420	0.0375
SSP2-4.5	5.54	4.08	1.09	0.689	0.186	0.143	0.0462	0.0411
SSP3-7.0	6.46	4.91	1.48	0.982	0.250	0.206	0.0646	0.0604
SSP5-8.5	7.68	6.03	2.12	1.47	0.333	0.269	0.0764	0.0685
Heatwave	10.5	9.31	4.68	3.58	0.958	0.691	0.217	0.180

Table 3.S3: Mean daily statistics of oxygen concentration, oxygen saturation, and temperature. Mean daily statistics (calculated using n days of N total observations) of dissolved oxygen concentration (μmol kg^{-1}), dissolved oxygen saturation (%), and temperature (°C) at each reef site (mean ± standard deviation; Table 3.S1, Fig. 3.1) using only complete days (i.e., full 24 hours.

Site	N	n	Dissolved Oxygen (μmol kg^{-1})			Dissolved Oxygen Saturation (%)			Temperature (°C)		
			Mean Daily Range	Mean Daily Min	Mean Daily Max	Mean Daily Range	Mean Daily Min	Mean Daily Max	Mean Daily Range	Mean Daily Min	Mean Daily Max
Bocas 1a	231	4	28.2 ± 8.6	156.2 ± 8.5	184.4 ± 4.8	15.9 ± 5.5	80.9 ± 4.5	96.8 ± 2.8	1.3 ± 0.3	29.7 ± 0.2	31 ± 0.3
Bocas 1b	765	15	41.7 ± 9.8	145.1 ± 7.8	186.8 ± 5.4	22.5 ± 5.3	75.8 ± 4.2	98.2 ± 2.9	0.7 ± 0.2	29.9 ± 0.3	30.6 ± 0.2
Bocas 1c	767	15	37.3 ± 7.1	134.3 ± 7.8	171.6 ± 6.5	19.6 ± 3.6	70.6 ± 3.9	90.2 ± 3.2	0.4 ± 0.2	30.1 ± 0.3	30.5 ± 0.2
Bocas 1d	273	5	27.3 ± 4.4	136.4 ± 7.4	163.7 ± 5.9	14.4 ± 2.3	71.8 ± 3.8	86.2 ± 3	0.3 ± 0.1	30.2 ± 0.1	30.5 ± 0.1
Bocas 2a	524	10	45.7 ± 13	141.6 ± 9	187.3 ± 10.1	24.4 ± 6.9	74.2 ± 4.6	98.6 ± 5.2	0.5 ± 0.2	30.1 ± 0.2	30.6 ± 0.2
Bocas 2b	523	10	49 ± 15.1	133.4 ± 15.5	182.4 ± 4.8	25.8 ± 8.2	70.3 ± 8.1	96.1 ± 2.7	0.4 ± 0.2	30 ± 0.2	30.4 ± 0.1
Crocker 1a	1128	45	87.4 ± 38.5	141.8 ± 22.3	229.2 ± 25.2	46.1 ± 20.2	74.1 ± 11.6	120.2 ± 13.6	0.6 ± 0.3	29.2 ± 0.4	29.8 ± 0.4
Crocker 1b	1096	45	48.2 ± 50.8	189.9 ± 9.7	238.1 ± 43	23.9 ± 25.1	93.4 ± 4.6	117.2 ± 21.4	0.8 ± 0.5	25 ± 1.1	25.8 ± 0.7
Crocker 1c	3006	124	133.1 ± 88.3	131.9 ± 36.9	265 ± 66.5	70.3 ± 46.9	69.1 ± 19.3	139.3 ± 35.7	0.6 ± 0.3	29.7 ± 0.9	30.3 ± 0.9
Hog 1a	2018	20	78.3 ± 29.7	200.7 ± 7.6	279 ± 28.3	41.1 ± 15.4	103.5 ± 3.9	144.6 ± 14.4	0.5 ± 0.2	28.1 ± 0.4	28.6 ± 0.4
Hog 1b	2018	20	54 ± 16.3	196.8 ± 10.7	250.8 ± 13.6	28.4 ± 8.6	101.4 ± 5.3	129.9 ± 6.9	0.4 ± 0.1	28.2 ± 0.4	28.6 ± 0.4
Heron 1	610	12	125.4 ± 46.1	128.2 ± 25	253.6 ± 29.7	65.1 ± 23.1	58.6 ± 11.5	123.7 ± 15	4.8 ± 1.1	20.7 ± 0.5	25.5 ± 1.1
Heron 2	293	5	58.4 ± 17.4	187.9 ± 18.1	246.3 ± 4.5	29.9 ± 9.3	87.6 ± 7.5	117.5 ± 3.3	1.9 ± 0.4	22.1 ± 0.6	24 ± 0.8
Heron 3	291	5	111.4 ± 21.1	153.9 ± 18.5	265.3 ± 9.7	57.7 ± 10.7	71.1 ± 7.6	128.8 ± 5.7	3.1 ± 0.5	21.8 ± 0.7	24.9 ± 0.9
Kaneohe 1a	624	12	164 ± 15.7	105.3 ± 11	269.2 ± 11.5	83.8 ± 8.5	51.6 ± 5.1	135.4 ± 6.5	1.7 ± 0.3	25.7 ± 0.4	27.4 ± 0.4
Kaneohe 1b	320	6	73.6 ± 24.4	90.9 ± 7	164.6 ± 29.3	37.1 ± 12.4	44.5 ± 3.2	81.6 ± 14.6	1 ± 0.5	25.5 ± 0.6	26.5 ± 0.3
Kaneohe 2	321	6	69.6 ± 31.6	145.4 ± 33.3	215 ± 12.9	35 ± 15.5	71.5 ± 16.7	106.5 ± 7.1	0.7 ± 0.2	25.7 ± 0.4	26.4 ± 0.5
Dongsha 1	710	6	187.5 ± 14.2	20.7 ± 17.1	208.1 ± 8.2	100.3 ± 7	10.8 ± 8.9	111.1 ± 4.5	2.3 ± 0.2	29.4 ± 0.4	31.7 ± 0.3
Dongsha 2	671	6	99.9 ± 59.6	93.8 ± 17.2	193.6 ± 45	52.6 ± 31.5	48.9 ± 8.7	101.6 ± 24.1	0.7 ± 0.1	29.7 ± 0.3	30.5 ± 0.3
Dongsha 3	1003	6	120 ± 45.6	83.9 ± 10.5	203.9 ± 36.4	63.3 ± 24	43.9 ± 5.5	107.2 ± 19.2	0.8 ± 0.2	30.1 ± 0.1	30.9 ± 0.2
Okinawa 1	909	18	31.6 ± 18.6	171.4 ± 9.5	203 ± 11.1	16.1 ± 9.6	84.5 ± 4.8	100.6 ± 5.8	0.5 ± 0.3	26.1 ± 0.2	26.7 ± 0.2
Okinawa 2	506	10	67.6 ± 19.7	185.7 ± 8.2	253.3 ± 16	34.1 ± 9.9	91.5 ± 3.9	125.6 ± 8.2	0.6 ± 0.2	26 ± 0.2	26.6 ± 0.2
Okinawa 3	503	10	80.3 ± 14.6	174.1 ± 8	254.4 ± 14.4	41 ± 7.7	85.5 ± 3.9	126.5 ± 7.8	0.9 ± 0.3	25.9 ± 0.2	26.8 ± 0.3
Taiping 1	374	2	258.1 ± 11.5	48.1 ± 11.2	306.1 ± 0.3	138.6 ± 4.5	24.2 ± 5.4	162.7 ± 0.9	3.8 ± 0.6	27.6 ± 0.3	31.4 ± 0.3
Taiping 2	376	2	123.1 ± 17	90.4 ± 5.4	213.4 ± 11.6	64.1 ± 9.2	46.1 ± 3.1	110.2 ± 6.1	1.2 ± 0	28.3 ± 0.1	29.5 ± 0.1
Baker	25716	2	35.1 ± 4.9	144.6 ± 1.5	179.8 ± 3.3	17.9 ± 2.1	74 ± 0.6	92 ± 1.5	0.8 ± 0.1	27.8 ± 0	28.6 ± 0.1
Jarvis	26530	2	32 ± 2.8	134.2 ± 4.4	166.2 ± 1.6	16.5 ± 1.3	67.8 ± 2.1	84.4 ± 0.8	0.4 ± 0.1	27.5 ± 0.1	27.8 ± 0
Palmyra 1a	13185	274	95.9 ± 21.2	140.1 ± 11.8	235.9 ± 20.2	50.1 ± 11.2	71.4 ± 5.9	121.4 ± 10.4	0.9 ± 0.4	28.1 ± 0.6	29 ± 0.6
Palmyra 1b	4701	195	73.5 ± 20.3	124.4 ± 10.2	197.9 ± 18.8	38.5 ± 10.7	63.7 ± 5.3	102.2 ± 9.8	0.7 ± 0.4	28.3 ± 0.6	29 ± 0.5
Palmyra 2	14852	308	76.7 ± 27	151.7 ± 14.3	228.4 ± 16.5	40.7 ± 14.7	77 ± 8.7	117.8 ± 8.6	1 ± 0.4	28.1 ± 0.6	29.1 ± 0.5
Palmyra 3	26761	2	40.9 ± 15.2	142.3 ± 10.2	183.2 ± 5	21.2 ± 8	73.5 ± 5.3	94.7 ± 2.7	0.2 ± 0.1	29.2 ± 0.1	29.4 ± 0
Tutuila	6878	23	22.9 ± 3.8	141.1 ± 2.9	164 ± 4	11.7 ± 1.9	72.3 ± 1.2	84 ± 2	0.2 ± 0.1	28.4 ± 0.4	28.6 ± 0.4

Table 3.S4: **Temperature projections by location.** Predicted temperature rise (ºC) for each location sourced from the CMIP6 CESM2-WACCM model (*81-82*).

Location	Predicted Temperature Rise (ºC)			
	SSP1-2.6	**SSP2-4.5**	**SSP3-7.0**	**SSP5-8.5**
Bocas del Toro	0.85	1.53	2.39	3.18
Crocker Reef	0.92	1.54	2.45	3.09
Hog Reef	0.68	1.23	2.43	3.38
Heron Island	0.95	1.87	2.72	3.76
Kaneohe Bay	0.36	1.90	2.22	3.47
Dongsha	0.97	1.11	2.34	3.03
Okinawa	1.07	1.06	2.32	2.94
Taiping	0.98	1.16	2.55	3.49
Baker	0.60	2.14	2.93	3.89
Jarvis	0.72	2.37	3.30	4.05
Palmyra	0.29	1.55	2.30	3.38
Tutuila	0.64	1.14	1.83	2.79

Table 3.S5: Changes in percent of observations below each hypoxia threshold under warming. Percent of total observations (N) that are hypoxic at present, under each temperature projection, and under a 6 °C heatwave scenario for each site under four thresholds: ≤ 153 µmol kg^{-1}, ≤ 122 µmol kg^{-1}, ≤ 92 µmol kg^{-1}, or ≤ 61 µmol kg^{-1} using the datasets standardized to 30-minute sampling intervals.

		Threshold = 153 µmol kg^{-1}						Threshold = 122 µmol kg^{-1}					
Site	**N**	**Present**	**SSP 1-2.6**	**SSP 2-4.5**	**SSP 3-7.0**	**SSP 5-8.5**	**Heatwave**	**Present**	**SSP 1-2.6**	**SSP 2-4.5**	**SSP 3-7.0**	**SSP 5-8.5**	**Heatwave**
Bocas 1a	231	0.3	1.1	1.9	3	4.2	11.6	0	0	0	0	0	0
Bocas 1b	765	2.7	3.8	4.6	5.9	7.7	13.7	0	0.1	0.1	0.1	0.2	1.9
Bocas 1c	767	6.3	8.7	10	12	13.5	16.5	0	0.1	0.3	0.5	1	4.6
Bocas 1d	273	9.2	11	12.5	14.5	15.9	16.7	0	0	0.1	0.3	0.9	5.5
Bocas 2a	524	2.4	4.1	6.1	8.3	9.8	15.3	0	0	0	0.2	0.3	1.8
Bocas 2b	523	6.9	8.1	9.6	11.1	12.3	15.5	0.7	1	1.2	1.8	2.3	5.7
Crocker 1a	2255	3.9	4.9	5.6	6.9	7.8	11.3	0.1	0.1	0.2	0.3	0.9	4.6
Crocker 1b	2191	0	0	0	0	0.1	0.5	0	0	0	0	0	0
Crocker 1c	6027	4.6	5.4	6.3	7.6	8.5	11.4	1.3	1.8	2.2	2.8	3.3	6.6
Hog 1a	1009	0	0	0	0	0	0	0	0	0	0	0	0
Hog 1b	1009	0	0	0	0	0.1	0.2	0	0	0	0	0	0
Heron 1	610	3.1	5.7	6.9	7.6	8.3	9.9	0.9	1.3	1.5	1.9	3.1	7.2
Heron 2	293	0	0	0	0	0.4	1.9	0	0	0	0	0	0
Heron 3	291	0.2	0.4	0.7	1.4	2.9	7.4	0	0	0.1	0.1	0.2	1
Kaneohe 1a	624	6.5	6.7	8.1	8.3	9.3	11.2	2.5	3	4.9	5.2	6.5	8.7
Kaneohe 1b	320	13.3	13.4	14.1	14.2	14.8	15.9	10.3	10.7	11.9	12	12.6	13.6
Kaneohe 2	321	2.2	2.3	3.6	3.9	5.7	11.2	0.7	0.8	1.1	1.3	1.7	2.6
Dongsha 1	355	10.9	11.7	11.9	12.8	13.4	16.5	8.6	9.4	9.4	10.4	11	14.1
Dongsha 2	336	12	13	13.2	14.4	15.3	16	6.3	7.7	7.8	9.4	10.1	13.2
Dongsha 3	335	11.3	11.9	12	12.7	12.9	14.7	8.7	9.2	9.3	9.7	10.1	12.5
Okinawa 1	909	0.2	0.3	0.3	0.7	0.8	4.2	0	0	0	0	0	0.1
Okinawa 2	169	0	0	0	0	0	1	0	0	0	0	0	0
Okinawa 3	168	0	0	0	0.4	0.7	5.3	0	0	0	0	0	0
Taiping 1	125	9.1	9.5	9.6	10.7	10.9	14.3	5.6	7.6	7.6	8.9	9.5	11.3
Taiping 2	126	7.5	9.5	9.5	11	12.4	16	3.2	3.7	4.1	6.5	7.3	10.7
Baker	143	1.4	2.7	8.7	11	13.4	16.3	0	0	0	0	0	0
Jarvis	148	11.1	12.5	16.7	16.7	16.7	16.7	0	0	0.1	0.5	1.7	6.2
Palmyra 1a	13185	3.1	3.5	5.3	6.3	7.7	10.2	0.1	0.1	0.4	0.8	1.5	5.1
Palmyra 1b	9401	8.6	9	10.2	10.8	11.7	13.7	0.8	1	2.5	3.5	5.3	9.3
Palmyra 2	14852	1.4	1.6	2.7	3.6	5.5	9.8	0.1	0.1	0.2	0.3	0.5	1.9
Palmyra 3	149	4.4	4.7	7.9	10.3	14.3	16.6	0	0	0	0.1	0.2	2.3
Tutuila	1147	9.7	12.5	14.1	15.6	16.5	16.7	0	0	0	0	0	1.3

Table 3.S5: Changes in percent of observations below each hypoxia threshold under warming. Percent of total observations (N) that are hypoxic at present, under each temperature projection, and under a 6 ºC heatwave scenario for each site under four thresholds: ≤ 153 µmol kg^{-1}, ≤ 122 µmol kg^{-1}, ≤ 92 µmol kg^{-1}, or ≤ 61 µmol kg^{-1} using the datasets standardized to 30-minute sampling intervals (continued).

	Threshold = 92 µmol kg^{-1}						Threshold = 61 µmol kg^{-1}					
Site	**Present**	**SSP 1-2.6**	**SSP 2-4.5**	**SSP 3-7.0**	**SSP 5-8.5**	**Heatwave**	**Present**	**SSP 1-2.6**	**SSP 2-4.5**	**SSP 3-7.0**	**SSP 5-8.5**	**Heatwave**
Bocas 1a	0	0	0	0	0	0	0	0	0	0	0	0
Bocas 1b	0	0	0	0	0	0	0	0	0	0	0	0
Bocas 1c	0	0	0	0	0	0	0	0	0	0	0	0
Bocas 1d	0	0	0	0	0	0	0	0	0	0	0	0
Bocas 2a	0	0	0	0	0	0	0	0	0	0	0	0
Bocas 2b	0	0	0	0	0	0.6	0	0	0	0	0	0
Crocker 1a	0	0	0	0	0	0.1	0	0	0	0	0	0
Crocker 1b	0	0	0	0	0	0	0	0	0	0	0	0
Crocker 1c	0.4	0.5	0.6	0.7	0.9	2.5	0.1	0.2	0.2	0.2	0.3	0.6
Hog 1a	0	0	0	0	0	0	0	0	0	0	0	0
Hog 1b	0	0	0	0	0	0	0	0	0	0	0	0
Heron 1	0.2	0.2	0.3	0.5	1	1.8	0	0.1	0.1	0.1	0.2	0.4
Heron 2	0	0	0	0	0	0	0	0	0	0	0	0
Heron 3	0	0	0	0	0	0.1	0	0	0	0	0	0
Kaneohe 1a	0.1	0.1	1.1	1.3	2.7	6.1	0	0	0	0	0.1	2
Kaneohe 1b	1.4	2.2	6.4	7	8.8	11	0	0	0	0	0	3.1
Kaneohe 2	0.1	0.1	0.3	0.3	0.5	0.9	0	0	0	0	0.1	0.1
Dongsha 1	6	6.9	6.9	8.2	8.7	11.4	2.5	3.6	3.8	5.4	6.1	9.1
Dongsha 2	1.3	2.1	2.3	3.5	4.4	8.1	0	0	0	0.1	0.1	2.2
Dongsha 3	0.9	2.4	2.6	5.5	6.6	9.5	0	0.1	0.1	0.2	0.2	4.2
Okinawa 1	0	0	0	0	0	0	0	0	0	0	0	0
Okinawa 2	0	0	0	0	0	0	0	0	0	0	0	0
Okinawa 3	0	0	0	0	0	0	0	0	0	0	0	0
Taiping 1	2.1	2.9	3.2	5.3	7.6	9.6	0.9	1.2	1.3	2	2.8	7.6
Taiping 2	0.4	1.3	1.3	2.4	3	6.5	0	0	0	0	0.1	2.4
Baker	0	0	0	0	0	0	0	0	0	0	0	0
Jarvis	0	0	0	0	0	0	0	0	0	0	0	0
Palmyra 1a	0	0	0	0	0	0.4	0	0	0	0	0	0
Palmyra 1b	0	0	0	0	0.1	1.5	0	0	0	0	0	0
Palmyra 2	0	0	0	0	0	0.1	0	0	0	0	0	0
Palmyra 3	0	0	0	0	0	0	0	0	0	0	0	0
Tutuila	0	0	0	0	0	0	0	0	0	0	0	0

Extended Materials and Methods

Detailed Site and Deployment Information

Heron Island, Australia

Heron Island (23.443°S, 151.915°E) is a small coral cay (~0.16 km^2) located on the Heron Reef platform (~28 km^2) in the Capricorn Group of the Southern Great Barrier Reef (*35-36*). The Heron Reef platform is characterized by reef flat and lagoon habitats dominated by calcium carbonate sands, some algae, and live coral, predominantly *Acropora spp.* (*37-38*). SeapHOx (*39*) sensors were deployed on the benthos at three sites along the Heron Reef platform along an east-west transect: close to Heron Island (Heron 1), in the middle of the lagoon (Heron 2), and on the reef flat (Heron 3) (*40*). All instruments were deployed starting on October 8, 2015, and recorded temperature, salinity, dissolved oxygen, and pH every 30 minutes. Heron 1 was deployed for 14 days at approximately 0.7 m depth and Heron 2 and Heron 3 were deployed for 7 days at approximately 2.1 m and 1.2 m depth, respectively (*40*; Table 3.S1).

Bocas del Toro, Panamá

Bocas del Toro (9.358°N, 82.244°W) is an archipelago on the northwest coast of Panamá, separated from the Caribbean Sea by the estuarine Almirante Bay (*41*). Almirante Bay is influenced by intense terrestrial runoff, freshwater discharge, and sedimentation from upstream rivers, streams, and plantations (*42*). Punta Caracol (9.377°N, 82.300°W) is a shallow reef site on the west coast of Isla Colón in Almirante Bay of Bocas del Toro, mostly protected from open ocean water flow and surrounded by dense mangroves (*41*). Punta Caracol is mainly composed of sandy sediments and large colonies of *Porites*, *Orbicella*, *Diploria*, *Montastrea* and

Colpophyllia at 2 to 4 m depth and a mixed community with muddy sediments from 4 to 12 m depth (*41*). Punta Vieja (9.259°N, 82.108°W) is a reef site at the southern tip of Isla Bastimentos, exposed to the Caribbean Sea and subject to much less terrestrial runoff and fewer anthropogenic inputs (*41*). The reef at Punta Vieja is dominated mainly by *Acropora cervicornis* and *Acropora palmata* from 2 to 5 m and drops off to a muddy bottom at 12 m depth (*41*).

Four SeapHOx (*39*) sensors were deployed on the benthos at Punta Caracol on November 3–4, 2015, at depths of 1 m, 3 m, 8 m, and 12 m depth (Bocas 1a, 1b, 1c, and 1d, respectively) and recorded temperature, salinity, dissolved oxygen, and pH every 30 minutes (Table 3.S1). The sensors at 3 m and 8 m remained in place for 16 days and were recovered on November 19. On November 9, the sensors at 1 m and 12 m were moved to Punta Vieja and deployed at 3 m and 8 m (Bocas 2a and Bocas 2b, respectively). The sensors at Punta Vieja were recovered on November 20 after 11-day deployments (*41*).

Kāneʻohe Bay, Oʻahu, Hawaiʻi, USA

Kāneʻohe Bay (21.463°N, 157.810°W) is a large bay on the northeastern (windward) coast of Oʻahu, home to a large barrier reef extending 13 km (alongshore) by 4 km (cross shore) (*43*). The reef area has a reef crest, reef and sand flats, and lagoon with many patch reefs (*44-45*). The reef flat is shallow and has a mixed benthic community, with some areas dominated by reef, rubble (coral skeletons with encrusting or turf algae), or sand (*44-45*). A SeapHOx sensor (*39*) was deployed on the benthos between June 17–30, 2016, at a reef site near the NOAA CRIMP2 buoy (https://www.pmel.noaa.gov/co2/story/CRIMP2), measuring temperature, salinity, pH, and dissolved oxygen every 30 minutes for the 13-day deployment (Kaneohe 1a). Two SeapHOx

sensors were also later deployed on the benthos in the fall at the same CRIMP2 reef site (Kaneohe 1b) and at a rubble site (Kaneohe 2) for 7 days from November 10 to17, 2016, recording the same parameters every 30 minutes (*43*; Table 3.S1).

Hog Reef, Bermuda

Hog Reef (32.457ºN, 64.835ºW) is a rim-reef on the northern side of the Bermuda carbonate platform dominated by macroalgae (35 ± 3 %), hard coral (27 ± 5 %), turf algae (20 ± 4 %), soft coral (16 ± 2 %), and some areas of sand, rock, rubble, and coralline algae (< 5 %; mean ± 1 SD benthic cover) (*46-48*). The depth at Hog Reef ranges from 4 to 25 m, with a mean (± 1 SD) of 10.3 ± 3.3 m, generally increasing offshore but with variable structure and complexity (*47-49*). A suite of autonomous sensors were deployed at Hog Reef in September of 2017, including Aanderaa oxygen optodes measuring dissolved oxygen and a CTD (Microcat, Sea-Bird Scientific) measuring temperature and salinity, among other parameters not included in the present study (*48*; Table 3.S1). Instruments were deployed either attached to (surface, Hog 1a) or on the benthos below (7 m; Hog 1b) the NOAA PMEL MAPCO2 buoy on Hog Reef (https://www.pmel.noaa.gov/co2/story/Hog+Reef) for 21 days from September 1-22, 2017, recording every 15 minutes. Salinity values for the Hog 1a sensors were taken from the MAPCO2 buoy and linearly interpolated to match the recording frequency of the sensors (every 15 minutes) (*48*).

Dongsha Atoll, Taiwan

Dongsha Atoll (20.682ºN, 116.808ºE) is a large (~23 km wide), circular atoll in the South China Sea (also known as one of the Pratas Islands) southwest of Taiwan, with a wide reef flat and

large lagoon containing thousands of patch reefs of varying size. Dongsha Island on the western side of the atoll is home to a large seagrass bed on its north shore, extending up to 1 km offshore with scattered patches of *Porites spp.* coral colonies. The lagoon patch reefs are dominated mainly by massive *Porites*, foliaceous *Echinopora*, *Pavona*, and *Turbinaria* corals (*50*). An Idronaut CTD was deployed on the bottom in the shallow seagrass (Dongsha 1) at ~0.5 m depth during July 1–8, 2018, recording temperature, salinity, pH, and dissolved oxygen every 15 minutes for 7 days. Another Idronaut CTD was deployed on the benthos of a large patch reef (Dongsha 2) near the center of the lagoon from July 1–8, 2018, at ~4 m for 7 days, also recording temperature, salinity, pH, and dissolved oxygen every 15 minutes. A Sea-Bird CTD sensor and Aanderaa oxygen optode were deployed on the benthos at a smaller patch reef on the eastern side of the lagoon at ~4 m depth for 7 days from July 1–8, 2018, measuring temperature, salinity, and dissolved oxygen every 10 minutes (Table 3.S1).

Taiping Island, Taiwan

Taiping Island (10.376ºN, 114.365ºE) or Itu Aba Island is the largest of the naturally occurring Spratly Islands in the South China Sea (0.57 km^2), ~ 500 km due west of Palawan Island, Philippines and ~1180 km southwest of Dongsha Atoll, Taiwan (*51*). The east-west oriented coral island is surrounded by shallow seagrass beds that transition into a reef flat (1–4 m in depth) extending ~50 m offshore before a steep reef drop off with low to no coral cover below 18 m depth (*52*). Previous work employing remote sensing data estimates that Taiping is home to 1.27 km^2 of reef flat and 2.46 km^2 sub-tidal reef area (*51*). The reef areas surrounding Taiping are high in coral cover, with less than 5 % cover of algae, most of which was crustose coralline algae (*53*). Surveys in 1994 identified 120 species of corals on the south side of the island,

dominated mainly by *Pocillopora* and *Acropora* species (*52*). A Sea-Bird CTD and PME MiniDOT were deployed in the shallow seagrass and a SeapHOx (*39*) sensor was deployed on the benthos of the reef flat on the south side of the island for 3 days from March 28–31, 2019. The Sea-Bird and MiniDOT measured temperature, salinity, and dissolved oxygen every 10 minutes and the SeapHOx sensor measured temperature, salinity, dissolved oxygen, and pH every 10 minutes (Table 3.S1).

Okinawa, Japan

Okinawa Island is the largest of the Ryuku Islands of southern Japan's Kyushu region. Onna Reef (26.449ºN, 127.796ºE), located in Onna Village near Nakadomari, is a fringing coral reef along Okinawa's central western side, extending 2.8 km alongshore with a 150 km wide reef flat. The reef flat has a mean depth of ~1.3 m and is composed mainly of carbonate rock, crustose coralline algae, sand, rubble, turf algae, and some small coral colonies (*54*). The lagoon (3–4 m depth) inshore from the reef flat is mainly sand, with scattered patch reefs, coral farms (*55*), seaweed farms, and has several deeper channels in the south and north. A SeapHOx (*39*) sensor was deployed on the benthos on the reef flat (Okinawa 1) and two Sea-Bird CTDs equipped with Aanderaa Oxygen Optodes were deployed in the lagoon near a coral farm (Okinawa 2) and in the southern boat channel (Okinawa 3) next to a group of artificially placed large *Porites* colonies (*54*). The sensors were deployed at ~0.5 m, 2 m, and 10 m, respectively from October 10–29, 2019; however, biofouling on the Sea-Bird and Aanderaa sensors led to unusable dissolved oxygen data after October 21 (*54*). Thus, the SeapHOx sensor recorded temperature, salinity, dissolved oxygen, and pH for 19 days every 30 minutes, and the other instruments recorded

temperature, salinity, and dissolved oxygen every 10 minutes for ~10 (Okinawa 3) and 11 days (Okinawa 2) (*54*; Table 3.S1).

Crocker Reef, Florida, USA

Crocker Reef (24.908ºN, 80.525ºW), located on the outer reef tract of the Florida Keys, is a "senile or dead reef" dominated mainly by rubble, sand, and scattered coral colonies (*56*). An autonomous sensor package including a SeapHOx (*39, 57*) sensor was deployed on the benthos (3.7 m) in a sandy patch next to hardbottom to capture temperature, salinity, dissolved oxygen, and pH every hour for 47 days during late summer (July 19–September 3, 2014; Crocker 1a), 46 days in winter (December 4, 2013–January 19, 2014; Crocker 1b), and 126 days from summer to fall (June 24, 2014–October 27, 2014; Crocker 1c) (*58*; Table 3.S1).

Baker Island, Phoenix Islands

Baker Island (0.194ºN, 176.478ºW) is a small (2.1 km^2), uninhabited atoll in the Central Pacific and part of the Baker Island National Wildlife Refuge and the Pacific Remote Island Marine National Monument. The low-lying island is surrounded by a narrow fringing reef extending mainly east to west, and deeper reef slopes and terraces that drop off precipitously (*59*), with a total reef area of about 4 km^2 (*60*). Benthic community composition on the southern reef slopes at Baker is dominated by *Acropora* corals (28.9 % cover), turf algae (22.3 %), macroalgae (15.6 %), and crustose coralline algae (24.2 %) (*60-61*). A Sea-Bird SBE43 dissolved oxygen sensor and Sea-Bird SBE19 plus CTD were deployed on the forereef benthos at 14.3 m for 3 days between June 12 and 15, 2018, recording temperature, salinity, and dissolved oxygen every 10 seconds (*62*; Table 3.S1).

Jarvis Island, Line Islands

Jarvis Island (0.372ºS, 159.997ºW) is a small (4.5 km^2), barren island in the Central Pacific surrounded by narrow fringing reefs and steep forereefs that drop off to depths of more than 3,000 m (*60, 63*). Total reef area at Jarvis is approximately 3 km^2, with less than 1 % live coral cover following mass bleaching in 2015 (*63*). A Sea-Bird SBE43 dissolved oxygen sensor and Sea-Bird SBE19 plus CTD were deployed on the forereef benthos at 17.1 m for 3 days between July 28 and 31, 2018, recording temperature, salinity, and dissolved oxygen every 10 seconds (*62*; Table 3.S1).

Tutuila, American Samoa

Tutuila (14.319ºS, 170.751ºW) is the main and largest island of American Samoa at 142.3 km^2. The island is surrounded by narrow fringing reefs, with highly variable coral and macroalgal cover (*63*). The benthic community of the reefs on the northwest side of the island is dominated by turf algae (~40 % cover), hard coral (~25 %), crustose coralline algae (<20 %), and some macroalgae (<4 %), with similar composition at shallow (0–6 m), mid (> 6–18 m), and deeper depths (18–30 m; *60, 63*). A Sea-Bird SBE43 dissolved oxygen sensor and Sea-Bird SBE19 plus CTD were deployed on the forereef benthos at 15.2 m for 24 days between June 23 and July 17, 2018, recording temperature, salinity, and dissolved oxygen every 5 minutes (*64*; Table 3.S1).

Palmyra Atoll, Line Islands

Palmyra Atoll (~2 km^2) of the northern Line Islands is a coral atoll in the South Pacific (5.882ºN, 162.081ºW) approximately due south of the Hawaiian Islands. Palmyra is a National Fish and

Wildlife Refuge and part of the Pacific Remote Island Areas National Marine Monument, and thus not exposed to recent anthropogenic influences such as fishing or pollution (*65-66*). The atoll runs east to west, with two large lagoons and shallow reef terraces on either side (*67*) and a total reef area of about 42 km^2 (*60*). The benthic community at Palmyra is dominated by live stony corals (28.5%), crustose coralline algae (18.9%), turf algae (24.3%), and macroalgae (12.8%) (*60, 68*). The forereef of Palmyra has been noted to contain a more diverse coral community, with higher cover of faster growing species like *Acropora* and *Pocillopora* (*69*).

SeapHOx (*39*) sensors were deployed at a site on the reef terrace in 2016–2017 and 2018–2019 and on the reef flat in 2016–2017. A SeapHOx sensor was deployed on the benthos of the reef terrace at approximately 5 m depth to record temperature, salinity, pH, and dissolved oxygen every 30 minutes from July 7, 2016–April 8, 2017 (275 days; Palmyra 1a) and October 30, 2018–May 14, 2019 (196 days; Palmyra 1b). The SeapHOx placed on the benthos of the back reef was deployed from July 7, 2016, to May 12, 2017 (309 days; Palmyra 2) at ~4 m depth, also recording temperature, salinity, pH, and dissolved oxygen every 30 minutes. An SBE43 dissolved oxygen sensor and Sea-Bird SBE19 plus CTD were also deployed at a site on the forereef benthos from August 3–6, 2018 (3 days; Palmyra 3) at 12.8 m depth, recording temperature, salinity, and dissolved oxygen every 10 seconds (*62*; Table 3.S1).

Potential Errors and Uncertainty

The accuracy of autonomous oxygen measurements depends on a number of factors including quality of the initial sensor calibration, subsequent sensor drift (during storage, transport, and/or deployment), and biofouling. (*72*). We note the oxygen data in the present study were collated

from multiple sources including both published (i.e., Crocker Reef, Heron Island, Bocas del Toro, Kāne‘ohe Bay, Jarvis, Baker, Tutuila, Palmyra 3, and Bermuda; *40, 41, 43, 48, 58, 62, 64*) and unpublished (i.e., Dongsha Atoll, Okinawa, Taiping Island, Palmyra, 1a, 1b, 2) datasets as well as different oxygen sensors, calibration protocols, deployment durations, and users. However, because of the dynamic nature of oxygen in coral reef benthic environments spanning the full range from anoxia (e.g., *9, 73-74*) to extensive super saturation (e.g., *75*), it is not straightforward to identify suboptimal measurements that remain within reasonable bounds. We have done our best to assess the validity of each dataset both technically (i.e., following calibration protocols, etc.) and holistically (i.e., if a range of observations from a given environment makes sense based on the local benthic community, geomorphology, hydrodynamics, and history), and have found no direct evidence of any outstanding problems with the datasets that would negate our main conclusions. If we consider a hypothetical mean bias of -5% of our oxygen measurements (*76*), this alters the percentage of observations below the different thresholds at present by at most -32 % (153 μmol kg^{-1}), -31 % (122 μmol kg^{-1}), -21 % (92 μmol kg^{-1}), and -6 % (61 μmol kg^{-1}) with mostly similar or smaller reductions under future warming projections (Table 3.S2). This would lessen the observed and projected hypoxia intensity and severity with respect to the defined thresholds, but it does not affect the ranges of oxygen variability and the projected decreases in dissolved oxygen under different warming scenarios. The same would be true for a positive measurement bias, although this would worsen the observed and projected intensity and severity for the different reefs. In either case, under projected future warming, there will be an increase in the frequency, intensity, duration, and severity of hypoxia for all reefs in this study compared to present, which emphasize the concerns raised here and elsewhere (*6-8*). It also highlights the need to further solidify relevant

physiological oxygen thresholds and their implications, and to continue developing methodological and technological improvements for making high quality, autonomous oxygen measurements in shallow, near-shore environments.

Box Model of DO Changes as a Result of Temperature Rise

A simple box model was used to validate the methodology and calculations performed as described in the Online Methods. The objective of the model was not to create a full-fledged biogeochemical coral reef model, but simply to create a model that could be used to conceptually validate the computational approximation of DO changes owing to the combined effect of decreasing gas solubility and increasing respiration rates resulting from ocean warming. The observations of DO from each reef location reflected the net effect of primary production, respiration, and physical transport processes, but without quantitative knowledge of these individual processes, we could only approximate the net effect of future warming on DO concentrations (see Online Methods). In the model, individual fluxes were prescribed and assessed independently, which allowed us to model the effect of warming on these processes and compare the net effect to the computational approximation applied to the global coral reef oxygen dataset.

The model calculations were assessed for a 1 m^3 seawater reservoir (1 m x 1 m x 1m) with dissolved oxygen concentration influenced by inflow ($F_{sw\text{-}i}$) and outflow ($F_{sw\text{-}o}$) of seawater and gross primary production (F_{PP}) and respiration (F_R). Gas exchange was negligible relative to these other fluxes and therefore not included in the model. The mass balance of oxygen was described by:

$$\frac{dDO}{dt} = F_{sw-i} - F_{sw-o} + F_{PP} - F_R \qquad \text{(Equation 14)}$$

All calculations were conducted at constant salinity, with the base scenario having a salinity of 35 g kg^{-1} and temperature of 25 ºC. At initial conditions, seawater was assumed to be at 100 % oxygen saturation. Seawater inflow was assumed constant from an open ocean end member at 100 % oxygen saturation throughout the simulation. Gross primary production was defined according to Falter et al. (*90*):

$$F_{PP} = P * \sin\left(\frac{\pi(t-t_{sr})}{(t_{ss}-t_{sr})}\right)^{1.2} \text{ for } t_{sr} \leq t \leq t_{ss} \qquad \text{(Equation 15)}$$

$$F_{PP} = 0 \qquad \text{in all other cases}$$

where P is the maximum rate of gross primary production, t is time, and t_{sr} and t_{ss} represent the time of sunrise and sunset. For this model we used a 12-hour day night cycle, with sunrise and sunset being at 6am and 6pm respectively. Respiration was assumed to be constant. Primary production and respiration rates were prescribed according to typical coral reef rates (*90* and references therein), and tuned to reproduce a typical diel cycle of reef oxygen variability (194 µmol kg^{-1} to 233 µmol kg^{-1}). Thus, the maximum rate of gross primary production was prescribed at 40 mmol m^{-2} h^{-1} (P = 40 mmol m^{-2} h^{-1}) and respiration at 12 mmol m^{-2} h^{-1} resulting in a daily net productivity of 0 mmol m^{-2} day^{-1} in the base scenario. Numerical integration was conducted with Matlab R2018a (*91*) using an ordinary differential equation solver (ode45) based on an explicit Runge-Kutta (4, 5) formula. The model was run for 7 days.

Sensitivity analyses were conducted with respect to different residence times (1 and 5 hours) and three temperature scenarios (25 ºC, 28 ºC, 31 ºC) to assess the influence on both the mean and the diel variability in DO concentrations. For each scenario, open ocean and initial seawater

conditions were assumed to be at 100% oxygen saturation calculated using the constant salinity and given temperature of the scenario. Gross primary production was assumed to be unaffected by warming whereas respiration rates changed according to the Q_{10} relationship previously described (Eq. 9). The computational approximation approach employed to the global coral reef dataset was used for each model scenario and compared to the exact model results of DO concentrations (Fig. 3.S4). These comparisons showed that the approximation approach reproduced oxygen concentrations to within 0 to 0.5 μmol kg^{-1} of the actual results for a 1 hour residence time and within 0.1 to 5.6 μmol kg^{-1} for a 5 hour residence time once the model reached a near quasi-steady state (Fig. 3.S4). This comparison provides confidence of the application of the calculations used to estimate the effect of warming on oxygen solubility and biological oxygen demand for the global coral reef dataset.

ACKNOWLEDGEMENTS

Chapter 3, in full, is currently in review at Nature Climate Change as Global coral reefs will experience moderate to severe hypoxia before the end of the century. Pezner, Ariel K.; Courtney, Travis A.; Barkley, Hannah C.; Chou, Wen-Chen; Chu, Hui-Chuan; Clements, Samantha M.; Cyronak, Tyler; DeGrandpre, Michael D.; Kekuewa, Samuel A. H.; Kline, David I.; Liang, Yi-Bei; Martz, Todd R.; Mitarai, Satoshi; Page, Heather N.; Rintoul, Max S.; Smith, Jennifer E.; Soong, Keryea; Takeshita, Yui; Tresguerres, Martin; Wei, Yi; Yates, Kimberly K.; Andersson, Andreas J. The dissertation author was the primary investigator and author of this paper.

REFERENCES

1. L. Stramma, G. C. Johnson, J. Sprintall, V. Mohrholz, Expanding oxygen-minimum zones in the tropical oceans. *Science* **320**, 655–658 (2008).

2. R. F. Keeling, A. Körtzinger, N Gruber, Ocean deoxygenation in a warming world. *Ann. Rev. Mar. Sci.* **2**, 199–229 (2010).

3. D. Breitburg, L. A. Levin, A. Oschlies, M. Grégoire, F. P. Chavez, D. J. Conley, V. Garçon, D. Gilbert, D. Gutiérrez, K. Isensee, G. S. Jacinto, K. E. Limburg, I. Montes, S. W. A. Naqvi, G. C. Pitcher, N. N. Rabalais, M. R. Roman, K. A. Rose, B. A. Seibel, M. Telszewski, M. Yasuhara, J. Zhang, Declining oxygen in the global ocean and coastal waters. *Science* **359**, eaam7240 (2018).

4. N. L. Bindoff, W. W. L. Cheung, J. G. Kairo, J. Arístegui, V. A. Guinder, R. Hallberg, N. Hilmi, N. Jiao, M. S. Karim, L. Levin, S. O'Donoghue, S. R. Purca Cuicapusa, B. Rinkevich, T. Suga, A. Tagliabue, P. Williamson, "Changing ocean, marine ecosystems, and dependent communities" in *IPCC Special Report on the Ocean and Cryosphere in a Changing Climate*, H.-O. Pörtner, D. C. Roberts, V. Masson-Delmotte, P. Zhai, M. Tignor, E. Poloczanska, K. Mintenbeck, A. Alegría, M. Nicolai, A. Okem, J. Petzold, B. Rama, N. M. Weyer, Eds. (IPCC, 2019), chap. 5.

5. L. Kwiatkowski, O. Torres, L. Bopp, O. Aumont, M. Chamberlain, J. R. Christian, J. P. Dunne, M. Gehlen, T. Ilyina, J. G. John, A. Lenton, H. Li, N. S. Lovenduski, J. C. Orr, J. Palmieri, J. Schwinger, R. Séférian, C. A. Stock, A. Tagliabue, Y. Takano, J. Tjiputra, K. Toyama, H. Tsujino, M. Watanabe, A. Yamamoto, A. Yoo, T. Ziehn, Twenty-first century ocean warming, acidification, deoxygenation, and upper-ocean nutrient and primary production decline from CMIP6 model projections. *Biogeosci* **17**, 3439–3470 (2020).

6. A. H. Altieri, S. B. Harrison, J. Seemann, R. Collin, R. J. Diaz, N. Knowlton, Tropical dead zones and mass mortalities on coral reefs. *Proc. Nat. Acad. Sci.* **114**, 3660–3665 (2017).

7. H. R. Nelson, A. H. Altieri, Oxygen: The universal currency on coral reefs. *Coral Reefs* **38**, 177–198 (2019).

8. D. J. Hughes, R. Alderdice, C. Cooney, M. Kühl, M. Pernice, C. R. Voolstra, D. J. Suggett, Coral reef survival under accelerating ocean deoxygenation. *Nat. Clim. Change* **10**, 296–307 (2020).

9. A. K. Kealoha, S. M. Doyle, K. E. F. Shamberger, J. B. Sylvan, R. D. Hetland, S. F. DiMarco, Localized hypoxia may have caused coral reef mortality at the Flower Garden Banks. *Coral Reefs* **39**, 119–132 (2020).

10. T. L. Frölicher, E. M. Fischer, N. Gruber, Marine heatwaves under global warming. *Nature* **560**, 360–364 (2018).

11. R. Vaquer-Sunyer, C. M. Duarte, G. Jordà, S. Ruiz-Halpern, Temperature dependence of oxygen dynamics and community metabolism in a shallow Mediterranean macroalgal meadow (*Caulerpa prolifera*). *Estuar. Coast.* **35**, 1182–1192 (2012).

12. W. J. Sutherland, P. W. Atkinson, S. Broad, S. Brown, M. Clout, M. P. Dias, L. V. Dicks, H. Doran, E. Fleishman, E. L. Garratt, K. J. Gaston, A 2021 horizon scan of emerging global biological conservation issues. *Trends Ecol. Evol*. **36**, 87–97 (2021).

13. J. S. Gray, R. S. S. Wu, Y. Y. Or, Effects of hypoxia and organic enrichment on the coastal marine environment. *Mar. Ecol. Prog. Ser.* **238**, 249–279 (2002).

14. R. Vaquer-Sunyer, C. M. Duarte, Thresholds of hypoxia for marine biodiversity. *Proc. Nat. Acad. Sci* **105**, 15452–15457 (2008).

15. R. Vaquer-Sunyer, C. M. Duarte, Temperature effects on oxygen thresholds for hypoxia in marine benthic organisms. *Glob. Change Biol.* **17**, 1788–1797 (2011).

16. A. F. Haas, J. E. Smith, M. Thompson, D. D. Deheyn, Effects of reduced dissolved oxygen concentrations on physiology and fluorescence of hermatypic corals and benthic algae. *PeerJ* **2**, (2014).

17. M. D. Johnson, S. D. Swaminathan, E. N. Nixon, V. J. Paul, A. H. Altieri, Differential susceptibility of reef-building corals to deoxygenation reveals remarkable hypoxia tolerance. *Sci. Rep.* **11**, 1–12 (2021).

18. P. M. Gravinese, A. Douwes, K. R. Eaton, E. M. Muller, Ephemeral hypoxia reduces oxygen consumption in the Caribbean coral *Orbicella faveolata*. *Coral Reefs*, 1–6 (2021).

19. G. E. Nilsson, S. Östlund-Nilsson, P. L. Munday, Effects of elevated temperature on coral reef fishes: loss of hypoxia tolerance and inability to acclimate. *Comp. Biochem. Phys.* **156**, 389–393 (2010).

20. T. M. DeCarlo, A. L. Cohen, G. T. F. Wong, K. A. Davis, P. Lohmann, K. Soong, Mass coral mortality under local amplification of 2°C ocean warming. *Sci. Rep.* **7**, 1–9 (2017).

21. C. Hauri, N. Gruber, A. M. P. McDonnell, M. Vogt, The intensity, duration, and severity of low aragonite saturation state events on the California continental shelf. *Geophys. Res. Lett.* **40**, 3424–3428 (2013).

22. H. M. Guzmán, J. Cortés, P. W. Glynn, R. H. Richmond, Coral mortality associated with dinoflagellate blooms in the Eastern Pacific (Costa Rica and Panama). *Mar. Ecol. Prog. Ser.* **60**, 299–303 (1990).

23. K. D. Raj, G. Mathews, D. O. Obura, R. L. Laju, M. S. Bharath, P. D. Kumar, A. Arasamuthu, T. K. A. Kumar, J. K. P. Edward, Low oxygen levels caused by *Noctiluca scintillans* bloom kills corals in Gulf of Mannar, India. *Sci. Rep.* **10**, 1–7 (2020).

24. M. D. Johnson, J. J. Scott, M. Leray, N. Lucey, L. M. Rodriguez Bravo, W. L. Wied, A. H. Altieri, Rapid ecosystem-scale consequences of acute deoxygenation on a Caribbean coral reef. *Nat. Comm.* **12**, 1–12 (2021).

25. J. W. A. Murphy, R. H. Richmond, Changes to coral health and metabolic activity under oxygen deprivation. *PeerJ* **4**, e1956 (2016).

26. R. Alderdice, D. J. Suggett, A. Cárdenas, D. J. Hughes, M. Kühl, M. Pernice, C. R. Voolstra, Divergent expression of hypoxia response systems under deoxygenation in reef-forming corals aligns with bleaching susceptibility. *Glob. Change Bio.* **27**, 312–326 (2021).

27. H. Jorissen, M. M. Nugues, Coral larvae avoid substratum exploration and settlement in low-oxygen environments. *Coral Reefs* **9**, 31–39 (2021).

28. R. D. Villanueva, H. T. Yap, M. N. E. Montaño, Survivorship of coral juveniles in a fish farm environment. *Mar. Poll. Bull.* **10**, 580–589 (2005).

29. R. J. Diaz, R. Rosenberg, Marine benthic hypoxia: A review of its ecological effects and the behavioural responses of benthic macrofauna. *Oceanog. Mar. Biol.* **33**, 245–303 (1995).

30. H.-O. Pörtner, C. Bock, F. C. Mark, Oxygen- and capacity-limited thermal tolerance: Bridging ecology and physiology. *J. Exp. Biol.* **220**, 2685–2696 (2017).

31. C. Deutsch, A. Ferrel, B. Seibel, H.-O. Pörtner, R. B Huey, Climate change tightens a metabolic constraint on marine habitats. *Science* **348**, 1132–1135 (2015).

32. A. H. Altieri, K. B. Gedan, Climate change and dead zones. *Glob. Change Biol.* **21**, 1395–1406 (2015).

33. A. Steckbauer, S. G. Klein, C. M. Duarte, Additive impacts of deoxygenation and acidification threaten marine biota. *Glob. Change Biol.* **26**, 5602–5612 (2020).

34. W. J. Cai, X. Hu, W. J. Huang, M. C. Murrell, J. C. Lehrter, S. E. Lohrenz, W. C. Chou, W. Zhai, J. T. Hollibaugh, Y. Wang, P. Zhao, Acidification of subsurface coastal waters enhanced by eutrophication. *Nat. Geosci.* **4**, 766–770 (2011).

REFERENCES OCURRING ONLY IN SUPPLEMENTARY MATERIAL

35. T. Cyronak, Y. Takeshita, T. A. Courtney, E. H. DeCarlo, B. D. Eyre, D. I. Kline, T. Martz, H. Page, N. N. Price, J. Smith, L. Stoltenberg, M. Tresguerres, A. J. Andersson, Diel temperature and pH variability scale with depth across diverse coral reef habitats. *Limnol. Oceanog. Lett.* **5**, 193–203 (2020).

36. C. Roelfsema, E. M. Kovacs, K. Markey, J. Vercelloni, A. Rodriguez-Ramirez, S. Lopez-Marcano, M. Gonzalez-Rivero, O. Hoegh-Guldberg, S. R. Phinn, Benthic and coral reef community field data for Heron Reef, Southern Great Barrier Reef, Australia, 2002–2018. *Sci. Data* **8**, 1–7 (2021).

37. W. Ahmad, D. T. Neil, An evaluation of Landsat Thematic Mapper (TM) digital data for discriminating coral reef zonation: Heron Reef (GBR). *Int. J. Remote Sens.* **15**, 2583–2597 (1994).

38. I. R. Santos, R. N. Glud, D. Maher, D. Erler, B. D. Eyre, Diel coral reef acidification driven by porewater advection in permeable carbonate sands, Heron Island, Great Barrier Reef. *Geophys. Res. Lett.* **38**, L03604 (2011).

39. P. J. Bresnahan, T. R. Martz, Y. Takeshita, K. S. Johnson, M. LaShomb, Best practices for autonomous measurement of seawater pH with the Honeywell Durafet. *Methods Oceanog.* **9**, 44–60 (2014).

40. S. A. H. Kekuewa, T. A. Courtney, T. Cyronak, T. Kindeberg, B. D. Eyre, L. Stoltenberg, A. J. Andersson, Temporal and spatial variabilities of chemical and physical parameters on the Heron Island coral reef platform. *Aq. Geochem.*, 1–28 (2021).

41. K. Pedersen, "Spatiotemporal variability in seawater carbonate chemistry at two contrasting reef locations in Bocas Del Toro, Panama", thesis, University of California, San Diego, La Jolla, California (2019).

42. L. D'Croz, J. B. Del Rosario, P. Góndola, The effect of fresh water runoff on the distribution of dissolved inorganic nutrients and plankton in the Bocas Del Toro Archipelago, Caribbean Panama. *Car. J. Sci.* **14**, 414–429 (2005).

43. H. N. Page, T. A. Courtney, E. H. De Carlo, N. M. Howins, I. Koester, A. J. Andersson, Spatiotemporal variability in seawater carbon chemistry for a coral reef flat in Kāneʻohe Bay, Hawaiʻi. *Limnol. Oceanog.* **64**, 913–934 (2018).

44. S. V. Smith, W. J. Kimmerer, E. J. Laws, R. E. Brock, T. W. Walsh, Kaneohe Bay sewage diversion experiment: Perspectives on ecosystem responses to nutritional perturbation. *Pac. Sci.* **35**, 279–395 (1981).

45. P. Jokiel, "Jokiel's Illustrated Scientific Guide to Kaneʻohe Bay, Oʻahu" (Hawaiʻi Institute of Marine Biology, 1991).

46. Marine Environmental Program, "Marine Environmental Program Annual Report, 2006-2007." (Bermuda Institute of Ocean Sciences, 2007).

47. T. A. Courtney, A. J. Andersson, N. R. Bates, A. Collins, T. Cyronak, S. J. de Putron, B. D. Eyre, R. Garley, E. J. Hochberg, R. Johnson, S. Musielewicz, T. J. Noyes, C. L. Sabine, A. J. Sutton, J. Toncin, A. Tribollet, Comparing chemistry and census-based estimates of net ecosystem calcification on a rim reef in Bermuda. *Front. Mar. Sci.* **3**, 1–15 (2016).

48. A. K. Pezner, T. A. Courtney, H. N. Page, S. N. Giddings, C. M. Beatty, M. D. DeGrandpre, A. J. Andersson, Lateral, vertical, and temporal variability of seawater carbonate chemistry at Hog Reef, Bermuda. *Front. Mar. Sci.* **8**, 1–18 (2021).

49. Y. Takeshita, T. Cyronak, T. R. Martz, T. Kindeberg, A. J. Andersson, Coral reef carbonate chemistry variability at different functional scales. *Front. Mar. Sci.* **5**, 1–12 (2018).

50. K. S. Tkachenko, K. Soong, Dongsha Atoll: a potential thermal refuge for reef-building corals in the South China Sea. *Mar. Environ. Res.* **127**, 112–125 (2017).

51. Y. Duan, Y. Liu, M. Li, M. Zhou, Y. Yang, Survey of reefs based on Landsat 8 Operational Land Imager (OLI) images in the Nansha Islands, South China Sea. *Acta Oceanol. Sinica* **35**, 11–19 (2016).

52. C. -F. Dai, T. Y. Fan, "Coral fauna of Taiping Island (Itu Aba Island) in the Spratlys of the South China Sea" (Atoll Research Bulletin, Smithsonian Institution, 436, 1996).

53. P. -C. Chen, S. -L. Liu, DNA-assisted barcoding of seaweed community in Taiping Island in South China Sea. *Phycologia* **56**, 31 (2017).

54. M. Rintoul, T. Courtney, J. Dohner, S. Giddings, K. Inoha, S. Kekuewa, S. Mitarai, S. Monismith, A. K. Pezner, A. J. Andersson, The effects of light intensity and flow speed on biogeochemical variability within a fringing coral reef in Onna-son, Okinawa, Japan. *Submitted to JGR Oceans.*

55. M. Omori, Y. Higa, C. Shinzato, Y. Zayasu, T. Nagata, R. Nakamura, A. Yokokura, S. Janadou, "Development of active restoration methodologies for coral reefs using asexual reproduction in Okinawa, Japan", paper presented at the 13th International Coral Reef Symposium, Honolulu, Hawai'i, 1 December 2016.

56. C. A. Kellogg, K. K. Yates, S. N. Lawler, C. S. Moore, N. A. Smiley, "Seasonal microbial and environmental parameters at Crocker Reef, Florida Keys, 2014–2015" (U.S. Geological Survey Open-File Report, 2015).

57. K. K. Yates, C. S. Moore, N. H. Goldstein, E. T. Sherwood, "Tampa bay ocean and coastal acidification monitoring quality assurance project plan" (U.S. Geological Survey Open-File Report. Open-File Report, 2019).

58. K. K. Yates, C. S. Moore, N. A. Smiley, "Time series of autonomous carbonate system parameter measurements from Crocker Reef, Florida, USA" (U.S. Geological Survey data release, https://doi.org/10.5066/P90NCI8T, 2019).

59. J. Maragos, J. Miller, J. Gove, E. De Martini, A. M. Friedlander, S. Godwin, C. Musburger, M. Timmers, R. Tsuda, P. Vroom, E. Flint, E. Lundblad, J. Weiss, P. Ayotte, E. Sala, S. Sandin, S. McTee, T. Wass, D. Siciliano, R. Brainard, D. Obura, S. Ferguson, B. Mundy, "US coral reefs in the Line and Phoenix Islands, central Pacific Ocean: history, geology, oceanography, and biology." in *Coral Reefs of the USA*, B. M. Riegl, R. E. Dodge, Eds. (Springer Netherlands, 2008) pp. 595–641.

60. S. Boyle, V. De Anda, K. Koenig, E. O'Reilly, M. Schafer, T. Acoba, A. Dillon, A. Heenan, T. Oliver, D. Swanson, B. Vargas-Ángel, M. Weijerman, L. Wegley Kelly, R. Brainard, I. Williams. "Coral reef ecosystems of the Pacific Remote Islands Marine National Monument:

a 2000-2016 overview" (NOAA Pacific Islands Fisheries Science Center, PIFSC Special Publication, SP-17-003, 2017).

61. P. S. Vroom, C. A. Musburger, S. W. Cooper, J. E. Maragos, K. N. Page-Albins, M. A. V. Timmers, Marine biological community baselines in unimpacted tropical ecosystems: spatial and temporal analysis of reefs at Howland and Baker Islands. *Biodiv. Conserv.* **19**, 797–812 (2010).

62. Ecosystem Sciences Division, "National Coral Reef Monitoring Program: diel seawater carbonate chemistry observations from a suite of instrumentation deployed at coral reef sites at Tutuila Island, American Samoa from June 23 to July 17, 2018" (Pacific Islands Fisheries Science Center, NCEI Accession 0240606, 2021).

63. B. Vargas-Ángel, B. Huntington, R. E. Brainard, R. Venegas, T. Oliver, H. Barkley, A. Cohen, El Niño-associated catastrophic coral mortality at Jarvis Island, Central Equatorial Pacific. *Coral Reefs* **38**, 731–741 (2019).

64. Ecosystem Sciences Division, "National Coral Reef Monitoring Program: diel seawater carbonate chemistry observations from a suite of instrumentation deployed at coral reef sites at Baker Island, Jarvis Island, and Palmyra Atoll in the Pacific Remote Islands Marine National Monument between 2018-06-12 and 2018-08-07" (Pacific Islands Fisheries Science Center, NCEI Accession 0240686, 2021).

65. J. E. Smith, R. Brainard, A. Carter, S. Grillo, C. Edwards, J. Harris, L. Lewis, D. Obura, F. Rohwer, E. Sala, P. S. Vroom, S. Sandin, Re-evaluating the health of coral reef communities: baselines and evidence for human impacts across the Central Pacific. *Proc. Royal Soc. B: Biol. Sci.* **283**, p20151985 (2016).

66. Y. Takeshita, W. McGillis, E. M. Briggs, A. L. Carter, E. M. Donham, T. R. Martz, N. N. Price, J. E. Smith, Assessment of net community production and calcification of a coral reef using a boundary layer approach. *J. Geophys. Res.: Oceans* **121**, 5655–5671 (2016).

67. J. D. Collen, D. W. Garton, J. P. A. Gardner, Shoreline changes and sediment redistribution at Palmyra Atoll (Equatorial Pacific Ocean): 1874–present. *J. Coastal Res.* **25**, 711–722 (2009).

68. S. A. Sandin, J. E. Smith, E. E. DeMartini, E. A. Dinsdale, S. D. Donner, A. M. Friedlander, T. Konotchick, M Malay, J. E. Maragos, D. Obura, O. Pantos, G. Paulay, M. Richie, F. Rohwer, R. E. Schroeder, S. Walsh, J. B. C. Jackson, N. Knowlton, E. Sala, Baselines and degradation of coral reefs in the Northern Line Islands. *PLoS ONE* **3**, e1548 (2008).

69. G. J. Williams, J. E. Smith, E. J. Conklin, J. M. Gove, E. Sala, S. A. Sandin, Benthic communities at two remote pacific coral reefs: effects of reef habitat, depth, and wave energy gradients on spatial patterns. *PeerJ* **1**, e81 (2013).

70. D. Kelley, C. Richards, WG127 SCOR/IAPSO. gsw: Gibbs Sea Water Functions. R package version 1.0-5, (2017). https://CRAN.R-project.org/package=gsw

71. RStudio Team. RStudio: Integrated Development for R. (RStudio, PBC, Boston, MA, 2020).

72. H. C. Bittig, A. Körtzinger, C. Neill, E. van Ooijen, J. N. Plant, J. Hahn, K. S. Johnson, B. Yang, S. R. Emerson. Oxygen optode sensors: principle, characterization, calibration, and application in the ocean. *Front. Mar. Sci.* **4**, 1–25 (2018).

73. A. J. Andersson, N. R. Bates, F. T. Mackenzie, Dissolution of carbonate sediments under rising *p*CO2 and ocean acidification: observations from Devil's Hole, Bermuda. *Aq. Geochem.* **13**, 237–264 (2007).

74. E. F. Camp, M. R. Nitschke, R. Rodolfo-Metalpa, F. Houlbreque, S. G. Gardner, D. J. Smith, M. Zampighi, D. J. Suggett, Reef-building corals thrive within hot-acidified and deoxygenated waters. *Sci. Rep*. **7**, 1–9 (2017).

75. F. Giomi, A. Barausse, C. M. Duarte, J. Booth, S. Agusti, V. Saderne, A. Anton, D. Daffonchio, M. Fusi, Oxygen supersaturation protects coastal marine fauna from ocean warming. *Sci. Adv.* **5**, eaax1814 (2019).

76. Y. Takeshita, T. R. Martz, K. S. Johnson, J. N. Plant, D. Gilbert, S. C. Riser, C. Neill, B. Tilbrook. A climatology-based quality control procedure for profiling float oxygen data. *J. Geophys. Res.: Oceans* **118**, 5640–5650 (2013).

77. M. Dowle, A. Srinivasan. data.table: Extension of `data.frame`. R package version 1.13.6. (2020). https://CRAN.R-project.org/package=data.table

78. R. Rosenberg, "Effect of oxygen deficiency on benthic macrofauna in fjords" in *Fjord Oceanography* (Springer, Boston, MA, 1980), pp. 499–514.

79. A. F. Hofmann, E. T. Peltzer, P. M. Walz, P. G. Brewer, Hypoxia by degrees: establishing definitions for a changing ocean. *Deep Sea Res Part I: Oceanog. Res. Papers* **58**, 1212–1226 (2011).

80. G. Danabasoglu. NCAR CESM2-WACCM model output prepared for CMIP6 CMIP, Earth System Grid Federation. (2019). https://doi.org/10.22033/ESGF/CMIP6.10028.

81. G. Danabasoglu. NCAR CESM2-WACCM Model Output Prepared for CMIP6 ScenarioMIP, Earth System Grid Federation. (2019). https://doi.org/10.22033/ESGF/CMIP6.10101.

82. H. E. Garcia, L. I. Gordon, Oxygen solubility in seawater: better fitting equations. *Limnol. Oceanog.* **37**, 1307–1312 (1992).

83. P. W. Hochachka, G. N. Somero, *Biochemical Adaptations* (Oxford University Press, Oxford, 2002).

84. J. H. Brown, J. F. Gillooly, A. P. Allen, V. M. Savage, G. B. West, Toward a metabolic theory of ecology. *Ecology* **85**, 1771–1789 (2004).

85. C. D. Clausen, A. A. Roth, Effect of temperature and temperature adaptation on calcification rate in the hermatypic coral *Pocillopora Damicomis*. *Mar. Biol.* **33**, 93–100 (1975).

86. S. A. Howe, A. T. Marshall, Thermal compensation of metabolism in the temperate coral, *Plesiastrea Versipora* (Lamarck, 1816). *J. Exp. Mar. Biol. Ecol.* **259**, 231–248 (2001).

87. P. Edmunds, R. Gates, D. Gleason, The biology of larvae from the reef coral *Porites Astreoides*, and their response to temperature disturbances. *Mar. Biol.* **139**, 981–989 (2001).

88. P. J. Edmunds, Effect of elevated temperature on aerobic respiration of coral recruits. *Mar. Biol.* **146**, 655–663 (2005).

89. P. J. Edmunds, Differential effects of high temperature on the respiration of juvenile Caribbean corals. *Bull. Mar. Sci.* **83**, 453–464 (2008).

90. J. L. Falter, R. J. Lowe, Z. Zhang, M. McCulloch, Physical and biological controls on the carbonate chemistry of coral reef waters: effects of metabolism, wave forcing, sea level, and geomorphology. *PloS ONE* **8**, e53303 (2013).

91. MATLAB R2018a, Natick, Massachusetts: The MathWorks Inc (2021).

CHAPTER 4: Effects of spatiotemporal gradients in pH and oxygen on coral growth in a naturally variable seagrass bed

Ariel K. Pezner, Christopher D. Charles, Wen-Chen Chou, Hui-Chuan Chu, Travis A. Courtney, Benjamin W. Frable, Samuel A. H. Kekuewa, Keryea Soong, Yi Wei, and Andreas J. Andersson

ABSTRACT

Coral reefs are facing threats from a variety of global change stressors, including warming, ocean acidification, and oxygen loss. Although low oxygen and low pH conditions tend to co-occur in the natural environment, few studies have examined the simultaneous impacts of hypoxia and acidification on coral calcification and growth. In this study, we investigated differences in coral growth rates across a natural gradient in seawater temperature, pH, and dissolved oxygen (DO) variability in a seagrass bed within Dongsha Atoll, Taiwan, South China Sea. We observed a strong spatial gradient in temperature (up to 5 ºC), pH (0.29 pH units), and DO (and 129 μmol kg^{-1}) across the 1-kilometer wide seagrass bed over a single day. Similarly, diel variability recorded by an autonomous sensor in the shallow seagrass measured daily ranges in temperature, pH, and DO of up to 2.6 ºC, 0.55, and 204 μmol kg^{-1}. Despite these highly variable conditions, we observed many massive *Porites* corals scattered throughout the seagrass bed along the gradient. Cores collected from 15 of these coral colonies at 4 sites revealed no significant differences in coral calcification rates between sites along the gradients. However, there were significant differences in extension rate and density between corals at some sites. Isotopic analyses of two cores from the extreme ends of the gradient demonstrated that coral skeletal $\partial^{18}O$ strongly tracked local sea surface temperatures for both corals, but the seasonality and mean values of skeletal $\partial^{13}C$ differed depending on growth location.

INTRODUCTION

Coral reefs are experiencing a myriad of environmental changes, from warming to acidification and hypoxia (e.g., Pandolfi et al., 2011; Breitburg et al., 2018; Nelson and Altieri, 2019). Coral cover has been declining worldwide in recent decades, with a global loss of 13.5 % between 2009 and 2020 (Status of the Coral Reefs of the World: 2020, 2020). Warming in coastal areas has led to mass coral bleaching events and significant coral mortality in tropical reefs around the world (e.g., Hoegh-Guldberg, 1999). In addition, ocean acidification (OA), caused by the uptake of excess anthropogenic CO_2 in seawater (Doney et al., 2009), has been predicted to potentially decrease calcification rates in scleractinian corals (Chan and Conolly, 2013). While the effects of both temperature and acidification on coral growth have become relatively well-studied, less is known about the impacts of low oxygen or hypoxia on coral growth (for a review, see Nelson and Altieri, 2019). However, experimental and field evidence suggests that hypoxia can lead to mass mortality for vulnerable species (e.g., Altieri et al., 2017; Johnson et al., 2021). Importantly, rising temperatures, low pH, and low oxygen are not occurring in isolation, and many of the processes that cause warming, acidification, or hypoxia are interconnected (Altieri and Gedan, 2015).

Management strategies proposed to help ameliorate the effects of OA and hypoxia have included proposals to grow marine photosynthesizers near corals or place corals in areas with a high cover of primary producers. Experimental evidence suggests that primary producers like macroalgae and seagrasses can modify local water chemistry in ways to oppose OA, potentially leading to benefits for calcifiers downstream (Anthony et al., 2011). Marine photosynthesizers such as seagrasses are also predicted to potentially benefit from increased ocean acidity, as an increase in the CO_2 available in seawater can enhance photosynthetic rates (Invers et al., 1997;

Zimmerman et al., 1997). Thus, the potential refugia created by the primary producers could be maintained under increasing acidification.

Seagrasses are known to be among the most productive marine primary producers, and it is well-documented that they have the capacity to change the biogeochemistry of the surrounding seawater (Duarte and Chiscano, 1999; Marbà et al., 2006). These modifications can be observed over large spatial scales (Manzello et al., 2012; Buapet et al., 2013; Cyronak et al., 2018), and throughout the water column (Frankignoulle and Distèche, 1984). Daytime photosynthesis by the seagrasses removes dissolved inorganic carbon (DIC) from the water and produces oxygen, leading to an increase in pH and dissolved oxygen (DO) concentration (Marbà et al., 2006). This has led many to hypothesize that seagrasses can create a pH-refuge for other species from OA (Manzello et al., 2012; Hendriks et al., 2014; Koweek et al., 2018; Ward et al., 2022). Studies in some temperate species have shown that the presence of primary producers can relieve pH stress from acidification, leading to higher calcification rates (Semesi et al., 2009; Bergstrom et al., 2019; Ricart et al., 2021). However, models estimate that the ability of seagrasses to ameliorate OA impacts will likely vary as a function of depth-averaged and seasonal productivity as well as seawater residence time (Koweek et al., 2018; Ward et al., 2022)

While elevations of pH and DO during the daytime in areas with a high cover of primary producers may be beneficial, nighttime respiration significantly lowers pH and DO, often to or past the point of hypoxia (e.g., Camp et al., 2017; Cyronak et al., 2018a). Compared to coral reefs, the magnitude of change in pH and DO over a single day in ecosystems dominated by primary producers such as seagrasses, macroalgae, or mangroves is immense (e.g., Challener et al. 2016; Camp et al., 2017, 2019), with extremely low pH and DO in early morning and high pH and DO in the late afternoon. Currently, it is unclear whether the benefits of elevated pH and DO

during the day outweigh the potential costs of extremely low pH and DO at night for calcifying organisms like corals. Significant time and effort have been put into researching the effects of OA on calcifying species like corals with mixed results (for a review, see Chan and Connolly, 2013). In addition, research on the impacts of variable pH on photosynthesizing calcifiers has shown that the majority are indifferent to variable pH regimes (Kaspenberg and Cyronak, 2019). This may be due to the fact that the daytime increases in pH are transient, and often accompanied by similar nighttime minima that lead to no overall change in the mean pH experienced (Kaspenberg and Cyronak, 2019). While the effect of low pH may be minimal for many marine calcifiers, the effects of low and variable oxygen has been shown to have strong impacts for some species. In temperate mollusks growing in eelgrass dominated areas, variable DO and temperature had stronger impacts on mollusk physiology compared to pH, which had no effect (Spencer et al., 2019). Low oxygen alone has also been demonstrated to have negative impacts on coral calcification in the laboratory (Wijgerde et al., 2012, 2014). In the field, research in mangrove ecosystems has shown that corals can successfully grow in dynamic oxygen and pH environments, but with lower calcification and photosynthetic rates than corals found on reefs (Camp et al. 2017, 2019), suggesting there may be physiological tradeoffs.

In this study, we used a seagrass bed as a natural laboratory to investigate: 1) What is the natural spatiotemporal variability in seawater temperature, carbonate chemistry, and dissolved oxygen across the seagrass bed in Dongsha?; 2) How do potential gradients in these environmental parameters drive differences in coral growth rates across the seagrass bed?; and 3) How do these gradients control skeletal stable isotopic composition in corals collected inside and outside of the seagrass? To address these questions, we characterized changes in water chemistry and DO across the seagrass bed over space and time using in situ sampling and deployment of an

autonomous sensor. We also quantified annual skeletal density, calcification, and extension rates in massive *Porites* collected from four sites across the seagrass bed to assess how the chemical gradients might have influenced these growth parameters. Lastly, we measured the stable isotopic composition of two coral cores to further elucidate the potential impacts of this environmental variability on patterns of skeletal isotopic signatures.

MATERIALS AND METHODS

Study Site

Dongsha Atoll (20°40' N, 116°48' E) is a nearly circular coral atoll located in the northern South China Sea ~ 420 km southwest of Kaohsiung, Taiwan. Dongsha has an approximate diameter of 23 km and an area of 460 km^2 (Tkachenko and Soong 2017; Figure 1). The atoll is composed of a ~ 3 km wide shallow reef flat and an inner lagoon dominated by patch reefs with an average depth of 10 m (Chou et al., 2018). Water exchange with the open ocean occurs mainly through large open channels on the western side of the atoll both north and south of Dongsha Island.

Positioned on the western edge of the atoll, Dongsha Island (2.86 km long, 1.75 km^2) is home to expansive seagrass meadows that extend up to 1 km offshore, covering an estimated area of between 8.2 and 11.85 km^2, depending on the survey year and season (Dai, 2006; Lin et al., 2005; Huang et al., 2015). The seagrass meadows on Dongsha have been found to contain seven species of seagrass from six genera and two families, though the meadows on the north shore where the present study was conducted are dominated by *Thalassia hemprichii*, *Cymodocea rotundata*, and *Cymodocea serrulata* (Lin et al., 2005; Huang et al., 2015; Lee et al., 2015). Seagrass percent cover along the north shore was estimated to be 81% in 2011, with a

mean shoot density of between 455 and 2522 shoots m^{-2} (Huang et al., 2015). The seagrass beds are shallow, with a depth of 0.5 to 2.2 m nearshore (tidal range of 0.85 ± 0.21 m; Lee et al., 2015; this study) and 3 m offshore (Chou et al., 2018). Within these seagrass meadows are also some small patches of scleractinian corals, mainly massive *Porites* and some *Acropora* colonies. The presence of coral colonies in the seagrass bed have been noted in the literature since at least 1994 (Dai, 2006; Dai et al., 1995).

The climate on Dongsha Atoll is tropical, with sea surface temperatures ranging between 19.61 ºC and 31.77 ºC (NOAA Coral Reef Watch 1985-2022). The atoll experiences a dry season from October to May, driven by northeast monsoonal winds, with mean monthly rainfall of < 50 mm (Dai, 2006; Lin et al., 2005). Between June and September, southwest winds bring rain (mean monthly rainfall > 170 mm) and warmer temperatures (Dai, 2006; Lin et al., 2005). Typhoons also occur regularly during the wet season from July to October (Lin et al., 2005; Tkachenko and Soong, 2017).

Coral biodiversity across Dongsha Atoll is high, with 267 coral species identified as of 2017 (Dai et al., 1995; Dai, 2006). Coral cover was historically very high across Dongsha, with cover ranging from 80 to 95 % in many parts of the atoll in 1994 (Dai et al., 1995). However, intense pressure from illegal fishing, including use of dynamite and poison, has led to severe declines in coral cover and diversity since the late 1990s (Li et al., 2000). In addition, this area of the South China Sea has experienced coral bleaching events in 1998, 2007, 2010, and 2015-2016 that have driven increased coral mortality (Tkachenko and Soong, 2017). The major bleaching event in 1998 led to mass mortality of corals across the atoll lagoon and an estimated 95 % reduction in coral cover (Soong et al., 2002; Dai, 2006). In June 2015, a combination of El Niño Southern Oscillation-driven sea surface temperature warming and a confluence of local

conditions (low flow and weak winds) led to mass mortality of the reef community on the eastern reef flat (up to 40 %; DeCarlo et al., 2017). During both events, species-specific trends were observed, with higher mortality among the *Acropora spp.* and *Pocillopora spp.* corals (Tkachenko and Soong, 2017).

Spatial Surveys

To assess the spatial and temporal variability of water chemistry parameters and dissolved oxygen (DO) across the seagrass bed, water samples were collected at 12 stations on the north shore of Dongsha Island in 2018. The sampling area covered approximately 0.7 km^2 across the seagrass bed. The spatial surveys were conducted a total of four times, with one in the early morning (~6:30 – 7:15 h) on June 30, two in the early to mid-afternoon (~11:00 – 13:30 h) on June 27 and June 30, one in the late afternoon (~15:00 – 16:30 h) on June 26.

Spatial surveys were conducted using a jet-ski, with one driver and one collector, as the water depth was too shallow for boat use. Water samples (N = 48 total) were collected at the surface in 250 mL Pyrex glass sample bottles by rinsing the bottle with seawater three times and then submerging the bottle in the water until filled (ensuring no bubbles were collected) at all stations. In situ temperature and salinity were measured with a YSI 556 Handheld Multiparameter Instrument (accuracy: temperature ±0.15°C, salinity ±1%). Once all of the samples were collected, the bottles were then handed off to scientists on the beach and immediately fixed with 100 µL of a saturated $HgCl_2$ solution and sealed for later analyses of dissolved inorganic carbon (DIC) and total alkalinity (TA) (Dickson et al., 2007).

The water samples were transported back to Scripps Institution of Oceanography (SIO), where DIC was measured using an Automated Infra-Red Inorganic Carbon Analyzer (AIRICA,

Marianda) with a Li-COR 7000 detector. TA was analyzed via an open-cell potentiometric acid titration system developed by the Dickson Lab at SIO (Dickson et al., 2007). Accuracy (± precision) of TA and DIC measurements were calculated as the mean offsets (± SD) from Certified Reference Materials provided by the Dickson Lab and were 1.5 ± 2.5 μmol kg^{-1} (n = 23) for DIC and -0.62 ± 2.1 μmol kg^{-1} (n = 20) for TA. Additional carbonate chemistry parameters were calculated using CO2SYS for Excel (Lewis and Wallace, 1998) and the Seacarb package in R (Gattuso et al., 2021). Constants and scales used included: the first and second dissociation constants of carbonic acid (K1 and K2) from Mehrbach et al. (1973) refit by Dickson and Millero (1987), the dissociation constants of bisulfate (K_{HSO4}) from Dickson (1990) and total boron by Uppström (1974), and total scale pH (pH_T). For TA:DIC analyses, TA, DIC, and DO were normalized to a mean salinity across all surveys of 34.2 PSU. $nDIC_{NCP}$ was also calculated by removing the influence of $CaCO_3$ calcification and dissolution on DIC using the following equation, assuming mean TA across all surveys serves as a reasonable source water value:

$$nDIC_{NCP} = nDIC + \left(\frac{TA_{mean} - nTA}{2}\right) \qquad \text{(Equation 1)}$$

Autonomous Measurements

An Ocean Seven 316 Plus CTD (IDRONAUT S.r.l, Italy) was deployed at a shallow, nearshore site in the seagrass meadow to collect high frequency, temporal measurements of seawater chemistry and DO. This deployment site overlapped with the central nearshore survey station (Figure 1). The CTD recorded temperature (accuracy: ± 0.003 °C), salinity (± 0.003 mS cm^{-1}), DO (± 0.01 ppm), and pH_{NBS} (± 0.01) every 15 minutes. The CTD was deployed on 25 June 2018 and was left to collect at the shallow station until 8 July 2018. However, a problem

with the battery led to a loss of data between 27 June and 1 July 2018. Thus, only data from 2 July to 8 July 2018 are reported in the present study. All CTD pH data was converted from NBS scale to total scale using the offset from the pH of a bottle sample collected next to the CTD during deployment. pH from the bottle sample (in total scale) was calculated in CO2SYS using measured TA and DIC. The offset (-0.059) was calculated as the difference between the bottle pH and the average of the two CTD pH values at time points before and after the water sample was collected.

Coral Core Collection and Analysis

Coral cores were drilled from 20 individual colonies of massive *Porites* along a transect perpendicular to the north shore of Dongsha Island and along the inshore-offshore axis of the spatial surveys. To compare growth rates between corals across and outside of the seagrass bed, we selected 4 sites to collect cores (n = 5 per site) located: ~15 m offshore in dense seagrass ("Nearshore"), ~300 m offshore in seagrass ("Mid"), ~600 m offshore in a patch with no seagrass ("Outer"), and ~1 km offshore outside the seagrass bed ("Outside"). There was a slight depth gradient from the nearshore to outside locations, with the shallowest coral collected at ~ 0.6 m depth and the deepest coral collected at ~ 2.4 m depth (as measured by a SUUNTO Zoop Wrist Scuba Diving Computer).

Cores were drilled using a handheld pneumatic drill (Nemo Power Tools) and a 3 cm drill bit from freestanding massive *Porites* colonies of approximately the same size (~50 cm tall). Holes in the corals from coring were sealed with epoxy. Cores measured 3 cm in diameter, and most were ~20 cm in length (excluding those that broke or were interrupted by low drill battery). Cores were cleaned, dried, and shipped back to SIO for processing. Cores were slabbed using a

double-bladed lapidary saw and then x-rayed with matching aluminum and aragonite (*Tridacna sp.* shell) wedges at 35 kVp and 0.3 mAs for 40 seconds using a Faxitron X-Ray in the SIO Marine Vertebrate Collection. Scans of each core were then analyzed in Coral XDS (Helmle et al., 2003) to identify growth bands and calculate annual density, annual calcification, and linear extension rates. Unfortunately, 5 cores were removed from the analyses (one core from the nearshore, mid, and outer sites and two cores from the outside site) due to limited or unidentifiable annual banding patterns.

Coral Isotope Measurements and Chronology Development

Two coral cores, one from the nearshore collection site and one from the outside site, were analyzed for skeletal $\partial^{13}C$ and $\partial^{18}O$ isotopic composition. Core slabs for each coral were sampled at 1 mm intervals along a transect perpendicular to the growth axis of each core. Mean annual extension rates derived from Coral XDS analyses for the outside and nearshore corals between 2003 and 2017 were 0.9 and 1.2 cm year^{-1}, respectively. Thus, this sampling scheme achieved approximately monthly resolution. The samples were analyzed using the Kiel IV Carbonate Device and ICP mass spectrometer in the Charles Lab at SIO to measure $\partial^{13}C$ and $\partial^{18}O$ stable isotopic ratios, where $\partial^{13}C$ and $\partial^{18}O$ were calculated as follows:

$$\partial^{18}O = \left[\frac{^{18}O/^{16}O_{sample}}{^{18}O/^{16}O_{standard}} - 1\right] * 1000\ ‰ \qquad \text{(Equation 2)}$$

$$\partial^{13}C = \left[\frac{^{13}C/^{12}C_{sample}}{^{13}C/^{12}C_{standard}} - 1\right] * 1000\ ‰ \qquad \text{(Equation 3)}$$

NBS 19 standards were used for each run of the device and mass spectrometer. Long-term precision of these instruments is better than 0.08 ‰ for $\partial^{18}O$ and 0.06 ‰ for $\partial^{13}C$ (Charles et al., 2003).

To assign dates to the collected isotope data, the $\partial^{18}O$ record of each coral was compared to the available SST data from the NOAA Coral Reef Watch Satellite SST products for Dongsha Atoll. Mean monthly SST was calculated as the average between the monthly minimum and monthly maximum SST data points in the absence of finer temporal scale data. Given the strong seasonality of the skeletal $\partial^{18}O$ record for both corals, we assumed that this record would closely follow the local SST trend. With this assumption, maxima and minima of the $\partial^{18}O$ record were matched with the maxima and minima of the mean monthly SST record, knowing that the most recent maxima would have occurred in winter 2017 (as the corals were collected in summer 2018). After assigning the month and year for the maxima and minima, the na.fill() function from the 'zoo' package (Zeileis and Grothendieck, 2005) in RStudio (R Core Team, 2019) was used to interpolate the missing dates for the $\partial^{18}O$ and $\partial^{13}C$ records of each coral. Due to differing growth rates as well as drill angle, the number of samples for each core representing the same time period differed. Thus, for all analyses and statistics, only data from July 2007 to January 2018 for both cores was used for equal comparison.

Calculations and Statistical Analyses

Spatial gradients in temperature, carbonate chemistry, and DO across the seagrass were calculated as the difference between the survey mean and the station value for each parameter. This was performed for each survey independently. A positive value thus indicates that the value

recorded at the station was higher than the survey mean, whereas a negative value indicates a value lower than the survey mean.

To statistically compare the spatial gradients within each survey, linear models were constructed with survey and location as fixed effects (parameter ~ Location*Survey) for temperature, DO, pH, DIC, and TA. Stations were grouped into four groups of three stations corresponding to the four locations along the inshore-offshore gradient (nearshore, mid, outer, and outside). The 'emmeans' package and emmeans() function with a Tukey adjustment (Lenth, 2022) in RStudio (R Core Team, 2019) was used to compute pairwise comparisons of the locations for each survey and parameter.

Similarly, to compare extension rates, annual density, and calcification rates between coral cores at different locations, linear mixed effects models were constructed with location and core as random effects (i.e., growth parameter ~ location, random = ~ location | core) using the lme() function from the 'nlme' package (Pinheiro et al., 2021) in RStudio (R Core Team, 2019). The 'emmeans' package and emmeans() function with a Tukey adjustment (Lenth, 2022) in RStudio (R Core Team, 2019) was used to compute pairwise comparisons of these growth parameters between each location. Linear models were also created for calcification ~ density, density ~ extension, and extension ~ calcification using the lmodel2() function (Legendre, 2018) in RStudio (R Core Team, 2019) to compute r^2, slopes, and p-values.

For the isotope data, an unpaired, two-sample t-test using the t.test() function in RStudio (R Core Team, 2019) was used to compare the mean values of the $\partial^{13}C$ and $\partial^{18}O$ time series from the coral cores between the nearshore and outside coral cores. In addition, linear models were constructed for $\partial^{18}O \sim \partial^{13}C$ using the lmodel2() function (Legendre, 2018) in RStudio (R Core Team, 2019) to compute r^2, slopes, and p-values for each coral core.

RESULTS

Spatial Variability of Carbonate Chemistry and Dissolved Oxygen

Repeat spatial surveys over the seagrass bed revealed gradients in many parameters from nearshore to outside stations (Figure 2, S1; Table 1). These gradients were most pronounced during the early morning and late afternoon surveys.

In the early morning, spatial gradients were observed for all measured parameters: temperature, dissolved oxygen (DO), pH, dissolved inorganic carbon (DIC), and total alkalinity (TA) (Figure 2, S1). DO recorded at the nearshore stations was up to 69 μmol kg^{-1} lower than the early morning survey average and up to 129 μmol kg^{-1} lower than the highest value recorded at the outside stations (Figure 2, S1; Table 1). DO concentrations recorded at two of the three nearshore stations were severely hypoxic (< 61 μmol kg^{-1}; Rosenberg, 1980). pH at the nearshore stations was up to 0.13 units lower than the survey average and up to 0.24 units lower than the highest pH recorded at the outside stations (Figure 2, S1; Table 1). In contrast, DIC recorded at the nearshore and mid stations were up to 57 μmol kg^{-1} higher than the survey average and up to 104 μmol kg^{-1} higher than the lowest value recorded at the outside stations (Figure 2, S1; Table 1). Temperature and TA were more uniform amongst the mid, outer, and outside stations, but were still distinct from the nearshore stations (Figure 1, S1). Temperature at the nearshore stations was up to 1.0 ºC warmer and TA was up to 50 μmol kg^{-1} lower than the early morning survey average and up to 1.3 ºC warmer and 95 μmol kg^{-1} higher, respectively, than the lowest recorded value at the other stations (Figure 2, S1; Table 1).

Post-hoc Tukey tests of the linear models of the spatial gradients of each parameter across the early morning survey revealed that both mean DO and pH were significantly ($p <$

0.01) higher at both the outer and outside stations compared to the nearshore stations (Figure 3). However, while there appeared to be differences in mean temperature, DIC, and TA between the nearshore and outside stations, these difference were not statistically significant ($p > 0.05$, Tukey test; Figure 3).

Even more pronounced spatial gradients were observed during the late afternoon survey for all measured parameters (Figure 2, S1). Temperature at the nearshore stations was up to 2.6 ºC warmer than the survey average and up to 5.0 ºC warmer than the coolest outside station (Figure 2, S1; Table 1). DO and pH were up to 62 μmol kg^{-1} and 0.17 units higher at the nearshore stations than the survey average, and up to 129 μmol kg^{-1} and 0.29 units higher than the lowest values recorded at the outside stations, respectively (Figure 2, S1; Table 1). DIC was up to 204 μmol kg^{-1} lower at the nearshore stations and up to 342 μmol kg^{-1} lower than the highest value recorded at the outside stations (Figure 2, S1; Table 1). The gradients in total alkalinity, similar to the early morning survey, were less clear because both the highest and lowest TA were measured at adjacent nearshore stations.

Post-hoc Tukey tests of the linear models of the spatial gradients for the afternoon survey revealed that the mean temperature and pH at the mid, outer, and outside stations were significantly lower than the temperature at the nearshore stations ($p < 0.001$), but not significantly different between the other stations (Figure 3). Similarly, mean DIC at the mid, outer, and outside stations was significantly higher than the DIC at the nearshore stations ($p < 0.001$), but not significantly different between the other stations (Figure 3). Mean DO at the nearshore sites was also significantly higher at the nearshore stations compared to the outside stations ($p < 0.05$), but not statistically different from the other stations (Figure 3).

Spatial gradients were also observed during the mid-morning and mid-day surveys (Figure 1,S1), however they were much less pronounced than the gradients observed in the early morning and late afternoon and followed similar patterns to those of the late afternoon surveys.

Comparing observations at each station between the late afternoon and early morning surveys revealed strong temporal variability in all parameters along this spatial gradient. At the nearshore stations, temperature was up to 6.6 ºC warmer, the DO concentration 332 µmol kg^{-1} higher, and pH 0.76 units higher in the late afternoon survey compared to the early morning survey (Figure 1, Table 1). At the offshore stations, temperature was up to 3.9 ºC warmer, the DO concentration 175 µmol kg^{-1} higher, and pH 0.40 units higher in the late afternoon compared to the early morning survey (Figure 1, Table 1). The differences observed between the mid and outer stations between the early morning and late afternoon surveys were of similar magnitude. In addition, the differences between all station locations between the mid-morning and mid-day surveys were much smaller than the differences observed between the early morning and late afternoon surveys (Table 1).

Metabolic Controls of Variability

A regression of salinity normalized DIC (nDIC) and TA (nTA) revealed a significant, positive relationship (slope = 0.18, $r^2 = 0.45$, $p < 0.01$) (Figure 4A,B) and a regression of salinity normalized DO (nDO) and NCP DIC ($nDIC_{NCP}$) revealed a significant negative slope (slope = -0.51, $r^2 = 0.87$, $p < 0.01$). (Figure 4C,D). Observations of both nDIC and nTA and nDO and $nDIC_{NCP}$ clustered strongly by survey, station locations, and pH (Figure 4).

Fine Scale Temporal Variability of Temperature, pH, and Dissolved Oxygen

High frequency measurements from the CTD sensor deployed at the shallow seagrass site revealed a strong diel pattern of variability in temperature, DO, and pH (Figure 5). Across the 7-day deployment, the temperature varied between 29.08 ºC to 32.24 ºC, DO from 0 to 224 µmol kg^{-1} (0 to 121 % saturation), and pH from 7.67 to 8.36 (Table 2). Salinity was relatively invariable during dry conditions but increased in association with precipitation events (33.67 ± 1.08 PSU; mean ± SD) (Figure 5). Temperature, DO, and pH peaked in the late afternoon, and were lowest in the early morning (Figure 5). Diel variability in temperature had a mean daily range (± SD) of 2.28 ± 0.22 ºC across the 7-day deployment. DO and pH had mean daily ranges of 187 ± 14 µmol kg^{-1} (100 ± 7 % saturation) and 0.53 ± 0.02, respectively (Table 2). The DO concentrations in the seagrass bed reached hypoxic concentrations (< 61 µmol kg^{-1}; Rosenberg, 1980) every evening of the deployment (Figure 5).

Coral Core Linear Extension, Density, and Calcification Rates

Annual linear extension rate, density, and calcification rate varied both between and across years in the same coral core as well as between cores from all sites (Figures 6,7). Across all cores, years, and sites, the mean extension rate was 0.94 ± 0.36 cm $year^{-1}$ (mean ± SD), the mean annual density was 2.11 ± 0.40 g cm^{-3} $year^{-1}$, and the mean calcification rate was 1.98 ± 0.82 g cm^{-2} $year^{-1}$. We observed no clear temporal trends in calcification, extension, or density over the growth record for any site (Figure 6).

Due to variations in growth rates, core geometry, core length, and banding patterns, the number of usable growth years varied between cores. The core with the longest record had growth years dating to as early as 1994. All cores (N = 15, with poor quality cores removed)

contained data for growth years 2012 to 2017. Thus, only data from this 6-year period were used in statistical comparisons between sites (Figure 7).

Between 2012 and 2017, linear mixed effects models and a Tukey's pairwise comparison revealed no significant differences in calcification rates between corals from different sites (Figure 7, Table 3). However, there were significant differences between annual density and extension rates between corals collected at different sites (Figure 7, Table 3). Corals collected from the mid site had significantly higher mean annual density and significantly lower mean annual extension rates compared to corals collected at the nearshore site ($p < 0.05$; Figure 7, Table 3). In addition, the corals collected at the outside site had significantly higher mean annual density than the corals collected at the nearshore site ($p < 0.001$) and significantly higher mean annual extension rates compared to the corals from the mid site ($p < 0.05$; Figure 7, Table 3).

Linear regressions of pairs of the growth parameters across all cores from 2012 to 2017 revealed a strong, significant positive relationship between annual calcification rate and annual extension rate ($r^2 = 0.76$, $p < 0.01$) and weakly positive but significant relationship between annual calcification rate and annual density ($r^2 = 0.12$, $p < 0.01$; Figure 7). The relationship between annual extension rate and annual density was very weakly negative and not significant ($r^2 = 0.02$, $p = 0.1$; Figure 7).

Coral Core Skeletal Isotopic Composition ($\partial^{18}O$ and $\partial^{13}C$)

The time series of $\partial^{18}O$ from both coral cores was highly seasonal, with the record covering a near decade-long period between July 2008 and January 2017 (Figure 8). $\partial^{18}O$ varied between -6.222 ‰ and -4.476 ‰ for the coral collected from the outside site and between -6.235 ‰ and -4.211 ‰ for the coral collected from the nearshore site (Figure 8). $\partial^{18}O$ was more

negative in the summer months and more positive in the winter months (Figure 8). The mean values of $\partial^{18}O$ across the time series were not significantly different between the two corals (t-test, $p = 0.881$; Figure 9). The time series of $\partial^{13}C$ from the coral collected at the outside site was also seasonal, with more positive values in summer and more negative values in winter (Figure 8). The $\partial^{13}C$ time series was significantly anti-correlated to the $\partial^{18}O$ time series in the same core, though this relationship was relatively weak (linear model slope = -0.54, $r^2 = 0.17$, $p < 0.01$; Figure 9). $\partial^{13}C$ varied between -4.284 ‰ and -1.836 ‰ across the entire time series for the outside coral (Figure 8). The seasonal trend in the $\partial^{13}C$ for the nearshore coral was weaker, with much more high frequency variability and two extremely low $\partial^{13}C$ events during the record in summer 2007 and 2015 (Figure 8). Despite this high variability, the $\partial^{13}C$ time series for the nearshore coral was also weakly but significantly negatively correlated with $\partial^{18}O$ (linear model slope = -0.32, $r^2 = 0.15$, $p < 0.01$; Figure 9). The range of $\partial^{13}C$ for the nearshore coral was between -4.320 ‰ and -1.747 ‰ (Figure 8). In addition, the mean value of $\partial^{13}C$ was significantly higher in the nearshore coral than the outside coral (t-test, $p < 0.0001$; Figure 9).

DISCUSSION

Spatiotemporal Variability of Carbonate Chemistry and Dissolved Oxygen

Here, we demonstrate that at times there were significant gradients in seawater temperature, dissolved oxygen (DO), and carbonate chemistry across the Dongsha seagrass bed from inshore to offshore. The spatial gradients were present during all daytime surveys, but were strongest in the early morning and late afternoon (Figure 2), highlighting the high daytime productivity and nighttime respiration rates of the Dongsha seagrass system (Figure 4). The

maximum ranges of pH (0.76) and DO (332 μmol kg^{-1}) recorded across the Dongsha seagrass bed were generally larger than ranges reported from other spatial surveys of tropical and subtropical seagrass beds (Cyronak et al., 2018a). This is supported by previous work around Dongsha Island that has shown that seagrass productivity here is higher than the global average and higher than measurements for the same species in other areas (Huang et al., 2015).

These extreme diel changes were also captured by the autonomous sensor deployed in the shallow seagrass, which recorded fluctuations in temperature, DO, and pH that exceed global projections of warming, oxygen loss, and pH decline by the end of the century for the open ocean (Kwiatkowski et al., 2020; Figure 5). Previous work in seagrass meadows around the globe have reported pH fluctuations ranging from 0.25 to > 1 pH units (Frankignoulle and Bouquegneau, 1990; Marbà et al., 2006; Semesi et al., 2009; Unsworth et al., 2012; Challener et al., 2016; Saderne et al., 2019) across time scales varying from hours to months. Thus, the 0.7 pH unit range observed in the Dongsha seagrass over just a few days is relatively high compared to some seagrass beds. Notably, DO concentrations as measured by the CTD were severely hypoxic (< 61 μmol kg^{-1}; Rosenberg, 1980) every single night of the deployment (Figure 5). This nighttime hypoxia was also observed in the spatial surveys, with all of the measurements at the nearshore stations during the early morning survey either below or very close to severely hypoxic (Figure 2).

In contrast to DO, pH and DIC, total alkalinity was not significantly different between sites during any survey and changes between surveys were relatively small compared to the changes in DIC (Figure 3). Based on the shallow nTA:nDIC slope of 0.18 from the TA:DIC regression analysis (Figure 4A,B; Andersson and Gledhill, 2013; Cyronak et al., 2018b), and the strong relationship between nDO and $nDIC_{NCP}$ (Figure 4C,D), we can conclude a dominance of

organic carbon cycling processes (i.e., photosynthesis and respiration) over the inorganic carbon cycle ($CaCO_3$ calcification and dissolution) across the seagrass bed over diel timescales. This pattern holds across the seagrass bed, and led to the more distinct gradients in DO, pH, and DIC over time compared to TA (Figure 2,3). A dominance of organic carbon over inorganic cycling has previously been documented in the same seagrass bed over short time scales (Chou et al., 2018), though the nTA:nDIC slope was steeper (0.35) for samples collected over several years (Chou et al., 2021). Similar spatial studies of seagrass beds in Bermuda and San Diego, California reported similarly low TA:DIC slopes of 0.12 and -0.09, respectively (Cyronak et al., 2018a). However, studies of other seagrass beds, such as one conducted at a site in the Red Sea have reported much higher nTA:nDIC slopes (0.65 ± 0.05; Saderne et al., 2019), suggesting a stronger influence of inorganic carbon cycling in this seagrass bed.

All of the observed spatial and temporal trends in biogeochemical parameters were heightened in the shallow, nearshore areas of the seagrass compared to the outside stations, which was likely driven by a combination of shallower depth and higher seagrass density. Our depth measurements of the coral core collection locations suggest a depth gradient of ~ 0.6 m to 2.4 m nearshore to outside, depending on the tide. The nearshore stations were almost completely covered in seagrass, which led to a higher biomass to water volume ratio compared to the deeper outside stations. The outside stations were located outside of the farthest extent of the seagrass bed, and thus had a lower density of seagrass and a lower biomass to water volume ratio, leading to smaller changes in the magnitude of DO, pH, and DIC over time. Previous work in other seagrass beds and on coral reefs have demonstrated the importance of depth as a property influencing both temperature and carbonate chemistry variability (Cyronak et al., 2020), in addition to flow speed, water residence time, and path of the water over the reef (Page et al.,

2018; Pezner et al., 2021). Shallower depths allow for the benthic community to modify the above seawater to a greater extent, leading to larger differences along inshore-offshore gradients as well as larger differences between day and night (Unsworth et al., 2012; Falter et al., 2013). Thus, the greater influence of the seagrass in these shallow depths likely led to the high pH and DO values observed in this area. While the observations of DO, pH, and DIC at the outside stations still followed patterns of diel seagrass metabolism, the strength of these seawater modifications was smaller.

Coral Core Linear Extension, Density, and Calcification Rates

The mean annual extension, density, and calcification rates measured for the corals in the seagrass bed in this study are within values reported for other Indo-Pacific massive *Porites* (e.g., Lough, 2008; Cooper et al., 2012; Tanzil, 2013; Lough and Cantin, 2014). Given a mean annual SST of 26 ºC (Pan et al., 2017), the mean calcification rate of the corals collected in the Dongsha seagrass (2.0 ± 0.8 g cm^{-2} year^{-1}) is slightly higher than what would be predicted by the relationship proposed for Indo-Pacific *Porites* by Lough and Cantin (2014; ~ 1.5 g cm^{-2} year^{-1} for annual mean SST of 26 ºC). This suggests that Dongsha seagrass corals are calcifying faster than what would be expected for them based on SST alone, suggesting that perhaps other environmental factors may be influencing their calcification rates. The mean annual extension rate of the seagrass corals was somewhat low (0.9 ± 0.4 cm year^{-1}), but within the range of reported extension rates for massive *Porites* growing in more typical reef environments in the Indo-Pacific (0.54 – 2.67 cm year^{-1}; Lough et al., 2016). In contrast, the mean annual density of the seagrass corals (2.1 ± 0.4 g cm^{-3} year^{-1}) was much denser than those measured in other areas of the Indo-Pacific (0.95 – 1.70 g cm^{-3} year^{-1}; Lough et al., 2016).

Typically, there is a significant inverse relationship between skeletal density and extension rates for Indo-Pacific massive *Porites* (Lough and Barnes, 2000; Lough and Cantin, 2014). However, we observed no significant relationship between those parameters for these cores (Figure 7). Similarly, Indo-Pacific massive *Porites* skeletal density is typically weakly inversely related to calcification (Lough and Barnes, 2000; Lough and Cantin, 2014), but we observed a weakly significant positive relationship (Figure 7). In line with other Indo-Pacific massive *Porites*, we did observe the strongest relationship between extension and calcification rates (Lough and Barnes, 2000; Lough et al., 2016), suggesting that extension rates were the most important drivers of calcification in these corals (Figure 7).

A previous study of coral cores collected from the eastern reef flat of Dongsha Atoll reported higher mean annual extension rates than the seagrass corals (1.5 cm $year^{-1}$ versus 0.9 cm $year^{-1}$, respectively; DeCarlo et al., 2017). In addition, the mean annual calcification rate for the reef flat corals was lower than that of the seagrass corals (1.4 g cm^{-2} $year^{-1}$ versus 2.0 g cm^{-2} $year^{-1}$, respectively; DeCarlo et al., 2017). However, the reef flat corals were older (70-100 years old) than the corals in the present study (20-25 years old), which may complicate direct comparisons due to the potential age-dependence of skeletal growth rates (Lough and Cooper, 2011). The eastern reef flat where these corals were collected, aside from being a mainly coral environment, has a similar depth to the seagrass bed and thus is vulnerable to bleaching under periods of anomalously warm SST, as evidenced in 2015 (DeCarlo et al., 2017). While we observed no obvious signs of bleaching during 2015 in the seagrass coral cores, we did note high density stress bands in the year 2007 in 4 of our 15 cores (27 %). Similarly, DeCarlo et al. reported identifying stress bands in 6 of 22 (27 %) of their cores from the year 2007, suggesting

that the 2007 bleaching event was an atoll-wide event and may have affected massive *Porites* in both environments.

Given the large temperature, pH, and DO gradients experienced by the corals in the Dongsha seagrass, we expected to see differences in coral growth parameters along these gradients. Despite high interannual and inter-colony differences in growth parameters, particularly for the outer corals, we did observe some significant differences in annual extension rate and annual density between the nearshore cores and the mid and outside cores.

Surprisingly, we found that both the nearshore and outside corals had significantly higher mean annual extension rates than the corals at the mid site (Figure 7). It is well-established that depth, and therefore the amount of light, influences coral growth rates (e.g. Lough and Cooper, 2011). Typically, linear extension and calcification rates decrease with increasing water depth, while density increases (Lough and Cooper, 2011). In the Dongsha seagrass corals we observed this trend in density, where the nearshore corals were significantly less dense than the mid and offshore corals (Figure 7). However, the expected trend for extension rates did not hold across the depth gradient of the collection sites. Other studies of corals along inshore to offshore gradients have recorded trends in coral growth parameters, which were attributed to differences in nutrient availability, heterotrophy versus autotrophy, turbidity, and/or wave action (for a review, see Lough and Cooper, 2011). Thus, we believe that the observed differences in the seagrass corals may not be entirely explained by depth or light availability alone, and could be due to other environmental parameters we were unable to measure or simply individual differences in corals (e.g., Lough and Cooper, 2011; Lough et al., 2016).

Notably, we observed no significant differences in mean annual calcification rates between corals at any site along the gradient (Figure 7). While models have predicted that coral

calcification could be up to 18 % higher in the presence of seagrass (Unsworth et al., 2012), we see no evidence of significant elevation of calcification between the corals in the nearshore seagrass compared to those found outside of the seagrass bed. The impacts of seagrass presence on calcification for calcifiers in temperate systems have been shown to be mixed, with some studies showing no changes in calcification in the presence of seagrass (Groner et al., 2018; Lowe et al., 2019), whereas others found more positive effects (Wahl et al., 2018; Ricart et al., 2021). However, even with positive effects, there can be tradeoffs. Ricart et al., (2021) observed an increase in oyster shell growth rates with seagrass density, but this newly formed shell was thinner and less dense. While we found no significant differences in overall calcification rate of corals at any site, there were significant differences in extension and density (Figure 7). Thus, perhaps while the nearshore corals were able to maintain similar calcification rates as their peers in less variable areas of the seagrass, there is a tradeoff of decreased density for increased extension rates, similar to the oysters in Ricart et al. (2021).

Growth rate data from massive *Porites* colonies living in seagrass beds is limited. However, other studies of changes in massive *Porites* growth under either experimental or natural exposure to low pH have found that calcification tends to be quite resistant to acidification either alone or in combination with other stressors. For example, in a study testing the interactive effects of low pH and high temperature on massive *Porites*, calcification was found to be unaffected by either treatment either alone or in combination (Edmunds et al., 2012). Other experimental studies have yielded mixed responses to various acidification treatments, varying by species, variable versus static exposure, and method of acidification (e.g., Chan and Connolly, 2012; Comeau et al., 2013; Edmunds et al., 2012; Kaspenberg and Cyronak, 2019). In a study of corals found at natural CO_2 seeps, researchers found no significant differences in

calcification rates of massive *Porites* growing near the low pH seeps versus outside of them (Fabricius et al., 2011). Similar to the Dongsha seagrass bed, there was low diversity of corals at the low pH site, with very few structurally complex "weedy" corals, suggesting that massive *Porites* may be particularly insensitive to low pH environments (Fabricius et al., 2011).

In addition to low pH, the corals in the shallow seagrass are also experiencing high temperatures and hypoxic oxygen concentrations on a daily basis. While the relationship between temperature and calcification is relatively well-known (e.g., Lough and Barnes, 2000; Lough et al., 2016), few studies have quantified the effects of hypoxia on tropical coral growth and no studies have tested the interactive effects of temperature, pH, and hypoxia together. Calcification rates and temperature generally scale linearly as discussed above, however extreme temperature events that lead to bleaching can lead to suspensions or cessations in coral growth (e.g., DeCarlo et al., 2017). The effects and mechanisms of hypoxia on calcification are not as well resolved. While one study recorded increases in daytime calcification rate under elevated oxygen (Colombo-Pallotta et al., 2010), another found that both hypoxia and hyperoxia decreased daytime calcification rates, regardless of coral nutrition (Wijgerde et al., 2012). Other studies have found that nighttime hypoxia decreases dark calcification rates (Al-Horani et al., 2007). In a study of both pH and oxygen, daytime hyperoxia was found to negate the positive effects of elevated pH on calcification (Wijgerde et al., 2014). Despite these findings, we recorded elevated calcification rate of the corals in the Dongsha seagrass bed relative to published data for other Indo-Pacific massive *Porites* and what would be expected based on temperature alone (e.g., Lough et al., 2016), as well as a lack of differences in calcification rate across the environmental gradient. We find it likely that the corals in the Dongsha seagrass have naturally acclimated or adapted to living in these conditions, and have thus been able to maintain

their calcification rates. Being one of the only coral species to inhabit the seagrass bed suggests that these massive *Porites* may be particularly resistant to environmental stressors compared to other species found on Dongsha Atoll.

Lastly, while other studies have found significant decreases in calcification, density, and extension rate in recent decades for massive *Porites*, *Pocillopora damicornis*, and other species (De'ath et al., 2009; Manzello 2010), we found no trends of declining growth in the seagrass corals over time (Figure 7). Similarly, the study of much older massive *Porites* from the eastern reef flat of Dongsha Atoll also found no significant decline in calcification rate over time (DeCarlo et al., 2017). Thus, corals on Dongsha Atoll appear to be doing well when compared to global trends of coral growth.

Coral Core Skeletal Isotopic Composition (∂^{18}O and ∂^{13}C)

While we observed significant differences in temperature between the nearshore and outside sites over the short time scale of this study, the similar mean skeletal ∂^{18}O of the corals collected at these sites suggests that on longer time scales, these corals experienced similar seasonal temperature and salinity conditions (Figure 8,9; Urey, 1974; McCrea, 1950; Epstein et al., 1953; Epstein and Mayeda, 1953). It is likely that these short-term, diel differences in temperature at the two sites led to overall equal monthly and annual average temperature values that were then incorporated as similar ∂^{18}O in the coral skeletons. In the absence of long term in situ temperature data for the nearshore and outside sites, our comparisons rely on satellite-sensed SST, which cannot be resolved to scales small enough to compare the two sites. Based on the NOAA satellite SST data for Dongsha, we observe the expected seasonal patterns of skeletal ∂^{18}O tracking SST, with lower values during the warm summer months and higher values during

the cooler winter months (Figure 8). It is well-established that skeletal $\partial^{18}O$ is a good proxy for both water temperature and the $\partial^{18}O$ of seawater (Urey, 1974; McCrea, 1950; Epstein et al., 1953; Epstein and Mayeda, 1953). Thus, these observations match previous measurements in many other corals. We do note, however that the range of values of $\partial^{18}O$ are quite high compared to most measurements made in other tropical corals (e.g., Fairbanks and Dodge, 1979; Gagan et al., 1994; Grottoli, 1999), highlighting the uniquely warm environment that these corals are able to persist in.

The differences in skeletal $\partial^{13}C$ between the nearshore and outside corals, as well as the differences in skeletal $\partial^{13}C$ over time in both corals, could be the result of one or more environmental and/or physiological processes. While the environmental controls on skeletal $\partial^{18}O$ have been long known, the environmental and physiological significance of skeletal $\partial^{13}C$ patterns are less well-resolved. Previous work has shown that variations in skeletal $\partial^{13}C$ can be the result of variations in symbiont respiration and photosynthesis (Goreau, 1977; Erez, 1978; Grottoli and Wellington 1999), light availability/depth (e.g. Weber et al., 1976; Fairbanks and Dodge 1979; Muscatine et al., 1989; Guzmán and Tudhope 1998; Grottoli 2002; Rosenfeld et al., 2003; Linsley et al., 2019), host reproduction and spawning (Gagan et al. 1994, 1995), kinetic effects related to calcification and growth rate (Land et al. 1975; McConnaughey 1989, 1997), and pH (Adkins et al., 2003; Martin et al., 2016).

We propose several hypotheses to explain the observed trends in skeletal $\partial^{13}C$ in the seagrass corals. In the first hypothesis, we propose that the seagrass is modifying the $\partial^{13}C$ of the DIC in the seawater. These modifications of the $\partial^{13}C$ of DIC may be related to seagrass productivity and thus may occur seasonally, leading to the clearer seasonal trends in skeletal $\partial^{13}C$ for the outside coral. Seagrass biomass and growth rates tend to follow seasonal patterns,

with higher growth in late summer and lower growth in winter (Duarte, 1989). These variations can also lead to seasonal patterns in the modification of the overlying seawater carbonate chemistry and DO concentrations (e.g., Ganguly et al., 2017; Challener et al., 2016). The skeletal $\partial^{13}C$ of the outside coral follows an approximately seasonal pattern, with lower $\partial^{13}C$ in winter and higher $\partial^{13}C$ in summer (Figure 8). This could be linked to increased uptake of local DIC for photosynthesis by the seagrasses in summer, wherein the seagrasses preferentially take up the lighter DIC with lower $\partial^{13}C$ for their photosynthesis. This leaves behind DIC with a heavier $\partial^{13}C$ signature for the coral symbionts to use during summer and thus be incorporated into the host skeleton. In winter, when the seagrasses are not as productive, the corals have access to more of the lighter $\partial^{13}C$ DIC and thus incorporate lower $\partial^{13}C$ values in their skeletons. Previous work on reefs in Florida have confirmed that the $\partial^{13}C$ of the DIC in seawater does change seasonally and these trends match those of the $\partial^{13}C$ of corals collected from those reefs (Swart et al., 1996). This seasonal trend is suggested to reflect the overall productivity of the community, with the heaviest $\partial^{13}C$ of DIC occurring during the periods of maximum light and productivity (Swart et al., 1996). The nearshore coral, in contrast, was growing in the shallowest and densest part of the seagrass bed, which we suggest likely remains fairly productive throughout the entire year. This maintenance of productivity, and thus uptake of lighter DIC may explain why the skeletal $\partial^{13}C$ record of the nearshore coral is much more variable without the clear same seasonal trend and significantly higher than the $\partial^{13}C$ of the outside coral throughout the entire record (Figure 8,9).

In our second hypothesis, we propose that depth and food source may have also driven some of the differences in skeletal $\partial^{13}C$ between the nearshore and outside coral. We observed significantly lower mean skeletal $\partial^{13}C$ in the outside coral (collected at 2.4 m depth) compared to the nearshore coral (collected at 1.2 m depth) (Figure 9). Many studies have found that skeletal

$\partial^{13}C$ decreases with depth (Weber et al., 1976; Weber and Woodhead, 1970; Fairbanks and Dodge 1979; Muscatine et al., 1989; Guzman and Tudhope 1998; Rosenfeld et al., 2003; Linsley et al., 2019). At increasing depths, less light is available for photosynthesis, leading to reduced coral symbiont photosynthetic rates. In order to maintain enough energy for growth, corals at depth or in areas of reduced light may rely more on heterotrophy, which in turn also reduces skeletal $\partial^{13}C$ (Grottoli-Everett, 1998; Grottoli, 2000). This also supports our observation that the seasonal pattern of $\partial^{13}C$ closely tracked that of the $\partial^{18}O$ for the deeper outside coral, whereas this was less clear for the nearshore coral. Reduced light during winter months led to a stronger reliance on heterotrophy, leading to lower $\partial^{13}C$ in the outside coral, and the high dependence on light led to a stronger seasonal pattern.

Lastly, we hypothesize that the two major decline events in the skeletal $\partial^{13}C$ of the nearshore coral may be due to bleaching or coral spawning events. The extremely low values of $\partial^{13}C$ both occurred during years that bleaching was either reported on Dongsha Atoll (2015; DeCarlo et al., 2017) or observed in the skeletal record of other cores from this study (2007). Previous studies of $\partial^{13}C$ in bleached corals have shown that bleaching can lead to sharp declines in $\partial^{13}C$ in Caribbean *Montastraea annularis* (Porter et al. 1989), Costa Rican *Porites lobata* (Carriquiry et al. 1994), *Porites* from Japan (Suzuki et al. 2003), and *Porites compressa* and *Montipora verrucose* from Hawai‘i (Grottoli et al. 2004). However, similar declines in $\partial^{13}C$ have also been observed in Indo-Pacific *Porites* following coral spawning events (Gagan et al., 1994, 1996). Without more data on spawning patterns for corals in this area or bleaching surveys, we cannot confirm which if either of these potential causes may be more likely for this coral.

CONCLUSION

Overall, we demonstrate that seagrass on Dongsha has the ability to strongly modify local water chemistry and dissolved oxygen concentrations over both time and space. While the seagrass elevates local pH and DO during the daytime, it also creates acidic and hypoxic conditions at night. Despite these variable conditions, we show that the corals in the Dongsha seagrass bed are persisting and growing at all sites along this extremely dynamic temperature, pH, and dissolved oxygen gradient, though perhaps with tradeoffs in terms of density or extension rate. However, we found no evidence to suggest that corals growing in shallow areas surrounded by seagrass had enhanced calcification rates compared to corals growing outside of the seagrass bed. Additional research is needed to investigate whether corals exposed to natural variability in pH and oxygen are better prepared for future exposure to low pH or oxygen. We believe environments such as seagrass beds that support corals can serve as natural laboratories to test how corals will fare under more extreme variable conditions as well as future studies investigating the mechanisms of this tolerance.

ACKNOWLEDGEMENTS

We thank National Sun Yat-sen University, the Coast Guard Administration of Taiwan, the Dongsha Atoll Marine National Park employees, Oscar Ng, Yuli Chiu, Hai-Jin Zhang, Di Bing Tam, Jeanie Lim, and Rong-Wei Syu for their help in coordinating and assisting with fieldwork. We also thank Dr. Phil Hastings and the Scripps Institution of Oceanography Marine Vertebrate Collection for access to x-radiography instruments as well as Dr. Jessica Carilli and Dr. Richard Norris for access to the aragonite and aluminum wedges used in the x-radiography. We also thank Noreen Garcia and Anna Golub for assistance in running the stable isotope samples. This research was supported by the National Science Foundation Graduate Research

Fellowship (DGE-2038238) and a Philanthropic Educational Organization (P.E.O.) Scholar Award to AKP as well as National Science Foundation OCE-1829778 (AJA).

TABLES

Table 4.1: Seagrass spatial survey statistics. Minimum, maximum, range, and mean (± standard deviation; n = 12 per survey) temperature, salinity, dissolved oxygen concentration, dissolved oxygen percent saturation, total scale pH (pH_T), dissolved inorganic carbon, and total alkalinity for all spatial surveys from in situ YSI measurements and bottle sample data.

		Survey			
		June 30 06:34–07:15	**June 27** 11:04–11:56	**June 30** 12:43–13:27	**June 26** 15:13–16:21
Temperature (°C)	*Min*	28.3	28.7	29.8	30.5
	Max	29.6	31	30.8	35.5
	Range	1.3	2.3	1	5
	Mean ± SD	28.6 ± 0.4	29.7 ± 0.8	30.3 ± 0.3	32.9 ± 1.6
Salinity (PSU)	*Min*	34.3	32.6	34.3	33.5
	Max	34.3	34.2	34.3	35.2
	Range	0	1.6	0	1.7
	Mean ± SD	34.3 ± 0	33.9 ± 0.5	34.3 ± 0	34.2 ± 0.4
Dissolved Oxygen (µmol kg^{-1})	*Min*	61.2	186.8	199.1	263.6
	Max	189.7	244.9	260.3	392.8
	Range	128.5	58.2	61.2	129.3
	Mean ± SD	130.1 ± 45.3	214.4 ± 19.5	227.4 ± 20	330.6 ± 41.7
Dissolved Oxygen Percent Saturation (%)	*Min*	32	95	103	142
	Max	97	127	138	224
	Range	65	32	35	82
	Mean ± SD	67 ± 23	111 ± 10	120 ± 11	181 ± 26
pH_T	*Min*	7.73	7.94	7.99	8.2
	Max	7.97	8.08	8.12	8.49
	Range	0.24	0.14	0.13	0.29
	Mean ± SD	7.86 ± 0.08	8.05 ± 0.05	8.05 ± 0.05	8.32 ± 0.11
Dissolved Inorganic Carbon (µmol kg^{-1})	*Min*	1952	1836	1819	1397
	Max	2056	1933	1904	1739
	Range	104	97	85	342
	Mean ± SD	1999 ± 37	1865 ± 32	1863 ± 35	1601 ± 102
Total Alkalinity (µmol kg^{-1})	*Min*	2168	2178	2161	2107
	Max	2263	2197	2223	2233
	Range	95	20	63	126
	Mean ± SD	2217 ± 24	2189 ± 7	2199 ± 17	2146 ± 37

Table 4.2: Seagrass CTD sensor statistics. Daily statistics (mean daily minimum, maximum, range, and mean ± SD) and deployment absolute minima and maxima for temperature, salinity, dissolved oxygen concentration, dissolved oxygen percent saturation, and total scale pH recorded by the autonomous sensor in the shallow seagrass. Only full days (i.e., complete 24-hour cycle) are included in daily means (2-7 July 2018).

	Temp (ºC)	Salinity (PSU)	DO (µmol kg^{-1})	DO Saturation (%)	pH_T
Mean daily min	29.4 ± 0.4	32.6 ± 1.8	20.7 ± 17.1	11 ± 9	7.76 ± 0.06
Mean daily max	31.7 ± 0.3	34 ± 0	208.1 ± 8.2	111 ± 4	8.3 ± 0.05
Mean daily range	2.3 ± 0.2	1.4 ± 1.8	187.5 ± 14.2	100 ± 7	0.53 ± 0.02
Mean daily mean	30.7 ± 0.3	33.8 ± 0.1	115.4 ± 5	61 ± 3	8.04 ± 0.04
Deployment min	29.1	23.6	0.0	0	7.67
Deployment max	32.2	34.0	224.1	121	8.36

Table 4.3: Mean coral core growth parameters by site between 2012 and 2017. Mean annual extension, density, and calcification rates between 2012 and 2017 for corals at the nearshore (n = 4), mid (n = 4), outer (n = 4), and outside sites (n = 3), as well as averaged across all sites (n = 15).

	Mean annual extension Rate (cm $year^{-1}$)	Mean annual density (g cm^{-3} $year^{-1}$)	Mean annual calcification Rate (g cm^{-2} $year^{-1}$)
Nearshore	1.10 ± 0.29	1.79 ± 0.12	1.95 ± 0.44
Mid	0.69 ± 0.18	2.38 ± 0.39	1.66 ± 0.51
Outer	0.94 ± 0.36	1.97 ± 0.38	1.93 ± 0.96
Outside	1.01 ± 0.24	2.26 ± 0.17	2.28 ± 0.53
Across all sites	0.93 ± 0.31	2.09 ± 0.38	1.93 ± 0.68

FIGURES

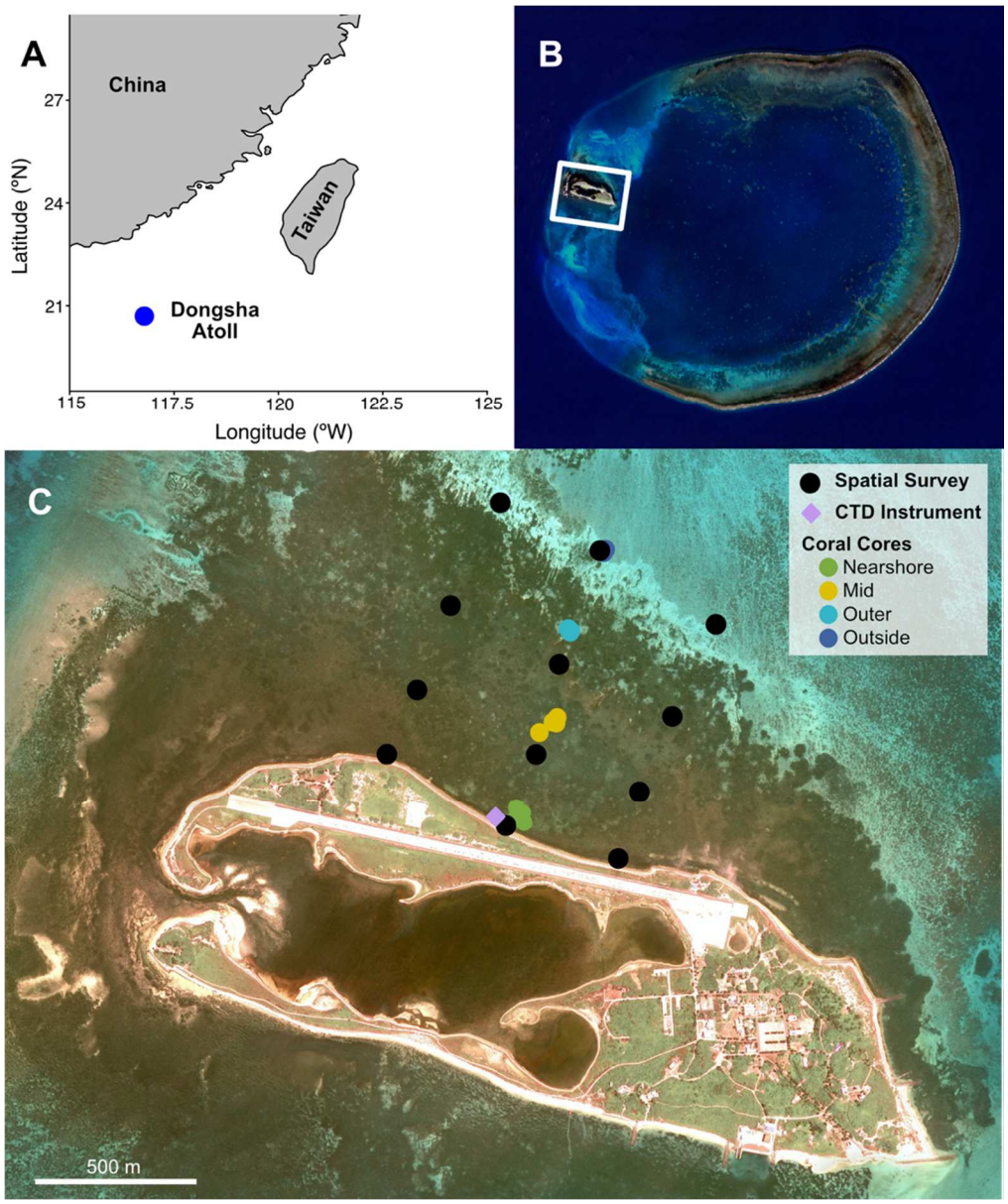

Figure 4.1: Map of study site and sampling locations. (A) Map of the South China Sea including coastal China, Taiwan (Republic of China), and Dongsha Atoll (blue circle); **(B)** Image of Dongsha Atoll (Taiwan News) and Dongsha Island study area (white rectangle); **(C)** Google Earth image of Dongsha Island and surrounding seagrass beds. Spatial survey locations are denoted by black circles, the CTD instrument deployment location is denoted by a pink diamond, and the coral core collection locations are shown in circles colored by collection location (nearshore – green, mid – yellow, outer – light blue, and outside – dark blue). These same names are used to refer to the groups of 3 spatial survey stations spanning northwest to southeast near the core collection locations.

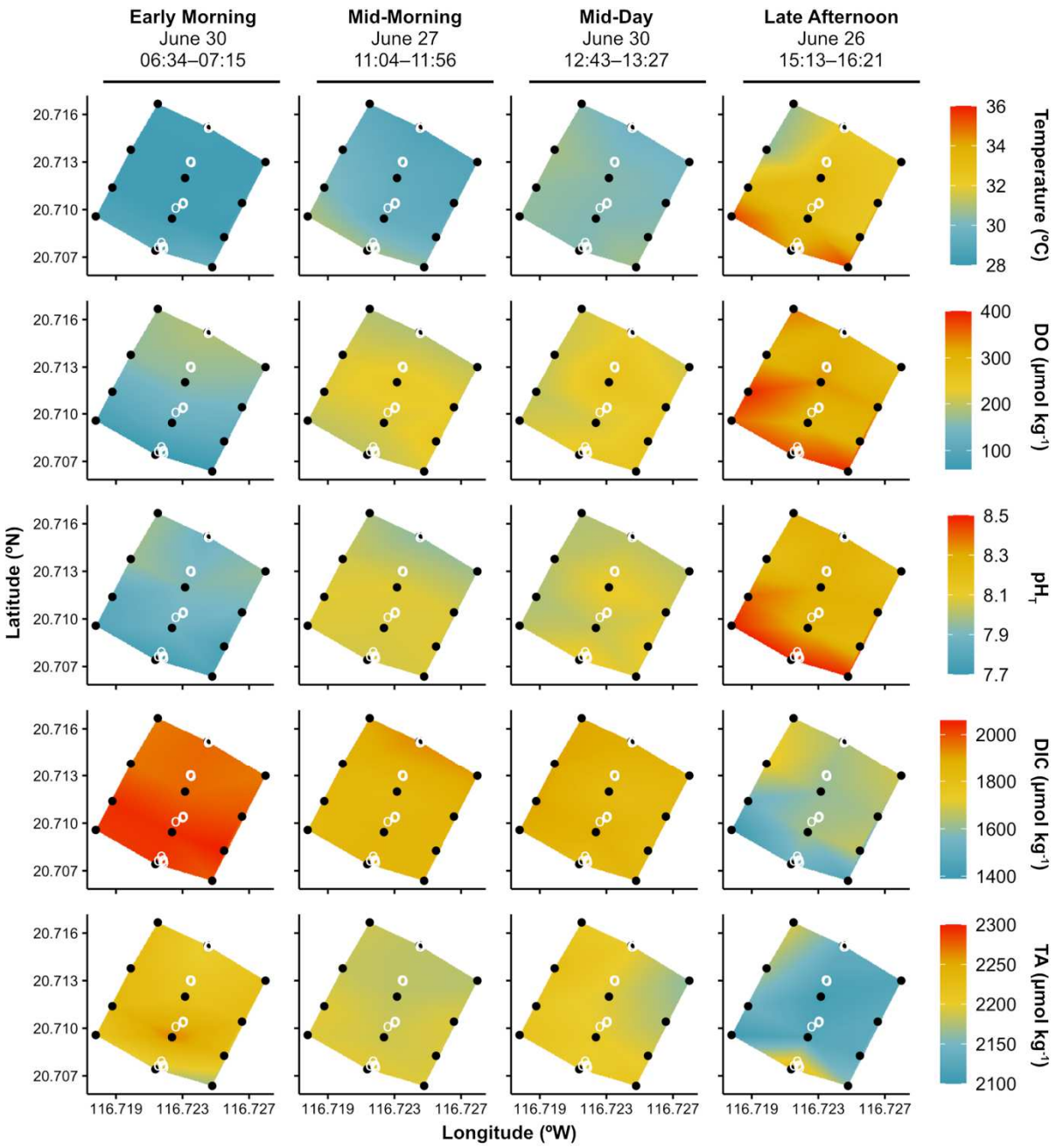

Figure 4.2: Spatial surveys of temperature, water chemistry, and dissolved oxygen across the seagrass. Spatiotemporal variability in temperature (ºC), dissolved oxygen (DO; µmol kg^{-1}), total scale pH (pH_T), dissolved inorganic carbon (DIC; µmol kg^{-1}); and total alkalinity (TA; µmol kg^{-1}) across the four spatial surveys (stations denoted by black circles) in the Dongsha Island north shore seagrass bed. Coral core collection locations are denoted by white open circles. Times listed below dates represent the time of collection of the first and last sample of the survey (local time).

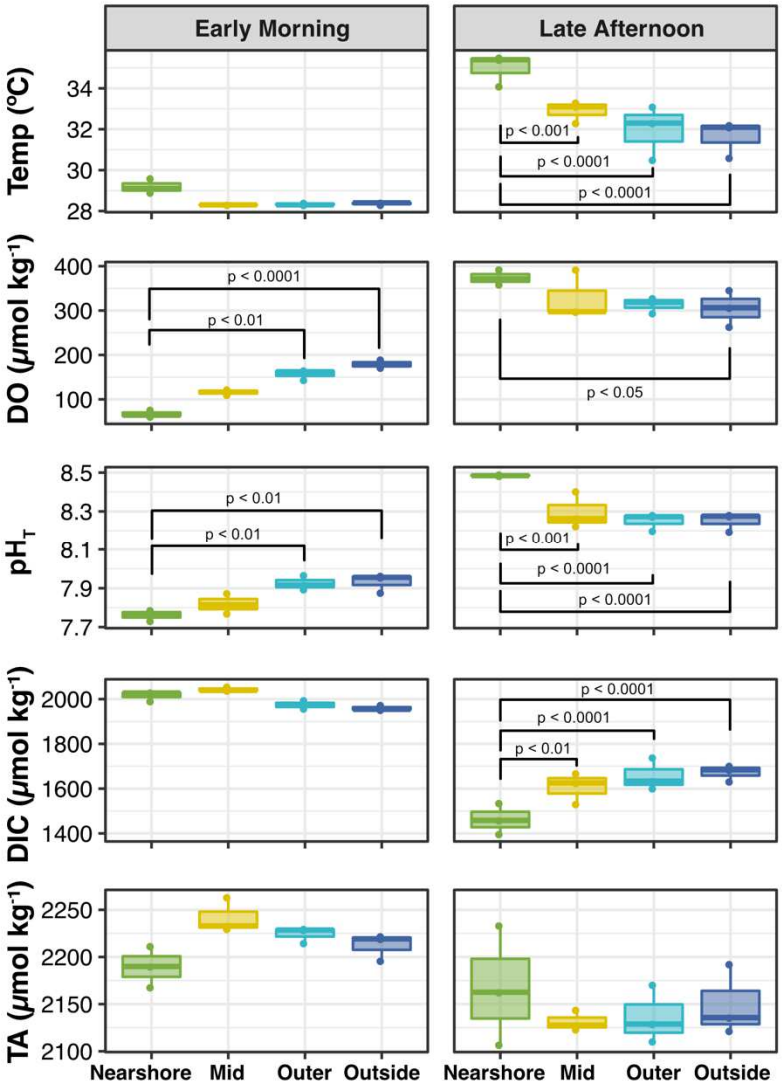

Figure 4.3: Spatial gradients in water chemistry and oxygen in the early morning and late afternoon. Boxplots of temperature (ºC), dissolved oxygen (DO; µmol kg^{-1}), total scale pH (pH_T), dissolved inorganic carbon (DIC; µmol kg^{-1}); and total alkalinity (TA; µmol kg^{-1}) for the grouped spatial survey locations (nearshore, mid, outer, and outside; n = 3 each) for the early morning and late afternoon surveys. Significant differences (Tukey) are denoted by brackets with listed p-values.

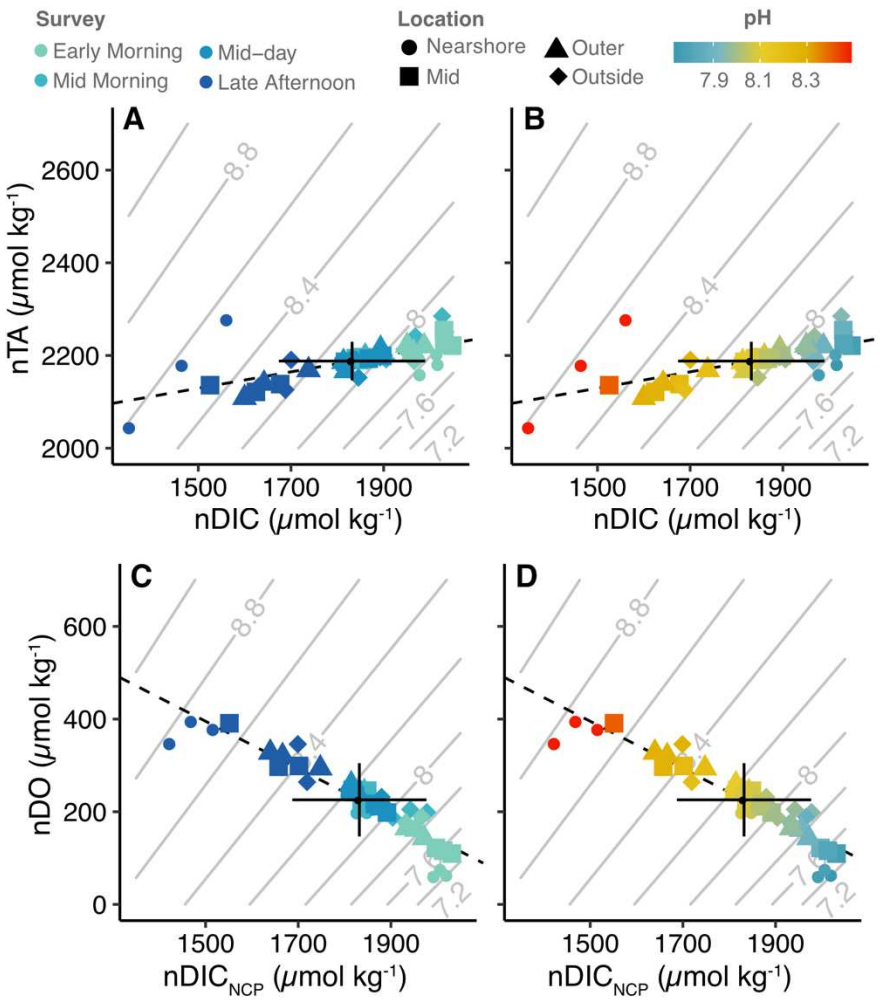

Figure 4.4: Salinity normalized TA, DIC, and DO property-property plots. Salinity normalized TA (nTA) and salinity normalized DIC (nDIC) shaped by location, colored by survey time **(A)** and by calculated pH **(B)**. Salinity normalized DO (nDO) and salinity normalized DIC accounting for NCP effects only ($nDIC_{NCP}$) shaped by location, colored by survey time **(C)** and colored by calculated pH **(D)**. All normalization was done to a mean salinity of 34.2.

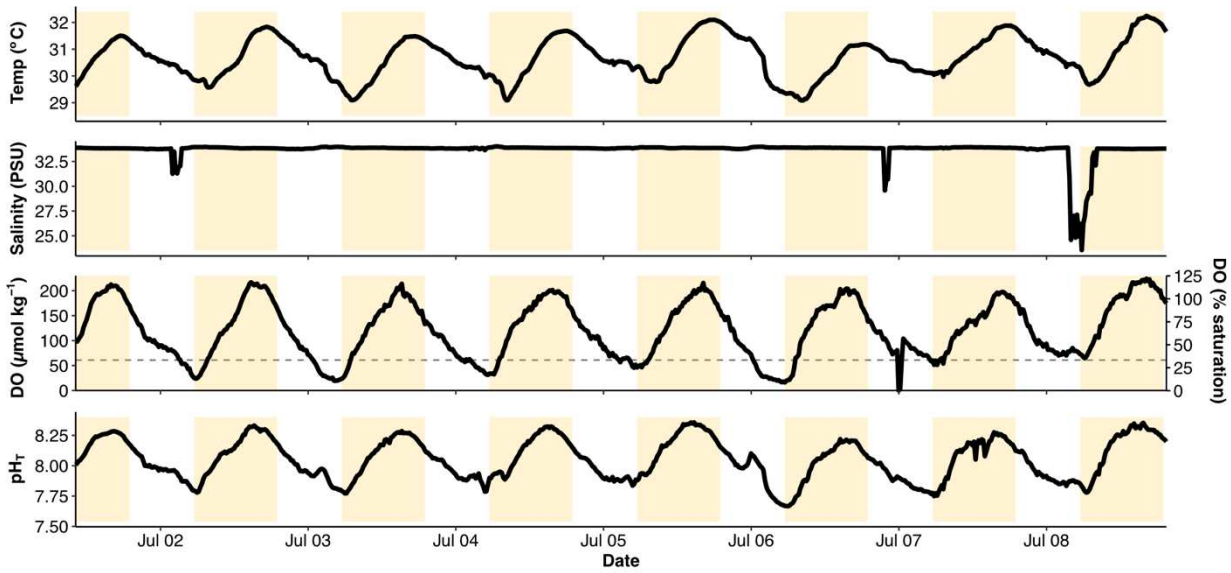

Figure 4.5: High frequency data from the seagrass CTD sensor. Time series of temperature (ºC), salinity (PSU), dissolved oxygen (DO; µmol kg^{-1} and percent saturation), and total scale pH (pH_T) from the IDRONAUT CTD sensor deployed in the shallow seagrass. Yellow shaded boxes denote local daylight hours. Dashed grey line on the DO panel denotes severe hypoxia (< 61 µmol kg^{-1}).

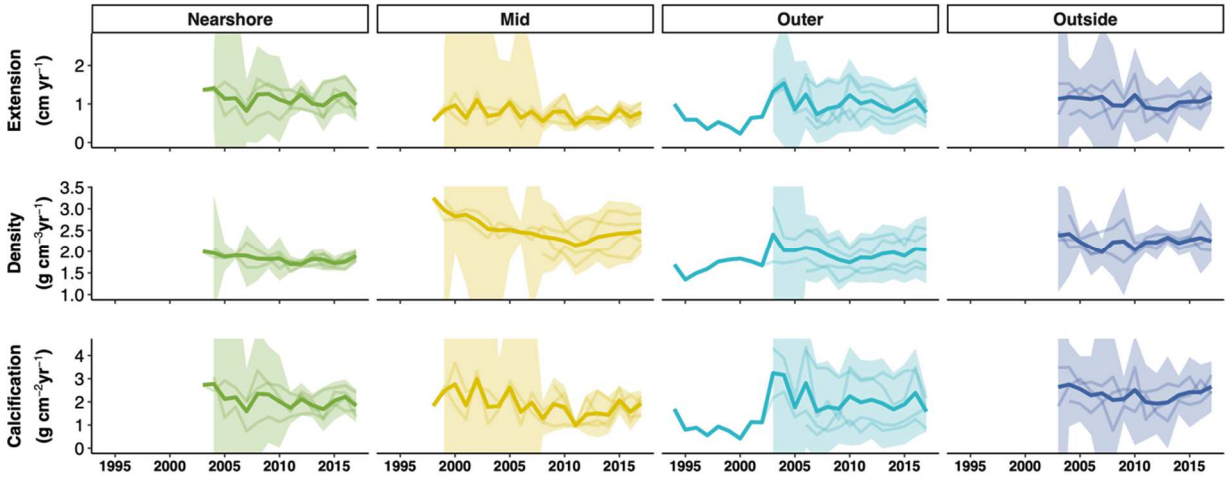

Figure 4.6: Trends of coral skeletal growth parameters over time. Time series of annual extension rate (cm $year^{-1}$), density (g cm^{-3} $year^{-1}$), and calcification rate (g cm^{-2} $year^{-1}$) for all years for all cores at each of the four collection locations (columns; n = 4 cores per location, but n = 3 at the outside site). Lighter color lines are time series for individual cores and darker lines are the mean for all cores at each location with 95 % confidence interval shading above and below.

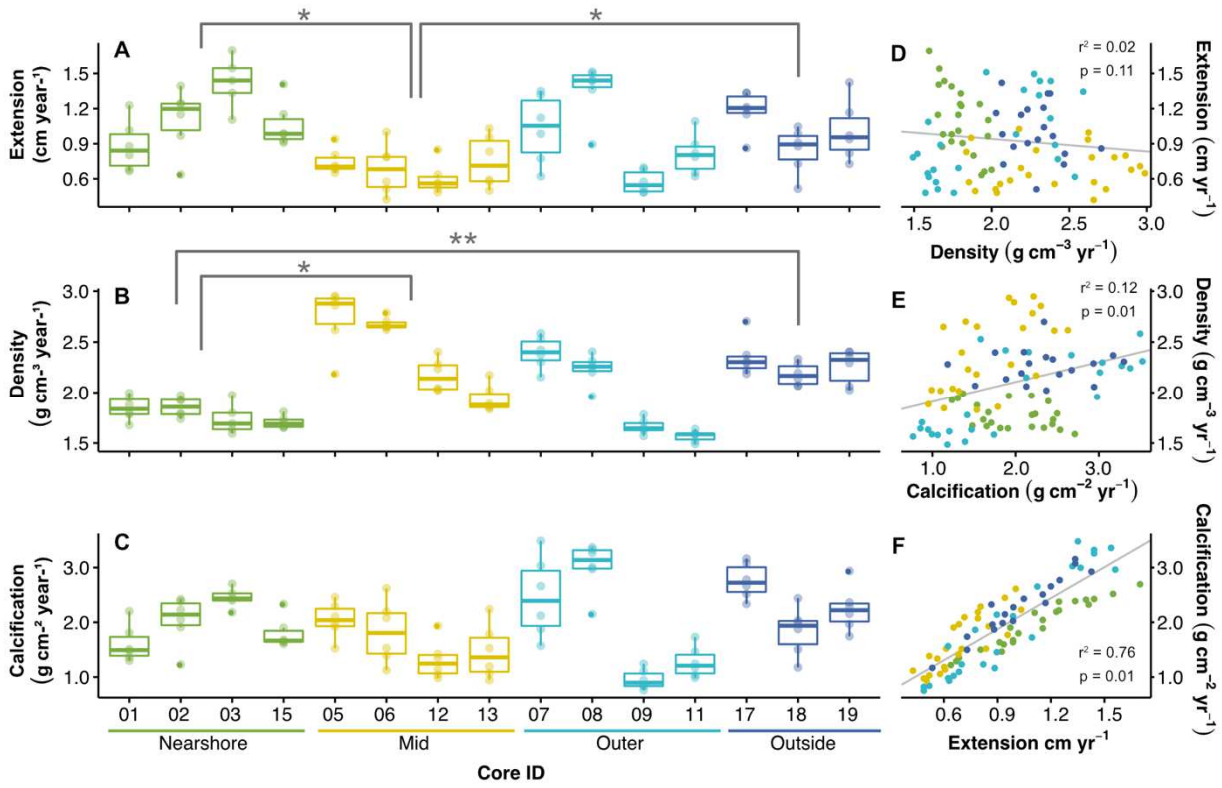

Figure 4.7: Differences in coral growth parameters between sites. Boxplots of annual extension rate (cm year^{-1}) **(A)**, density (g cm^{-3} year^{-1}) **(B)**, and calcification rate (g cm^{-2} year^{-1}) **(C)** for the years 2012 to 2017 for all cores at each collection location. Significant differences between mean growth parameters grouped by site are indicated by a grey bracket and asterisk (*p < 0.06. **p < 0.01; Tukey). Property-property plots of extension rate, density, and calcification rate for all cores **(D-F)** colored by location, with linear regression lines (grey) and linear model statistics.

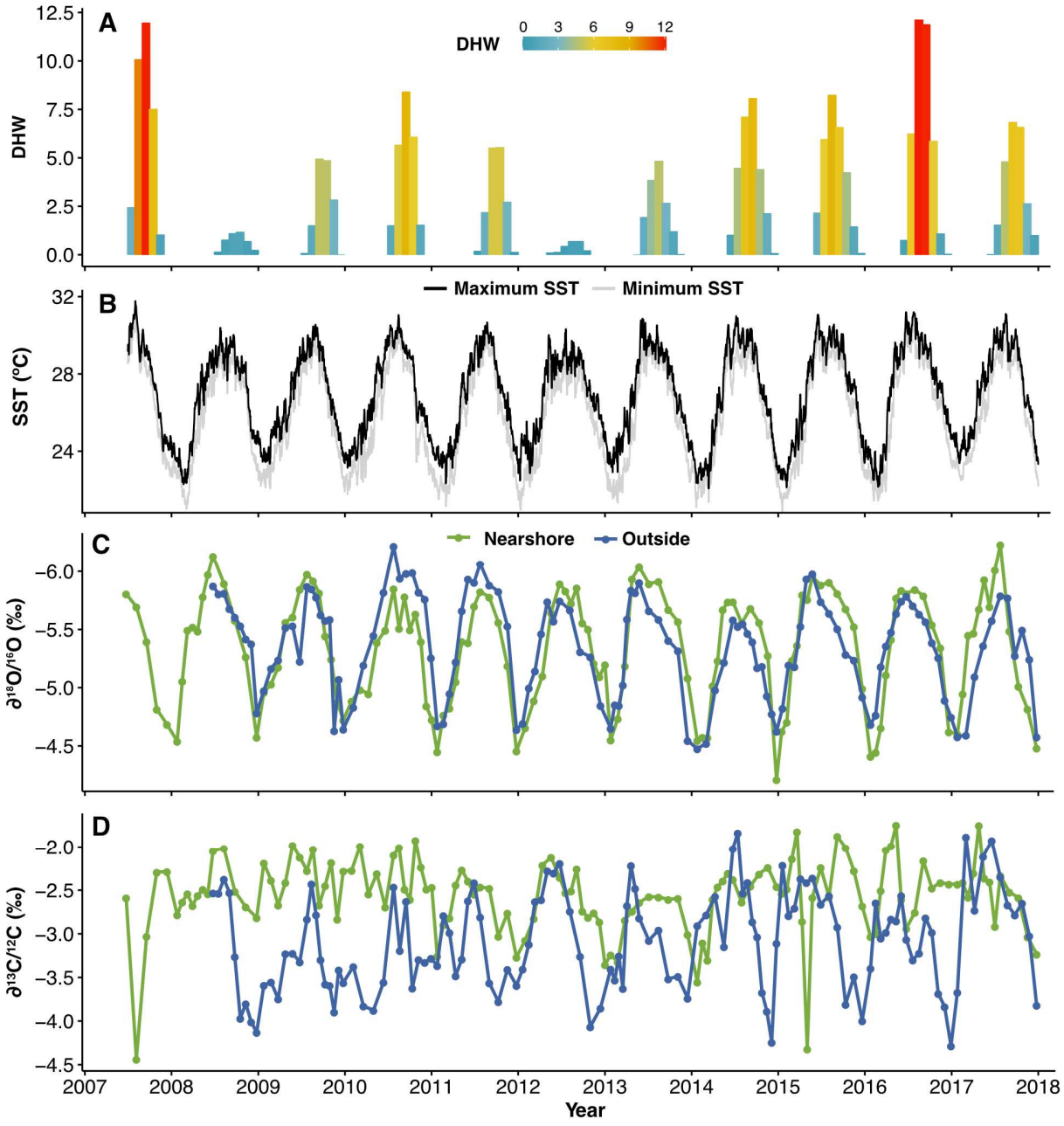

Figure 4.8: Time series of degree heating weeks, temperature, and coral skeletal isotopic ratios. (A) Mean monthly degree heating weeks (DHW), **(B)** maximum and minimum mean monthly satellite-derived sea surface temperature (° C), **(C)** skeletal $\partial^{18}O/^{16}O$ isotopic ratio (‰) for the nearshore and outside coral, and **(D)** skeletal $\partial^{13}C/^{12}C$ (‰) for the nearshore and outside coral.

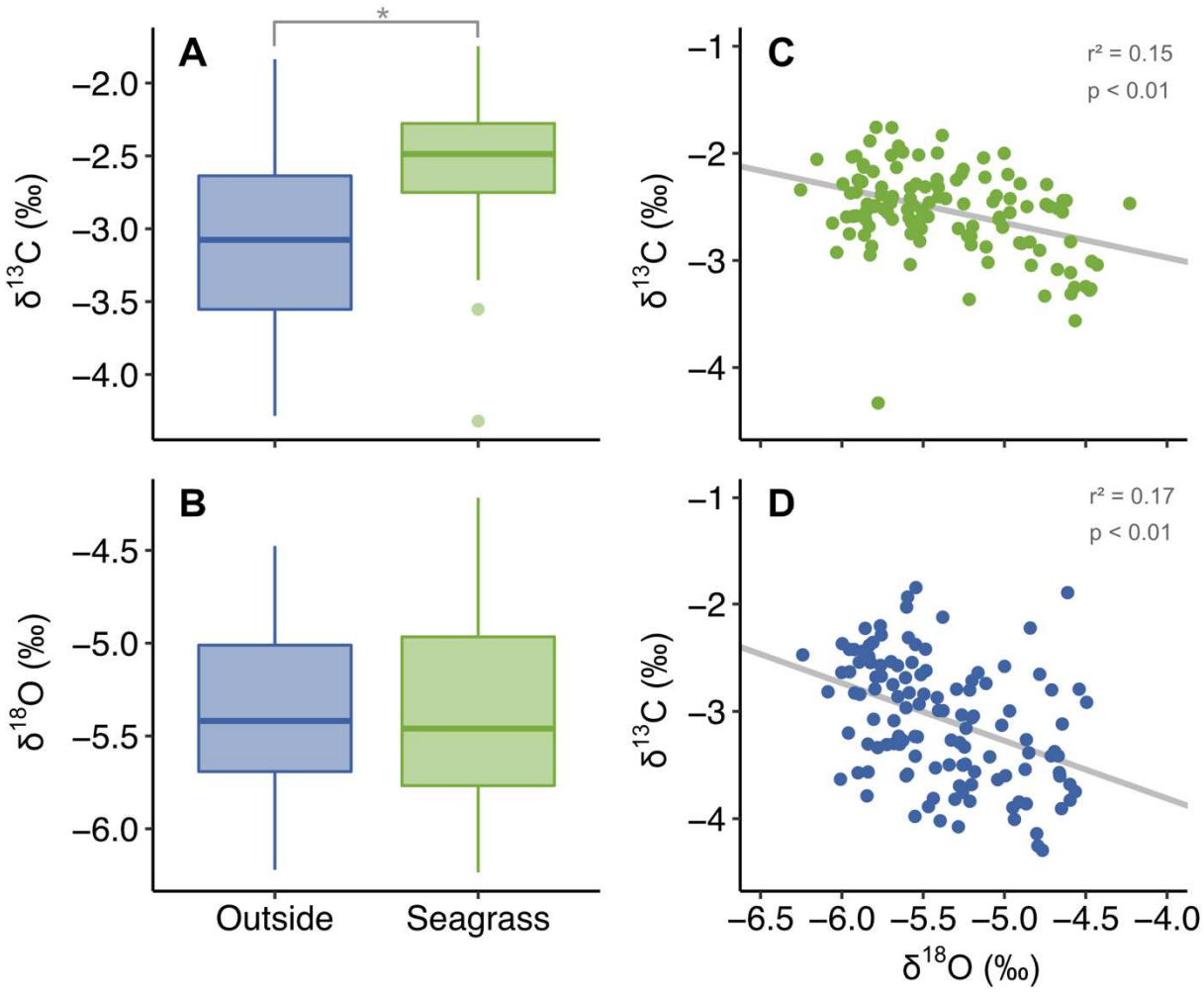

Figure 4.9: Comparisons of $\partial^{13}C$ and $\partial^{18}O$ between corals and property-property plots of isotopes. Boxplots of $\partial^{13}C$ (A) and $\partial^{18}O$ (B) for the outside (blue) and seagrass (green) core. Significant differences ($p < 0.01$, t-test) in mean values denoted by gray bracket and asterisk. Property-property plots of $\partial^{13}C$ and $\partial^{18}O$ for the seagrass coral (C) and the outside coral (D) with linear regression line in gray and linear model statistics.

SUPPLEMENTARY MATERIAL

FIGURES

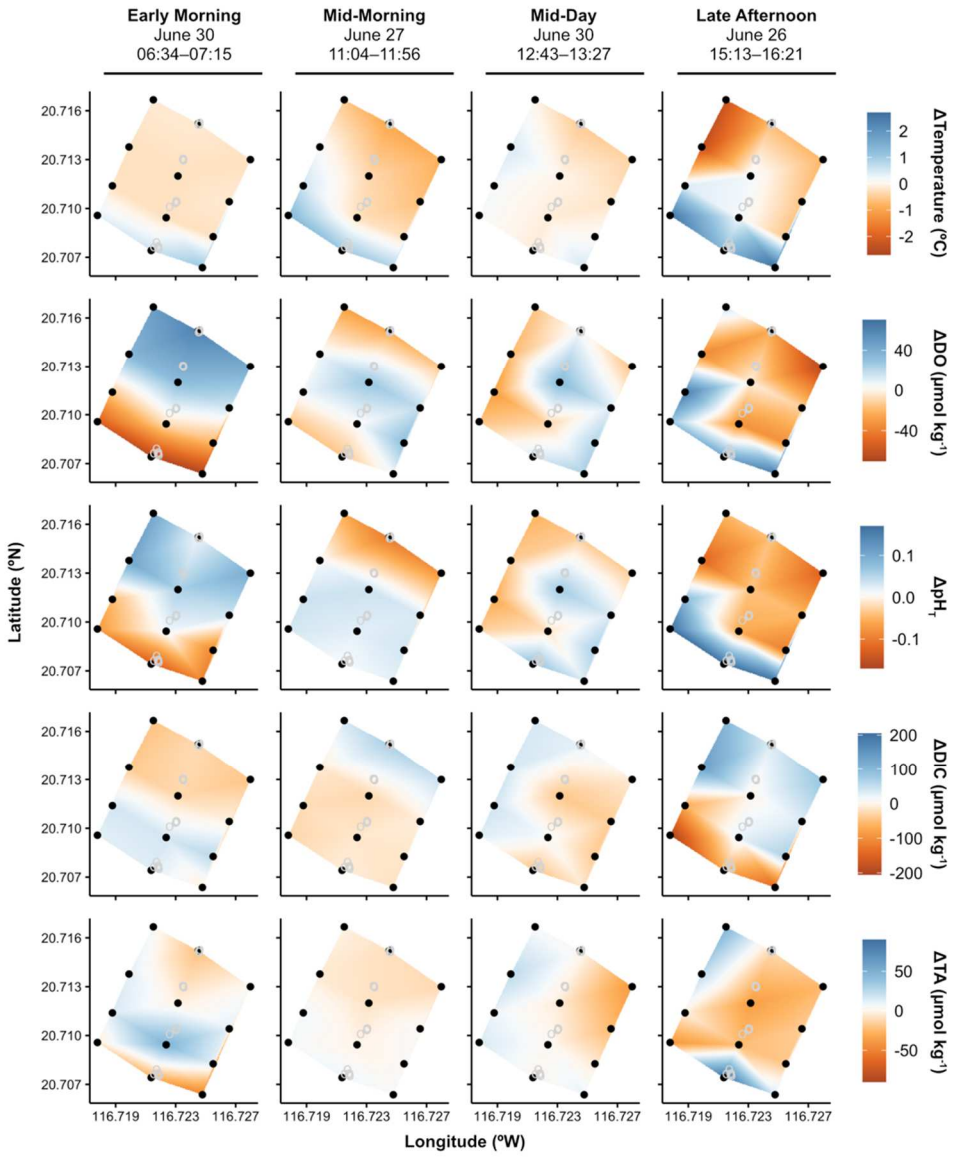

Figure 4.S1: Gradients in temperature, water chemistry, and dissolved oxygen across the seagrass spatial surveys. Spatial gradients in temperature (ºC), dissolved oxygen (DO; µmol kg^{-1}), total scale pH (pH_T), dissolved inorganic carbon (DIC; µmol kg^{-1}); and total alkalinity (TA; µmol kg^{-1}) across the four spatial surveys (stations denoted by black circles) in the Dongsha Island north shore seagrass bed. Coral core collection locations are denoted by white open circles. Times listed below dates represent the time of collection of the first and last sample of the survey (local time). Delta values reported were calculated as the difference between the survey mean and the value recorded at a given station (i.e., positive values indicate that the value recorded at that station was higher than the survey average and negative values indicate that the value recorded at the station was lower than the survey average).

ACKNOWLEDGEMENTS

Chapter 4, in full, is currently being prepared for submission for publication of the material. Pezner, Ariel K.; Charles, Christopher D.; Chou, Wen-Chen; Chu, Hui-Chuan; Courtney, Travis A.; Frable, Bejamin W.; Kekuewa, Samuel A. H.; Soong, Keryea; Wei, Yi; Andersson, Andreas J. The dissertation author was the primary researcher and author of this material.

REFERENCES

Adkins, J. F., Boyle, E. A., Curry, W. B., and Lutringer, A. (2003). Stable isotopes in deep-sea corals and a new mechanism for "vital effects." *Geochimica et Cosmochimica Acta* 67, 1129–1143. doi: 10.1016/S0016-7037(02)01203-6.

Al-Horani, F. A., Tambutté, É., and Allemand, D. (2007). Dark calcification and the daily rhythm of calcification in the scleractinian coral, *Galaxea fascicularis*. *Coral Reefs* 26, 531–538. doi: 10.1007/s00338-007-0250-x.

Altieri, A. H., and Gedan, K. B. (2015). Climate change and dead zones. *Global Change Biology* 21, 1395–1406. doi: 10.1111/gcb.12754.

Altieri, A. H., Harrison, S. B., Seemann, J., Collin, R., Diaz, R. J., and Knowlton, N. (2017). Tropical dead zones and mass mortalities on coral reefs. *Proceedings of the National Acadamies of Science* 114, 3660–3665. doi: 10.1073/pnas.1621517114.

Andersson, A., and Gledhill, D. (2012). Ocean acidification and coral reefs: Effects on breakdown, dissolution, and net ecosystem calcification. *Annual Review of Marine Science* 5. doi: 10.1146/annurev-marine-121211-172241.

Anthony, K. R. N., A. Kleypas, J., and Gattuso, J.-P. (2011). Coral reefs modify their seawater carbon chemistry – implications for impacts of ocean acidification. *Global Change Biology* 17, 3655–3666. doi: 10.1111/j.1365-2486.2011.02510.x.

Bergstrom, E., Silva, J., Martins, C., and Horta, P. (2019). Seagrass can mitigate negative ocean acidification effects on calcifying algae. *Scientific Reports* 9, 1932. doi: 10.1038/s41598-018-35670-3.

Breitburg, D., Levin, L. A., Oschlies, A., Grégoire, M., Chavez, F. P., Conley, D. J., Garçon, V., Gilbert, D., Gutiérrez, D., Isensee, K., Jacinto, G. S., Limburg, K. E., Montes, I., Naqvi, S. W. A., Pitcher, G., Rabalais, N. N., Roman, M. E., Rose, K. A., Seibel, B. A., Telszewski, M., Yasuhara, M., and Zhang, J. (2018). Declining oxygen in the global ocean and coastal waters. *Science* 359, eaam7240. doi: 10.1126/science.aam7240.

Buapet, P., Gullström, M., Björk, M., Buapet, P., Gullström, M., and Björk, M. (2013). Photosynthetic activity of seagrasses and macroalgae in temperate shallow waters can alter seawater pH and total inorganic carbon content at the scale of a coastal embayment. *Marine Freshwater Research* 64, 1040–1048. doi: 10.1071/MF12124.

Camp, E. F., Edmondson, J., Doheny, A., Rumney, J., Grima, A. J., Huete, A., and Suggett, D. J. (2019). Mangrove lagoons of the Great Barrier Reef support coral populations persisting under extreme environmental conditions. *Marine Ecological Progress Series.* 625, 1–14. doi: 10.3354/meps13073.

Camp, E. F., Nitschke, M. R., Rodolfo-Metalpa, R., Houlbreque, F., Gardner, S. G., Smith, D. J., Zampighi, M., Suggett, D. J. (2017). Reef-building corals thrive within hot-acidified and deoxygenated waters. *Scientific Reports* 7, 2434. doi: 10.1038/s41598-017-02383-y.

Carriquiry, J. D., Risk, M. J., and Schwarcz, H. P. (1994). Stable isotope geochemistry of corals from Costa Rica as proxy indicator of the EL Niño/Southern Oscillation (ENSO). *Geochimica et Cosmochimica Acta* 58, 335–351. doi: 10.1016/0016-7037(94)90468-5.

Challener, R. C., Robbins, L. L., and McClintock, J. B. (2016). Variability of the carbonate chemistry in a shallow, seagrass-dominated ecosystem: implications for ocean acidification experiments. *Marine Freshwater Research* 67, 163. doi: 10.1071/MF14219.

Chan, N. C. S., and Connolly, S. R. (2013). Sensitivity of coral calcification to ocean acidification: a meta-analysis. *Global Change Biology* 19, 282–290. doi: 10.1111/gcb.12011.

Charles, C. D., Cobb, K., Moore, M. D., and Fairbanks, R. G. (2003). Monsoon–tropical ocean interaction in a network of coral records spanning the 20th century. *Marine Geology* 201, 207–222. doi: 10.1016/S0025-3227(03)00217-2.

Chou, W.-C., Chu, H.-C., Chen, Y.-H., Syu, R.-W., Hung, C.-C., and Soong, K. (2018). Short-term variability of carbon chemistry in two contrasting seagrass meadows at Dongsha Island Implications for pH buffering and CO_2 sequestration. *Estuarine, Coastal and Shelf Science* 210, 36–44.

Chou, W.-C., Fan, L.-F., Yang, C.-C., Chen, Y.-H., Hung, C.-C., Huang, W.-J., Shih, Y.-Y., Soong, K., Tseng, H.-C., Gong, G.-C., Chen, H.-Y., and Su, C.-K. (2021). A unique diel pattern in carbonate chemistry in the seagrass meadows of Dongsha Island: The enhancement of metabolic carbonate dissolution in a semienclosed lagoon. *Frontiers in Marine Science* 8, 1–16.

Colombo-Pallotta, M. F., Rodríguez-Román, A., and Iglesias-Prieto, R. (2010). Calcification in bleached and unbleached *Montastraea faveolata*: evaluating the role of oxygen and glycerol. *Coral Reefs* 29, 899–907. doi: 10.1007/s00338-010-0638-x.

Comeau, S., Edmunds, P. J., Spindel, N. B., and Carpenter, R. C. (2013). The responses of eight coral reef calcifiers to increasing partial pressure of CO_2 do not exhibit a tipping point. *Limnology and Oceanography* 58, 388–398. doi: 10.4319/lo.2013.58.1.0388.

Cyronak, T., Andersson, A. J., D'Angelo, S., Bresnahan, P., Davidson, C., Griffin, A., Kindeberg, T., Pennise, J., Takeshita, Y., White, M. (2018a). Short-term spatial and temporal carbonate chemistry variability in two contrasting seagrass meadows: Implications for pH buffering capacities. *Estuaries and Coasts* 41, 1282–1296. doi: 10.1007/s12237-017-0356-5.

Cyronak, T., Andersson, A. J., Langdon, C., Albright, R., Bates, N. R., Caldeira, K., Carlton, R., Corredor, J. E., Dunbar, R. B., Enochs, I., Erez, J., Eyre, B. D., Gattuso, J.-P., Gledhill, D., Kayanne, H., Kline, D. I., Koweek, D. A., Lantz, C., Lazar, B., Manzello, D., McMahon, A., Meléndez, M., Page, H. N., Santos, I. R., Schulz, K. G., Shaw, E., Silverman, J., Suzuki, A., Teneva, L., Watanabe, A., and Yamamoto, S. (2018b). Taking the metabolic pulse of the world's coral reefs. *PLoS ONE* 13, e0190872. doi: 10.1371/journal.pone.0190872.

Cyronak, T., Takeshita, Y., Courtney, T. A., DeCarlo, E. H., Eyre, B. D., Kline, D. I., Martz, T., Page, H., Price, N. N., Smith, J., Stoltenberg, L., Tresguerres, M., and Andersson, A. J. (2020). Diel temperature and pH variability scale with depth across diverse coral reef habitats. *Limnology and Oceanography Letters* 5, 193–203. doi: 10.1002/lol2.10129.

Dai, C. (2006). Dongsha Atoll in the South China Sea: Past, present, and future. 6.

Dai, C.-F., Fan, T.-Y., and Wu, C.-S. (1995). Coral fauna of Tungsha Tao (Pratas Islands). *Acta Oceanographica Taiwanica* 34, 1–16.

De'ath, G., Lough, J. M., and Fabricius, K. E. (2009). Declining coral calcification on the Great Barrier Reef. *Science* 323, 116–119. doi: 10.1126/science.1165283.

DeCarlo, T. M., Cohen, A. L., Wong, G. T. F., Davis, K. A., Lohmann, P., and Soong, K. (2017). Mass coral mortality under local amplification of 2°C ocean warming. *Scientific Reports* 7, 44586. doi: 10.1038/srep44586.

Dickson, A. G. (1990). Thermodynamics of the dissociation of boric acid in synthetic seawater from 273.15 to 318.15 K. *Deep Sea Research Part A. Oceanographic Research Papers* 37, 755–766. doi: 10.1016/0198-0149(90)90004-F.

Dickson, A. G., and Millero, F. J. (1987). A comparison of the equilibrium constants for the dissociation of carbonic acid in seawater media. *Deep Sea Research Part A. Oceanographic Research Papers* 34, 1733–1743. doi: 10.1016/0198-0149(87)90021-5.

Dickson, A. G., Sabine, C. L., Christian, J. R., Bargeron, C. P., and North Pacific Marine Science Organization eds. (2007). *Guide to best practices for ocean CO_2 measurements*. Sidney, BC: North Pacific Marine Science Organization.

Doney, S. C., Fabry, V. J., Feely, R. A., and Kleypas, J. A. (2009). Ocean acidification: The other CO_2 problem. *Annual Review of Marine Science* 1, 169–192. doi: 10.1146/annurev.marine.010908.163834.

Duarte, C. M. (1989). Temporal biomass variability and production/biomass relationships of seagrass communities. *Marine Ecological Progress Series* 51, 269–276. doi: 10.3354/meps051269.

Duarte, C. M., and Chiscano, C. L. (1999). Seagrass biomass and production: A reassessment. *Aquatic Botany* 65, 159–174. doi: 10.1016/S0304-3770(99)00038-8.

Edmunds, P. J., Brown, D., and Moriarty, V. (2012). Interactive effects of ocean acidification and temperature on two scleractinian corals from Moorea, French Polynesia. *Global Change Biology* 18, 2173–2183. doi: 10.1111/j.1365-2486.2012.02695.x.

Epstein, S., Buchsbaum, R., Lowenstam, H. A., and Urey, H. C. (1953). Revised carbonate-water isotopic temperature scale. *Bulletin of the Geological Society of America* 64, 1315–1326.

Epstein, S., and Mayeda, T. (1953). Variation of O^{18} content of waters from natural sources. *Geochimica et Cosmochimica Acta* 4, 213–224. doi: 10.1016/0016-7037(53)90051-9.

Erez, J. (1978). Vital effect on stable-isotope composition seen in foraminifera and coral skeletons. *Nature* 273, 199–202. doi: 10.1038/273199a0.

Fabricius, K. E., Langdon, C., Uthicke, S., Humphrey, C., Noonan, S., De'ath, G., Okazaki, R., Muehllenhner, N., Glas, M. S., and Lough, J. M. (2011). Losers and winners in coral reefs acclimatized to elevated carbon dioxide concentrations. *Nature Climate Change* 1, 165–169. doi: 10.1038/nclimate1122.

Fairbanks, R. G., and Dodge, R. E. (1979). Annual periodicity of the $^{18}O/^{16}O$ and $^{13}C/^{12}C$ ratios in the coral *Montastrea annularis*. *Geochimica et Cosmochimica Acta* 43, 1009–1020. doi: 10.1016/0016-7037(79)90090-5.

Falter, J. L., Lowe, R. J., Zhang, Z., and McCulloch, M. (2013). Physical and biological controls on the carbonate chemistry of coral reef waters: Effects of metabolism, wave forcing, sea level, and geomorphology. *PLoS ONE* 8, e53303. doi: 10.1371/journal.pone.0053303.

Frankignoulle, M., and Bouquegneau, J. M. (1990). Daily and yearly variations of total inorganic carbon in a productive coastal area. *Estuarine, Coastal and Shelf Science* 30, 79–89. doi: 10.1016/0272-7714(90)90078-6.

Frankignoulle, M., and Distèche, A. (1984). CO_2 chemistry in the water column above a posidonia seagrass bed and related air-sea exchanges. *Oceanologica Acta* 7, 209–219.

Gagan, M. K., Chivas, A. R., and Isdale, P. J. (1994). High-resolution isotopic records from corals using ocean temperature and mass-spawning chronometers. *Earth and Planetary Science Letters* 121, 549–558. doi: 10.1016/0012-821X(94)90090-6.

Gagan, M. K., Chivas, A. R., and Isdale, P. J. (1996). Timing coral-based climatic histories using ^{13}C enrichments driven by synchronized spawning. *Geology* 24, 1009–1012. doi: 10.1130/0091-7613(1996)024<1009:TCBCHU>2.3.CO;2.

Ganguly, D., Singh, G., Ramachandran, P., Selvam, A. P., Banerjee, K., and Ramachandran, R. (2017). Seagrass metabolism and carbon dynamics in a tropical coastal embayment. *Ambio* 46, 667–679. doi: 10.1007/s13280-017-0916-8.

Gattuso, J.-P., Epitalon, J.-M., Lavigne, H., and Orr, J. (2021). seacarb: Seawater carbonate chemistry. Available at: https://CRAN.R-project.org/package=seacarb.

Goreau, T. J. (1977). Coral skeletal chemistry: Physiological and environmental regulation of stable isotopes and trace metals in *Montastrea annularis*. *Proceedings of the Royal Society of London. Series B. Biological Sciences* 196, 291–315. doi: 10.1098/rspb.1977.0042.

Groner, M. L., Burge, C. A., Cox, R., Rivlin, N. D., Turner, M., Van Alstyne, K. L., Wyllie-Echeverria, A., Bucci, J., Staudigel, P., and Friedman, C. S. (2018). Oysters and eelgrass: Potential partners in a high pCO_2 ocean. *Ecology* 99, 1802–1814. doi: 10.1002/ecy.2393.

Grottoli, A. G. (1999). Variability of stable isotopes and maximum linear extension in reef-coral skeletons at Kaneohe Bay, Hawaii. *Marine Biology* 135, 437–449. doi: 10.1007/s002270050644.

Grottoli, A. G. (2000). Stable carbon isotopes ($\delta^{13}C$) in coral skeletons. *Oceanography* 13, 93–97.

Grottoli, A. G. (2002). Effect of light and brine shrimp on skeletal $\delta^{13}C$ in the Hawaiian coral Porites compressa: A tank experiment. *Geochimica et Cosmochimica Acta* 66, 1955–1967. doi: 10.1016/S0016-7037(01)00901-2.

Grottoli, A. G., Rodrigues, L. J., and Juarez, C. (2004). Lipids and stable carbon isotopes in two species of Hawaiian corals, *Porites compressa* and *Montipora verrucosa*, following a bleaching event. *Marine Biology* 145, 621–631. doi: 10.1007/s00227-004-1337-3.

Grottoli, A. G., and Wellington, G. M. (1999). Effect of light and zooplankton on skeletal $\delta^{13}C$ values in the eastern Pacific corals *Pavona clavus* and *Pavona gigantea*. *Coral Reefs* 18, 29–41. doi: 10.1007/s003380050150.

Guzmán, H. M., and Tudhope, A. W. (1998). Seasonal variation in skeletal extension rate and stable isotopic ($^{13}C/^{12}C$ and $^{18}O/^{16}O$) composition in response to several environmental variables in the Caribbean reef coral *Siderastrea siderea*. *Marine Ecology Progress Series* 166, 109–118. doi: 10.3354/meps166109.

Helmle, K. P., Kohler, K. E., and Dodge, R. E. (2003). CoralXDS - Coral X-radiograph Densitometry System. *Nova Southeastern University*. Available at: https://hcas.nova.edu/tools-and-resources/coralxds/index.html.

Hendriks, I. E., Olsen, Y. S., Ramajo, L., Basso, L., Steckbauer, A., Moore, T. S., Howard, J., and Duarte, C. M. (2014). Photosynthetic activity buffers ocean acidification in seagrass meadows. *Biogeosciences* 11, 333–346. doi: 10.5194/bg-11-333-2014.

Hoegh-Guldberg, O. (1999). Climate change, coral bleaching and the future of the world's coral reefs. *Marine Freshwater Research* 50, 839–866. doi: 10.1071/mf99078.

Huang, Y.-H., Lee, C.-L., Chung, C.-Y., Hsiao, S.-C., and Lin, H.-J. (2015). Carbon budgets of multispecies seagrass beds at Dongsha Island in the South China Sea. *Marine Environmental Research* 106, 92–102. doi: 10.1016/j.marenvres.2015.03.004.

Invers, O., Romero, J., and Pérez, M. (1997). Effects of pH on seagrass photosynthesis: A laboratory and field assessment. *Aquatic Botany* 59, 185–194. doi: 10.1016/S0304-3770(97)00072-7.

Johnson, M. D., Swaminathan, S. D., Nixon, E. N., Paul, V. J., and Altieri, A. H. (2021). Differential susceptibility of reef-building corals to deoxygenation reveals remarkable hypoxia tolerance. *Scientific Reports* 11, 23168. doi: 10.1038/s41598-021-01078-9.

Kapsenberg, L., and Cyronak, T. (2019). Ocean acidification refugia in variable environments. *Global Change Biology* 25, 3201–3214. doi: 10.1111/gcb.14730.

Koweek, D. A., Zimmerman, R. C., Hewett, K. M., Gaylord, B., Giddings, S. N., Nickols, K. J., Ruesink, J. L., Stachowicz, J. J., Takeshita, Y., and Caldeira, K. (2018). Expected limits on the ocean acidification buffering potential of a temperate seagrass meadow. *Ecological Applications* 28, 1694–1714. doi: 10.1002/eap.1771.

Kwiatkowski, L., Torres, O., Bopp, L., Aumont, O., Chamberlain, M., Christian, J. R., Dunne, J. P., Gehlen, M., Ilyina, T., John, J. G., Lenton, A., Li, H., Lovenduski, N. S., Orr, J. C., Palmieri, J., Santana-Falcón, Y., Schwinger, J., Séférian, R., Stock, C. A., Tagliabue, A., Takano, Y., Tjiputra, J., Toyama, K., Tsujino, H., Watanabe, M., Yamamoto, A., Yool, A., and Ziehn, T.(2020). Twenty-first century ocean warming, acidification, deoxygenation, and upper-ocean nutrient and primary production decline from CMIP6 model projections. *Biogeosciences* 17, 3439–3470. doi: 10.5194/bg-17-3439-2020.

Land, L. S., Lang, J. C., and Barnes, D. J. (1975). Extension rate: A primary control on the isotopic composition of West Indian (Jamaican) scleractinian reef coral skeletons. *Marine Biology* 33, 221–233. doi: 10.1007/BF00390926.

Lee, C.-L., Huang, Y.-H., Chung, C.-Y., Hsiao, S.-C., and Lin, H.-J. (2015). Herbivory in multi-species, tropical seagrass beds. *Marine Ecology Progress Series* 525, 65–80. doi: 10.3354/meps11220.

Legendre, P. (2018). lmodel2: Model II regression. Available at: https://CRAN.R-project.org/package=lmodel2.

Lenth, R. V. (2022). emmeans: Estimated marginal means, aka least-squares means. Available at: https://CRAN.R-project.org/package=emmeans.

Lewis, E., and Wallace, D. (1998). CO2SYS - program developed for the CO2 system calculations.

Li, J.-J., Lee, T.-F., Tew, K. S., and Fang, L.-S. (2000). Changes in the coral community at Dong-Sha Atoll, South China Sea from 1975 to 1998. *Acta Zoologica Taiwanica* 11. doi: 10.6576/AZT.2000.11.(1).1.

Lin, H.-J., Hsieh, L.-Y., and Liu, P.-J. (2005). Seagrasses of Tongsha Island, with descriptions of four new records to Taiwan. *Botanical Bulletin of Academia Sinica* 46, 163–168.

Linsley, B. K., Dunbar, R. B., Dassié, E. P., Tangri, N., Wu, H. C., Brenner, L. D., and Wellington, G. M. (2019). Coral carbon isotope sensitivity to growth rate and water depth with paleo-sea level implications. *Nature Communications* 10, 2056. doi: 10.1038/s41467-019-10054-x.

Lough, J. M. (2008). Coral calcification from skeletal records revisited. *Marine Ecological Progress Series* 373, 257–264. doi: 10.3354/meps07398.

Lough, J. M., and Barnes, D. J. (2000). Environmental controls on growth of the massive coral *Porites*. *Journal of Experimental Marine Biology and Ecology* 245, 225–243. doi: 10.1016/S0022-0981(99)00168-9.

Lough, J. M., and Cantin, N. E. (2014). Perspectives on massive coral growth rates in a changing ocean. *The Biological Bulletin* 226, 187–202. doi: 10.1086/BBLv226n3p187.

Lough, J. M., Cantin, N. E., Benthuysen, J. A., and Cooper, T. F. (2016). Environmental drivers of growth in massive *Porites* corals over 16 degrees of latitude along Australia's northwest shelf: Environmental drivers of massive coral growth. *Limnology and Oceanography* 61, 684–700. doi: 10.1002/lno.10244.

Lough, J. M., and Cooper, T. F. (2011). New insights from coral growth band studies in an era of rapid environmental change. *Earth-Science Reviews* 108, 170–184. doi: 10.1016/j.earscirev.2011.07.001.

Lowe, A. T., Kobelt, J., Horwith, M., and Ruesink, J. (2019). Ability of eelgrass to alter oyster growth and physiology is spatially limited and offset by increasing predation risk. *Estuaries and Coasts* 42, 743–754. doi: 10.1007/s12237-018-00488-9.

Manzello, D. P. (2010). Coral growth with thermal stress and ocean acidification: lessons from the eastern tropical Pacific. *Coral Reefs* 29, 749–758. doi: 10.1007/s00338-010-0623-4.

Marbà, N., Holmer, M., Gacia, E., and Barrón, C. (2006). "Seagrass beds and coastal biogeochemistry," in *Seagrasses: Biology, ecology, and conservation*, eds. A. W. D. Larkum, R. J. Orth, and C. M. Duarte (Dordrecht, The Netherlands: Springer), 135–157.

Martin, P., Goodkin, N. F., Stewart, J. A., Foster, G. L., Sikes, E. L., White, H. K., Hennige, S., and Roberts, J. M. (2016). Deep-sea coral $\delta^{13}C$: A tool to reconstruct the difference between seawater pH and $\delta^{11}B$-derived calcifying fluid pH. *Geophysical Research Letters* 43, 299–308. doi: 10.1002/2015GL066494.

McConnaughey, T. (1989). ^{13}C and ^{18}O isotopic disequilibrium in biological carbonates: I. Patterns. *Geochimica et Cosmochimica Acta* 53, 151–162. doi: 10.1016/0016-7037(89)90282-2.

McConnaughey, T. A., Burdett, J., Whelan, J. F., and Paull, C. K. (1997). Carbon isotopes in biological carbonates: Respiration and photosynthesis. *Geochimica et Cosmochimica Acta* 61, 611–622. doi: 10.1016/S0016-7037(96)00361-4.

McCrea, J. M. (1950). On the isotopic chemistry of carbonates and a paleotemperature scale. *The Journal of Chemical Physics.* 18, 849–857. doi: 10.1063/1.1747785.

Mehrbach, C., Culberson, C. H., Hawley, J. E., and Pytkowicx, R. M. (1973). Measurement of the apparent dissociation constants of carbonic acid in seawater at atmospheric pressure. *Limnology and Oceanography* 18, 897–907. doi: 10.4319/lo.1973.18.6.0897.

Muscatine, L., Porter, J. W., and Kaplan, I. R. (1989). Resource partitioning by reef corals as determined from stable isotope composition. *Marine Biology* 100, 185–193. doi: 10.1007/BF00391957.

Nelson, H. R., and Altieri, A. H. (2019). Oxygen: The universal currency on coral reefs. *Coral Reefs* 38, 177–198. doi: 10.1007/s00338-019-01765-0.

Page, H. N., Courtney, T. A., De Carlo, E. H., Howins, N. M., Koester, I., and Andersson, A. J. (2018). Spatiotemporal variability in seawater carbon chemistry for a coral reef flat in Kāneʻohe Bay, Hawaiʻi. *Limnology and Oceanography* 64, 913–934. doi: 10.1002/lno.11084.

Pan, X., Wong, G. T. F., DeCarlo, T. M., Tai, J.-H., and Cohen, A. L. (2017). Validation of the remotely sensed nighttime sea surface temperature in the shallow waters at the Dongsha Atoll. *Terrestrial, Atmospheric, and Oceanic Sciences.* 28, 517–524. doi: 10.3319/TAO.2017.03.30.01.

Pandolfi, J. M., Connolly, S. R., Marshall, D. J., and Cohen, A. L. (2011). Projecting Coral Reef Futures Under Global Warming and Ocean Acidification. *Science* 333, 418–422. doi: 10.1126/science.1204794.

Pezner, A. K., Courtney, T. A., Page, H. N., Giddings, S. N., Beatty, C. M., DeGrandpre, M. D., and Andersson, A. J. (2021). Lateral, vertical, and temporal variability of seawater carbonate chemistry at Hog Reef, Bermuda. *Frontiers in Marine Science.* 8, 562267. doi: 10.3389/fmars.2021.562267.

Pinheiro, J., Bates, D., DebRoy, S., Sarkar, D., and R Core Team (2021). nlme: Linear and Nonlinear Mixed Effects Models. Available at: https://CRAN.R-project.org/package=nlme.

Porter, J. W., Fitt, W. K., Spero, H. J., Rogers, C. S., and White, M. W. (1989). Bleaching in reef corals: Physiological and stable isotopic responses. *Proceedings of the National Academy of Sciences* 86, 9342–9346. doi: 10.1073/pnas.86.23.9342.

R Core Team (2019). R: A language and environment for statistical computing. Available at: https://www.R-project.org/.

Ricart, A. M., Gaylord, B., Hill, T. M., Sigwart, J. D., Shukla, P., Ward, M., Ninokawa, A., and Sanford, E. (2021). Seagrass-driven changes in carbonate chemistry enhance oyster shell growth. *Oecologia* 196, 565–576. doi: 10.1007/s00442-021-04949-0.

Rosenberg, R. (1980). "Effect of oxygen deficiency on benthic macrofauna," in *Fjord Oceanography*, eds. J. H. Freeland, D. M. Farmer, and C. D. Levings (New York, NY: Plenum Publication Corporation), 499–514.

Rosenfeld, M., Yam, R., Shemesh, A., and Loya, Y. (2003). Implication of water depth on stable isotope composition and skeletal density banding patterns in a Porites lutea colony: results from a long-term translocation experiment. *Coral Reefs* 22, 337–345. doi: 10.1007/s00338-003-0333-2.

Saderne, V., Baldry, K., Anton, A., Agustí, S., and Duarte, C. M. (2019). Characterization of the CO_2 system in a coral reef, a seagrass meadow, and a mangrove forest in the central Red Sea. *Journal of Geophysical Research: Oceans* 124, 7513–7528. doi: 10.1029/2019JC015266.

Semesi, I., Beer, S., and Björk, M. (2009). Seagrass photosynthesis controls rates of calcification and photosynthesis of calcareous macroalgae in a tropical seagrass meadow. *Marine Ecological Progress Series* 382, 41–47. doi: 10.3354/meps07973.

Soong, K., Dai, C.-F., and Lee, C.-P. (2002). Status of Pratas Atoll in South China Sea. Proceedings of the 4th Conference on the Protected Areas of East Asia (IUCN/WCPA/EA-4), Taipei, 739–742.

Spencer, L. H., Horwith, M., Lowe, A. T., Venkataraman, Y. R., Timmins-Schiffman, E., Nunn, B. L., and Roberts, S. B. (2019). Pacific geoduck (*Panopea generosa*) resilience to natural pH variation. *Comparative Biochemistry and Physiology Part D: Genomics and Proteomics* 30, 91–101. doi: 10.1016/j.cbd.2019.01.010.

Status of the Coral Reefs of the World: 2020 (2020). Global Coral Reef Monitoring Network.

Suzuki, A., Gagan, M. K., Fabricius, K., Isdale, P. J., Yukino, I., and Kawahata, H. (2003). Skeletal isotope microprofiles of growth perturbations in *Porites* corals during the 1997-1998 mass bleaching event. *Coral Reefs* 22, 357–369. doi: 10.1007/s00338-003-0323-4.

Swart, P. K., Leder, J. J., Szmant, A. M., and Dodge, R. E. (1996). The origin of variations in the isotopic record of scleractinian corals: II. Carbon. *Geochimica et Cosmochimica Acta* 60, 2871–2885. doi: 10.1016/0016-7037(96)00119-6.

Tanzil, J. T. I. (2013). Environmental controls of coral growth: Data driven multi-scale analyses of rates and patterns of growth in massive *Porites* corals around the Thai-Malay Peninsula. Thesis, University of Amsterdam.

Tkachenko, K. S., and Soong, K. (2017). Dongsha Atoll: A potential thermal refuge for reef-building corals in the South China Sea. *Marine Environmental Research* 127, 112–125. doi: 10.1016/j.marenvres.2017.04.003.

Unsworth, R. K. F., Collier, C. J., Henderson, G. M., and McKenzie, L. J. (2012). Tropical seagrass meadows modify seawater carbon chemistry: Implications for coral reefs impacted by ocean acidification. *Environmental Research Letters.* 7, 024026. doi: 10.1088/1748-9326/7/2/024026.

Uppström, L. R. (1974). The boron/chlorinity ratio of deep-sea water from the Pacific Ocean. *Deep Sea Research and Oceanographic Abstracts* 21, 161–162. doi: 10.1016/0011-7471(74)90074-6.

Urey, H. C. (1947). The thermodynamic properties of isotopic substances. *Journal of the Chemical Society* 562–581. doi: 10.1039/JR9470000562.

Wahl, M., Schneider Covachã, S., Saderne, V., Hiebenthal, C., Müller, J. D., Pansch, C., and Sawall, Y. (2018). Macroalgae may mitigate ocean acidification effects on mussel calcification by increasing pH and its fluctuations. *Limnology and Oceanography* 63, 3–21. doi: 10.1002/lno.10608.

Ward, M., Kindinger, T. L., Hirsh, H. K., Hill, T. M., Jellison, B. M., Lummis, S., Rivest, E. B., Waldbusser, G. G., Gaylord, B., and Kroeker, K. J. (2022). Reviews and syntheses: Spatial and temporal patterns in seagrass metabolic fluxes. *Biogeosciences* 19, 689–699. doi: 10.5194/bg-19-689-2022.

Weber, J. N., Deines, P., Weber, P. H., and Baker, P. A. (1976). Depth related changes in the $^{13}C/^{12}C$ ratio of skeletal carbonate deposited by the Caribbean reef-frame building coral *Montastrea annularis*: Further implications of a model for stable isotope fractionation by scleractinian corals. *Geochimica et Cosmochimica Acta* 40, 31–39. doi: 10.1016/0016-7037(76)90191-5.

Weber, J. N., and Woodhead, P. M. J. (1970). Carbon and oxygen isotope fractionation in the skeletal carbonate of reef-building corals. *Chemical Geology* 6, 93–117. doi: 10.1016/0009-2541(70)90009-4.

Wijgerde, T., Jurriaans, S., Hoofd, M., Verreth, J. A. J., and Osinga, R. (2012). Oxygen and heterotrophy affect calcification of the scleractinian coral *Galaxea fascicularis*. *PLOS ONE* 7, e52702. doi: 10.1371/journal.pone.0052702.

Wijgerde, T., Silva, C. I. F., Scherders, V., van Bleijswijk, J., and Osinga, R. (2014). Coral calcification under daily oxygen saturation and pH dynamics reveals the important role of oxygen. *Biology Open* 3, 489–493. doi: 10.1242/bio.20147922.

Zeileis, A., and Grothendieck, G. (2005). zoo: S3 infrastructure for regular and irregular time series. *Journal of Statistical Software* 14, 1–27. doi: 10.18637/jss.v014.i06.

Zimmerman, R. C., Kohrs, D. G., Steller, D. L., and Alberte, R. S. (1997). Impacts of CO_2 enrichment on productivity and light requirements of eelgrass. *Plant Physiology* 115, 599–607. doi: 10.1104/pp.115.2.599.

CHAPTER 5: Conclusions

This dissertation explores multidimensional variability in carbonate chemistry and oxygen across reefs (Chapter 2), the prevalence of present and future hypoxia exposure on global reefs (Chapter 3), and how spatial gradients in water chemistry and oxygen impact coral calcification in a seagrass bed (Chapter 4). Together, these results contribute to our growing understanding of the controls on coral reef biogeochemical variability and how corals themselves may fare in a changing ocean.

Chapter 2

- In addition to benthic production (photosynthesis and respiration), water column production was quantitatively important at Hog Reef, contributing to the observed strong diel signals in dissolved oxygen (DO), pH, and seawater pCO_2.
- The total alkalinity (TA) signal was driven mainly by biogeochemical processes occurring only on the benthos (calcification and dissolution) and modified by local hydrodynamics, leading to higher frequency variability.
- Lateral spatial gradients in water chemistry parameters across the reef were larger than vertical gradients and were strongly influenced by the geomorphology of the reef, water current speed, and flow direction.
- While the gradients between surface and benthic water chemistry parameters were small, the non-zero differences suggest that the assumption of a well-mixed water column should be assessed for specific reef cases.

Chapter 3

- Baseline oxygen concentrations and variability differ both within and between reef locations around the world, leading to different definitions of "normoxia" for each reef habitat.
- Low oxygen conditions are pervasive on reefs across the globe under present-day conditions, with nearly all sites experiencing weak to moderate hypoxia and some already experiencing severe hypoxia.
- Calculations of changing oxygen solubility and biological oxygen demand under modeled warming reveal an increase in hypoxic event intensity, duration, and severity for all reef sites by the end of the century, with more than a third experiencing severe hypoxia.
- Assessments and predictions of hypoxia exposure depend strongly on the thresholds set to define hypoxic conditions; thus, continued quality measurements of DO on reefs as well as quantitative exploration of relevant oxygen thresholds for tropical reef taxa is needed to improve predictions.

Chapter 4

- Seagrasses strongly modify the surrounding seawater environment on diel and spatial scales, creating significant inshore to offshore gradients in temperature, pH, dissolved inorganic carbon (DIC), and DO.
- High frequency autonomous sensor data reveal that the corals in the shallowest part of the seagrass experience severe hypoxia and low pH every night, and hyperoxia and high pH during the day.

- Despite the observed spatial gradient, there was no evidence of significant elevation of coral calcification for corals inside the seagrass bed.
- Significant differences in coral skeletal extension rate, density, and $\partial^{13}C$ between corals collected across the seagrass may be driven by a combination of depth, feeding strategy, seagrass modifications of local DIC, or individual differences between corals.
- More research is needed to assess whether corals exposed to natural variability in temperature, pH, and DO are better prepared to cope with warming, acidification, and deoxygenation in the future.

Ultimately, this dissertation highlights the many interactive processes that shape carbonate chemistry and oxygen variability on reefs over both time and space and how this variability translates to differences in coral growth. Measurements of both biological and physical processes on reefs are needed for proper assessment of changes in reef biogeochemistry under climate change. In addition to warming and acidification, oxygen loss and hypoxia are likely to be important drivers of reef scale changes in the future, and additional research is needed to elucidate the impacts of low oxygen on coral reefs.